Development of, and signalling to, oligodendrocytes and their precursors

Laura Clarke

A thesis submitted to University College London for the degree of Doctor of Philosophy

Department of Neuroscience, Physiology and Pharmacology
University College London

June 2012

Statement of the candidate's contribution to this thesis

With the exceptions listed below, all of the work in this thesis was carried out by Laura Clarke. She was responsible, with normal supervisorial input, for planning the work, carrying out the electrophysiological, immunocytochemical, cell proliferation and cell death experiments, and analysing and interpreting the data she had collected.

The exceptions are as follows.

(i) The work on the electrophysiological and anatomical properties of oligodendrocytes derived from different regions of the CNS (Chapter 3) depended on the use of transgenic mice that were developed and characterised by Richa Tripathi in Bill Richardson's lab. The injection of tracer into the primary motor cortex and red nucleus was carried out by Patrick Anderson because of his expertise at this difficult technique. Some details of the mouse characterisation and results of the tracer injection are included in Chapter 3 in order to give a complete scientific account of this study. This work has been published in the Journal of Neuroscience, with Laura Clarke as joint first author.

(ii) The work on the electrophysiological properties and fate of OPCs in different brain regions (Chapter 4) included an analysis of cell proliferation that required EdU administration to living animals. For Home Office Licence animal legislation reasons this administration was done by Kaylene Young in Bill Richardson's lab. This work has been accepted for publication by the Journal of Neuroscience, with Laura Clarke as joint first author.

(iii) The work on the effects of GABA on oligodendrocyte development (Chapter 5) were partly carried out on cultured cortical slices - a preparation developed by Nicola Hamilton in the lab. This work has been submitted to Neuron, with Laura Clarke as joint first author.

Laura Clarke wrote all of the thesis.

Signed: David Attwell, Jodrell Professor of Physiology, PhD Supervisor

Laura Clarke

Abstract

Oligodendrocytes myelinate axons in the CNS to increase the speed of action potential conduction. Myelinating oligodendrocytes develop from oligodendrocyte precursor cells (OPCs). OPCs can express voltage-gated sodium and potassium channels, and receive excitatory and inhibitory synaptic input from axons. The functional relevance of voltage-gated and synaptic currents in OPCs is unknown, but electrical signalling from axons might regulate OPC development and myelination. In this thesis I investigate the electrical properties of OPCs, and how signalling to these cells regulates their proliferation, differentiation and myelination. I studied the electrical properties of OPCs in different brain areas, to investigate whether their electrical properties differ between embryonic sites of origin (in dorsal versus ventral parts of the CNS), and between brain regions (white matter versus grey matter). Firstly, using a dual reporter mouse line to colour code ventrally- and dorsally-derived oligodendrocyte lineage cells, I demonstrated that oligodendrocyte lineage cells derived from different embryonic sites are electrically similar. However, despite having indistinguishable electrical properties, dorsally-derived oligodendrocytes myelinated specific tracts in the spinal cord. Secondly, I have shown that OPCs in different brain regions have a similar expression of ion channels and precursor proteins, are all mitotically active, and generate differentiated oligodendrocytes but not neurons. Finally, having determined that all OPCs apparently have similar membrane properties, I investigated whether the inhibitory neurotransmitter GABA can regulate OPC proliferation, differentiation and myelination. I found that both oligodendrocytes and their precursors respond to GABA via the activation of $GABA_A$ receptors. In addition, endogenously released GABA was found to reduce the number of oligodendrocyte lineage cells formed, reduce the amount of myelin per axon and increase internode length. These results demonstrate that GABA, presumably released from inhibitory interneurons, can regulate myelination, and raise the possibility that GABA could also modulate CNS remyelination.

Contents

List of figures

List of tables

Acknowledgements

First and foremost, I would like to express my sincere thanks to my supervisor David Attwell for his encouragement, guidance, advice and the time he has spent supervising me throughout my PhD and in the preparation of this thesis.

During my time in the Attwell lab, I have greatly benefitted from being surrounded by people with such vast knowledge and expertise. In particular, I would like to thank Dr Kaylene Young for all her help over the years with the research for our joint project, and for her invaluable input during the preparation of this thesis. I am also extremely grateful to Dr Nicola Hamilton for teaching me to make cultures and record compound action potentials, to Dr Yamina Bakiri for teaching me to patch-clamp at the beginning of my PhD, and to Valeria Burzomato and Richa Tripathi for their help and expertise during our collaboration.

I would also like to express a special thank you to my collegues of past and present: Julia Harris, Clare Reynell, Nicola Hamilton, Valeria Burzomato, Kaylene Young, Lorena Arancibia Carcamo, Catherine Hall, Karolina Kolodziejczwk, Yamina Bakiri, Renaud Jolivet, Fergus O'Farrell, Lee Cossell, Johanne Egge Rinholm, Christian Madry, Anusha Mishra and Antonia Langfelder for creating a wonderful friendly lab environment full of inspiring scientific discussions, support and encouragement, which I have been very fortunate to work in.

In addition, I owe special gratitude to Justin Read and my friends in London and elsewhere, for their patience, encouragement and support over the years and especially during the preparation of this thesis.

Finally, I am most grateful to my parents and my brother for their unconditional love, guidance and support, without whom, I would not have been able to follow my dreams.

Chapter 1: Introduction

1.1 An overview of glia

The central nervous system is composed of two main types of cell, neurons and glia. Neurons are the excitable cells within the CNS and were thought to be solely responsible for information processing. On the other hand glia, as the Greek name implies, were thought to be the 'glue' of the CNS, providing structural, metabolic and trophic support for the surrounding neurons. Glia can be subdivided into three main types: (1) oligodendrocytes which wrap myelin around neuronal axons, (2) astrocytes which have diverse functions within the CNS, including providing trophic support to neurons, buffering extracellular [K^+], and taking up neurotransmitters released at neuronal synapses, and (3) microglia which are the resident immune cells of the brain. In recent years recognition of the importance of glial cells and their interactions with neurons has increased, especially in terms of the role of glia in the modulation of neurotransmission. My thesis focuses on investigating the properties of oligodendrocyte lineage cells and their interactions with neurons. In this chapter I will provide the background needed to understand the thesis: I will review the development of oligodendrocytes, their expression of cell surface proteins and ion channels, their functional roles in the CNS, and how they can be damaged in diseases.

1.2 An overview of the function of oligodendrocytes

The term oligodendrocyte means a cell with a few branches, and originates from the Greek words oligo (few), dendro (branches) and cytes (cells). The primary role of oligodendrocytes in the CNS is the synthesis and wrapping of layers of myelin around neuronal axons, which provides electrical insulation, effectively lowering the capacitance and increasing the resistance of the axonal membrane. Myelin is essential for rapid action potential conduction. Myelinated axons are wrapped by myelin in a series of sheaths, which are interrupted by unmyelinated segments rich in voltage-gated Na^+ channels, called the nodes of Ranvier. The nodes are essential for the conduction of action potentials, which sequentially activate Na^+ channels in the series of nodes (saltatory conduction). Although myelin is one of best studied mammalian membranes, surprisingly little is known about the oligodendrocyte-neuron interactions that determine which axons are selected for myelination, and how myelination is initiated and regulated.

1.3 The development of oligodendrocytes

Mature myelinating oligodendrocytes develop from glial precursors (oligodendrocyte precursor cells or OPCs) which express the proteoglycan NG2 and platelet-derived growth factor receptor α (PDGFRα) (Fig. 1.1). In addition to making oligodendrocytes during brain development, OPCs are also present in the adult CNS, where they comprise ~5% of the cells (7% in the white matter and 3% in the grey matter), and are the main proliferating cell type (Dawson et al., 2003). OPCs express a variety of cell surface receptors, and can respond to a multitude of neuronally derived signals including neurotransmitters, growth factors and cell adhesion ligands. In the following sections I will review the CNS sites of origin of OPCs, their development and differentiation into myelinating oligodendrocytes, and their electrical properties.

1.3.1 Birth of oligodendrocytes

The brain and spinal cord develop in the embryo by the process of neurulation. Firstly, neurulation begins with the formation of the neural plate from a thickening of the cells within the ectoderm. Next, the edges of the neural plate thicken to form the neural groove before folding inwards to form the neural tube (this process occurs at embryonic day 12 (E12) in mice). Finally, differentiation of the neural tube gives rise to the embryonic brain and spinal cord, and proliferation of the neuroepithelial cells within the neural tube gives rise to all of the neural cells (i.e. neurons, glia and ependymal cells). The notochord, a transient mesodermally-derived structure, is located ventrally to the developing neural tube and instructive signals released from the notochord have been shown to be involved in the formation of the dorsal-ventral axis in the developing CNS, and the specification of distinct populations of neurons within the spinal cord (Van Straaten et al., 1988).

1.3.1.1 Birth of oligodendrocytes in the embryonic spinal cord

Oligodendrogenesis within different parts of the brain and spinal cord occurs during the late gestational and early postnatal periods, after neuronal differentiation has taken place (Altman and Bayer, 1984). During development, OPCs arise from neural precursors located within discrete regions within the CNS. The newly generated OPCs proliferate and migrate long distances in order to populate the entire CNS, before differentiating into myelinating oligodendrocytes. In vertebrates, the majority of myelination occurs postnatally and is thought to continue throughout life (Fields, 2008).

The ventral ventricular zone (VZ) of the developing spinal cord is composed of a series of discrete progenitor domains known as p3, pMN, p2, p1, and p0 in the

ventral half of the cord and dP6 to dP1 in the dorsal half (Fig. 1.2). Each progenitor domain contains cells expressing specific transcription factors and generates a characteristic subset of spinal neurons before switching to production of glial cells (astrocytes and/or oligodendrocytes). In the developing spinal cord oligodendrocytes are produced in two separate waves. Initially, from E12.5, OPCs, identified by their expression of PDGFRα, arise from the VZ of the pMN domain of the spinal cord (Zhou et al., 2001) (Fig. 1.3A). The pMN domain generates the majority (~85%) of the oligodendrocytes in the spinal cord (Cai et al., 2005; Fogarty et al., 2005; Vallstedt et al., 2005; Tripathi et al., 2011). A change of transcription factor expression generates a developmental switch within the pMN domain, which initially gives rise to motor neurons but later generates oligodendrocytes. The pMN progenitors initially express the *Olig2*, *neurogenin1* and *neurogenin2* transcription factors, which results in the production of motor neurons. The pMN progenitors then downregulate their expression of *neurogenin1 and neurogenin 2,* and upregulate their expression of *Nkx2.2*. Cells that express both *Olig2* and *Nkx2.2* transcription factors develop into spinal cord oligodendrocytes instead of motor neurons (Zhou et al., 2001). This initial specification of oligodendrocytes in the embryonic spinal cord is also dependent on the ventral signalling molecule Sonic hedgehog (Shh) (Tekki-Kessaris et al., 2001) secreted from the notochord and floor plate, which is thought to induce cell type specific expression of *Olig* genes (Lu et al., 2000; Zhou et al., 2000) and to enhance the survival of oligodendrocytes (Davies and Miller, 2001).

The remainder of the oligodendrocytes within the spinal cord are thought to arise from more dorsal progenitor domains in the cord (Fig. 1.3A), independently of Shh signalling. The first evidence for the existence of alternative sources of oligodendrocytes, came from *Nkx6.1* and *Nkx6.2* double-mutant studies*. Nkx6* transcription factors are expressed in the progenitor domains of p3, pMN, p2 and p1 (Fig. 1.2). In knockout *Nkx6* spinal cords, Shh signalling from the notochord and floor plate fails to induce *Nkx6*-dependent activation of *Olig2* transcription, and this completely blocks oligodendrocyte production in the pMN (Cai et al., 2005). Surprisingly however, oligodendrocytes, expressing the characteristic markers PDGFRα and OLIG2, continue to be produced in the dorsal spinal cord of the *Nkx6*-null mice (Cai et al., 2005). These dorsal precursors expressed the transcription factor *Pax7*, confirming their dorsal origin (Cai et al., 2005). Furthermore, some oligodendrocytes in wild-type mice were also found to express PAX7, indicating that dorsal generation of oligodendrocytes also occurs in normal development. The

generation of dorsal oligodendrocytes, was found to begin a couple of days later than that of the ventral ones (from E15 compared to ~E15.5) (Cai et al., 2005).

Cre-lox fate-mapping experiments have also shown that the transcription factor *Dbx1*, which is restricted to ventral and dorsal progenitors in p1, p0, dP6 and dP5, labels a small number of oligodendrocytes (~3%) (Fogarty et al., 2005) (Fig. 1.2). Interestingly, these oligodendrocytes were found to transiently co-express the radial glial marker RC2, which suggests that these oligodendrocytes are formed from the direct transformation of radial glia (Fogarty et al., 2005). Finally, more recent fate-mapping studies, with *Gsh2-Cre* and *Msx3-Cre* transgenic mice, have demonstrated that ~10% and ~17% of oligodendrocytes, respectively, arise from the dP1-dP2 and dP3–dP5 domains (Tripathi et al. (2011) and chapter 3 of this thesis).

1.3.1.2 Birth of oligodendrocytes in the embryonic brain

Within the developing brain, as in the spinal cord, oligodendrocytes arise from distinct ventral and dorsal progenitor domains within the developing brain. Recent fate-mapping studies using *Nkx2.1*-Cre transgenic mice, which label neural precursors in the ventral regions of the telencephalon (in particular the medial ganglionic eminence (MGE) and the anterior entopeduncular region (AEP)), showed that OPCs first arrive in the cortex at ~E16 after migrating from the MGE/AEP at ~ E12.5 (Fig. 1.4) (Kessaris et al., 2006). This first wave of oligodendrocytes populates the whole cortex by E18, before being joined by a second wave of oligodendrocytes which arise from Gsh2-expressing precursors which reside in the lateral ganglionic eminences (LGE) (Fig. 1.4) (Kessaris et al., 2006). Until E18, all oligodendrocyte lineage cells in the forebrain are ventral in origin. After E18, the percentage contribution of the ventrally-derived oligodendrocytes begins to decrease as they are joined by a third wave of cells produced by *Emx1*-expressing progenitors found locally in the cortex (Fig. 1.4) (Kessaris et al., 2006). Interestingly, the original population of MGE/AEP-derived precursors disappears after birth, being rapidly eliminated from the cortex and more gradually from all other parts of the brain. Almost no trace can be found of the initial *Nkx2.1*-derived oligodendrocyte population anywhere in the adult (Kessaris et al., 2006). At present, it is not clear whether the *Nkx2.1*-derived oligodendrocyte population fails to survive, or just becomes diluted by the later-forming LGE- and dorsally-derived oligodendrocytes. Perhaps these early-forming oligodendrocytes have a specialised function in brain development, and are no longer required in the adult brain. Indeed, the majority (~80%) of OL lineage cells in the postnatal corpus callosum are generated

locally from *Emx1*-expressing progenitors, with the remaining (~20%) of OPCs migrating in from the LGE (Tripathi et al., 2011 and chapter 3 of this thesis).

Sonic Hedgehog signalling (Shh) has also been demonstrated to be important in oligodendrocyte specification in the embryonic ventral forebrain (Nery et al., 2001; Spassky et al., 2001; Tekki-Kessaris et al., 2001). Shh signalling however has not been detected within the postnatal cerebral cortex (Richardson et al., 2006), so the final wave of oligodendrocytes generated from the cortical *Emx1*-expressing progenitors is presumably controlled by an alternative signalling molecule. For example, fibroblast growth factor (FGF) can induce the generation of oligodendrocytes from cortical progenitor cells (Davis and Temple, 1994; Qian et al., 1997), and is perhaps involved in oligodendrocyte specification within the cortex.

1.3.1.3 Are oligodendrocytes derived from different progenitors functionally distinct?

Oligodendrocytes arise from dorsal and ventral progenitor populations under the influence of different instructive signals, however it is not known whether they are functionally identical or differ functionally in some way. In general, oligodendrocytes are morphologically distinct, with four different types of myelinating oligodendrocyte having been defined: types I and II, which have small cell bodies and 5-10 processes which myelinate small diameter axons (< 2 µm diameter), type III, which have large cell bodies and 1-2 processes which myelinate large diameter axons (> 4 µm diameter); and type IV oligodendrocytes which have large cell bodies without any processes and lie directly over the single large axon that they ensheath (del Rio-Hortega, 1921, 1928; Stensaas and Stensaas, 1968; Remahl and Hildebrand, 1990; Bjartmar et al., 1994; Vinet et al., 2010). Thus, these different types of oligodendrocyte myelinate different numbers of axons, in a manner which is highly correlated with the axon diameter. Those wrapping large diameter axons synthesise only one myelin internode, whereas other oligodendrocytes can make many internodes to myelinate several small diameter axons (Butt et al., 1997). Differences in the migration and maturation properties of dorsally- and ventrally-derived oligodendrocytes have been described in the spinal cord oligodendrocytes, with dorsally-derived OPCs maturing more slowly than their ventral counterparts (Cai et al., 2005). In addition, OPCs have been described to differ in terms of their ion channel expression (Karadottir et al., 2008), proliferative capacity (Rivers et al., 2008; Psachoulia et al., 2009; Guo et al., 2010; Simon et al., 2011), and response to injury (Keirstead et al., 1998). However, despite all these reported differences in the morphological and functional properties of oligodendrocyte lineage cells, a study by

Kessaris et al. (2006) revealed that if one specific developmentally-defined population cortical oligodendrocytes is killed, they could be replaced by the remaining population of oligodendrocytes. Interestingly, this replacement was sufficient to ensure the normal development of the animal, suggesting that in the forebrain the subpopulations of oligodendrocytes are functionally equivalent, as they can replace each other.

Chapter 3 of my thesis addresses the question of whether dorsally- and ventrally-derived oligodendrocyte lineage cells are functionally distinct, with the use of a dual-reporter mouse line in which oligodendrocyte lineage cells are labelled green or red, depending on their developmental origin within the embryonic brain or spinal cord.

1.3.2 Migration of oligodendrocytes

As a result of arising from highly restricted progenitor domains, OPCs must migrate long distances in order to populate the whole brain and spinal cord. OPC migration is guided by many soluble and membrane bound cues (Miller, 2002) to ensure the cells reach their final destination. In the optic nerve, the majority of OPC migration was found to be unidirectional, with OPCs migrating from the optic chiasm to the retina (Sugimoto et al., 2001). This unidirectional migration was shown to be due to chemorepellent signals (in particular netrin-1 and semaphorin-3a and 4f) produced by the optic chiasm (Sugimoto et al., 2001; Armendariz et al., 2012). Similarly, netrin-1 is also thought to be involved in the dispersal of OPCs from the VZ of the spinal cord (Miller, 2002). The soluble signalling molecule Slit, which is secreted by cells within the midline, also repels OPC migration by activating roundabout (Robo) receptors expressed on the OPCs (Liu et al., 2012). Vascular endothelial growth factor (VEGF), a soluble signalling molecule known to regulate angiogenesis, has been recently reported to promote OPC migration by reorganisation of the actin cytoskeleton within the leading-edge processes of migrating OPCs (Hayakawa et al., 2011).

OPCs are often defined by their expression of the proteins NG2 and PDGFRα on their cell surface (Fig. 1.1), and both of these proteins have been reported to play a role in OPC migration. Firstly, when the external interactions of NG2 was blocked by the binding of an antibody to an extracellular domain of the NG2 protein, OPC migration was impaired (Hayakawa et al., 2011; Trotter, 2005). NG2 is known to serve as a co-receptor for PDGFRα (Goretzki et al., 1999) and the intracellular domain of NG2 contains a PDZ-binding motif which can interact with many intracellular signalling proteins that also contain the motif. In particular, NG2 has been found to interact with the PDZ-binding protein syntenin-1 which aids OPC migration (Chatterjee et al., 2008). Secondly, activation of PDGFRα receptors, by the growth factor PDGF-AA, enhances

OPC migration (and proliferation: see next section). PDGFRα is a tyrosine kinase receptor which activates numerous signalling pathways. A recent study has demonstrated that the ERK signalling pathway mediates PDGF-AA-dependent OPC migration (Vora et al., 2011).

OPCs also express integrins, in a developmentally regulated fashion, which interact with extracellular matrix proteins including laminin and fibronectin, to regulate contact-mediated OPC migration (Milner and Ffrench-Constant, 1994). Interestingly, neurotransmitter receptor signalling has been demonstrated to regulate integrin function to modulate OPC migration. Gudz et al. (2006) suggested that, like in migrating neurons (in which the amplitude and frequency of intracellular calcium ($[Ca^{2+}]_i$) fluctuations in the soma provide a signal that controls the rate of cell migration (Pende et al., 1994; Kumada and Komuro, 2004)), OPC motility could also be controlled by $[Ca^{2+}]_i$ fluctuations. Gudz et al. (2006) provided evidence that Ca^{2+} modulates integrin-dependent OPC migration, by showing that disruption of Ca^{2+} signalling in OPCs leads to an alteration of integrin function and to a reduction of the cells' movement. The distribution of integrins on the OPC cell membrane provided an insight into how Ca^{2+} signalling controls OPC motility. During the 'migratory' phase of OPC development, OPCs were found to express higher levels of the $\alpha_v\beta_3$ integrin receptor on the leading edge of their processes when compared with their rear processes (Gudz et al., 2006). This regional distribution of integrin receptors, produced by different recycling/endocytosis rates at the leading edge and rear of the cell, was controlled by $[Ca^{2+}]_i$. Furthermore, the neurotransmitter glutamate was shown to increase $[Ca^{2+}]_i$ in OPCs and accelerate integrin-mediated OPC migration (Gudz et al., 2006).

The inhibitory neurotransmitter GABA can also regulate OPC migration. A gradient of low to high immunoreactivity for GABA has been observed from the ventricular zone to the cortical plate of the developing telencephalon, which may allow the involvement of endogenous GABA signalling in directional cortical cell migration (Heng et al., 2007). Like glutamate, $GABA_A$ receptor activation evokes Ca^{2+} transients in OPCs, however, these Ca^{2+} transients are not mediated by opening of voltage-gated Ca^{2+} channels but instead involved GABA depolarising OPCs by activating a Cl^- efflux through $GABA_A$ receptors (the Cl^- reversal potential is more positive than the resting potential: Lin and Bergles, 2004). The depolarisation then activates voltage-gated Na^+ channels, which raises $[Na^+]_i$. Finally the rise of $[Na^+]_i$ reverses Na^+/Ca^{2+} exchange and raises $[Ca^{2+}]_i$ (Tong et al., 2009). This unique Ca^{2+} signalling pathway in OPCs regulated their migration (Tong et al., 2009).

The factors described above are all thought to enhance OPC migration, but less is known about the factors which stop OPC migration when they reach their target destination. A few candidate stop signals have been described for OPCs in the optic nerve, which include the ECM molecule tenascin-C (Miller, 2002) and the chemokine CXCL-1 (Miller, 2002).

1.3.3 Proliferation of oligodendrocytes

OPC proliferation is regulated at least in part by signals released from neurons and astrocytes, in order to produce sufficient of OPCs to differentiate into myelinating cells and ensheath the length of neuronal axons. Several mechanisms have been suggested to control OPC proliferation. In culture, OPC proliferation was reported to be limited by an intrinsic clock, which makes OPCs undergo a finite number of divisions before differentiating into myelinating oligodendrocytes (Temple and Raff, 1986). This intrinsic clock mechanism was, however, found to be dependent on surrounding environmental signals, as when OPCs were cultured in the absence of exogenous growth factors they rapidly died (Calver et al., 1998)

Several growth factors released from neurons act as potent mitogens for OPCs. Perhaps the most well studied OPC mitogen is the growth factor PDGF-AA (the active homodimer of PDGF-A), which binds to its receptor PDGFRα. PDGFRα receptors are abundantly expressed by OPCs, and become down-regulated as they differentiate into myelinating oligodendrocytes. Over-expression of the PDGF-A gene results in a dramatic increase in the number of OPCs (Calver et al., 1998), while in PDGF-A knockout mice the number of OPCs is dramatically reduced (Fruttiger et al., 1999). The mechanism by which PDGF-AA regulates OPC proliferation is thought to involve increased expression of delayed outward-rectifying K^+ channels (Chittajallu et al., 2005), since inhibition of K^+ channels produced by glutamatergic signalling to OPCs reduces their proliferation (Knutson et al., 1997).

NG2 is also thought to influence the proliferation of OPCs, in part by acting as a co-receptor for PDGFRα (Goretzki et al., 1999). The expression of NG2 potentiates the activity of growth factor receptors such as PDGFRα by enhancing ligand binding (Goretzki et al., 1999). When NG2 is knocked out in mice, the numbers of proliferative OPCs are reduced, indicating that NG2 promotes OPC proliferation (Kucharova and Stallcup, 2010).

The growth factor fibroblast growth factor (FGF), which appears to be widely distributed throughout the embryonic CNS, also enhances OPC proliferation. FGF-

induced OPC proliferation is thought to extend the time period over which OPCs are proliferative and prevent their differentiation into myelinating oligodendrocytes (Gard and Pfeiffer, 1993; Mayer et al., 1993). The mitogenic action of FGF on OPCs is regulated by developmental changes of FGF receptor expression, with FGF-3 receptors being abundantly expressed by OPCs and downregulated as OPCs differentiate into myelinating oligodendrocytes (Bansal et al., 1996). Several other growth factors including neurotrophin-3 (NT-3) (Barres et al., 1994b), brain derived neurotrophic factor (BDNF) (Van't Veer et al., 2009) and neuregulin (Roy et al., 2007; Brinkmann et al., 2008; Taveggia et al., 2008) also act as mitogens to increase OPC proliferation.

Some messengers have been reported to inhibit OPC proliferation. In particular, retinoic acid, glucocorticoid and thyroid hormone are all suggested to cause OPCs to exit the cell cycle and differentiate (Barres et al., 1994a). For example, when the receptor for thyroid hormone is knocked out in mice, OPCs continuously proliferate and fail to differentiate, resulting in altered myelination in adult optic nerves (Baas et al., 2002). However, the mechanisms by which these molecules instruct OPCs to exit the cell cycle and induce differentiation are yet to be determined.

In addition to growth factors, neurotransmitters may regulate OPC proliferation, OPCs receive excitatory and inhibitory synaptic input mediated by glutamate and GABA (Bergles et al., 2000; Lin and Bergles, 2004; Kukley et al., 2007; Ziskin et al., 2007; Karadottir et al., 2008; Ge et al., 2009), raising the question of whether these neurotransmitters also regulate OPC development. So far, conflicting results exist in the literature on this issue. Glutamate has been suggested to block the proliferation and lineage progression of OPCs (Gallo et al., 1996; Yuan et al., 1998), as was shown earlier for neuronal precursor cells (LoTurco et al., 1995), but on the other hand glutamate has also been shown to promote myelin formation (Wake et al., 2011). Surprisingly, despite stimulating OPC migration (Tong et al., 2009), GABA has been reported to have no effect on OPC proliferation and differentiation (Gallo et al., 1996; Yuan et al., 1998). In chapter 5 I re-visit this issue.

OPC proliferation has recently been reported to be regulated by circadian rhythms. It is well known that, in a variety of mammalian organs, cell cycle progression is under the control of circadian oscillatory mechanisms (Bjarnason et al., 1999), and disruption of clock-associated genes significantly affects DNA replication and cell division in regenerated tissues and tumours (Gery et al., 2006; Chen-Goodspeed and Lee, 2007). The division of adult neural progenitor cells in the neurogenic sub-granular

zone of the hippocampus is controlled by time-of-day regulated mechanisms. More neural precursors proliferate during the night time (the active period in mice), when compared with the day time (resting time in mice) (Guzman-Marin et al., 2007; Matsumoto et al., 2011). Interestingly, the number of proliferating OPCs is also controlled by the time of the day, however, in contrast to neuronal precursors more OPCs proliferate during the resting period when compared to the active period (Matsumoto et al., 2011). This difference in time-of-day proliferation between neuronal precursors and OPCs was linked to a difference in the expression of cyclin proteins.

Voluntary physical exercise was reported to increase the number of proliferating OPCs in the hippocampus of mice (Matsumoto et al., 2011), and this increase was accompanied by an increase in the expression of c-Fos, a gene product which is upregulated in response to an increase in neuronal activity, indicating that OPC proliferation may be regulated by neuronal activity. In contrast, in a different brain region, the cerebral cortex, voluntary physical exercise led to an increase in the number of OPCs exiting the cell cycle, which was followed by enhanced differentiation of OPCs into oligodendrocytes (Simon et al., 2011). The evidence provided by both of these studies indicates that an increase in neuronal activity can influence OPC development.

To summarise, many signalling molecules can regulate OPC proliferation. In this thesis, I investigate the proliferative capacity of OPCs in Chapter 4, and whether OPC proliferation can be regulated by neurotransmitters in Chapter 5.

1.3.4 Differentiation of oligodendrocytes

During development a large proportion of OPCs differentiate into premyelinating oligodendrocytes, which then differentiate further into myelinating oligodendrocytes (Trapp et al., 1997; Zhu et al., 2008; De Biase et al., 2010; Kukley et al., 2010). The differentiation of OPCs is characterised by changes in the expression pattern of molecular markers and a dramatic change in cell morphology. Throughout development, all oligodendrocyte lineage cells express SOX10 and OLIG2 (Nishiyama et al., 2009), but as OPCs undergo terminal differentiation, they lose expression of precursor proteins including NG2 and PDGFRα, and begin to express the immature marker O4, followed by PLP, galactocerebroside and myelin basic protein (MBP) (Nishiyama et al., 2009) (Fig. 1.1). Morphometric analysis by single cell dye-filling has revealed that premyelinating oligodendrocytes have larger somas and longer processes which cover a greater area, when compared with OPCs (Kukley et al., 2010). Mature myelinating oligodendrocytes possess fewer processes than both

premyelinating cells and OPCs, but clearly show 1-60 myelin sheaths (internodes) (Fig. 1.1).

As OPCs differentiate, the changes in expression of molecular markers and cell morphology are also accompanied by a loss of synaptic connections and a change in ion channel expression (Kukley et al., 2010). These changes in ion channel expression within the oligodendrocyte lineage are described in detail in section 1.4 below.

From birth, OPCs are more or less evenly distributed throughout the brain (Nishiyama et al., 1996; Dimou et al., 2008; Rivers et al., 2008), and continue to produce myelinating oligodendrocytes long into adulthood (Rivers et al., 2008; Psachoulia et al., 2009). However, not all OPCs differentiate into myelinating oligodendrocytes: a large proportion of these cells persist as OPCs in the adult, where they represent 5% of the cells in the brain (Dawson et al., 2003). In order to maintain a constant number of OPCs and produce new oligodendrocytes, OPC divide asymmetrically giving rise to one OPC and one differentiating cell (Sugiarto et al., 2011; Zhu et al., 2011a). When OPCs divide asymmetrically NG2 expression becomes polarised and segregates onto the surface of the cell that remains an OPC, and is lost from the other cell which then differentiates (Sugiarto et al., 2011; Zhu et al., 2011a). In addition, OPCs can also divide symmetrically giving rise to two new NG2 expressing OPCs (Zhu et al., 2011a).

As mentioned above, OPCs are reported to possess an intrinsic clock which results in OPCs undergoing a finite number of divisions before differentiation (Temple and Raff, 1986). This intrinsic clock mechanism for regulation of OPC differentiation was found when OPCs were cultured in the absence of other cell types. In contrast, when OPCs are cultured in the presence of neurons, an intrinsic timer may not be responsible for the initiation of differentiation, instead the density of OPCs may be vital, since OPCs need to reach a critical density before differentiation occurs (Rosenberg et al., 2008). In fact, if OPCs reached a sufficient density they could even differentiate and myelinate axons fixed with paraformaldehyde (Rosenberg et al., 2008). This evidence suggests that spatial constraints may be able to induce OPC differentiation.

Several molecular signals have been reported to instruct OPCs to exit the cell cycle and differentiate. These include messengers such epidermal growth factor (EGF) (Sugiarto et al., 2011), retinoic acid, glucocorticoid and thyroid hormone (Barres et al., 1994a), and the neurotransmitter glutamate (Gallo et al., 1996; Yuan et al., 1998). However, the question of how proliferating OPCs rapidly switch to postmitotic oligodendrocytes that synthesise myelin remained unanswered until recently, when it

was discovered that differentiating OPCs express a series of microRNAs (miRNAs) which provide a hitherto unrecognised level of gene expression control. miRNAs are small, noncoding RNA molecules expressed by many eukaryotic organisms. These miRNAs are generated from longer hairpin-loop RNA sequences, which are trimmed by successive cleavages by the miRNA processing enzymes Drosha and Dicer1, and incorporated into an RNA-induced silencing complex (RISC) (Bartel, 2004). When the mitogen PDGF-AA was withdrawn from OPCs, this induced the expression of specific miRNAs (Dugas et al., 2010; Zhao et al., 2010). These miRNAs efficiently attenuated the expression of the PDGFRα protein and downregulated the responsiveness of OPCs to PDGF-AA, which was followed by a change in OPC gene expression to promote differentiation (Dugas et al., 2010; Zhao et al., 2010). This new finding provides a link between the signalling molecules which regulate OPC development and the changes in gene expression required for their differentiation.

1.3.5 Survival of newly formed oligodendrocytes

OPC cell number is controlled by regulating both cell proliferation and cell death. The final number of oligodendrocytes is thought to be regulated by competition for local survival factors (Barres et al., 1992; Barres and Raff, 1994). In addition, only OPCs that make the appropriate contacts with axons are thought to survive and initiate myelination (Trapp et al., 1997), suggesting that axon derived signals are also important for oligodendrocyte survival. Quantitative analysis of OPC proliferation and cell death reveals that as many as 50% of newly formed oligodendrocytes die during normal development (Barres et al., 1992). In vitro, both PDGF-AA and insulin-like growth factors can rescue newly formed oligodendrocytes from cell death (Barres et al., 1992). Increasing the amount of available PDGF-AA in the postnatal optic nerve reduced oligodendrocyte death by up to 90% (Barres et al., 1992), indicating that competition for survival factors likely contributes to the death of oligodendrocytes.

Ultimately, the number of oligodendrocytes generated must be directly matched to the number of axons that require myelination. Accordingly, increasing experimentally the number of axons results in an increase in the number of oligodendrocytes that survive (Burne et al., 1996). In addition, oligodendrocytes can form multiple myelin internodes. Therefore, both the generation of the correct number of oligodendrocytes and the coordination of the number of internodes formed requires the presence of precise temporal and spatial cues. At present, surprisingly little is known about the neuron-glial interactions which exist to control the process of myelination.

1.3.6 Myelination

In the CNS, oligodendrocytes wrap axons with multiple layers of compact myelin (Fig. 1.5). The myelin membrane contains a high percentage of lipids, of which cholesterol is the major constituent. In addition to lipids, myelin also contains an array of proteins which include myelin basic protein (MBP), proteolipid proteins (PLP/DM20), myelin oligodendrocyte glycoprotein (MOG), the 2', 3'-cyclic nucleotide 3'-phosphodiesterase (CNPase) and myelin associated glycoprotein (MAG) (Dubois-Dalcq et al., 1986) (Fig. 1.1). Myelin has a high electrical resistance so, because of the multiple membrane layers wrapped around axons, it lowers the capacitance of the axon. This, in turn, reduces the current flow through the internodal membranes, making it easier to charge the internodal membrane, thus facilitating rapid saltatory conduction from node to node.

The process of myelination requires the formation of small gaps in the myelin sheath, referred to as the nodes of Ranvier (Fig. 1.6). These are highly complex structures, of 0.5-1 µm in length, which allow ion influx into the axon to generate the action potential. Early in the process of myelination, an axo-glial junction forms between the distal, uncompacted loops of myelin and the axolemma, which gives rise to the paranode that separates the node from the juxtaparanode (Fig. 1.6) (reviewed by Salzer, 2003). Each of these domains contains specific membrane proteins which are highly organised. The paranode contains the axonal protein contactin-associated protein (Caspr) and contactin which form complexes with the glial 155 kDa isoform of neurofascin, that generate septate-like junctions between the myelin and the axon (Sherman and Brophy, 2005). The juxtaparanodes lie just under the compact myelin sheath immediately adjacent to the paranodes and have high densities of voltage-gated K^+ channels and neuron-glial-related nodal axonal cell adhesion molecules (NrCAMs), Caspr2 and TAG-1 (Fig. 1.6). These cell adhesion molecules form a complex and interact with TAG-1, which is expressed by the oligodendrocyte cell membrane (Poliak et al., 2003). The nodes of Ranvier are the sites for action potential regeneration, and are therefore highly enriched in voltage-gated Na^+ channels. The Na^+ channels are clustered and anchored at the nodes via interactions with several cytoskeletal/scaffolding proteins, including transmembrane neurofascin-186 and NrCAM (which interact with extracellular matrix proteins), and intracellular ankyrin-G and βIV spectrin (Fig. 1.6). Concentration of Na^+ channels at the nodes allows for the action potential to be regenerated at each node, as it propagates from one node to the next by saltatory conduction.

The processes of myelination and node formation must be tightly linked, however the precise mechanistic relationship between the two events is unclear. These processes could be coordinated by axons, by myelinating glia, or by a mixture of both. Substantial evidence suggests that interactions with myelinating glia are vital for the assembly of nodal domains in the axon. Na^+ channels and ankyrin G, which are diffusely expressed on axons cultured in the absence of glia, cluster in the presence of glia (Kaplan et al., 1997). Also, when oligodendrocytes are ablated, Na^+ channel clustering disappears at the nodes and the protein expression at the paranodes becomes disrupted (Mathis et al., 2001). Additional studies in mice deficient in myelin glycolipid synthesis were also found to have substantial axonal paranodal abnormalities (Honke et al., 2002), providing further evidence that myelinating glia play an important role in axon domain localisation.

The mechanisms of node assembly are best characterised in the PNS, where Schwann cells instead of oligodendrocytes myelinate axons. Prior to myelination, components of the node, paranode and juxtraparanode are diffusely expressed along the axon (Zhang et al., 2012). In the PNS, the first stage of node assembly occurs with the diffusion of NF186 along the axon surface to the node. Gliomedin is released by the Schwann cell, and it binds to NrCAM expressed by the Schwann cell microvilli, forming the NrCAM-gliomedin complex (Feinberg et al., 2010). NF186 becomes trapped via interactions with the NrCAM-gliomedin complex on the Schwann cell microvilli, which promotes the clustering of NF186 at the node (Feinberg et al., 2010). NF186 then recruits ankyrin G, followed by the Na^+ channels and βIV spectrin which are trafficked to the node in transport vesicles (Zhang et al., 2012). The paranodal junctions that form after the adhesion molecules have already accumulated limit the diffusion of node components in and out of the node. Finally, the nodal components still present along the internodes become downregulated, reinforcing the localisation of the node components (Zhang et al., 2012).

Some differences have been reported in CNS node formation. In the PNS, Schwann cells make contacts with the axon at two distinct sites: the developing nodes and the adjacent paranodal junction. At the developing and mature PNS nodes, axoglial contacts are formed between Schwann cell microvilli and the axon, and these direct contacts are necessary for the clustering of the nodal complex (Arroyo et al., 2004). In the CNS, oligodendrocytes make contacts with the axon at the paranodal junction but, unlike Schwann cells, oligodendrocytes are devoid of microvilli and do not contact the developing node. Despite this lack of microvilli, nodes still form beyond the ends of the oligodendrocyte processes. Interestingly, astrocytes and OPCs are

reported to extend processes to nodes (Butt et al., 1999), and these could play a role similar to the Schwann cell microvilli in aiding the clustering and maintenance of the nodal complex. However, these perinodal glial processes only project to large CNS axons (Melendez-Vaquez et al., 2001), suggesting that they are not required for node formation in all CNS axons. Also, in contrast to the PNS, Ankyrin G is the first molecule to be recruited during node formation in the CNS, not neurofascin (Jenkins and Bennett, 2002).

Oligodendrocytes myelinate axons which have diameter of at least 0.2 µm (Waxman and Bennett, 1972; Voyvodic, 1989), and axons which have a diameter of less than this normally remain unmyelinated. Furthermore, the number of layers in the myelin sheath is tightly correlated with the axonal diameter, increasing in proportion to the inner axonal diameter. The ratio of the axonal diameter to the outer diameter of the myelin sheath, referred to as the g-ratio, is constant, around 0.75 in the CNS, and 0.6 in the PNS (Friede, 1972). In addition, each oligodendrocyte is capable of myelinating up to 60 axons (Remahl and Hildebrand, 1990), all of which may have different axonal diameters and subsequently require differing amounts of myelin. The strong correlation between axon diameter and myelin thickness points to the existence of axonal signals that both initiate the myelination process and determine exactly how many times the myelinating process wraps around the axon before compaction occurs to form the mature myelin sheath. Surprisingly, the processes of axonal ensheathment and myelin compaction are still not fully understood.

Several studies have helped to decipher the glial-axonal interactions which occur during the initial stages of myelination. So far, two axonal ensheathment models have been described. In the original model of myelination from electron microscopy studies, it has been suggested that the leading edge of the myelin sheath aligns along the axon in a sheet-like manner, which forms the initial wrap. Then subsequent wraps are laid down inside the previous ones, forming a smooth surface with all the myelin membranes running in parallel to the long axis of the axon, reminiscent of a rolled up carpet (Bunge et al., 1989). More recent studies have suggested an alternative model of myelination, in which a narrow oligodendrocyte process spirals around the axon and, when sufficient wraps have been generated, the spirals then extend laterally along the long axis of the axon to form overlapping sheets, as described by the ‘serpent’ model (Sobottka et al., 2011). A recent study by Ioannidou et al. (2012), using real time imaging to visualise dynamic glial-axonal interactions occurring during myelination, demonstrated that oligodendrocyte processes initially spiral around the axon in a

corkscrew-like manner, similar to the ‘serpent model’ of myelination, after which the myelin membrane spreads out along the axon to form the myelin internode.

Molecular studies have provided information about the signalling molecules regulating various stages of myelination. Many axonal-derived signals have been reported to regulate myelination. For example, neurons are reported to change their patterns of expression of axonal proteins before the onset of, and during the early stages of myelination (Coman et al., 2005). In particular, polysialylated neural cell adhesion molecule (PSA-NCAM) and the adhesion molecule L1 CAM are expressed on the axonal surface at the beginning of myelination, but soon disappear as axons become myelinated (Coman et al., 2005), suggesting that these molecules promote myelination. In addition to axon-derived signals regulating myelination, there has been much interest in the possibility that electrical activity can provide instructive signals which promote myelination. Initial evidence of activity-dependent myelination came from studies demonstrating that when neuronal action potentials are blocked by TTX, myelination is impaired (Barres and Raff, 1993; Demerens et al., 1996).

In addition, neuronal activity triggers the release of several promyelinating factors such as PDGF-AA (Richardson et al., 1988), neurotrophin-3 (Barres et al., 1994b), neuregulin (Roy et al., 2007; Brinkmann et al., 2008; Taveggia et al., 2008) and adenosine (Stevens et al., 2002). One of the most well studied promyelinating factors in the PNS is the growth factor neuregulin 1 (NRG1). In the developing CNS and PNS, the EGF-like growth factor NRG1 activates its receptors, the family of ErbB tyrosine kinases, on oligodendrocytes and Schwann cells, respectively (Miller, 2002). In the PNS, NRG1 is essential for myelination. A threshold level of axonal NRG1 type III is required to induce myelination by Schwann cells, and the amount of NRG1 type III expressed on axons determines the thickness of the myelin sheath (Michailov et al., 2004; Taveggia et al., 2005; Brinkmann et al., 2008).

The role of neuregulin in CNS myelination remains controversial. Some studies have suggested that, like the PNS, NRG1 signalling plays a role in oligodendrocyte differentiation and myelination in the CNS (Park et al., 2001; Sussman et al., 2005). In ErbB knockout mice, oligodendrocytes were unable to differentiate into myelinating oligodendrocytes (Sussman et al., 2005) and ensheath axons with myelin (Park et al., 2001). In contrast, a recent study from Brinkmann et al. (2008) suggested that CNS myelination does not depend on NRG1. When the NRG1 gene was conditionally knocked out of virtually all projection neurons of the forebrain at P5 before subcortical myelination occurs, surprisingly, myelination proceeded normally (Brinkmann et al.,

2008). Furthermore, to completely eliminate neuregulin signalling, Brinkmann et al. (2008) knocked out all of the ErbB receptors on which neuregulins act. Despite the lack of neuregulin signalling, myelination proceeded normally in ErbB knockout mice (Brinkmann et al., 2008). However, given that many other signalling pathways are involved in myelination, it is possible that an alternative signalling pathway could compensate for the lack of neuregulin signalling in the neuregulin deficient mice, to ensure that myelination occurs.

As mentioned above, neuregulin regulates myelin sheath thickness in the PNS. Recently, fibroblast growth factor (FGF) has been reported to play a role similar to that of neuregulin in the PNS, to regulate the myelin sheath thickness of CNS axons. FGFs are a family of growth factors that activate their receptors, the family of Fgfr1-2 receptor tyrosine kinases, on oligodendrocytes (Bansal et al., 1996). Oligodendrocyte lineage cells express FGF receptors in a developmentally regulated manner. Fgfr1 is expressed by all oligodendrocyte lineage cells, Fgfr3 is only expressed by OPCs, and Fgfr2 is only expressed by myelinating oligodendrocytes (Bansal et al., 1996; Bryant et al., 2009). The differential expression of FGF receptors in the oligodendrocyte lineage raises the possibility that FGF receptor signalling may have distinct functions in OPCs and myelinating oligodendrocytes. Indeed, in a recent study, Furusho et al. (2012) knocked-out Fgfr1 and Fgfr2 receptors from all oligodendrocyte lineage cells and found that OPC development was unaffected but the myelin sheath thickness was altered. In the absence of Fgfr1 and Fgfr2 receptors, OPCs proliferated and differentiated normally, and produced a similar number of myelinating oligodendrocytes (Furusho et al., 2012), suggesting that Fgfr1/Fgfr2 receptor activation is not important for OPC lineage progression. In addition, axonal ensheathment and myelination were initiated at a similar time to that of normal mice. However, the rapid growth of myelin, normally occurring the second postnatal week, was severely inhibited in Fgfr1/Fgfr2 knockout mice (Furusho et al., 2012). Furthermore, in adulthood in the absence of Fgfr1 and Fgfr2 receptors, myelinating oligodendrocytes were found to transcribe fewer myelin genes, and the myelin sheath remained disproportionately thin relative to the axon diameter (Furusho et al., 2012). This study suggests that FGF receptor signalling in myelinating oligodendrocytes plays a vital role in regulating the thickness of the myelin sheath in the CNS.

In addition to growth factors, neurotransmitters may regulate myelination, OPCs receive excitatory and inhibitory synaptic input mediated by glutamate and GABA (Bergles et al., 2000; Lin et al., 2005; Kukley et al., 2007; Ziskin et al., 2007; Karadottir et al., 2008; Ge et al., 2009), raising the question of whether such synaptic

communication between individual axons and OPCs might initiate myelin formation on electrically active individual axons. Interestingly, Wake et al. (2011) provided the first evidence for the involvement of OPC synapses in myelination, in culture. Wake et al. (2011) showed that glutamate release from synaptic vesicles along axons promoted myelination by stimulating the formation of cholesterol-rich signalling domains in oligodendrocytes and increasing the local synthesis of a major protein in the myelin sheath, MBP (Wake et al., 2011). However, the role of OPC synapses in myelination has yet to be demonstrated *in vivo*, and it is not yet known whether other neurotransmitters such as GABA can regulate myelination. In chapter 5 of this thesis, I investigate whether GABA can regulate myelination.

Like neurons, astrocytes also release factors which can regulate myelination. Ishibashi et al. (2006) found that astrocytes respond to ATP released from active axons by releasing LIF (leukaemia inhibitory factor) which promotes myelination by mature oligodendrocytes. Interestingly, astrocytes release different factors depending on their activation phenotype. In particular, in a myelinating culture system, inclusion of normal quiescent astrocytes induced the formation of less myelinated fibres when compared with the inclusion of reactive astrocytes (Nash et al., 2011). The cytokine ciliary neurotrophic factor (CNTF) was found to activate astrocytes, and increase myelination. In the absence of astrocytes, CNTF had no promyelinating effect on oligodendrocytes, suggesting that, in response to CNTF, reactive astrocytes secrete a soluble factor to increase myelination. In contrast, CXCL10 was identified as a potential candidate molecule released from quiescent astrocytes to reduce myelination since, when CXCL10 was neutralised with an antibody, the effect of quiescent astrocytes on myelination was eliminated (Nash et al., 2011). Collectively, these data demonstrate that astrocytes may play an important role in controlling myelination.

1.3.7 Regulation of internode length in the tuning of action potential conduction speed

During development, adjustment of myelin thickness or of the internode length may be used to tune the conduction speed of action potentials in myelinated axons. In some cases in the CNS, myelination is organised to promote synchronicity of neuronal firing (Sugihara et al., 1993; Lang and Rosenbluth, 2003), make the action potential conduction velocity almost independent of the length of the axon transmitting information between areas (Salami et al., 2003), or adjust action potential conduction delays to mediate sound localization in the auditory system (Jeffress, 1948; McAlpine and Grothe, 2003; Seidl et al., 2010).

In addition to the adjustment of myelination during development, myelination may also change during adult life (Ullen, 2009). For example, it has been reported that only around 30% of corpus callosal axons are myelinated even in eight month-old mice (Sturrock, 1980), suggesting that there is still plenty of scope for de novo myelination of axons to occur throughout life. In the human brain, myelination is known to continue well into the third decade of life (Fields, 2008). Interestingly, magnetic resonance imaging data in humans have indicated that myelination can change when people learn motor tasks such as piano playing (Bengtsson et al., 2005) and juggling (Scholz et al., 2009), suggesting that myelin plasticity may be involved in learning.

The regulation of internode length provides one mechanism for action potential conduction speed tuning, however, the length of each internode must be within a certain range to achieve a high action potential conduction speed (Huxley and Stampfli, 1949; Brill et al., 1977). Deviations from the optimum internode length lead to a decrease in action potential conduction velocity. Despite this, the mechanisms by which internode length is determined are not well understood. Recently, intercellular interactions between competing myelinating oligodendrocytes have been reported to influence the number and length of internodes. One signal regulating internode number, in a myelinating co-culture system, was identified to be Nogo-A (Chong et al., 2012), which decreases the number of myelin segements per oligodendrocyte. Additional potent cues probably remain unidentified in oligodendrocyte membranes which contribute to the patterning and spatial arrangement of internodes. Additional signals regulating internode formation may include receptors responding to neurotransmitters released from axons. The effects of the neurotransmitter GABA on the regulation of internode length were investigated in chapter 5.

1.4 Ion channel expression in oligodendrocytes and their precursors

In this section I will review the main ion channels expressed in oligodendrocyte lineage cells, as a background to understanding signalling to these cells, and some of the experiments I have performed.

1.4.1 Voltage-gated ion channels

In chapters 3 and 4 of this thesis, I report experiments investigating voltage-gated ion channel expression in oligodendrocyte lineage cells.

1.4.1.1 Potassium channels

Oligodendrocyte lineage cells express many voltage-gated K^+ channels, which are differentially expressed at specific stages within the oligodendrocyte lineage (Soliven et al., 1988, 1989; Sontheimer et al., 1989). In OPCs, depolarising voltage steps from the resting potential elicit rapidly activating and sustained K^+ currents, due to the expression of A-type K^+ channels and delayed rectifying K^+ channels. The proliferative capacity of OPCs has been linked to the expression of delayed rectifying K^+ channels, and in particular, expression of the Kv1.3 subunit is thought to promote the G1/S transition in the cell cycle (Attali et al., 1997; Chittajallu et al., 2002). Furthermore, over-expression of Kv1.3 or Kv1.4 subunits increases the proliferation rate of OPCs in the absence of mitogens (Vautier et al., 2004). Interestingly, the amplitude of voltage-gated K^+ currents decreases as OPCs stop dividing and start to differentiate (Kukley et al., 2010), providing further evidence for a role of K^+ channels in OPC lineage progression.

OPCs also express inwardly rectifying K^+ currents, which are likely to result from the activity of ATP-sensitive K^+ (K_{ATP}) channels and inwardly rectifying K^+ (K_{ir}) channels (Chittajallu et al., 2004). Mature oligodendrocytes predominantly express inwardly rectifying K^+ channel currents, and small delayed outwardly rectifying K^+ channel currents (Barres et al., 1990; Attali et al., 1997). The inwardly rectifying K^+ channels pass little outward current when the membrane is depolarised and pass large currents at hyperpolarised potentials. Inwardly rectifying K^+ channels act to set the membrane potential close to the K^+ equilibrium potential, and also act to buffer K^+ released during neuronal activity (Reimann and Ashcroft, 1999). In addition, inwardly rectifying K^+ channels are thought to be involved in myelination, as mice with a null mutation in the $K_{ir}4.1$ subunit of inwardly rectifying K^+ channel, have hypomyelinated spinal cords (Neusch et al., 2001).

1.4.1.2 Sodium channels

Like neurons, OPCs express voltage-gated Na^+ channels, but at a density much lower than the density of Na^+ channels found in neurons. There are some discrepancies in data on the proportion of OPCs that express Na^+ channels. Some studies point to a heterogeneity in the Na^+ channel expression of OPCs, and define two classes of OPC: one type that expresses and another type that lacks Na^+ channels (Karadottir et al., 2008). On the other hand, other studies suggest Na^+ channel expression is a universal property of OPCs in white and grey matter regions of the

brain (Bergles et al., 2000; Chittajallu et al., 2004; De Biase et al., 2010; Kukley et al., 2010).

The expression of Na^+ channels by OPCs raised the question of whether these cells are able to generate action potentials. Interestingly, despite the low density of Na^+ channels and the comparatively large K^+ conductance present, some OPCs in the rat cerebellar white matter were reported to generate action potentials on depolarisation (Karadottir et al., 2008). In other species and brain areas, OPCs were not reported to generate *bona fide* action potentials on depolarisation, but could generate single Na^+ spikes that had a higher threshold for activation than action potentials in neurons, with amplitudes that increased with larger current injections, and which did not substantially overshoot 0 mV (Chittajallu et al., 2004; Ge et al., 2009; De Biase et al., 2010). It is not currently known whether OPCs receive sufficient depolarising input from neurons *in vivo* to generate these Na^+ spikes. However, whether or not OPCs fire true action potentials *in vivo*, the Na^+ influx through Na^+ channels could act to amplify any depolarising stimuli, such as the excitatory post-synaptic currents (EPSCs) that OPCs receive from neurons. For example, Na^+ channel activation in OPCs, in response to GABA-activated membrane depolarisation, can lead to Ca^{2+} influx though Na^+/Ca^{2+} exchangers (Tong et al., 2009). This unique signalling pathway involving Na^+ channels and the Na^+/Ca^{2+} exchanger, was demonstrated to be important for OPC migration (Tong et al., 2009).

In contrast, Na^+ channel currents have not been observed in differentiating or mature myelinating oligodendrocytes (Barres et al., 1990; Kukley et al., 2010). Further evidence for the downregulation of Na^+ channels during oligodendrocyte lineage cell maturation came from the transcriptome database published by Cahoy et al. (2008), which demonstrated that Na^+ channel gene expression strongly decreases as oligodendrocytes mature.

In chapter 3 of this thesis I investigate voltage-gated ion channel expression in oligodendrocyte lineage cells with different developmental origins, and in chapter 4 I investigate Na^+ channel expression and action potential generation in OPCs in different brain regions.

1.4.1.3 Calcium channels

Ca^{2+} channels play a vital role in coupling membrane depolarisation to changes in cell physiology. Ca^{2+} influx across the cell membrane can occur via many routes, for example Ca^{2+} can move into the cells through ligand-gated ion channels,

such as glutamate receptors (as described below) or through voltage-gated Ca^{2+} channels. Many studies have investigated the expression of voltage-gated Ca^{2+} channels in oligodendrocyte lineage cells, but they have reported somewhat differing results. In culture and in brain slices, respectively, Barres et al. (1990) and Tong et al. (2009) reported that OPCs did not express voltage-gated Ca^{2+} channels. In contrast, low and high voltage-gated Ca^{2+} channels are reported to be expressed by OPCs (Akopian et al., 1996; Fulton et al., 2010; Paez et al., 2010). In these studies Ca^{2+} channel activation was also reported to play a role in OPC process extension and migration (Paez et al., 2010). Ca^{2+} influx into OPCs via Na^{+}/Ca^{2+} exchangers, instead of via voltage-gated Ca^{2+} channels, was also found to control OPC migration (Tong et al., 2009).

Although Ca^{2+} channel expression was reported to decrease as oligodendrocytes mature, some low and high voltage-gated Ca^{2+} channels could still be detected in mature oligodendrocytes (Fulton et al., 2010). However, other studies reported that mature oligodendrocytes did not express voltage-gated Ca^{2+} channels (Barres et al., 1990). Finally, in the transciptome database for oligodendrocyte lineage cells, voltage-gated Ca^{2+} channel genes were only found to be expressed in mature myelinating oligodendrocytes (Cahoy et al., 2008). The reason for these apparent differences in Ca^{2+} channel expression in oligodendrocyte lineage cells is uncertain, but increases in the intracellular Ca^{2+} concentration (by whatever mechanism) could lead to changes in cell physiology and gene expression, which could regulate the proliferation and lineage progression of these cells.

1.4.2 Neurotransmitter-gated ion channels

Oligodendrocyte lineage cells express receptors for many neurotransmitters such as glutamate, GABA, ATP and acetylcholine. In this section I will review the expression of glutamate and GABA receptors in oligodendrocyte lineage cells, as a background to understanding my experiments on the excitatory and inhibitory signalling to these cells.

1.4.2.1 Glutamate receptors

Oligodendrocyte lineage cells express AMPA, kainate and NMDA receptors, and the expression of some of these channels are reported to change during OPC lineage progression.

1.4.2.1.1 AMPA receptors

AMPA receptors are composed of subunits GluA1-GluA4, and they can assemble as either homo- or heterotetramers, with functional properties that are dictated by their subunit composition. The functional properties of AMPA receptors can be modulated by the presence of auxiliary transmembrane AMPA receptor regulatory proteins (TARPs) (Rouach et al., 2005). Furthermore, expression of the GluA2 subunit suppresses the Ca^{2+} permeability of AMPA receptors (Geiger et al., 1995).

Several studies have demonstrated that glutamate, AMPA and kainate evoke membrane currents in oligodendrocyte lineage cells in culture (Barres et al., 1990; Fulton et al., 1992; Borges et al., 1994; Patneau et al., 1994; Borges and Kettenmann, 1995; Gallo et al., 1996; Yuan et al., 1998) and in brain slices (Berger et al., 1992; Karadottir et al., 2005; Karadottir et al., 2008). Molecular studies have also reported that oligodendrocyte lineage cells express mRNA for AMPA receptor subunits (Jensen and Chiu, 1993; Patneau et al., 1994; Yoshioka et al., 1995; Matute et al., 1997). OPCs are reported to express a mixture of GluA2-lacking calcium permeable AMPA receptors and GluA2-containing calcium impermeable AMPA receptors (Zonouzi et al., 2011). This expression of neurotransmitter receptors by oligodendrocyte lineage cells sparked an interest in discovering the function of these channels in OPCs. The most exciting finding came with the discovery that AMPA receptors in OPCs are activated during transmission at discrete neuron-OPC synapses in the hippocampus, and that these synapses shared many similarities to neuronal synapses (Bergles et al., 2000), including the presence of action potential–evoked transmitter release that is calcium dependent and quantal in nature. Additional evidence from electron microscopy studies revealed an accumulation of synaptic vesicles at contact sites between neuronal axons and the processes of OPCs (Bergles et al., 2000; Lin and Bergles, 2004) in the hippocampus.

Since the discovery of glutamatergic synapses between neurons and OPCs, several other groups have reported that OPCs receive synaptic input from neurons throughout the grey matter (Bergles et al., 2000; Lin and Bergles, 2004; Mangin et al., 2008; Ge et al., 2009; Velez-Fort et al., 2010). In addition, synaptic input onto OPCs has been reported to occur in many white matter brain regions (Kukley et al., 2007; Ziskin et al., 2007; Karadottir et al., 2008), and in particular OPCs establish excitatory glutamatergic synapses with unmyelinated axons passing through the white matter (Kukley et al., 2007; Ziskin et al., 2007), which may play a role in controlling the development of myelination.

Although the physiological function of OPC synapses is yet to be determined, recent studies have suggested that glutamate receptor expression in OPCs is highly dynamic, and can be regulated by mechanisms similar to those found at neuronal synapses. For example, high-frequency presynaptic activity at neuron-OPC synapses is generates a form of long-term potentiation (LTP) that is associated with a rapid rise in the proportion of calcium-permeable AMPA receptors (Ge et al., 2006). In addition, key signalling molecules regulating glutamate receptor expression at neuronal synapses have recently been reported to regulate AMPA receptor expression in OPCs. In particular, activation of group 1 metabotropic glutamate receptors triggers an increase in the proportion of Ca^{2+} permeable AMPA receptors, whereas activation of purinergic P2Y receptors decreases the proportion of Ca^{2+} permeable AMPA receptors (Zonouzi et al., 2011). Furthermore, TARPs, which are an essential modulator of AMPA receptor expression in neurons, were also found to regulate AMPA receptor expression in OPCs (Zonouzi et al., 2011).

1.4.2.1.2 NMDA receptors

NMDA receptors are activated by two co-agonists: glutamate and glycine (or D-serine). NMDA receptors are tetramers. GluN2 subunits (of which there are 4 types) bind glutamate, while the GluN1 subunit binds glycine (or D-serine). GluN3 subunits (of which there are 2 types) can also bind glycine (Chatterton et al., 2002). The majority of NMDA receptors are heterotetramers, composed of two GluN1 subunits and two GluN2 subunits. Current flow through activated NMDA receptors is subject to a voltage-dependent magnesium block. As a result, at the resting potential, most neuronal NMDA receptors barely pass any current when activated, and can only pass significant current when the magnesium block is removed by sufficient depolarisation, so that cations (sodium, potassium and calcium) can then flow through the channel (Dingledine et al., 1999). However, receptors containing GluN3 subunits have a weaker Mg^{2+} block, so that significant current can flow at the resting potential.

NMDA receptors were initially thought to be absent from oligodendrocyte lineage cells, both in culture (Barres et al., 1990; Patneau et al., 1994; Pende et al., 1994) and in brain slices (Berger et al., 1992). The first evidence for the possible expression of NMDA receptors in oligodendrocytes came when Matute et al. (1997) reported NMDA receptor mRNA in extracts from the corpus callosum. Later, this molecular evidence for NMDA receptors in the white matter was confirmed by immunohistochemistry and patch-clamping studies, which demonstrated that functional NMDA receptors were expressed in oligodendrocyte lineage cells at all developmental

stages in the cerebellar white matter and corpus callosum (Karadottir et al., 2005). Furthermore, immunogold electron microscopy demonstrated the expression of GluN1 subunits in myelin (Karadottir et al., 2005). Similarly, in the optic nerve, Salter and Fern (2005) reported the presence of mRNA for GluN1 and GluN2 subunits within the myelin, and Micu et al. (2006) reported GluN1, GluN2 and GluN3 protein expression in myelin by immunohistochemistry and immunoprecipitation. Activation of NMDA receptors in ischaemia has also been reported to induce a $[Ca^{2+}]_i$ rise in oligodendrocyte lineage cells (Micu et al., 2006), raising the possibility that signalling through these receptors modulates oligodendrocyte lineage cell behaviour, especially since glutamate can alter proliferation, differentiation, and migration of OPCs (Gallo et al., 1996; Gudz et al., 2006; Wake et al., 2011). Oligodendrocyte NMDA receptors were suggested to contain GluN1, GluN2C and GluN3A subunits, and show a weak Mg^{2+} block, passing significant current even at the resting potential (Karadottir et al., 2005; Burzomato et al., 2010).

As mentioned above, OPCs receive glutamatergic synaptic inputs from neurons. The glutamatergic synaptic current in neurons is usually made up of an AMPA receptor component and an NMDA receptor component. However, in OPCs, NMDA receptors are not thought to contribute significantly to glutamatergic synaptic currents. This was assessed by voltage-clamping OPCs at positive potentials (+40 mV) to remove the block of NMDA receptors by magnesium. At positive potentials, glutamatergic synaptic currents were still completely blocked by AMPA/kainate receptor antagonists, in both the white matter (Kukley et al., 2007) and grey matter (Lin et al., 2005), suggesting that glutamatergic synaptic currents in OPCs are almost entirely mediated by AMPA/kainate receptors.

Many studies have investigated the functional role of NMDA receptors in oligodendrocyte lineage cells, but have reported somewhat differing results. NMDA receptor expression on oligodendrocytes has been widely reported to have a detrimental effect on these cells in diseases such as ischaemia (as discussed in detail in section 1.7 below), mediating glutamate toxicity and damage or death of oligodendrocyte lineage cells (Matute et al., 1997; Karadottir et al., 2005; Karadottir et al., 2008). However, the functional role of oligodendrocyte NMDA receptors in the healthy brain has recently been investigated and has given conflicting results. De Biase et al. (2011) examined the function of NMDA receptor expression on oligodendrocytes, by genetically deleting the obligatory NMDA receptor subunit GluN1. Surprisingly, OPCs lacking NMDA receptors exhibited normal rates of proliferation, achieved normal densities in grey and white matter, and matured into myelinating oligodendrocytes to

form the major white matter tracts of the CNS without appreciable delay (De Biase et al., 2011). Moreover, the majority of the characteristic physiological and morphological properties of OPCs were preserved in the absence of NMDA receptors, and OPCs continued to receive glutamatergic synaptic input (De Biase et al., 2011). The only observable differences after NMDA receptor deletion, were firstly, a reduction in the Na^+ channel density in OPCs, and secondly an alteration in the subunit composition of AMPA receptors in OPCs (De Biase et al., 2011). In particular, a higher number of Ca^{2+}-permeable AMPA receptors were found in OPCs following NMDA receptor deletion. The increase in Ca^{2+}-permeable AMPA receptors in OPCs might represent an attempt to compensate for a reduction in Ca^{2+} influx through NMDA receptors when they are deleted from the cell.

In another study, Guo et al. (2012) deleted the obligatory GluN1 subunit from OPCs and found that it did not interrupt the normal maturation and differentiation of OPCs. Furthermore, deletion of the GluN1 or the modulatory GluN3A subunit from oligodendrocyte lineage cells did not alter the clinical severity of experimental autoimmune encephalomyelitis (EAE) an animal model of multiple sclerosis (Guo et al., 2012), suggesting that oligodendrocyte NMDA receptors do not significantly contribute to the pathophysiology of EAE. Collectively, the studies by De Biase et al. (2011) and Guo et al. (2012) suggested that NMDA receptor signalling in OPCs does not play a significant role in OPC development or myelination, and does not contribute to the pathology of some diseases involving oligodendrocytes, such as EAE.

In contrast Wake et al. (2011), studying myelination of dorsal root ganglion neurons by OPCs, reported that glutamate release from synaptic vesicles along axons promoted myelination by stimulating the formation of cholesterol-rich signalling domains in oligodendrocytes and increasing the local synthesis of the major protein in the myelin sheath, MBP. Interestingly in this study, the glutamatergic signalling to OPCs was partly mediated by NMDA receptors and metabotropic glutamate receptors, (Wake et al., 2011), suggesting that NMDA receptors play an important role in activity-dependent myelination. It is not clear why these separate studies report contradictory findings on the importance of NMDA receptor signalling in oligodendrocyte lineage cells. Perhaps these differences result from compensatory mechanisms, such as an upregulation of Ca^{2+}-permeable AMPA receptors, which occur after the genetic deletion of NMDA receptors, to ensure that OPC maturation and myelination proceed. Thus, further work will be required to shed light on the functional role of NMDA receptor signalling at OPC synapses, and in OPC development and myelination.

1.4.2.2 GABA receptors

$GABA_A$ receptors are pentameric assemblies of subunits that form a central anion channel. Nineteen $GABA_A$ receptor subunits have been cloned from the mammalian CNS (α_{1-6}, β_{1-3}, γ_{1-3}, δ, ε, θ, π and ρ1-3), but the most abundantly expressed receptor subtype in the brain is formed from α_1, β_2 and γ_2 subunits (Pirker et al., 2000). The minimum requirement for a functional channel is the expression of α and β subunits, which form the binding site for GABA, and in some cases γ, δ, ε and π subunits are also included in $GABA_A$ receptors. The principle action of the inhibitory neurotransmitter GABA, which is mediated by $GABA_A$ receptors, is to increase membrane permeability to Cl^- ions. In most neurons, this leads to a net influx of Cl^- and a hyperpolarising response, however the direction of Cl^- flow depends on the intracellular concentration of Cl^- ($[Cl^-]_i$) and HCO_3^- (which also permeates the channel), as discussed below.

Several studies have demonstrated that GABA can evoke membrane currents in oligodendrocyte lineage cells (Bormann and Kettenmann, 1988; Gilbert et al., 1984; Kettenmann et al., 1984; Pastor et al., 1995; Barres et al., 1990; Von et al., 1991). However, previously $GABA_A$ receptor expression has been reported to be downregulated as OPCs mature into myelinating oligodendrocytes (Kirchhoff and Kettenmann, 1992). I investigate GABA signalling in oligodendrocyte lineage cells in chapter 5 of this thesis.

In addition to receiving glutamatergic input from neurons, OPCs also receive synaptic input from GABAergic interneurons in the grey matter (Lin and Bergles, 2004; Velez-Fort et al., 2010) and from inhibitory projection axons in some white matter tracts (Karadottir et al., 2008). Activation of $GABA_A$ receptors on neurons is known to induce either a depolarisation or a hyperpolarisation, depending on whether the reversal potential is more positive or more negative than the resting potential. This is partly determined by the $[Cl^-]_i$, which is regulated by the expression of Cl^- cotransporters on the cell membrane, and also by the presence of HCO_3^- which permeates the channels and makes the reversal potential more positive (since E_{HCO3-}=-20 mV). The relative expression of the Na^+-K^+-Cl^- cotransporter 1 (NKCC1) which transports Cl^- into the cell, and K^+-Cl^- cotransporter 2 (KCC2) which transports Cl^- out of the cell, determines the $[Cl^-]_i$ (Ben-Ari, 2002; Tyzio et al., 2011). Immature neurons maintain a high $[Cl^-]_i$ because of their high expression of NKCC1, relative to their low expression of KCC2, and consequently GABA exerts a depolarising action on immature neurons, triggering activation of voltage-gated Na^+ channels, and perhaps Ca^{2+} channels to elevate $[Ca^{2+}]_i$

(Ben-Ari, 2002). Similarly, activation of $GABA_A$ receptors in hippocampal OPCs induces membrane depolarisation, due to the high $[Cl]_i$, and subsequent efflux of Cl^- through $GABA_A$ receptors in OPCs (Lin and Bergles, 2004). Activation of $GABA_A$ receptors in OPCs also induced a transient inhibition of AMPA receptor mediated currents (Lin and Bergles, 2004), suggesting that GABA can somehow also regulate the efficacy of glutamatergic signalling in OPCs.

The function of the GABAergic input to OPCs has yet to be determined, and so far contradictory results have been reported concerning the effects of GABA on oligodendrocyte lineage cells. On the one hand GABA has been reported to have no effect on OPC development (Gallo et al., 1996; Yuan et al., 1998), while on the other hand, GABA has been reported to induce Ca^{2+} transients in OPCs which can stimulate their migration (Tong et al., 2009). Recently, the structure of interneuron–OPC synapses has been reported to change during development, so that at later times the peak GABA concentration experienced by the OPCs is reduced (Velez-Fort et al., 2010), suggesting that GABA signalling to OPCs may become reduced during development. OPCs may themselves modify the GABA concentration that they experience, since they are thought to express plasma membrane GABA transporters (Cahoy et al., 2008). In chapter 5 of this thesis, I investigate whether GABA can regulate OPC proliferation, differentiation and myelination.

1.5 Adult oligodendrocyte precursor cells

Adult OPCs were first identified in the rat optic nerve and later in other parts of the adult mammalian CNS (Ffrench-Constant and Raff, 1986; Wolswijk and Noble, 1989; Engel and Wolswijk, 1996; Reynolds and Hardy, 1997; Chang et al., 2000; Horner et al., 2000). Like perinatal OPCs, adult OPCs express NG2 and PDGFRα, and (*in vitro*) respond to the mitogen PDGF-AA by dividing and migrating (Shi et al., 1998; Wolswijk and Noble, 1989). A few prominent differences have been identified when adult OPCs were compared to their perinatal counterparts. For example, adult OPCs are reported to have more extensive processes, longer cell cycle times, and slower differentiation (Psachoulia et al., 2009) and slower migration rates (Wolswijk and Noble, 1989), when compared to perinatal OPCs. However, if their intracellular levels of cAMP were sufficiently elevated, adult OPCs could be induced to divide as rapidly as perinatal OPCs (Shi et al., 1998), suggesting that adult OPCs may have the capacity to proliferate at a faster rate under the correct environmental conditions.

Due to their obvious similarities to perinatal OPCs, adult OPCs have been widely presumed to be glial precursors, playing a role in CNS maintenance, and replacing oligodendrocytes that die as a result of injury, disease or as part of the ageing process. However, given the significant numbers of OPC in the adult brain, which represent 5% of all the cells in the CNS (Dawson et al., 2003), and their distribution throughout white and grey matter areas, it has been suggested that they might also have another role unrelated to myelination. Moreover, the complex process-bearing morphology of OPCs *in vivo* seems more in keeping with differentiated cells than immature precursors. Anatomical studies have revealed that OPCs form close contacts with neurons - with axons at nodes of Ranvier and in close proximity to synapses at neuronal cell bodies (Butt et al., 1999; Wigley and Butt, 2009). Furthermore, since OPCs receive glutamatergic and GABAergic synaptic input from neurons in both white and grey matter brain areas (Bergles et al., 2000; Lin and Bergles, 2004; Kukley et al., 2007; Ziskin et al., 2007; Karadottir et al., 2008; Mangin et al., 2008; Ge et al., 2009; De Biase et al., 2010; Velez-Fort et al., 2010), it seems possible that OPCs might participate in neural processing, by sensing neuronal activity and reporting this activity to neighbouring neurons or glia. At present, however, no output signal, such as neurotransmitter vesicle release, has been reported to occur in OPCs (Bakiri et al., 2009). Therefore, it is currently thought that signals that OPCs receive from neurons play an intrinsic role within the OPCs to regulate their proliferation, differentiation and myelination. In addition, this communication from neurons may also lead to an enhanced myelination of active circuits, contributing to circuit plasticity during adulthood. In chapter 4, I compare the properties of perinatal OPCs with young adult OPCs.

1.6 Cell fate of oligodendrocyte precursor cells

The idea that OPCs are multipotential began almost 30 years ago, with the discovery of a class of glial precursor - “O-2A progenitors” - that could generate oligodendrocytes or type-2 astrocytes in cultures of perinatal rat optic nerve cells (Raff et al., 1983). These O-2A progenitors expressed a range of defining molecular markers including NG2 and the PDGFRα, and later became known as NG2 cells or OPCs. More recently it was demonstrated that OPCs purified from early postnatal (P6) rat optic nerves could be reprogrammed into multipotent stem cells by first treating with fetal calf serum or bone morphogenetic proteins (BMPs) to generate type-2 astrocytes, followed by growth in basic fibroblast growth factor (bFGF) to generate free-floating balls of cells (neurospheres) containing neural stem cells (Kondo and Raff, 2000). Individual cells from these neurospheres could give rise to colonies containing a mixture of

neurons, astrocytes, and oligodendrocytes (Kondo and Raff, 2000), therefore indicating that OPCs are indeed multipotential *in vitro*.

With the development of Cre-lox technology in transgenic mice (described in chapter 2), many labs investigated the cell fate of OPCs *in vivo*. These studies demonstrated that the most common cell type generated by OPCs are myelinating oligodendrocytes, both in the normal and injured CNS (Rivers et al., 2008; Zhu et al., 2008; Psachoulia et al., 2009; Kang et al., 2010; Zhu et al., 2011a). However, in addition to oligodendrocytes, OPCs were also found to generate protoplasmic astrocytes within the grey matter of the ventral forebrain and spinal cord of perinatal mice (Zhu et al., 2008; Zhu et al., 2011a). In contrast, when the cell fate of OPCs was traced in the postnatal CNS, no astrocytes were found among the progeny of OPCs (Rivers et al., 2008; Kang et al., 2010; Zhu et al., 2011a). These data suggest that there are two distinct subtypes of OPC - astrogenic and oligodendrogenic OPCs in the embryonic CNS, whereas only the oligodendrogenic type of OPCs exists in the post-natal CNS.

Following the discovery that when OPCs are exposed to the appropriate environmental signals they can revert to a multipotent state, giving rise to neurons, oligodendrocytes and astrocytes in culture (Kondo and Raff, 2000), widespread interest arose in the idea that OPCs could provide new neurons and glia in diseases involving neuronal and glial cell loss. A number of studies encouraged this idea, with the findings that OPCs express neuronal precursor markers such as doublecortin (DCX), which is expressed by migratory neuronal progenitors (Tamura et al., 2007; Guo et al., 2010). Furthermore, SVZ and hippocampal stem cells have been reported to express NG2 (Belachew et al., 2003; Aguirre and Gallo, 2004) and PDGFRα (Jackson et al., 2006), indicating that OPCs may be neural stem cells.

Interestingly, although Cre-lox fate mapping studies, using independent transgenic mouse lines (*Pdgfrα-CreER^{T2}: Rosa26-YFP* mice (Rivers et al., 2008) and *Plp1-Cre^{T2}: Rosa26-YFP* mice (Guo et al., 2010), demonstrated that OPCs predominantly generated oligodendrocytes, in addition, new projection neurons derived from OPCs were reported to be added to the piriform cortex (see section 1.8.4 of this chapter) throughout life (Rivers et al., 2008; Guo et al., 2010). These neurons gradually appeared and accumulated solely in layers 2 and 3 of the piriform cortex (Fig. 1.7B), they acquired NeuN reactivity and they resembled piriform projection neurons morphologically. In addition, these neurons did not label for the cell proliferation marker BrdU (even after several months of BrdU exposure), suggesting that they were formed

by the direct transformation of a functionally distinct post-mitotic population of OPCs in the piriform cortex (Rivers et al., 2008; Psachoulia et al., 2009; Guo et al., 2010). These studies provided the most convincing evidence that OPCs may generate neurons *in vivo*.

In contrast, using an independently generated line of *Pdgfrα-CreER* ^{T2} mice, Kang et al. (2010) failed to detect any newly generated long-term surviving neurons, derived from OPCs, in the piriform cortex or elsewhere in the forebrain. The reason for the observed differences in the generation of neurons by OPCs remains unclear. However, these data suggest that new neurons are being produced (possibly from OPCs) in the adult piriform cortex. The anterior piriform cortex is part of the olfactory bulb circuit, which is known to be highly plastic with new neurons being added to the olfactory neuroepithelium of the nose and to the olfactory bulb, in adulthood (Young et al., 2007). These new neurons are generated from epithelial stem cells and from SVZ stem cells, respectively. Furthermore, these studies raise the question of whether OPCs in the piriform cortex are functionally distinct from OPCs in other brain regions. Indeed, some OPCs in the piriform cortex are reported to express the neuroblast marker PSA-NCAM and the neural precursor markers Sox2 and Pax6 (Seki and Arai, 1993; Hayashi et al., 2001; Nacher et al., 2002; Pekcec et al., 2006; Shapiro et al., 2007; Bullmann et al., 2010; Guo et al., 2010), suggesting they might be a functionally distinct cell population.

In chapter 4 of this thesis, I investigate whether OPCs in the piriform cortex have physiological properties inherently different from those in other brain regions.

1.7 Death of oligodendrocytes in ischaemia

Both oligodendrocytes and their precursors are damaged, leading to mental and physical disabilities, in conditions such as cerebral palsy (Back et al., 2001), spinal cord injury (Park et al., 2004), stroke (Tomimoto et al., 2003), multiple sclerosis (Werner et al., 2001) and the genetic leukodystrophies (Lappe-Siefke et al., 2003). Preventing oligodendrocyte damage is crucial to maintaining action potential transmission along axons.

Ischaemia is a restriction in blood supply, which consequently restricts the energy supply, because the blood supplies cells with oxygen and glucose, both of which are indispensable for cell viability. Brain ischaemia occurs when the blood supply is cut-off during cardiac arrest or in stroke when the blood supply to a localised region of the brain is interrupted as a result of a blood clot occluding a vessel or a vessel

bursting. Ischaemia causes a depletion of cellular ATP and intra- and extracellular acidification. While there are several alternatives to glucose (such as lactate and fatty acids), there are no alternatives to oxygen, which is vital for driving mitochondrial respiration and the production of ATP by oxidative phosphorylation. The fall in intracellular ATP levels inhibits all ATP-dependent processes, notably the Na^+-K^+-ATPase which uses 75% of all brain energy (Attwell and Laughlin, 2001). The Na^+-K^+-ATPase is vital for maintaining ionic gradients within the brain, and therefore if its function is inhibited all ion and voltage-gradients run down. As a result, the extracellular K^+ concentration rises, ultimately to approximately 50-60 mM in the grey matter (15 mM in the white matter) which evokes depolarisation (Hansen, 1985; Ransom et al., 1992), and triggers an initial increase in neuronal action potential firing (Hamann et al., 2005), followed by an cessation of action potential activity. A high extracellular K^+ concentration also leads to an increase in neurotransmitter release from neurons and glia (Li et al., 1999). Both neurons and oligodendrocytes release glutamate in response to ischaemia, by a reversal of their sodium-dependent glutamate transporters (driven by the alteration of the ion gradients) (Li et al., 1999; Rossi et al., 2000). The resulting rise in the extracellular glutamate concentration triggers damage to neurons and glial cells.

As all oligodendrocyte lineage cells express glutamate receptors, part of their ischaemic damage results probably from the released glutamate activating NMDA receptors (Matute et al., 1997; Karadottir et al., 2005; Karadottir et al., 2008;) and AMPA/kainate receptors (Matute et al., 1997; Fern and Moller, 2000; Tekkok and Goldberg, 2001; Deng et al., 2003) on oligodendrocytes and their precursors. However, other mechanisms and transmitters involved in the death of oligodendrocyte lineage cells in pathological conditions are largely unknown.

GABAergic signalling may play a role in many pathological conditions. GABA is released in the white matter during ischaemia (Shimada et al., 1993) and may activate $GABA_A$ receptors present on oligodendrocytes and their precursors. It is currently unclear whether GABA release exerts a beneficial effect by limiting depolarisation produced by glutamate release (Lutz, 1992) or a harmful effect since Cl^- influx facilitates water influx leading to cell swelling (Allen and Attwell, 2004). In chapter 5 of this thesis, I investigate GABAergic signalling to oligodendrocytes during ischaemia.

In response to demyelinating diseases such as multiple sclerosis, adult OPCs are reported to divide and differentiate, providing a major source of new oligodendrocytes for remyelination (Levine, 1994; Gensert and Goldman, 1997; Levine

et al., 2001). In addition, transplantation of OPCs has been suggested as a potential therapeutic strategy to repair damage caused to oligodendrocytes in neurological diseases (Windrem et al., 2008). Importantly, the efficiency of remyelination following experimental demyelination is reported to decrease with age, which might be attributed to an age-related decline in the regenerative properties of OPCs (Sim et al., 2002). The factors that cause these age-related changes in OPCs are currently unknown, but they are likely to be related to changes in the ability of OPCs to proliferate and generate new oligodendrocytes as the brain ages. If these changes in OPC behaviour with age could be understood, it might be possible to manipulate the properties of OPCs in the ageing brain to improve their regenerative properties.

1.8. The structure and function of the brain areas studied

1.8.1 The corpus callosum

In chapters 3 and 4, I report experiments on white matter oligodendrocyte lineage cells in the corpus callosum. The corpus callosum is the largest white matter structure in the brain, consisting of hundreds of millions of axons (Fig. 1.8). The corpus callosum connects and transfers motor, sensory and cognitive information between the left and right cerebral hemispheres. The majority of the corpus callosal fibres are excitatory, and originate from pyramidal cells in layers II/III and V of the cortex. These axons terminate on the spines of pyramidal cells in the contralateral cortex (Kumar and Huguenard, 2001). In addition, inhibitory fibres have been detected in the corpus callosum perinatally, however, these fibres disappear during development (Kimura and Baughman, 1997).

The corpus callosum was studied in chapter 3, because the oligodendrocyte lineage cells in this region are derived from separate dorsal and ventral progenitor pools within the developing brain (Kessaris et al., 2006). Since it was not known whether oligodendrocyte lineage cells derived from dorsal and ventral progenitors are functionally distinct, I compared their physiological properties in the corpus callosum. The corpus callosum was also studied in chapter 4, firstly, in order to compare the properties of OPCs in this white matter area with OPCs in grey matter areas (such as the motor cortex and the anterior piriform cortex), and secondly so that the properties of OPCs could be compared at different stages of myelination (at P9 when myelination is beginning, and at P35 when ~70% of the fibres are myelinated (Hamano et al., 1998)).

1.8.2 The cortex

In chapters 4 and 5, I report experiments on grey matter oligodendrocyte lineage cells in the motor cortical area (henceforth called the motor cortex or Ctx). The motor cortex is located in the posterior portion of the frontal lobe (Fig. 1.8). The motor cortex is centrally involved in mammalian motor behaviour and the cortical control of movement. Multiple long-range excitatory input pathways converge on primary somatic motor cortex (M1) (Weiler et al., 2008). These include corticocortical projections (carrying ipsi- and contralateral sensorimotor information), thalamocortical projections (carrying cerebellar and basal ganglionic information via the thalamic ventrolateral nucleus, as well as sensory and other information via multiple additional thalamocortical pathways) and neuromodulatory projections from brainstem and other areas (Weiler et al., 2008). Major outputs from M1 include projections to spinal motor centers, striatum, cerebellum, thalamus, subthalamus, red nucleus and pons (Weiler et al., 2008). All of the excitatory neurons in M1 are pyramidal neurons projecting to one or several of these long-distance targets (Weiler et al., 2008).

Myelination of motor cortical axons can be detected between the second and third postnatal week in the rodent brain (Bjelke and Seiger, 1989), and new myelinating oligodendrocytes continue to be added to the cortex throughout adulthood - a process which can even be detected in the aged brain (Psachoulia et al., 2009; Rivers et al., 2008).

The motor cortex was studied in chapter 4, firstly, so that a comparison could be made between grey matter OPCs in this region and white matter OPCs, and secondly so that the properties of OPCs could be compared at different stages of myelination (at P9 before cortical myelination has begun, and at P35 when some fibres in the motor cortex have been myelinated (Bjelke and Seiger, 1989)). In addition, in chapters 5 and 6, a cultured cortical model of myelination was used, as described by Rinholm et al. (2011), in which the progress of myelination can be observed. Briefly, myelination develops over a period of about 2 weeks in these cultured slices (see chapter 5). Initially many oligodendrocyte lineage cells are visible but no myelination can be detected then, as neuronal processes develop, gradually myelin basic protein appears.

1.8.3 The cerebellum

In chapters 4 and 5, I report experiments on oligodendrocyte lineage cells in the white and grey matter regions within the cerebellum. The cerebellum is located behind

the cerebral cortex, and it plays an important role in the coordination, precision, and accurate timing of motor movements. Anatomically, the cerebellum can be divided into three lobes: the flocculonodular, the anterior and the posterior lobes. The latter two can be further divided into the central vermis and the two lateral cerebellar hemispheres. My experiments were carried out in the grey matter and white matter areas of the vermis. The cerebellar vermis is composed of a series of folia, and within each folium three cell layers can be distinguished: the molecular, the Purkinje and the granular layers (Fig. 1.9). In addition, in the first 2 postnatal weeks there is an extra outer layer of developing granule cells (the external granular layer). The outermost layer of the adult cerebellar cortex is the molecular layer, which contains two types of inhibitory interneuron: the stellate and basket cells. It also contains the dendritic arbors of Purkinje neurons and the parallel fibre axon tracts from the granule cells (Fig. 1.9). Both stellate and basket cells form GABAergic synapses onto the Purkinje cell. The middle neuronal layer is the Purkinje cell layer which contains the cell bodies of the Purkinje neurons (Fig. 1.9). As these cells are the sole output neurons of the cerebellar cortex they are central to cerebellar cortical information processing. The innermost neuronal layer is the granular layer which contains the cell bodies of the small densely packed excitatory granule cells and inhibitory Golgi cells (Fig. 1.9). OPCs can be found throughout all of these grey matter layers by the end of the first postnatal week. Finally, the white matter layer, which is primarily composed of axons, oligodendrocyte lineage cells and astrocytes, lies underneath the granular layer.

There are two main afferents to the cerebellar cortex, the climbing fibres which make direct excitatory contact with the Purkinje cells, and the mossy fibres which terminate in the granular layer and make excitatory contacts with the granule cells and the Golgi cells (Apps and Garwicz, 2005) (Fig. 1.9). The granule cells recode mossy fibre information (modulated by Golgi cell inhibition) into action potentials which propagate along the parallel fibres that excite both the Purkinje cells and the molecular layer interneurons (the stellate and basket cells).

The climbing and mossy fibre axons also form collaterals with the deep cerebellar nuclei (Fig. 1.9). The output from the cerebellar cortex passes along GABAergic axons from the Purkinje cells, which synapse onto the cells in the deep cerebellar nuclei, which then in turn send excitatory axons to many areas of the brain including the pons, the spinal cord, the red nucleus, the cortex and the thalamus. With the exception of the granule cells, all the cerebellar cortical neurons, including the Purkinje cells, make inhibitory synaptic connections with their target neurons (Apps and Garwicz, 2005).

The oligodendrocyte lineage cells in the cerebellum arise from neural progenitors in the fourth ventricle (Reynolds and Wilkin, 1988). Myelination of the axons entering and leaving the cerebellar cortex (but not within the cortex itself) begins at the end of the first postnatal week and continues until myelination is complete, at the end of the first postnatal month (Hamano et al., 1998).

The experiments in chapter 4 were performed at P9 and P35 to compare the properties of OPCs when myelination is beginning and when myelination is almost complete. Furthermore, the properties of OPCs in the cerebellar white matter have been extensively studied in the rat (Karadottir et al., 2008), so I could compare their properties with transgenically labelled OPCs in the mouse, and subsequently with OPCs in other grey and white matter areas at different developmental stages. The experiments in chapter 5 were performed in the white matter of the cerebellum, at P7 when OPCs reach their peak density (Levine et al., 1993), and at P12 when myelination has begun, in order to locate myelinating oligodendrocytes for patch clamp recordings. These experiments were performed in the cerebellar white matter, because the morphological and electrophysiological characteristics of OPCs and mature myelinating oligodendrocytes have been previously characterised in this region (Bakiri et al., 2011).

1.8.4 The piriform cortex

In chapter 4, I describe experiments on oligodendrocyte lineage cells in the piriform cortex. The primary function of the piriform cortex (which is also known as the primary olfactory cortex) is to process odorant information from the olfactory bulb. The piriform cortex is divided into the anterior (aPC) and the posterior (pPC) regions (Fig. 1.7A). The piriform cortex has a laminar structure, with three layers and receives direct input from the olfactory bulb via the lateral olfactory tract (LOT) (Suzuki and Bekkers, 2007) (Fig. 1.7B). Layer I contains many axons and dendrites, but only a few neuronal somata. The more superficial part (Layer Ia) receives afferent axons from the LOT, whereas the deeper part (Layer Ib) receives associational fibres from within the piriform cortex (Suzuki and Bekkers, 2007). Layer II is densely packed with the somata of glutamatergic principal neurons, the main cells receiving input in the piriform cortex (Suzuki and Bekkers, 2007). Layer III contains a lower density of neuronal somata and, like Layer Ib, a high density of associational fibres (Suzuki and Bekkers, 2007).

The main input layer of the piriform cortex, layer II, contains two functionally distinctive types of principle neurons, semilunar cells which receive strong input from the olfactory bulb and superficial pyramidal cells which receive strong intracortical

(associative) input from fibres within the piriform cortex (Suzuki and Bekkers, 2006) (Fig. 1.7B). The olfactory circuit has long been known to be highly plastic, with new neurons being added to the olfactory neuroepithelium of the nose and to the olfactory bulb, in adulthood (Young et al., 2007). These new neurons are generated from epithelial stem cells and from SVZ stem cells, respectively. In addition, new projection neurons are added to layer II of the piriform cortex throughout life, and importantly these neurons are thought to be generated by OPCs (Rivers et al., 2008; Guo et al., 2010). Furthermore, these new neurons generated by OPCs displayed similar morphologies to the principal neurons in layer II (Rivers et al., 2008; Guo et al., 2010), suggesting that these neurons mature and may integrate into the olfactory circuit.

The piriform cortex appears to be the only brain region where OPCs generate neurons, which accumulate in significant numbers (Rivers et al., 2008; Guo et al., 2010), raising the question of whether OPCs in this region are functionally distinct. Therefore in chapter 4, I compare the properties of OPCs in the piriform cortex with OPCs in other brain regions (including the corpus callosum and motor cortex), to determine whether they differ.

1.8.5 The optic nerve

In chapter 6 I describe experiments searching for activity-dependent nodal adjustments, which could affect the conduction speed of action potential propagation, in the optic nerve.

The optic nerve transmits visual information from the retina to the brain. In the retina, the photoreceptors which absorb light, form glutamatergic synapses with retinal bipolar interneurons which in turn form glutamatergic synapses with retinal ganglion cells. Two layers of inhibitory interneurons, the horizontal and amacrine cells, modulate information flow through this pathway. The retinal ganglion cell axons converge to form the optic nerve. The majority of the retinal ganglion axons project to, and form synapses with the neurons in, the lateral geniculate nucleus, which in turn projects to the primary visual cortex of the brain.

The oligodendrocytes in the optic nerve are derived from neural progenitor cells in the third ventricle, which migrate from the optic chiasm towards the retina (Ono et al., 1997). Myelination of the optic nerve begins at the end of the first postnatal week, and by P21 (the age at which my experiments were performed) myelination is ~70% complete (Foster et al., 1982). The optic nerve was used for the experiments described in chapter 6, because it is a myelinated white matter tract which lacks neuronal cell

bodies, and therefore allows white matter and nodal plasticity to be studied without any confounding effects from neurons.

1.8.6 The spinal cord

In chapter 3 I describe experiments on white matter oligodendrocyte lineage cells in the spinal cord. The spinal cord is the main pathway for information connecting the brain and peripheral nervous system. In cross-section, the outermost region of the spinal cord consists of motor and sensory axons, the majority of which are myelinated (~12-40% of axons are unmyelinated in the adult mammalian spinal cord (Chung and Coggeshall 1983; Chung et al., 1985)). These axons transmit information either up or down the spinal cord (Fig. 1.3B). The innermost region at the centre of the spinal cord contains the cell bodies of motor neurons, ascending sensory neurons, and interneurons (Fig. 1.3B). The spinal cord can be divided into segments based on the origins of the spinal nerves, which include the cervical, thoracic, lumbar, sacral and coccygeal nerves. Each segment of the spinal cord is associated with a pair of ganglia, called dorsal root ganglia, which are situated just outside of the spinal cord.

Somatosensory information is transmitted up the spinal cord via the dorsal column-medial lemniscus tract and the anterolateral system. These sensory pathways transmit information from sensory receptors located in the peripheral nervous system to the thalamus and cerebral cortex. In both pathways, primary sensory neuron cell bodies are found in the dorsal root ganglia, and their central axons project into the spinal cord. The corticospinal tract serves as the motor pathway for upper motor neuronal signals coming from the cerebral cortex and transmits information to motorneurons projecting to the periphery, which regulate fine movements by distal muscles. The spinal cord begins to myelinate at the end of the first postnatal week and myelination is complete by the end of the first postnatal month (Hamano et al., 1996).

The spinal cord was studied in chapter 3, because the oligodendrocyte lineage cells in this region are derived from separate dorsal and ventral progenitor pools (Cai et al., 2005; Fogarty et al., 2005). Currently, it is not known whether oligodendrocyte lineage cells derived from dorsal and ventral progenitors are functionally distinct, so I compared their physiological properties in the spinal cord.

1.9 Aims of thesis

The experiments performed in this thesis had the following aims:

1. The experiments in Chapter 3 investigate functional differences between oligodendrocyte lineage cells, in the same region of the CNS (brain or spinal cord) that are derived from dorsal and ventral progenitor populations. I used a dual reporter mouse line in which OLs are fluorescently labelled green or red, depending on their developmental origin, and I patch-clamped dorsally- and ventrally-derived OLs and compared their electrophysiological and morphological properties to investigate whether they are functionally distinct.
2. The experiments in Chapter 4 investigate whether OPCs in different brain regions have similar properties. OPCs were originally assumed to be a homogenous class of cell, but have since been subdivided according to their electrical properties, gene expression profiles, proliferation rates, response to injury and their capacity to generate different cell types including neurons. To better understand the diversity of OPCs, I patch-clamped OPCs to investigate their expression of voltage-gated ion channels, their proliferative capacity and their cell fate in different brain regions.
3. The experiments in Chapter 5 investigate the properties of GABA-evoked currents in oligodendrocyte lineage cells, and how GABAergic signalling regulates their proliferation, differentiation and myelination.
4. The experiments described Chapter 6, describe other less developed research projects I performed during my PhD. In this chapter, I investigate nitric oxide signalling to oligodendrocyte lineage cells and activity-dependent nodal plasticity.

The results of each chapter are assessed in a discussion section within each chapter. In chapter 7, a global summary is provided and future directions for carrying on this work are suggested.

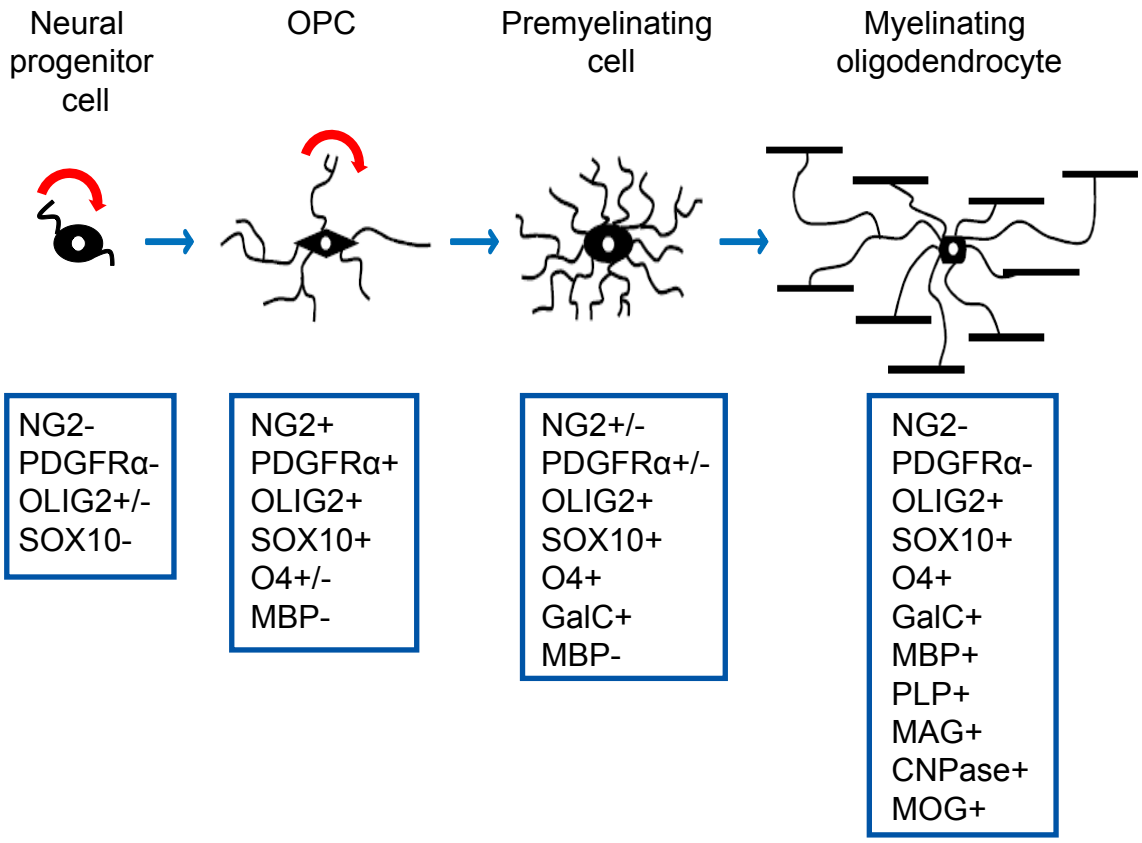

Figure 1.1. Oligodendrocyte lineage cell development.
Oligodendrocyte lineage cells are derived from proliferative neural progenitor cells, which lack expression of NG2 and PDGFRα, but some of these progenitors express OLIG2 (proliferation is indicated by red arrows). As the neural progenitors differentiate into proliferative oligodendrocyte precursor cells (OPCs) they express the precusor markers NG2 and PDGFRα, as well as the oligodendrocyte lineage cell markers OLIG2 and SOX10. As OPCs exit the cycle cell and undergo terminal differentiation, they lose expression of NG2 and PDGFRα, and begin to express the immature marker O4, followed by PLP, galactocerebroside (GalC), myelin associated protein (MAG), 2',3'-cyclic nucleotide 3'-phosphodiesterase, myelin oligodendrocyte glycoprotein (MOG) and myelin basic protein (MBP). The differentiation of OPCs is also accompanied by a change in morphology. Premyelinating cells have longer processes which cover a larger area, when compared with OPCs. Myelinating oligodendrocytes have numerous processes which are aligned with the axons that they myelinate.

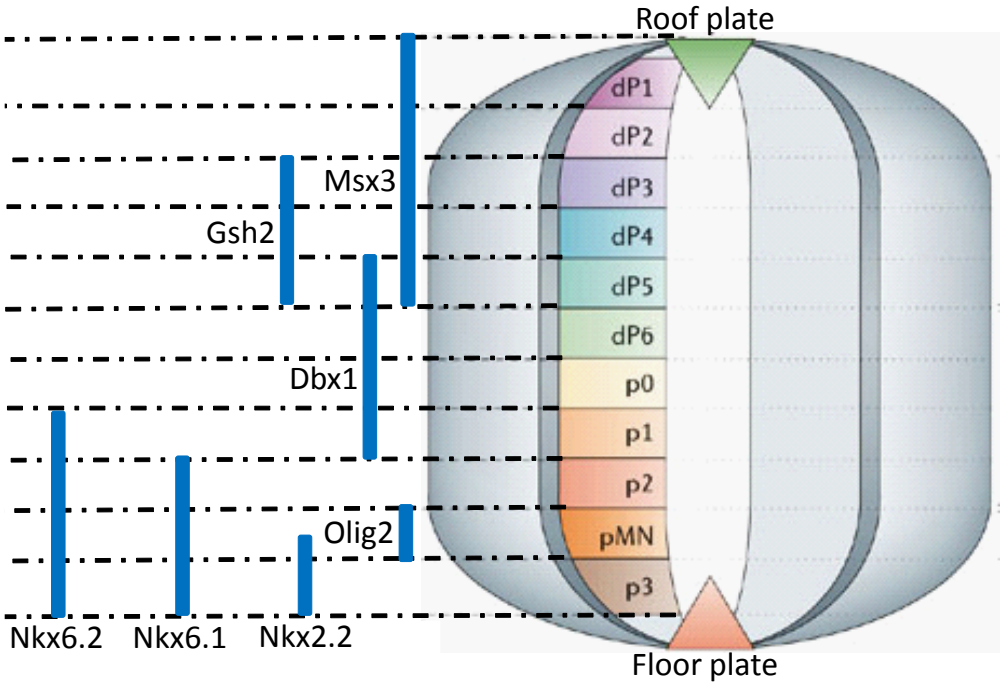

Figure 1.2. Progenitor domains in the embryonic spinal cord
Schematic diagram illustrating the progenitor domains in the embryonic spinal cord which generate the oligodendrocyte lineage cells, astrocytes and neurons. The transcription factors expressed by the progenitor cells in each domain are indicated. The majority (~85%) of the oligodendrocytes in the spinal cord originate from the pMN domain. A small number of oligodendrocytes also originate from the p1 and p0 domains. Later in development, OPCs arise from more dorsal domains, such as dP1-dP6.

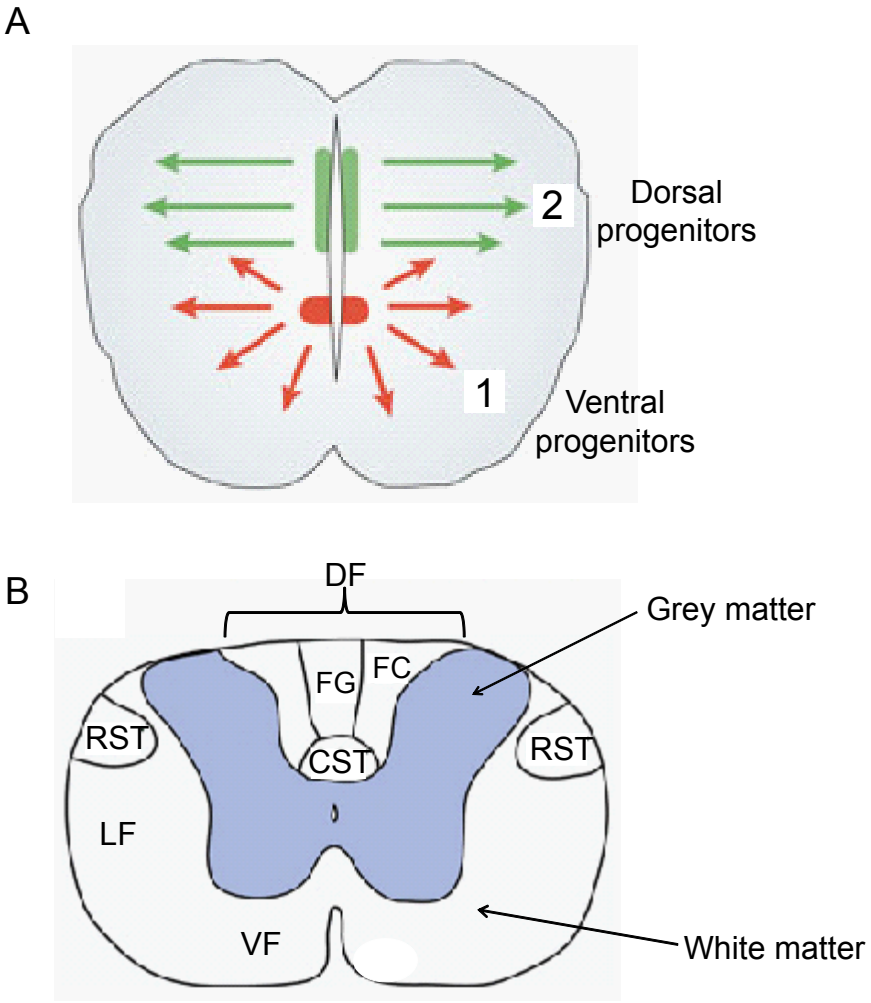

Figure 1.3. Origins of oligodendrocytes in the spinal cord
A. In the mouse spinal cord ~85% of the oligodendrocyte lineage cells are generated from the pMN domain in the ventral ventricular zones at ~E12.5 (red arrows). At about ~E15, a second wave of oligodendrocytes is generated from more dorsal progenitor regions (green arrows). **B.** A schematic diagram of the adult spinal cord showing grey matter regions (coloured grey) and white matter regions (coloured white). The dorsal funiculus (DF) contains the cortical spinal tract (CST), fasciculus gracilis (FG) and fasciculus cuneatus (FC) white matter tracts. The ventral funiculus (VF) is located in the ventral part of the spinal cord. The lateral funiculus (LF) contains the rubrospinal white matter tracts (RST).

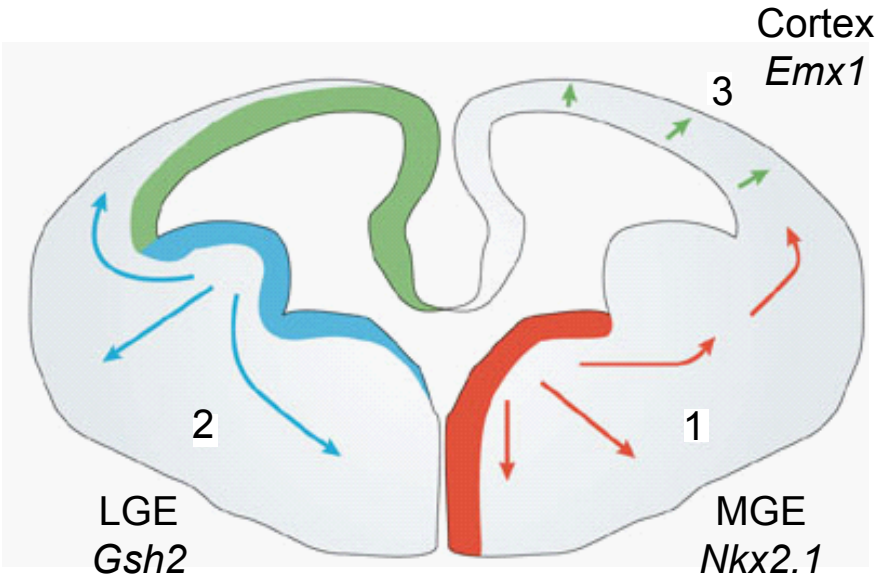

Figure 1.4. Progenitor domains in the telencephalon
In the telencephalon,oligodendrocytes are produced in three waves. Firstly, the ventral-most progenitors in the medial ganglionic eminence (MGE), expressing the transcription factor *Nkx2.1*, produce oligodendrocytes from about E12.5 (1). Next, progenitors in the lateral ganglionic eminence (LGE), expressing the transcription factor *Gsh2*, generate oligodendrocytes a few days later (2). The last wave of oligodendrocytes are produced from cortex-derived precursors, expressing the transcription factor *Emx1*, mainly after birth (3).

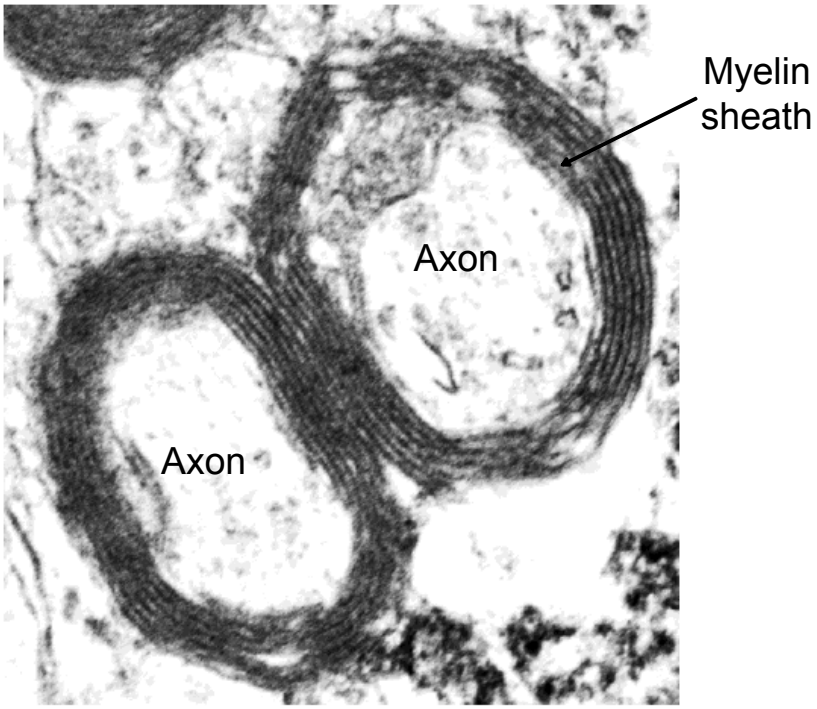

Figure 1.5. Myelin sheaths enwrapping axons
An electron micrograph showing myelinated axons in the corpus callosum of an adult mouse. Axons are surrounded my multiple layers of myelin. (Image provided by Kaylene Young).

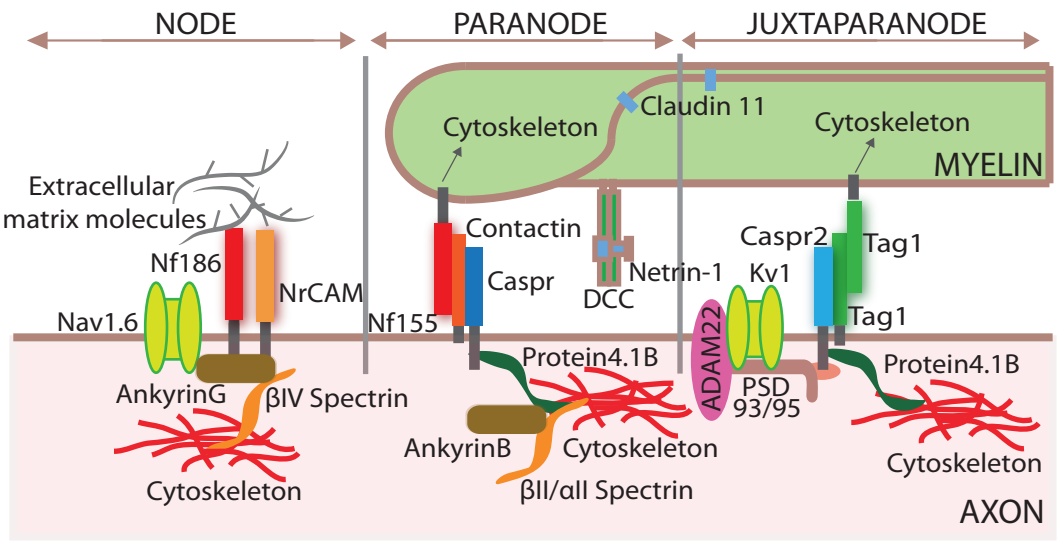

Figure 1.6. Node of Ranvier in the CNS
Diagram displaying the molecular composition of the domains at the node of Ranvier, with one adjacent myelin sheath shown on the right (another exists to the left of the node). The nodes of Ranvier are the sites for action potential regeneration, and are therefore highly enriched in voltage-gated Na^+ channels (Nav1.6), which are clustered and anchored at the nodes via interactions with axonal neurofascin-186 (NF186), neuron-glial-related nodal axonal cell adhesion molecule (NrCAM), ankyrin-G and βIV spectrin. The paranode contains the axonal protein contactin-associated protein (Caspr) and contactin which form complexes with the glial 155 kDa isoform of neurofascin, which form of the septate-like junctions between the myelin and the axon. The juxtaparanodes lie just under the compact myelin sheath immediately adjacent to the paranodes and have high densities of voltage-gated K^+ channels (Kv1) and NrCAMs, Caspr2 and TAG-1.

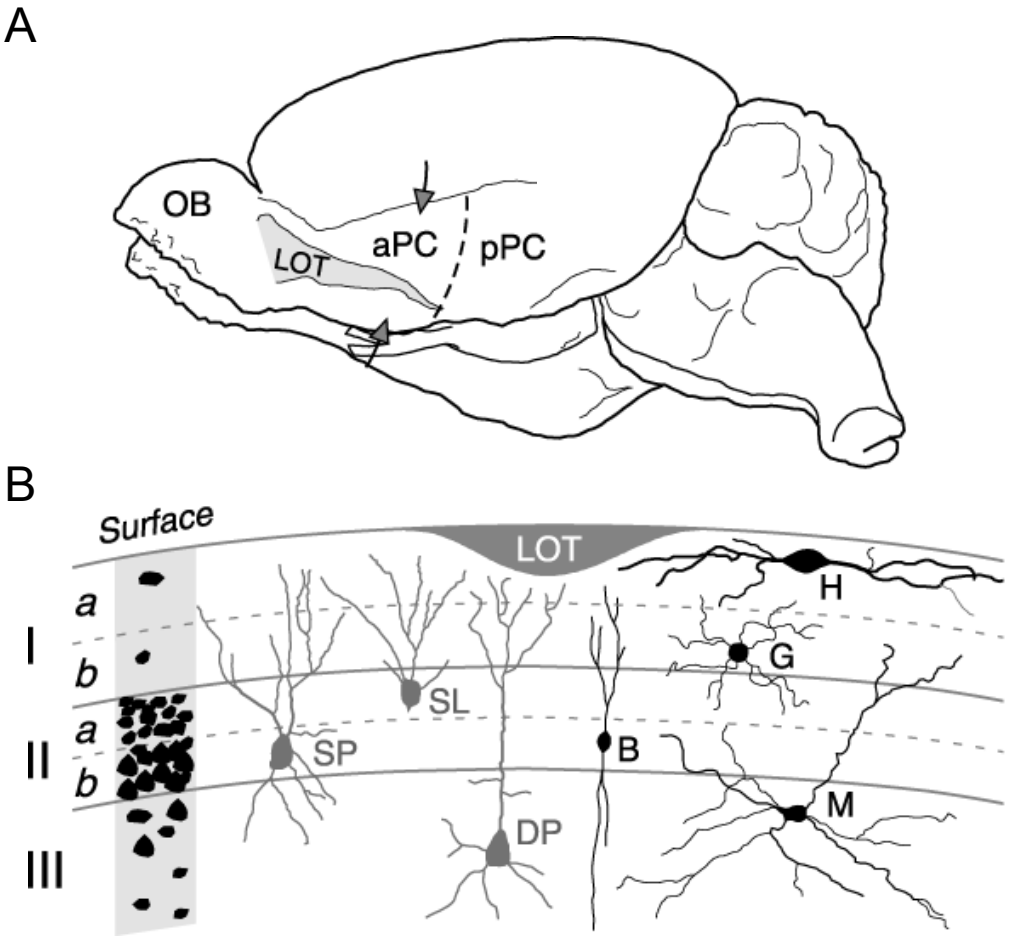

Figure 1.7. Structure of the piriform cortex
Schematic diagram of the location and anatomy of the piriform cortex (PC). **A.** Ventrolateral aspect of the rat brain, showing the olfactory bulb (OB), lateral olfactory tract (LOT) and the locations of the anterior (a) and posterior (p) PC. A coronal slice of the aPC, taken between the arrows, shows the laminar structure illustrated schematically in (**B**). **B**. The three main layers of the PC, with superficial and deep sublaminae (a and b, respectively). At the left is a schematic representation of the density of neuronal somata in each layer, showing the high density of mainly principal cells in Layer II and a lower density of neurons in Layers I and III. Schematic diagrams of the dendritic trees of the two main types of Layer II principal cells (SP, superficial pyramidal; SL, semilunar) and one type of Layer III principal cell (DP, deep pyramidal) are shown in grey. Schematic diagrams of the dendritic trees of four types of GABAergic interneurons are shown in black (B, bitufted; G, neurogliaform; H, horizontal; M, multipolar).

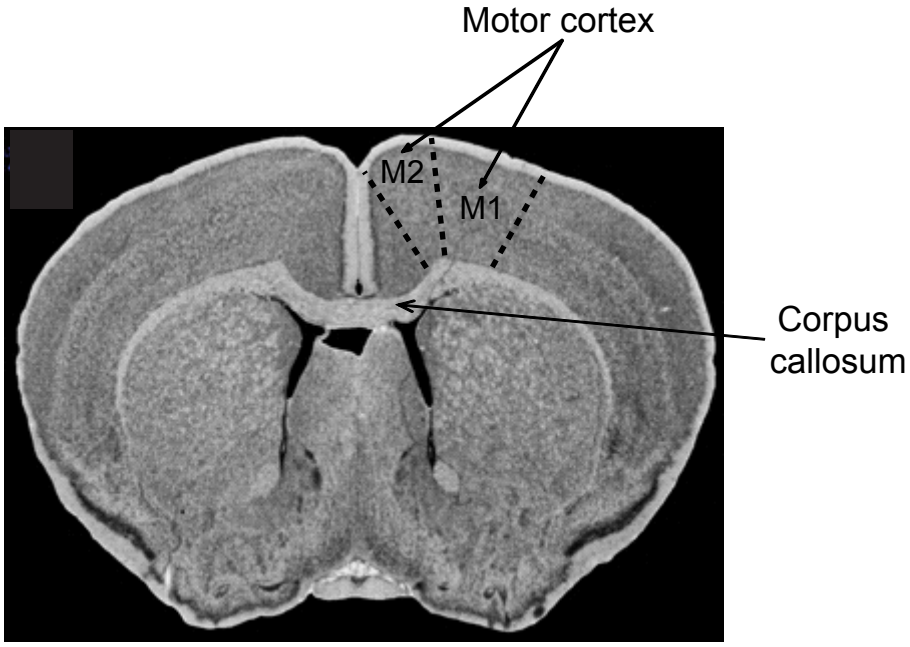

Figure 1.8. Coronal section of the mouse forebrain
The corpus callosum is the largest white matter tract in the brain which connects the right and the left hemispheres. The majority of the corpus callosal fibres are excitatory, and originate from pyramidal cells in layers II/III and V of the cortex. They terminate on the spines of pyramidal cells in the contralateral cortex. The motor cortex (consisting of the primary motor cortex (M1) and secondary motor cortex (M2), highlighted by the regions inside the black dotted lines) is located above the corpus callosum in the posterior portion of the frontal lobe, and is centrally involved in mammalian motor behaviour and the cortical control of movement. Both of these brain regions were studied in this thesis.

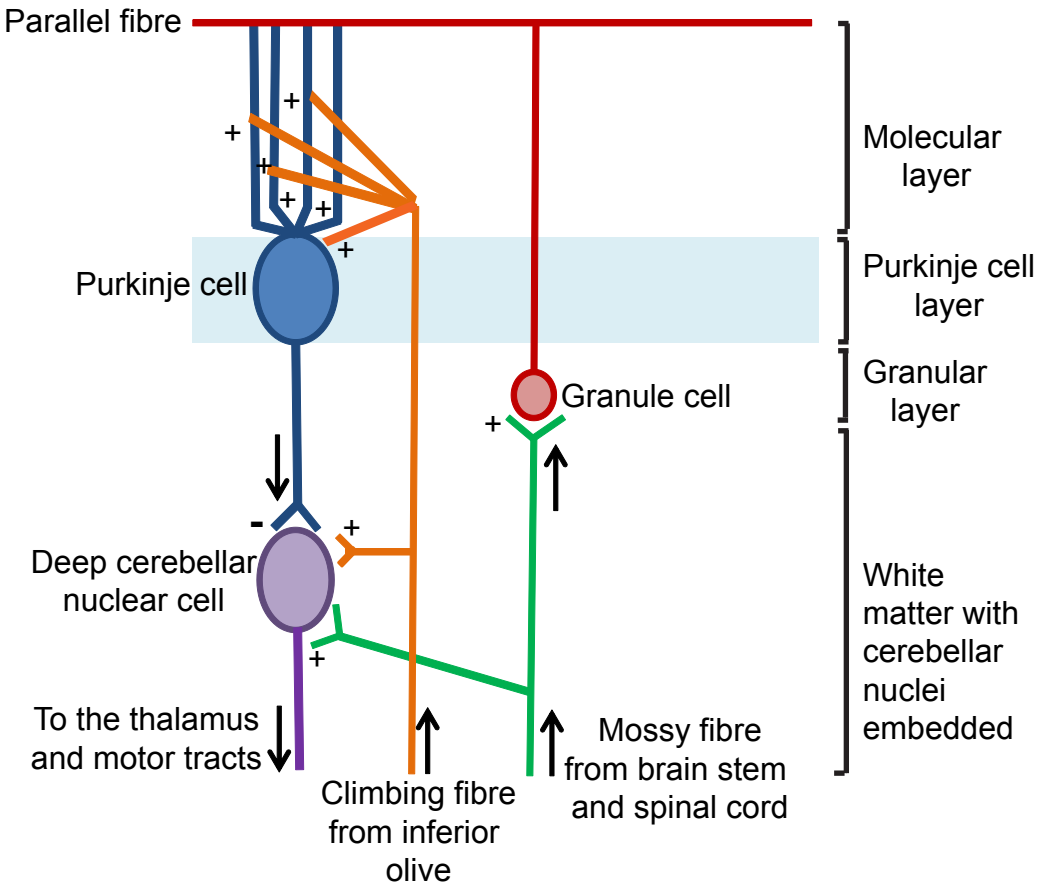

Figure 1.9. Simplified organisation of the cerebellar cortex.
The diagram shows the cytoarchitecture of the cerebellar cortex in a single folium of the cerebellar vermis. Each folium is composed of 3 layers (the molecular layer, the Purkinje layer and the granular layer). The white matter is located beneath the granular layer and the deep cerebellar nuclei are embedded in the white matter. Oligodendrocyte lineage cells are located thoroughout the cerebellar cortex, both myelinating oligodendrocytes in the white matter and OPCs in the molecular and granular layers. The cerebellar cortex recieves two types of excitatory afferent. The mossy fibres orginate from the brain stem, spinal cord and cortex, and contact the granule cells, deep cerebellar nuclear cells and Golgi cells (not represented here). Climbing fibres from the inferior olive directly synapse with the Purkinje cells, and also send collaterals to the deep cerebellar nuclei and the Golgi cells (not represented here). The granule cells, through their parallel fibre axons, excite Purkinje cells, which are the sole output of the cerebellar cortex and send inhibitory synaptic connections to the deep cerebellar nuclear neurons. The parallel fibres also excite three types of inhibitory interneuron: the stellate and basket cells (not shown here) which inhibit the Purkinje cells and the Golgi cells that inhibit the granule cells. The deep cerebellar nuclei send excitatory axons to the motor system and the thalamus.

Chapter 2: Methods

This chapter explains the general methods used for experiments throughout the thesis. Further details of the specific methods used are provided in each results chapter.

2.1 Slice and tissue preparation

2.1.1 Preparation of cerebellar slices

Sprague-Dawley rats, aged postnatal day 6-12 (P6-12), were used for the preparation of cerebellar slices for the experiments in Chapter 4 and 5. Animals were killed by cervical dislocation followed by decapitation. The head was immediately immersed in ice-cold oxygenated slicing solution, contained the following (in mM): 126 NaCl, 24 $NaHCO_3$, 2.5 KCl, 1 NaH_2PO_4, 2.5 $CaCl_2$, 2 $MgCl_2$, 10 D-glucose, Na-kynurenate 1 (to block glutamate receptors during the slicing process), pH 7.4 (bubbled with 95% O_2/5% CO_2). The skin was removed and the skull was opened by cutting between the eyes, followed by lateral cuts on both sides of the head from the anterior to the posterior. The excised region of the skull was lifted and the brain was removed and placed in ice-cold oxygenated slicing solution. To obtain parasagittal slices of the cerebellar vermis, the cerebellum was separated from the rest of the brain by making cuts through, and removing the inferior colliculus and the spinal cord. The cerebellar hemispheres on either side of the vermis were also removed to isolate the vermis. The cerebellum was mounted on one of these parasagittal cut surfaces on the stage of a vibrating tissue slicer (Vibratome) using superglue. The tissue was also stabilised using an agar block attached to the Vibratome stage. The cerebellum was immersed in ice-cold oxygenated slicing solution throughout the slicing process. The cerebellar slices were cut at a thickness of 225 µm, and placed in oxygenated slicing solution at room temperature until they were used for recording.

2.1.2 Preparation of forebrain slices

Coronal forebrain slices were made from transgenic mice (aged P2-P40) in which GFP or tdTomato is expressed in oligodendrocyte lineage cells (*Gsh2-Cre:Sox10-GFP/tdTom* mice (Tripathi et al., 2011) were used in chapter 3, *Sox10-GFP* mice (Kessaris et al., 2006) or *Pdgfrα-GFP* mice (Hamilton et al., 2003) were used in Chapters 4-6); these mice are described in detail below. Animals were killed and the brains were removed as described in section 2.1.1. Coronal sections of the forebrain were obtained by firstly removing the cerebellum to provide a flat surface by which to

attach the remaining forebrain to the slicing stage, and to ensure that the slices were prepared in the coronal plane. The forebrain was mounted on the stage of the Vibratome using superglue and stabilised using an agar block. The two hemispheres were separated by making a cut down the midline of the forebrain, and 225 µm slices were made in ice-cold oxygenated slicing solution. The slices were placed in oxygenated slicing solution at room temperature until they were used for recording.

2.1.3 Preparation of spinal cord slices

Msx3-Cre:Sox10-GFP/tdTom and Gsh2-Cre:Sox10-GFP/tdTom mice (Tripathi et al., 2011) in which GFP or tdTomato is expressed in oligodendrocyte lineage cells (as explained below), aged P6–P14, were used for the preparation of the longitudinal spinal cord slices used in chapter 3. Animals were killed as described in section 2.1.1. The spinal cord was removed by cutting the skin from the back of the head to the caudal end of the spine and peeling back the skin. The vertebral column was cut between the first vertebra and the skull, and then cuts were made along both sides of the vertebral columns, before making a transverse cut through the sacral region of the vertebral column. The intact spinal cord was then removed from the vertebrae by pulling the meninges at the cervical end. The meninges were removed by cutting along the midline of the spinal cord and then peeling the meninges back along the whole length of the cord. The spinal cord was transversely cut into separate ~1 cm segments before mounting on the stage of the Vibratome with superglue. The spinal cord segments were then sliced longitudinally at a thickness 150–160 µm in ice cold oxygenated slicing solution. The slices were placed in oxygenated slicing solution at room temperature until they were used for recording.

2.1.4 Isolated optic nerve preparation

Sprague-Dawley rats, aged P21-28, were used for the preparation of isolated optic nerves for the experiments in Chapter 6. After cervical dislocation, and removal of the skin surrounding the skull, a cut was made behind the eyeball to transect the optic nerve as distally as possible. The brain was removed as described in section 2.1.1, however as the brain was lifted from the skull the optic nerves were drawn through their optic canals, before transecting them at the optic chiasm. The isolated optic nerves were then placed in oxygenated slicing solution at room temperature until they were used for recording.

2.2 Solutions

2.2.1 Extracellular solutions

Brain slices and isolated tissue were perfused with solutions mimicking cerebrospinal fluid. For the experiments in chapter 3, HEPES-buffered solution was used, whereas for the experiments in chapters 4-6, bicarbonate-buffered solution was used. HEPES-buffered solution contained the following (in mM): 144 NaCl, 2.5 KCl, 2.5 $CaCl_2$, 1 $MgCl_2$, 10 HEPES, 1 NaH_2PO_4, and 10 D-glucose, pH 7.4 (adjusted with NaOH). Bicarbonate-buffered solution contained the following (in mM): 126 NaCl, 24 $NaHCO_3$, 2.5 KCl, 1 NaH_2PO_4, 2.5 $CaCl_2$, 1 $MgCl_2$, 10 D-glucose, pH 7.4 (bubbled with 95% O_2/5% CO_2). The HEPES-buffered solution was oxygenated with 100% oxygen, maintained at room temperature, and the solution was applied to the recording chamber using a gravity-fed perfusion system at a rate of 6-10 ml/min. The bicarbonate-buffered solution was applied to the recording chamber by a peristaltic pump at a flow rate of 4 ml/min, and additionally it was passed through a heating block (in which the temperature was controlled by adjusting the current through a series of resistors attached to the heating block) to adjust the temperature to 33 ± 2℃.

For the experiments in chapter 5, ischaemic conditions were mimicked *in vitro* by inhibiting glycolytic and mitochondrial ATP production by removing glucose and O_2, and pharmacologically blocking ATP production. The bicarbonate-buffered solution described above was amended by replacing glucose with sucrose (7 mM), bubbling the solution with 95% N_2/5% CO_2 instead of 95% O_2/5% CO_2, and iodoacetate (2 mM) was added to block glycolysis and antimycin (25 μM) to block oxidative phosphorylation (Allen et al., 2005).

2.2.2 Intracellular solutions

Whole-cell patch clamping experiments in chapters 3-6 were performed using different intracellular solutions appropriate for each experiment. In general, a potassium gluconate based solution was used to record from OPCs in both voltage- and current-clamp modes, whereas a caesium gluconate based solution was used to record from mature oligodendrocytes, to increase their membrane resistance and thus increase the cells' electrical space constant. All internal solutions contained a fluorescent dye (Lucifer yellow, Alexa Fluor 488 or Alexa Fluor 568 were used depending on the genetically encoded florescent label expressed by the patch clamped cell) in order to visualise their morphology and allow post-recording immunohistochemistry. All of the internal solutions used are described in Table 2.1, and in each chapter.

2.3 Preparation and maintenance of organotypic slices

Sox10-GFP mice (in which GFP is expressed in oligodendrocyte lineage cells (Kessaris et al., 2006)), aged P8, were killed as described in section 2.1.1. Brains were removed (as described in section 2.1.1) and placed into ice-cold Earle's Buffered Saline Solution (EBSS; Invitrogen) containing 10 mM HEPES (Invitrogen), with the pH set to 7.3. Coronal forebrain slices (of thickness 325 µm) were prepared as described in section 2.1.2 in ice-cold sterile EBSS containing HEPES. Each forebrain slice was then plated onto an insert (Millipore) within a 6 well plate, containing 1 ml of medium composed of 50% Minimal Essential Medium (MEM), 23% Earl's Balanced Salt Solution (EBSS), 25% horse serum, penicillin (25 units/ml) and streptomycin (25 µg/ml) all from Gibco-Invitrogen, and 1.125% nystatin (12.5 units/ml), 36 mM glucose and 5 mM Tris base all from Sigma-Aldrich. The slices were maintained for up to 14 days in at 37℃ in a humidified atmosphere with 5% CO_2, and the medium was replaced every 3-4 days.

2.4 Mechanical and optical set-up for electrophysiology

All experiments were performed with an Olympus BX51W upright microscope equipped with a halogen lamp and filter sets for fluorescence microscopy, mounted on a fixed stage with a microscope-moving table. Cell were visualised with 10x and 40x water immersion objectives using differential interference contrast (DIC) optics. Filter sets (Glen Spectra and Chroma; components listed below in brackets) were used to visualise transgenically labelled eGFP [ET500/20X (500nm excitation), T515LP (515nm dichroic), ET535/30M (535nm emission)] and tdTomato cells [XF1067 (560nm excitation), XF2029 (595nm dichroic), XF3081 (645 nm emission)], or cells filled with Lucifier yellow [D425/40X (425nm excitation), 460DCLP (460nm dichroic) D540/50M (540nm emission)], Alexa Fluor 488 [ET500/20X (500nm excitation), T515LP (515nm dichroic), ET535/30M (535nm emission)] and Alexa Fluor 568 [560AF55 (560nm excitation), 595DRLP (595nm dichroic), 645AF75 (645 nm emission)]. A video camera (COHU, 2700 series) was attached to the microscope so that cells could also be visualised on a TV monitor.

The microscope and recording chamber were mounted on a vibration isolation table to reduce movements which could affect recordings. A grounded Faraday cage surrounded the microscope and recording chamber to reduce electrical noise. All other metallic surfaces were also grounded by low-resistance cables connected to the patch-clamp amplifier's ground, to reduce any remaining electrical noise.

2.5 Pipettes and electrical set-up

Patch pipettes were made from thick-walled filament-containing borosilicate glass capillaries (outer diameter 1.5 mm, inner diameter 0.86 mm, type GC150F-10 from Harvard Apparatus) using a two-step vertical (Narishige PC-10) or a four-step horizontal (Sutter instruments P-97) puller. Pipettes were filled with an appropriate intracellular solution (described in section 2.22 and the individual results chapters). Recording electrodes had resistances of between 5-8 MΩ for recording from oligodendrocyte lineage cells and 2-4 MΩ for recording from neurons.

The recording electrode was inserted into the pipette holder of a patch-clamp headstage (Axopatch CV202AU, Axon Instruments), which was attached to and controlled by an electrical micro-manipulator (SM1, Luigs and Neumann) attached to the pipette holder. Both the electrode in the pipette holder and the bath electrode were a silver wire/silver pellet coated with silver chloride (AgCl). The external and internal solutions (section 2.2) also contained chloride ions which are reversibly exchanged with the electrode via the following reaction:

$$Ag + Cl^- \leftrightarrow AgCl + e^- \quad (2.1)$$

To ensure that Cl^- exchange was maintained, both the silver wire and bath electrode were regularly chlorided by placing them in a solution containing chloride ions (10% bleach, NaOCl). The majority of membrane currents were recorded at a sampling rate of 10 kHz, except for spontaneous synaptic currents which were recorded at 1 kHz, with an Axopatch 200B amplifier. Data were collected using pClamp 9 (Axon Instruments) or Axoscope 9 (Axon Instruments), and analysed off-line using Clampfit 9 (Axon Instruments).

2.6 Patch-clamp recordings

All patch-clamp recordings were performed in the conventional whole cell configuration (Hamill et al., 1981; Edwards et al., 1989). Firstly, the patch electrode was lowered into the bath, while at the same time a 5 mV voltage step (of duration 200 ms) was applied to monitor the resistance of the recording electrode before and after contacting the cell membrane. Additionally, while lowering the patch electrode towards the cell membrane, positive pressure was applied (through a 1 ml syringe attached to perfusion tubing) to prevent the tip of the recording electrode from becoming blocked by debris from either the external solution or the brain slice. Secondly, when the patch electrode came into contact with the cell membrane, gentle suction was applied to form

a high resistance seal (typically 1-10 GΩ) between the cell membrane and the patch electrode, so the electrode was in the cell-attached mode (Fig. 2.1A). Thirdly, after formation of a high resistance seal in the cell-attached mode, compensation of the pipette capacitance was made, and the holding potential was adjusted to -60 mV which is close to the cell's resting membrane potential. Finally, the whole-cell configuration was achieved by applying further gentle suction to rupture the section of membrane at the tip of the patch electrode. The whole-cell configuration allows the diffusion of ions between the patch electrode and the cell cytoplasm, and electrical access to the interior of the cell (Fig. 2.1B).

2.7 The electrical circuit for whole-cell patch-clamp recording in spatially compact cells

The cell membrane, which is composed of a lipid bilayer and embedded proteins, is an electrical insulator. In contrast, the extracellular and intracellular solutions are composed of salt solutions which are excellent conductors of current. This combination of the cell membrane (an insulator) and the surrounding intra- and extracellular solutions (conductors) forms a capacitor, which can store charge. The charge stored (Q) is proportional to the applied voltage (V), Q=CV, where capacitance (C) is a measure of the ability of the membrane to store charge. The physical dimensions of the membrane are important for determining the capacitance: the more membrane, the more charge can accumulate, therefore capacitance is proportional to membrane surface area. Importantly, capacitors prevent instantaneous changes in voltage which affects both the conduction of electrical signals in biology and electrophysiology recordings. For example, in excitable cells, local changes in membrane potential, such as an action potential travelling along an axon, are subject to a delay in propagation due to the time needed for charging of the cell membrane, therefore limiting the speed of action potential propagation. Similarly, during whole-cell voltage-clamp recordings, a step change in desired membrane potential can only be produced after the charging time of the membrane capacitance. The current flowing through a capacitor (C) is proportional to the rate of voltage change (∆V) with time (∆T):

$$I = C\,\frac{\Delta V}{\Delta T} \qquad 2.2$$

In addition to being a capacitor, the cell membrane is also a conductor due to the presence of ion channels in the membrane which allow the passage of charged ions. Currents flowing through these ion channels can charge or discharge the

membrane capacitance and therefore cause variations in membrane potential. The electrical circuit equivalent of a cell in the whole cell configuration is represented by a capacitor (the membrane capacitance Cm), and a resistor (the membrane resistance R_m) connected in parallel, both connected in series with the patch electrode (electrode series resistance R_s) (Fig. 2.2A).

The current flow (I) through this circuit in response to a voltage step (Vs), can be predicted by (Tessier-Lavigne et al., 1988):

$$I(t) = \left(\frac{Vs}{Rm + Rs}\right).\left(1 + \frac{Rm \cdot e^{-t/\tau}}{Rs}\right) \quad 2.3$$

where t is the time after the onset of the voltage step, and τ, the decay time constant of the current transient, is:

$$\tau = Cm \cdot \frac{Rs \cdot Rm}{Rs + Rm} \quad 2.4$$

At the onset of the voltage step (t=0), the cell capacitance is uncharged and the voltage across it is zero. Consequently, just as the voltage step is applied, the voltage across the series resistance is the applied voltage step, and the initial current flowing allows the calculation of the series resistance (from equation 2.3 at t=0) as:

$$Rs = \frac{Vs}{I(t=0)} \quad 2.5$$

When the current reaches a steady state (t=∞), the cell capacitance is fully charged and no current flows through it, and then the membrane resistance can be determined from the voltage step and the current at t=∞, by rearranging equation 2.3 with t=∞:

$$Rm = \frac{Vs}{I(t=\infty)} - Rs \quad 2.6$$

Substituting Rs from equation 2.5 gives:

$$Rm = Vs \cdot \frac{I\,(t=0) - I(t=\infty)}{I(t=0) \cdot I(t=\infty)} \quad 2.7$$

The membrane capacitance can be calculated by rearranging equation 2.4 to give:

$$Cm = \tau \cdot \frac{Rs + Rm}{Rs \cdot Rm} \qquad 2.8$$

Substituting R_s from equation 2.5 and R_m from equation 2.4 gives:

$$Cm = \tau \cdot \frac{(I\ (t = 0)^2}{Vs \cdot (I(t = 0) - I(t = \infty))} \qquad 2.9$$

The time constant (τ), was obtained by fitting the current transient with a single exponential using Clampfit 9. An example of a fitted capacity transient for an electrically compact cell, such as an oligodendrocyte precursor cell, which can be represented by a single-compartment model (Fig. 2.2A), is shown in Fig. 2.2B. The current change at t=0 was obtained by extrapolating the exponential back to the time of the voltage step.

2.8 The electrical circuit for whole-cell patch-clamp recordings in cells with complex morphology

Cells with more complex morphology, such as mature oligodendrocytes and neurons, do not conform to a single compartment model. For example the thin long myelinating processes of mature oligodendrocytes, or the complex geometry of neurons with a soma, an axon and large branching dendritic trees, may cause a lack of voltage uniformity. The degree of voltage non-uniformity in neurons has been analysed by Major (1993), who showed that the voltage control in the dendrites of CA1 pyramidal cells was very poor. A similar problem is expected to occur in the long processes of mature oligodendrocytes. Cells with complex morphologies need to be represented by two or more compartments (Fig. 2.3A and B). In these more complex cells the capacity transient cannot be fitted satisfactorily with a single exponential, but equation 2.5 can still be used for the initial amplitude of the current response to a voltage step in order to calculate the series resistance (equation 2.5). An approximation of the cell membrane resistance was obtained by taking the difference of the input resistance calculated at t=∞ and the series resistance (although this measurement includes the axial resistance of the processes linking distant membrane areas to the soma).

2.9 Series resistance and its compensation

In whole-cell patch-clamp experiments the electrode resistance leads to voltage errors. This voltage error is due to the electrode and the membrane resistance being in series in an electrical circuit, which results in a voltage drop across the electrode's

resistor when current flows through the cell membrane. The higher the series resistance of the electrode, the larger the voltage drop, which results in the cell not being clamped at the voltage applied to the top of the patch electrode. For example, using Ohms law ($V=I \cdot R$), for a series resistance (R_s) of 10 MΩ and a current flowing of 1 nA, the voltage error would be 10 mV. In my experiments R_s was typically between 10-20 MΩ, and the largest currents passed were typically 100 pA, giving a maximum voltage error of ~2 mV. Data were excluded if R_s increased significantly throughout recordings or if R_s was greater than 25 MΩ. The series resistance can also be partially compensated for, using a positive feedback circuit in which a signal proportional to the measured current is used to increase the command potential applied to the pipette, to compensate for the voltage drop across the patch electrode. The R_s compensation allows for more accurate control of the cell voltage, nevertheless it is impossible to reach 100% compensation for R_s. A low electrode series resistance is also desirable because the combination of Rs and the cell capacitance acts as a filter, slowing down changes in the membrane voltage applied to the cell and measured currents.

2.10 Liquid junction potential and its compensation

A potential difference (the junction potential) exists at the interface between two solutions with different compositions. For example, in whole-cell patch-clamp experiments when the patch electrode is placed in the bath, a junction potential exists at the tip of the electrode because the ionic composition of the internal solution inside the electrode differs from the external solution in the bath. However, this junction potential disappears in the whole cell mode when the pipette contents diffuse into the cell. The junction potential depends on the diffusion coefficients of the anions and cations present in each solution (which depends on their molecular weight and charge, which affects the mobility of ions). In particular, for my solutions, the principal ions responsible for generating the junction potential are K^+, Na^+, Cl^- and gluconate$^-$. K^+ ions diffuse out of the patch electrode more quickly ($D_K=1.99\times10^{-9}$ m^2 s^{-1}) than Na^+ ions ($D_{Na}=1.36\times10^{-9}$ m^2 s^{-1}) diffuse in, and gluconate ions ($D_{Gluconate}= 1.06\times10^{-9}$ m^2 s^1) diffuse out more slowly than chloride ions diffuse in ($D_{Cl}=1.99\times10^{-9}$ m^2 s^{-1}) (Robinson and Stokes, 1965), so the patch electrode potential becomes more negative than the bath potential (Fig. 2.4). The junction potential can be measured experimentally, as described below.

In order to measure the junction potential, an agar bridge was used (containing 4 M NaCl) to connect the bath solution to the reference electrode, to avoid changes in the reference electrode potential following a change in the external solution. Junction potentials were then measured by comparing the zero current voltage value obtained

when both the patch electrode and bath contained the same solution (when there is no junction potential), to the value obtained when the bath solution was that used for experiments. The junction potential was measured to be -10 mV for my K-gluconate and Cs-gluconate based internal solutions, and all of the voltage data have been adjusted accordingly (i.e -10 mV was added to all of the voltages measured with the patch clamp).

2.11 Voltage-gated ion channel analysis

In order to reveal and quantify voltage-gated currents, the passive components of current responses evoked by voltage steps can be removed from the data. The current response to a hyperpolarising voltage step with no active components, which only contained the capacity current and an ohmic leak conductance, was selected. This passive current is proportional to the size of the voltage step, and was linearly scaled according to the size of the voltage steps applied. This linearly scaled passive component was then subtracted from all of the current responses evoked by voltage steps, which revealed voltage-gated Na^+ and K^+ channel current responses evoked by depolarising voltage steps.

2.12 Optic nerve recordings

To make recordings from the axons in the optic nerve, suction electrodes were used. Thick walled capillary glass was shaped by heat to a 45° angle approximately 5 mm from the end of the capillary. The angled opening of each suction electrode was then fire-polished to the correct size to allow the nerve to be positioned inside the electrode securely during the recording, but without damaging it. Both of the suction electrodes contained an Ag/AgCl wire and extracellular recording solution, but one was used for stimulation whilst the other was used for recording (Fig. 2.5).

Compound action potentials were recorded from optic nerves by firstly drawing both ends of the optic nerve into the two suction electrodes, by applying slight negative pressure using syringes attached to the other end each glass capillary. The optic nerve was then stimulated via one suction electrode attached to a stimulator, and the compound action potential was recorded through the second electrode.

2.13 Using transgenic mice to label and trace neural cells

The transgenic mouse lines that were used for the work described in this thesis are listed below.

2.13.1 Transgenic mice expressing fluorescent constructs

Pdgfrα-H2BGFP knock-in mice (Hamilton et al., 2003), referred to as *Pdgfrα-GFP* mice, were purchased from Jackson Laboratories (line B6.129S4-Pdgfra tm11(EGFP)Sor /J). These mice have a histone-GFP fusion gene knocked into the *Pdgfrα* locus, resulting in nuclear labelling of PDGFRα-expressing cells, including OPCs. This transgenic line was maintained as a heterozygous breeding colony and was genotyped using the primers specified in table 2.2. *Sox10-GFP* mice were also used (see below).

2.13.2 Cre transgenic mouse lines

Emx1-iCre, *Gsh2-iCre* (Fogarty et al., 2005; Kessaris et al 2006) and *Msx3-iCre* (Tripathi et al 2011) transgenic mice are PAC transgenic mice that express a constitutively active form of improved Cre (iCre) recombinase in *Emx1-*, *Gsh2-* and *Msx3-* expressing cells, respectively. These transgenic lines were maintained as heterozygous breeding colonies and were genotyped by PCR amplification of their genomic DNA, to detect the presence of the iCre coding sequence, using primers specified in table 2.2.

Pdgfrα-CreER^{T2} transgenic mice (Rivers et al., 2008) express a tamoxifen inducible form of Cre recombinase under the regulation of the *Pdgfrα* gene promoter. This PAC (Phage Artificial Chromosome) transgenic mouse line was maintained as a homozygous breeding colony.

2.13.3 Reporter mouse lines (transgenic mice that contain loxP sites)

Rosa26-YFP transgenic reporter mice (Srinivas et al., 2001) were maintained as a homozygous breeding colony. Following Cre-mediated recombination, cells within these mice will express the yellow fluorescent protein (YFP) under the regulation of the ubiquitous *Rosa26* promoter.

Sox10-GFP transgenic reporter mice (Kessaris et al., 2006) express a PAC DNA construct containing the targeting construct *Sox10-lox-GFP-poly(A)-lox-DTA* driven by the Sox10 promoter. In the absence of Cre, these mice express enhanced GFP (eGFP) in all Sox10^{+} cells, and their GFP was used as a general marker of oligodendrocyte lineage cells. Following recombination by Cre, the eGFP sequence is removed, and the diphtheria toxin A chain (DTA) is expressed in the recombined cells. Expression of the active component of the diphtheria toxin results in the targeted ablation of the recombined cells. For experiments reported here, these mice were

maintained as a heterozygous breeding colony and were not crossed with any Cre-expressing line, so the diphtheria toxin was not expressed. Mice were identified (genotyped) as being positive for the *Sox10-GFP* transgene by exposing the P0-P4 pups to a UV light source – the positive pups fluoresced.

Sox10-GFP/tdTom dual reporter mice express a PAC DNA construct containing the targeting construct *Sox10-lox-GFP-pA-lox-tomato-pA* driven by the *Sox10* promoter (Tripathi et al., 2011). In the absence of Cre, these mice express enhanced GFP (eGFP) in all $Sox10^{+}$ cells. Following recombination by Cre, the eGFP sequence is removed, and the cells instead turn on the expression of the red fluorescent protein, tandem-duplicated tomato (td-Tom). The generation of the *Sox10-GFP/tdTom* dual reporter mice will be described in more detail in Chapter 3.

Tau-mGFP transgenic reporter mice (Hippenmeyer et al., 2006) contain a *lox-pA-lox-mGFP-IRES-NLS-LacZ-pA* targeting cassette in exon 2 of the *Tau* genomic locus. Following recombination by Cre, these mice express a membrane targeted form of GFP under the control of the *Tau* promoter, directing its expression within the central nervous system to differentiating/differentiated oligodendrocytes and neurons. This transgenic line was maintained as a heterozygous breeding colony and mice were genotyped by PCR using primers that identify the GFP coding sequence (Table 2.2)

2.13.4 Cre mediated recombination

The Cre-lox system is a genetic tool used to produce site and cell specific recombination events in genomic DNA. It was discovered in P1 bacteriophages, which use this mechanism to circularize and facilitate replication of their genomic DNA when reproducing as part of their life cycle (Sternberg and Hamilton 1981). This system is now artificially reproduced in the cells of transgenic mice and requires co-expression of two components: loxP sites (specific DNA sequences) within the target DNA sequence, and expression of the enzyme Cre recombinase, which recognises and catalyses the recombination and excision of DNA between the loxP sites (Sternberg and Hamilton, 1981). This system allows the labelling and tracing of specific cell types with visible proteins, the deletion of genes of interest or the targeted ablation of whole populations of cells.

Mice expressing the constitutive form of Cre (section 2.13.2) were crossed with one of the reporter mouse lines (see 2.13.3) to generate double heterozygous mice for experimental use. In cells that express Cre, the enzyme recombines the loxP sites within the reporter transgene, forming a circular region of DNA (Abremski and Hoess,

1984). The DNA between the loxP sites is then excised (Orban et al., 1992). This recombination event is permanent within the cell and all of its progeny (Fig. 2.6).

2.13.5 CreER^{T2} mediated recombination

Mice expressing a tamoxifen-inducible form of Cre (*Pdgfrα-CreER^{T2}*) (see 2.13.2) were crossed with one of two reporter mouse lines: *Rosa26-YFP* or *Tau-mGFP* (see 2.13.3). Cre recombination does not spontaneously occur in adult CreER^{T2}/reporter double transgenic mice, as Cre is bound to the estrogen receptor (ER^{T2}), and held inactive in the cell cytoplasm (Metzger et al., 1995). When tamoxifen, an estrogen analogue, is administered to double heterozygous mice, tamoxifen will bind to the ER^{T2} allowing Cre to translocate from the cytoplasm to the nucleus. In the nucleus, activated Cre recognises sequences in the DNA that correspond to lox-P sites and recombines the lox-P sites, excising the DNA sequence was between them. When tamoxifen is withdrawn Cre is again inactive.

Tamoxifen was administered orally to CreER^{T2}/reporter mice. 40 mg/ml tamoxifen in corn oil was sonicated for 40 minutes and administered by oral gavage into the stomach. Adult mice received 300 mg/kg body weight of tamoxifen daily for 4 consecutive days. Kaylene Young performed the tamoxifen administration.

2.13.6 Genotyping of transgenic mice

Genomic DNA was extracted from a tissue biopsy and used for PCR amplification. The primers used for genotyping each transgenic mouse line were designed to specifically amplify only stretches of DNA within the targeting construct (see Table 2.2). PCR genotying was performed by Ulla Dennhey, Sabrina Pacheco, Kaylene Young, Huiliang Li or Richa Tripathi. Alternatively, where stated, mice were identified visually by GFP fluorescence under a UV light source between P0-P4.

2.13.7 In vivo and in vitro EdU labelling of dividing cells

5-ethynyl-2'-deoxyuridine (EdU) (Invitrogen) is a thymidine analogue that is incorporated into the DNA of cells as they undergo DNA replication as part of the cell division process. EdU was administered to mice either by subcutaneous (s.c.) injections (for mice ≤ P10) or via the drinking water (for mice ≥ P20) by Kaylene Young. EdU was also added to the organotypic slice medium, at a concentration of 10 µM to quantify the percentage of dividing cells in vitro. For s.c. injections, EdU was dissolved to 1mg/ml w/v in PBS and each pup was injected with 50µl at 7:30am, 10:30am, 1:30pm, 4:30pm and 7:30pm for 5 consecutive days. Alternatively EdU was dissolved

in the drinking water (0.3 mg/ml) which was available ad libitum replaced every 2-3 days.

2.14 Immunohistochemistry

2.14.1 Perfusion fixation, tissue collection and freezing

Tissue sections were prepared by Richa Tripathi or Kaylene Young for the immunohistochemistry experiments in chapters 3 and 4, respectively. Briefly, mice were anaesthetized with pentobarbitone (2ml/kg body weight), and an incision was made at the base of the sternum extending along the base of the rib cage and then up the side of the body through the ribs allowing the rib cage to lift up. The diaphragm and connective tissue around the heart were dissected away and a small incision was made in the atrium. A needle connected to a peristaltic pump containing 4% paraformaldehyde (wt/vol, PFA, Sigma, in PBS) was inserted into the apex (left ventricle). 4% PFA was delivered at a rate of 5 ml/minute until there was no blood exiting the right atrium. Brains were removed and sliced into 2 mm coronal slices using a rodent brain matrix (Agar Scientific). Brain slices were immersion fixed in 4% PFA in PBS at 4ºC overnight (except for PDGFRα immuno-labelling where tissue was immersion fixed for 45' at room temperature), cryoprotected in 20% (w/v) sucrose in PBS at 4ºC for 6 hours before embedding in Optimal Cutting Temperature medium (Tissue Tek). Frozen tissue was stored at -80ºC. Cryosections (30 μm) were collected and immunohistochemistry performed on floating sections as described by Tripathi et al. (2011).

2.14.2 Antibody labelling

To label acute slices or organotypic slice cultures, slices were fixed in 4% paraformaldehyde in PBS for 1 hour, then rinsed three times (for 10 minutes) in PBS followed by preincubation in 0.5% Triton and 10% goat serum in PBS for 6-8 hours at room temperature. The slices were then incubated with primary antibodies for 36 hours at room temperature with slight agitation, rinsed in PBS three times (for 10 minutes), and then incubated with secondary antibodies for 3 hours before being rinsed again in PBS 3 times (for 10 minutes). All primary and secondary antibodies used in this thesis are listed in tables 2.3 and 2.4. Slices were then incubated with DAPI to label nuclei (300 nM in PBS, Molecular Probes) for 20 minutes, and rinsed in PBS three times (10 minutes), before finally mounting slices on a microscope slide with Citifluor (glycerol/PBS, Citifluor), covered with a 0.17 mm thick glass cover slip, and sealed with nail varnish (Boots, UK).

2.14.3 EdU detection

Following fixation, acute slices were washed once with PBS and subsequently incubated for 20 minutes in 0.8% (v/v) Triton X-100 in PBS, on an orbital shaker, at 21ºC. The slices were again washed in PBS before EdU detection with the Click-iT EdU Alexa Fluor-647 Imaging Kit (Invitrogen). Each slice was immersed in ~120µl of Click-iT developing cocktail, prepared according to the manufacturer's instructions and incubated for 45 minutes at 21ºC, in the dark. Slices were washed once with PBS before continuing with immunohistochemistry (see section 2.14.2).

For cryosections, EdU developing was performed immediately following immunohistochemistry, as some antibodies failed if the order was reversed. Sections were incubated at 21ºC for 15 minutes in PBS / 0.5% triton-x100. The reagents provided in the Click-iT EdU Alexa Fluor-647 Imaging Kit were combined according to the manufacturer's instructions. Floating cryosections were transferred into the developing cocktail and incubated in the dark at 21ºC, for 40 minutes. Sections were then washed three times in PBS. Cell nuclei were visualized by post-staining with Hoechst 33258 (1:1000; Sigma). All sections were coverslipped using fluorescent mounting medium (DAKO).

2.14.4 Confocal imaging and set up

Fixed slices were imaged with a confocal laser scanning microscope (LSM). The confocal microscope was either a Zeiss LSM 510 or a Zeiss LSM 710. Images were taken with x10, x20, x40 or x63 oil DIC objectives.

All imaging with multiple wavelengths was carried out with sequential scans, in order to minimise 'bleed through' from one channel to another. The argon laser line 488 nm was used to excite eGFP and Alexa Fluor 488 containing antibodies, the 458 nm laser line of the argon laser was used for tdTomato, Alexa Fluor 555, and Alexa Fluor 568 containing antibodies, and the 633 laser line was used for Cy5, Alexa Fuor 633 and Alexa Fuor 647 containing antibodies. The ultraviolet laser 364 nm laser line was used for the detection of DAPI. Scanning of areas of interest in slices was done in the x-y and z directions, and averaged 2-6 times depending on the signal. The size of the z stack largely depended on the region of interest from (15-90 µm depth), taken in continuous 0.2 µm sections. The gain and offset settings were initially chosen for each set of images in an experiment depending on the signal intensity being detected, and the settings were kept constant for all slices within an experiment.

2.15 Data analysis and statistics

Data are presented as mean ± sem. Statistical significance was normally assessed with 2-tailed Student's t-tests. T-tests were either paired, to analyse whether responses in a single cell changed after drug application, or unpaired when comparing the mean responses between different groups of cells. A correction procedure equivalent to the Holm-Bonferroni method was used when making multiple comparisons (for N comparisons in a given experiment, the most significant p value is multiplied by N, the 2nd most significant by N-1, the 3rd most significant by N-2, etc; the resulting corrected p values are significant at the 5% level when less than 0.05). Two-sample Kolmogorov-Smirnov tests were used to compare distributions.

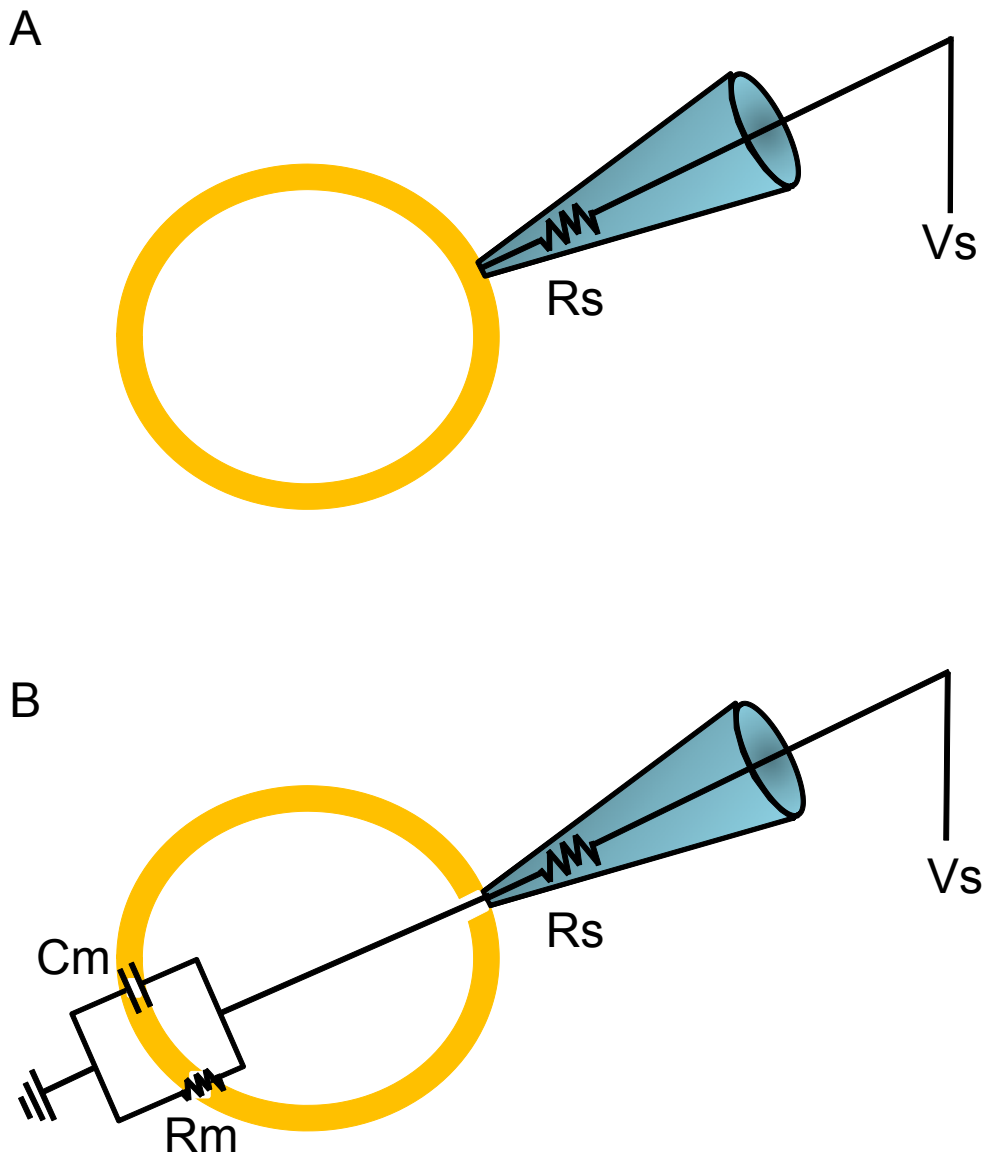

Figure 2.1. Schematic diagram of patch clamp configurations.
A. Seal formation, where the patch electrode comes into contact with the cell membrane and forms a high resistance seal. Very little current flows into the cell because of the high resistance of the membrane patch. **B.** Whole-cell configuration, where the membrane beneath the patch electrode is ruptured by application of gentle suction. The whole-cell configuration allows the diffusion of ions between the patch electrode and the cell cytoplasm, and electrical access to the interior of the cell. Vs is the voltage step applied to the patch electrode, Cm is the cell capacitance, Rs is the series resistance of the patch electrode, and Rm is the resistance of the cell membrane.

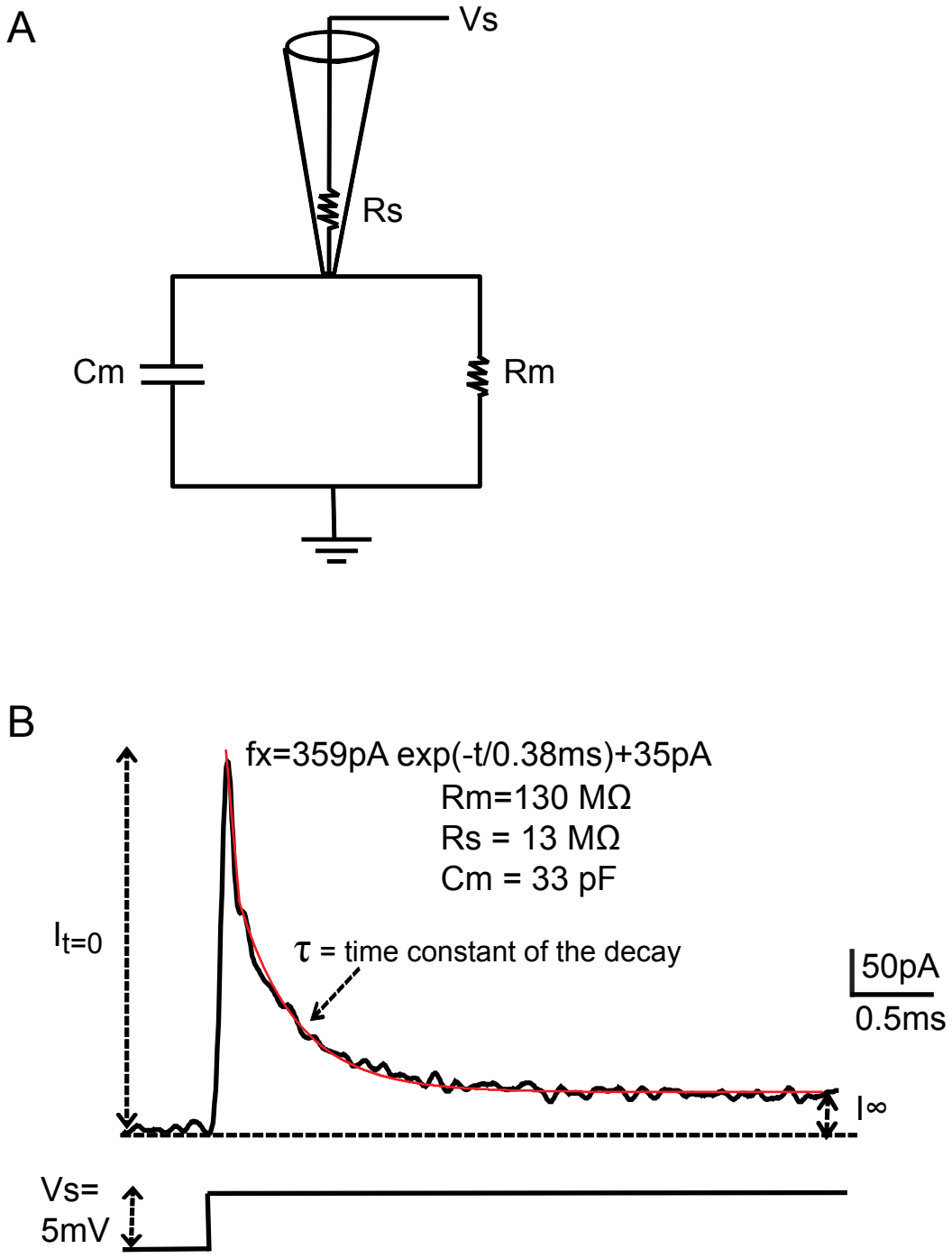

Figure 2.2. Electric circuit and capacity transient analysis for spatially compact cells.
A. Electric circuit model for spatially compact cells, such as oligodendrocyte precursor cells (OPCs). **B.** The top black trace displays the current response to a 5mV voltage pulse in a spatially compact OPC. The top red trace displays a single exponential fit to the current waveform. The bottom trace displays the applied voltage step. The series resistance (Rs) is calculated by the peak current recorded when the voltage pulse was applied (I(t=0)), the membrane resistance is calculated by measuring the current at t=∞, when the membrane is fully charged, as described in the text associated with equations 2.5 and 2.7.

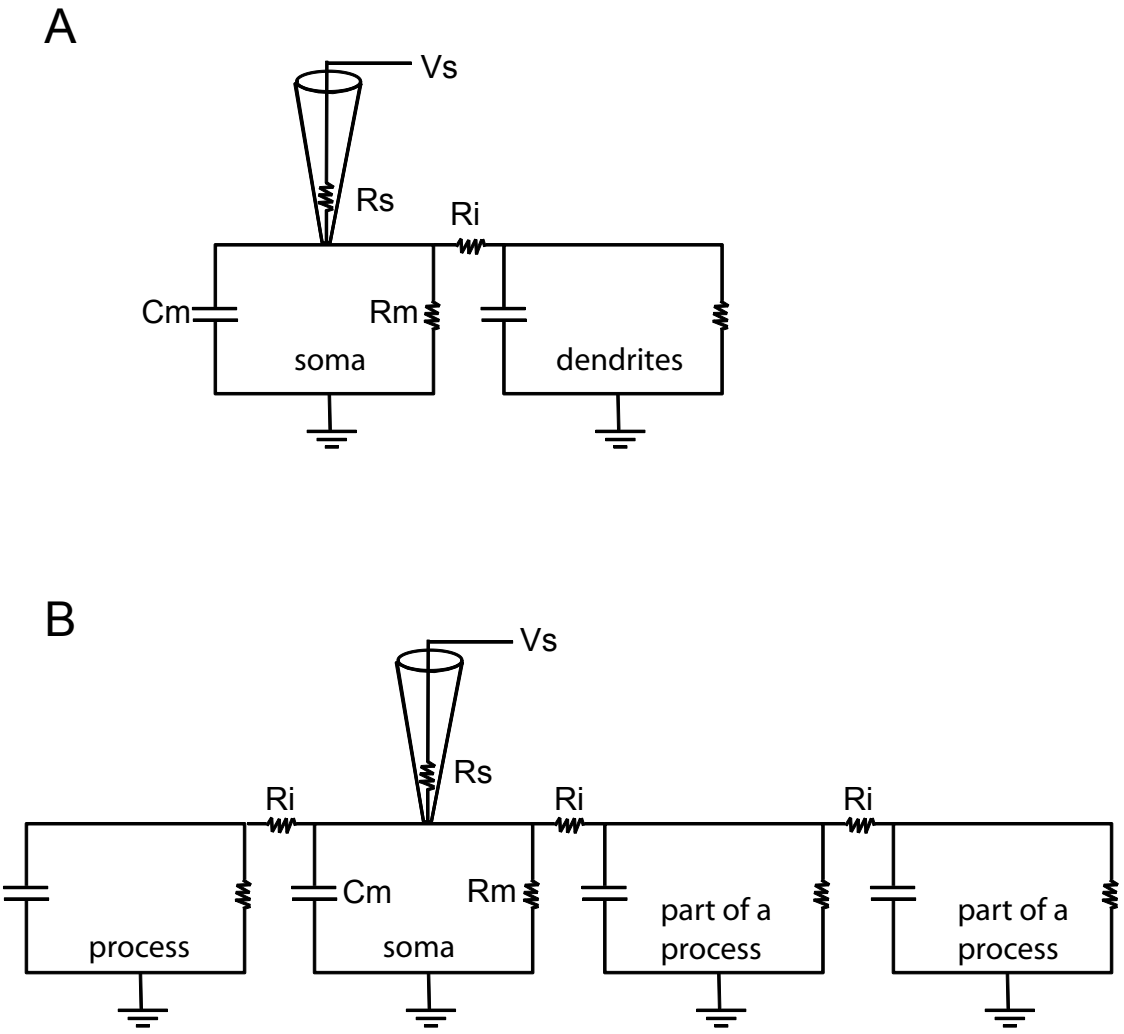

Figure 2.3. Electrical circuits of cells with complex morphology.
A. Electrical circuit model for a neuron. The dendrites are treated as an extra electrical compartment, where Ri is the intracellular resistance along the dendrites **B.** Electrical circuit model for a mature oligodendrocyte. Each myelinated process (Ri) is treated as a series of electrical compartments. In these more complex cells the capacity transient could not be fitted satisfactorily with a single exponential, but the initial amplitude of the current response to a voltage step was measured to calculate the series resistance as in Fig. 2.2, and the steady state input resistance was also measured.

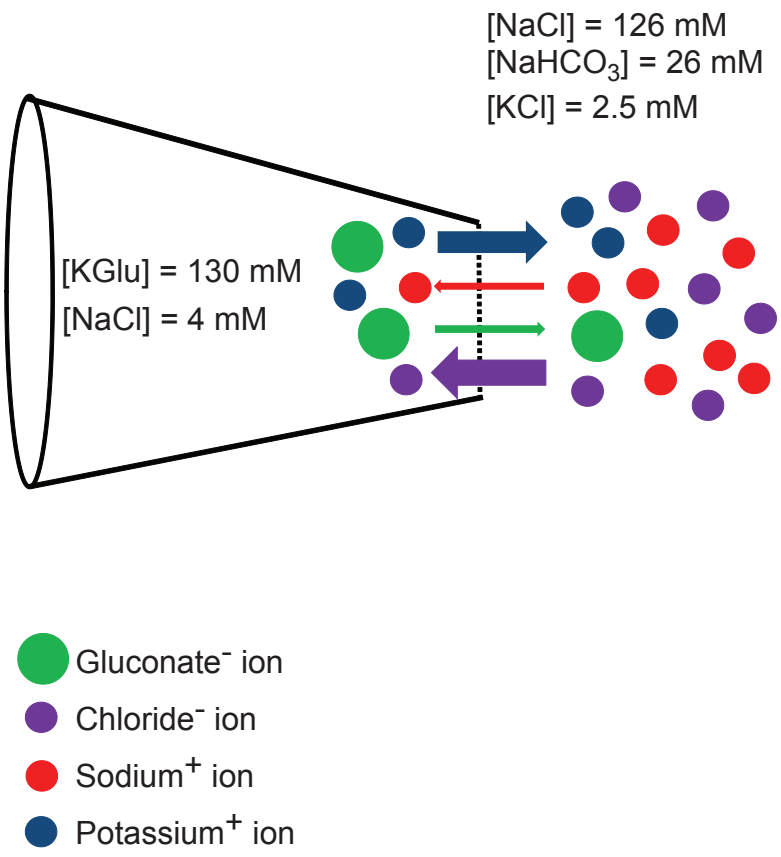

Figure 2.4. Liquid junction potential.
A potential difference (the junction potential) exists at the interface between two solutions with different compositions. When the patch electrode is placed in the bath a junction potential exists at the tip of the electrode because the ionic composition of the internal solution inside the electrode differs from the external solution in the bath. This junction potential does not exist in whole-cell mode because the electrode solution diffuses into the cell. The junction potential present with the electrode in the extracellular solution depends on the diffusion coefficients of the anions and cations present in each solution (which depends on their molecular weight and charge, which affects the mobility of ions). For my solutions the principal ions responsible for generating the junction potential are K^+, Na^+, Cl^- and gluconate$^-$, all of which are represented here.

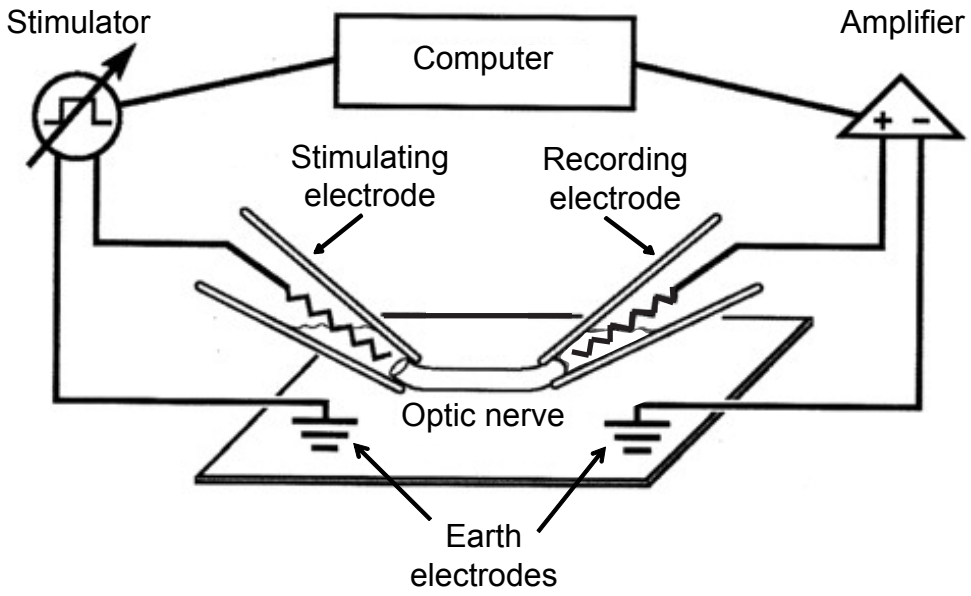

Figure 2.5. Optic nerve compond action potential (CAP) set up.
CAPs were measured using suction electrodes. Optic nerves were drawn into recording and stimulating electrodes. Both recording and stimulating electrodes were filled with external solution and Ag/AgCl chlorided wires.The optic nerve was then simulated via the electrode attached to a stimulator, and the compound action potential was recorded through the second electrode. Earth electrodes made of Ag/AgCl pellets were placed in the external bath solution.

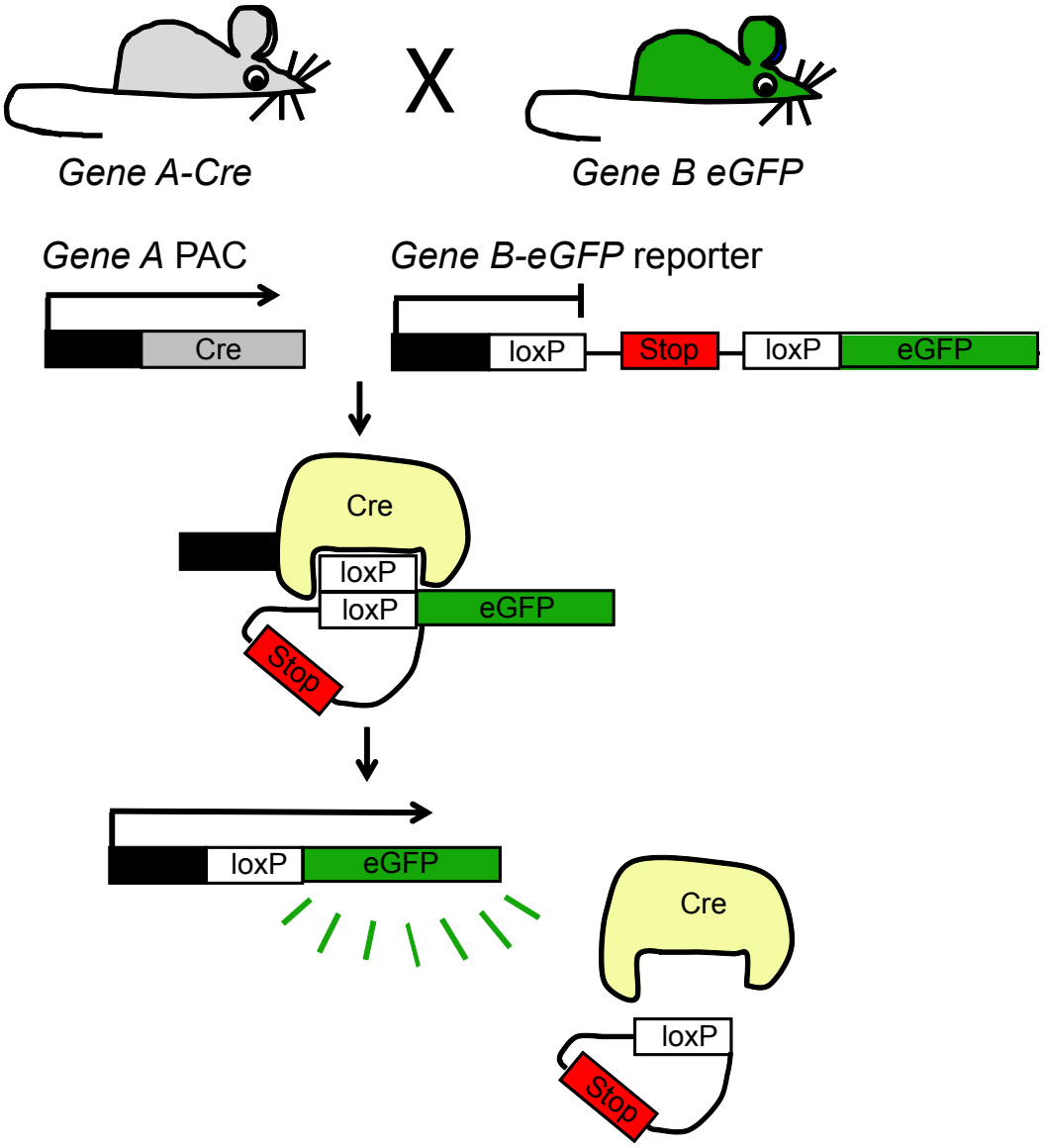

Figure 2.6. Cre-lox transgenics.
Cre-mediated recombination of loxP sites in *GeneA-Cre*/*GeneB-eGFP* double transgenic mice. In the absence of Cre, eGFP is not expressed by the *GeneB-eGFP* reporter mouse. When *GeneA-Cre* transgenic mice are crossed with *GeneB-eGFP* reporter mice, in cells expressing Cre, the Cre will bind to the loxP sites recombining and excising the loxP-flanked stop sequence of DNA. The removal of the sequence of DNA between the loxP sites by Cre then switches on the expression of the eGFP reporter gene.

	Concentration of main ion (mM)	
	K gluconate solution	**Cs gluconate solution**
K-gluconate	130	n/a
Cs-gluconate	n/a	130
NaCl	4	4
HEPES	10	10
BAPTA	10	10
$CaCl_2$	0.5	0.5
Na_4GTP	0.5	0.5
Mg_2ATP	4	4
Lucifer yellow	n/a	2
Alexa Fluor 488 or 568	0.1	n/a
pH adjusted to 7.3 with	KOH	CsOH

Table 2.1. Composition of the internal solutions used for the experiments described in this thesis.

Transgenic mouse line	Genotyping primers
Pdgfrα-CreER^{T2} mice	CAGGTCTCAGGAGCTATGTCCAATTTACTGAACGTA/GGTGTTATAAGCAATCCCCAGAA
Pdgfrα-GFP mice	ACGAAGTTATTA GGT CCC TCGC/CCCTTGTGGTCATGCCAAAC
Gsh2-Cre mice	TTGGCGCGCCTGTGAAGCGTTGGACAGAGGCCC/AGGTACAGGAGGTAGTCCCTC
Msx3-Cre mice	GAAACCTGGACTCTGAGACTGGG/GGCTGTCCAATAACCGAAGACG
Emx1-Cre mice	GCCAAGGATGACTCTGGGCA/GCGGTGGCCAAAGAAGCGATTCCG
Tau-mGFP reporter mice	CCCTGAAGTTCATCTGCACCAC/TCGTTGGGGTC GCTC
Sox10-GFP/tdTom reporter mice	GCCACGAGTTCGAGATCGAG/GGCTTCTTGGCCATGTAGATGG

Table 2.2. The genotyping primers used for the experiments described in this thesis.

Primary Antibody	Supplier	Dilution
Rat anti-PDGFRα	BD Pharmingen	1:400
Guinea pig anti-SOX10	Gift from M.Wegner	1:2000
Mouse anti-NeuN	Chemicon	1:500
Mouse anti-PSA-NCAM IgM	Chemicon	1:1000
Rabbit anti-Ng2	Chemicon	1:500
Rabbit anti-Olig2	Chemicon	1:1000
Rat anti-myelin basic protein (MBP)	Chemicon	1:200
Chicken anti-200kD neurofilament heavy (NF200) IgY	Abcam	1:1000
Rabbit anti-ankyrin G	Santa Cruz	1:400
Mouse anti-APC/CC1 IgM	Calbiochem	1:50-1:100
Rabbit anti-GFP serum	Synaptic Systems	1:1000
Rat anti-GFP IgG2a	Nacalai Tesque	1:3000
Mouse anti-glial fibrillary acidic protein (GFAP)	Sigma	1:2000
Rabbit anti-somatostatin (SST)	Peninsular laboratories	1:100
Rabbit anti-neuropeptide Y (NPY)	Insight	1:1000
Rabbit anti-parvalbumin	Chemicon	1:1000
Mouse anti-calbindin	Swant	1:1000
Rabbit anti-calretinin	Swant	1:1000
Mouse anti-reelin	Gift from A. Goffinet	1:2000
Rabbit anti-Iba1	Synaptic Systems	1:1000
Rabbit Ki67 polyclonal	Novacastra	1:200
Rabbit cleaved caspase 3	Cell signalling	1:200

Table 2.3. Primary antibodies used for the experiments described in this thesis, their dilution and supplier.

Secondary Antibodies	Supplier	Dilution
Donkey anti-rabbit 647	Molecular Probes	1:1000
Goat anti-mouse IgG 568	Molecular Probes	1:200-1000
Goat anti-mouse IgM 488	Molecular Probes	1:1000
Goat anti-rat 555	Molecular Probes	1:200-500
Goat anti-rat 350	Molecular Probes	1:200
Goat anti-rabbit 568	Molecular Probes	1:200
Goat anti-rabbit 633	Molecular Probes	1:200
Goat anti-chicken IgY CY5.5	Abcam	1:200

Table 2.4. Secondary antibodies used for the experiments described in this thesis, their concentration and supplier.

Chapter 3: Dorsally- and ventrally-derived oligodendrocytes have similar electrical properties but myelinate preferred tracts

3.1 Introduction

Oligodendrocytes are generated from both dorsal and ventral germinal regions of the embryonic neural tube, under the influence of different inductive signals (see chapter 1.3.1). In the developing spinal cord, most OPCs arise from the ventral ventricular zone (VZ) under the influence of Sonic Hedgehog (SHH), but a minority are generated from the dorsal VZ in a SHH-independent manner (possibly under the influence of Wnt, FGF and BMP signalling). In the developing forebrain too, OPCs arise from both the ventral and the dorsal VZ. Since the discovery of both dorsally and ventrally derived populations of OL lineage cells in the brain and spinal cord, an important question has been whether they are functionally identical or specialised in some way. In order to visualise dorsally and ventrally derived OLs, I used a dual reporter mouse line in which OLs are fluorescently labelled green or red, depending on their origin in the VZ (see Chapter 2.13). In both the spinal cord and corpus callosum I patch-clamped dorsally- and ventrally-derived OLs, at different developmental stages of the oligodendrocyte lineage, and compared their electrophysiological and morphological properties to investigate whether they are functionally distinct.

3.2 Methods

Transgenic mice generation

An OL lineage-specific dual reporter mouse line *Sox10-lox-eGFP-STOP-lox-tdTomato* (referred to as *Sox10-GFP/tdTom*) was generated by PAC (Phage Artificial Chromosome) transgenesis by Richa Tripathi (see methods, chapter 2 section 2.13). This line was designed to label Sox10-expressing OPCs and differentiated OLs constitutively with enhanced GFP or conditionally (in the presence of Cre recombinase) with tandem-duplicated Tomato (tdTom).

A 120 kb fragment of the *Sox10* genomic PAC (Phage Artificial Chromosome) (RP21-427-F18) was used, which includes 60 kb upstream and 50 kb downstream of *Sox10* (Fig. 3.1A)**.** The genomic region spanning exons 3–5 was replaced by *loxP-eGFP-polyA-loxP-tdTomato-frt-Cm^r-frt* (Fig. 3.1A) by homologous recombination in *Escherichia coli* bacteria (Lee et al., 2001). The chloramphenicol resistance cassette (*Cm^r*), inserted to allow selection of correctly recombined clones in bacteria, was

removed by transient activation of Flp recombinase with arabinose (Fig. 3.1A) before pronuclear injection into mouse embryos. In the absence of Cre recombinase, only eGFP is expressed since the *polyA4* cassette directs the cleavage of the RNA transcript upstream of the tdTom. Ten founders were generated by pronuclear injection, eight of which transmitted the transgene in roughly Mendelian ratios and expressed eGFP strongly in the expected pattern. One male founder was used to establish a line for further study.

These *Sox10-GFP/tdTom* mice were crossed to *Gsh2-iCre, Emx1-iCre* lines (Kessaris et al., 2006), or to a *Msx3-iCre* line. In *Sox10*$^{+}$ cells that express Cre recombinase, the *eGFP-polyA* cassette is removed, activating expression of *tdTom* instead (Fig. 3.1A).

Brain and spinal cord slices

Coronal forebrain slices (225 µm thick) were prepared from P9-12 *Gsh2-Cre:Sox10-GFP/tdTom* mice (in which dorsally derived cells are green and ventrally derived cells are red) and longitudinal spinal cord slices (150-160µm thick) were prepared from P6-14 *Msx3-Cre:Sox10-GFP/tdTom* mice (in which dorsally derived OL cells are red, and ventrally derived cells are green). Slices were superfused at room temperature (~23℃) with HEPES-buffered solution, containing (mM) 144 NaCl, 2.5 KCl, 2.5 $CaCl_2$, 10 HEPES, 1 NaH_2PO_4, and 10 glucose, pH 7.4 (adjusted with NaOH).

Patch clamp recordings

Whole-cell recordings were made from OPCs and OLs that expressed GFP or tdTom. OPCs were distinguished from differentiated OLs by morphology (OPCs are bipolar or stellate cells, OLs have long processes aligned with axons) and by the change in membrane current induced by changing the cell membrane potential from −110 to +30 mV in 20 mV steps. The steady-state I–V plots are approximately ohmic (linear) with mild outward rectification for mature OLs and more outwardly rectifying for OPCs (see Fig. 3.4 and 3.5). Electrodes were pulled from thick-walled borosilicate glass to a resistance of 6–9 MΩ and filled with a K-gluconate-based solution containing the following (in mM): 130 K-gluconate, 4 NaCl, 0.5 $CaCl_2$, 10 HEPES, 10 BAPTA, 4 MgATP, 0.5 Na_2GTP, and 2 K-Lucifer yellow (or 0.052 Alexa Fluor 568), pH 7.3 (adjusted with KOH). Drugs (NMDA 60 µm, kainate 100 µm, and GABA 100 µm) were applied in the superfusion solution.

Antibody labelling

Cryosections were prepared and labelled as described in detail in chapter 2, section 2.14.

Cell counts

For cell counts in the corpus callosum, at least three sections per animal were examined. For cell counts in the dorsal funiculus, three sections at each spinal level (cervical, thoracic, and lumbar) were examined. This was because the corticospinal axons are still extending caudally during early postnatal development. For cell counts in the rubrospinal tract and ventral funiculus, three sections at cervical level only were examined. Data are quoted as mean ± SEM (n = number of mice). The length of the cervical spinal cord (C1–C8) was measured in fixed, dissected spinal cords at P13 (5.3 ± 0.4 mm) and P67 (8.0 ± 0.1 mm).

Tract tracing

The anterograde tracer biotinylated dextran amine (BDA, Invitrogen) was used to label the corticospinal tract (CST) and the rubrospinal tracts (RSTs) in *Msx3-Cre:Sox10-GFP/tdTom mice* (Hossain-Ibrahim et al., 2007). The mice (P51–P64) were anesthetized and the skull opened. Then, 10% (w/v) solution of BDA in 0.1 M PBS was injected using stereotactic apparatus in the right primary motor cortex (4 sites, 0.4 µl at each site) and the right red nucleus (2 µl at one site) to label the CST and RST, respectively. The mice were humanely killed 12 days after BDA injection (P63–P72, referred to as P67).

Statistics

This is described in detail in chapter 2, section 2.15.

3.3 Results

3.3.1 Generation of SOX10 GFP/tdTom dual reporter mice

An OL lineage-specific dual reporter mouse line *Sox10-lox-eGFP-STOPlox-tdTomato* (referred to as *Sox10-GFP/tdTom*) was generated by PAC transgenesis (Fig. 3.1A and chapter 2 section 2.13) (Tripathi et al., 2011). This line was designed to label Sox10-expressing OPCs and differentiated OLs constitutively with enhanced GFP (Zhang et al., 1996) (e.g., Fig. 3.1B,E) or conditionally (in the presence of Cre recombinase) with tandem-duplicated Tomato (tdTom) (Shaner et al., 2004). In the

absence of Cre, 96% ± 0.2% (n=3 mice) of SOX10-immunoreactive cells also expressed GFP in the corpus callosum at P12/13 (Fig. 3.1H). In P10–P13 spinal cord white matter, 86 ± 4% (n=4 mice) of SOX10+ cells were GFP+ (Fig. 3.1H). In both brain and spinal cord, 98 ± 1% of GFP+ cells were also SOX10+ (not shown). In addition, immunolabelling with anti-GFP together with monoclonal antibody CC-1, which labels differentiated OLs (Fig. 3.2A–C), or anti-OLIG2, which labels all stages of the OL lineage (Fig. 3.2D–E), confirmed that the vast majority of OL lineage cells were labelled by GFP (94.6 ± 0.7% (n=3 mice) of CC1+ cells and 91.9 ±1.6% of OLIG2+ cells (n=3 mice) in the corpus callosum between P10 and P13 were GFP+). As expected, there was no expression of tdTom in brain or spinal cord in the absence of Cre (not shown). In the presence of Cre, the *eGFP-STOP* cassette was excised and tdTom was expressed instead (see Fig. 3.3 and below), thereby fluorescently labelling OLs green or red, depending on their origin.

3.3.2 The postnatal corpus callosum is mainly populated by dorsally derived OLs

It has been shown previously that NG2-expressing OPCs in the postnatal rat cerebellar white matter and corpus callosum fall into two classes—those that express voltage-gated Na^+ channels and receive synaptic input and others that do not (Karadottir et al., 2008). It has also been reported that the postnatal corpus callosum is firstly populated by OPCs that migrate from the ventral telencephalon before birth, intermingled with OPCs that develop locally within the cortex after birth (Kessaris et al., 2006). This raised the possibility that the two electrical subtypes of OPCs might correspond to the two developmental subgroups. I tested this by patch clamping OPCs in *Gsh2-Cre:Sox10-GFP/tdTom* double-transgenic mice.

In the telencephalon, *Gsh2-Cre* is expressed in the lateral ganglionic eminence (LGE) and the dorsal part of the medial ganglionic eminence (MGE) (i.e., the region coloured red in Fig. 3.3A). The ventral MGE (which expresses *Nkx2.1* but not *Gsh2*) makes a negligible contribution to the cortical OL population after P10 (Kessaris et al., 2006). In *Gsh2-Cre : Sox10-GFP/tdTom mice*, OL lineage cells derived from the LGE and dorsal MGE should have their GFP coding sequences removed by Cre recombinase and consequently fluoresce red (tdTom), while those from the developing cortex, which do not undergo Cre recombination, fluoresce green (GFP) as schematised in Fig. 3.1A. As expected, the cortical grey and white matter contained intermingled red- and green-labelled cells, reflecting a mixture of ventrally and dorsally derived OL lineage cells (Fig. 3.3C). In these mice, the red cells are undoubtedly ventral in origin, but green cells could either be genuinely dorsal in origin or else

ventrally derived cells that somehow escaped Cre recombination, e.g., because Cre protein is expressed at too low a level to bind the *lox* recombination sites efficiently. This uncertainty was resolved by crossing *Sox10-GFP/tdTom to Emx1-Cre* mice, which express Cre (hence activating tdTom expression) in a reciprocal pattern to *Gsh2-Cre*, i.e., in the cortical VZ but not in the LGE or MGE (i.e. the region coloured red in Fig.3.3B). Cells that are labelled red by *Gsh2-Cre* will remain green in *Emx1-Cre* and vice versa. It follows that the proportion of OL lineage cells that is labelled red by *Gsh2-Cre* plus the proportion that is labelled red by *Emx1-Cre* should equal 100%. We found that 23 ± 1% (n = 7 mice) of OL lineage cells in the P12/13 corpus callosum were recombined red by *Gsh2-Cre* and 81 ± 1% (n = 5 mice) by *Emx1-Cre* (Fig. 3.3C-G). Since the sum of these contributions is not significantly different from 100%, we can infer that (1) Cre recombination efficiency is close to 100% in both *Emx1-Cre* and *Gsh2-Cre* (i.e., no cells escape the action of Cre) and (2) ~80% of OL lineage cells in the postnatal corpus callosum are generated locally in the cortical VZ, the remaining ~20% migrating in from the LGE and MGE.

3.3.3 Dorsally and ventrally derived OL lineage cells in the corpus callosum have similar electrical properties

Having determined that the dual reporter system reliably distinguishes ventrally and dorsally derived cells, I made electrophysiological recordings from dorsally and ventrally defined cells with the morphology of OPCs (dOPCs and vOPCs) in the corpus callosum of acute vibratome forebrain slices of *Gsh2-Cre:Sox10-GFP/tdTom* mice at P9–P12 (median age P11). Figure 3.4, A and B, shows representative images and current traces obtained from vOPCs (tdTom-expressing, red) and dOPCs (eGFP-expressing, green). Before recording, the cells were identified by their expression of red or green fluorescence (Fig. 3.4A,B, top images). They were then whole-cell clamped using an internal solution containing a green or red dye (for the red and green cells, respectively: Fig. 3.4A,B, middle images), allowing colocalization of the fluorescent reporter protein and the pipette dye to demonstrate that the correct cell had been patch clamped (Fig. 3.4A,B, bottom images). OPC status (as opposed to OL) was defined by their morphology (recognising that this might include some cells that were differentiating and downregulating their voltage-gated Na^+ channels: see chapter 4).

On applying 20 mV voltage steps from a holding potential of −70 mV (Fig. 3.4A, B, top traces), depolarization was seen to evoke a transient inward (Na^+) current in the majority of cells, followed by a more sustained outward (K^+) current (Karadottir et al., 2008). Subtraction of the linearly scaled capacity transient and (ohmic) current evoked

by hyperpolarizing steps revealed a clear transient inward Na^+ current (I_{Na}) that partly overlapped with the onset of the K^+ current (Fig. 3.4A, B, bottom traces). As previously reported (Karadottir et al., 2008), ~35% of fluorescing cells with OPC morphology lacked detectable Na^+ current, but the presence or absence of I_{Na} did not correlate with the developmental origin of the cells (10 of 17 vOPCs and 11 of 15 dOPCs displayed Na^+ currents; not significantly different, $p = 0.63$). Some of the I_{Na}-negative cells presumably were OPCs that were differentiating into mature OLs (De Biase et al., 2010; Kukley et al., 2010), while others were NG2-expressing OPCs that lacked significant Na^+ current (Karadottir et al., 2008).

The capacitance of OPCs (Fig. 3.4C), their membrane resistance near the resting potential (Fig. 3.4D), and the net inward current that I_{Na}-expressing OPCs generated on depolarization from −70 mV to +10 mV (Fig. 3.4E) did not differ significantly between dOPCs and vOPCs. Similarly, the responses of I_{Na}-expressing OPCs to neurotransmitter application did not differ significantly. Kainate and NMDA evoked inward currents at −70 mV, while GABA evoked an outward current at −40 mV (Fig. 3.4F) but the amplitudes of these currents were indistinguishable between the OPCs of different origin (Fig. 3.4G). Thus, although I confirmed the existence of two electrical subtypes of cell with OPC morphology in the corpus callosum, I determined that these do not correspond to dOPCs versus vOPCs.

Similarly, the electrical properties of cells with the morphology of mature myelinating OLs derived from the ventral VZ (tdTom-expressing vOLs, red) (Fig. 3.5A) or dorsal VZ (eGFP-expressing dOLs, green) (Fig. 3.5B) did not differ significantly. Their current response to voltage steps was approximately ohmic with slight outward rectification (Fig. 3.5A, B), with a membrane resistance at −70 mV that was not significantly different between dOLs and vOLs (Fig. 3.5C). dOLs and vOLs were found to myelinate a similar range of numbers of internodes (between 2 and 21, the distribution of which did not differ significantly: $p = 0.45$ comparing dOLs and vOLs) (Fig. 3.5D). Accordingly, the mean number of internodes was not different for dOLs and vOLs ($p = 0.2$) (Fig. 3.5E). Their responses to kainate and NMDA were also not significantly different from one another (Fig. 3.5F, G).

3.3.4 Dorsally and ventrally derived OL lineage cells in the spinal cord have similar electrical properties

The VZ of the developing spinal cord is composed of a series of discrete progenitor domains, known as p3, pMN, p2, p1, and p0 in the ventral half of the cord

and dP6 to dP1 in the dorsal half (reading ventral to dorsal) (Fig. 3.6A). Each progenitor domain generates a characteristic subset of spinal neurons before switching to production of glial cells (astrocytes and/or OPCs). Most OPCs in the spinal cord are generated from the pMN domain in the ventral VZ, but a minority are generated outside pMN, mainly from the dorsal VZ (Cai et al., 2005; Fogarty et al., 2005; Vallstedt et al., 2005).

Dorsal OPCs and their differentiated dOL progeny were specifically marked by crossing *Sox10-GFP/tdTom* mice with *Msx3-Cre* mice (Msx3 is expressed in progenitor domains dP1–dP5), with or *Gsh2-Cre* mice (Gsh2 is expressed in dP3–dP5, Fig. 3.6A). In P12/13 double-transgenic animals, *Gsh2*-derived cells were 10 ± 2% (n = 3 mice) of all OL lineage cells in the cord, whereas *Msx3*-derived cells were 17 ± 1% (n = 5 mice) of the total. This is in keeping with the broader expression domain of *Msx3* and indicates that dP1 and/or dP2 give rise to some OL lineage cells in addition to dP3–dP5. Thereafter, *Msx3-Cre* was used to label dorsally derived OPCs and OLs in the spinal cord. *Msx3*-derived OL lineage cells (red) were concentrated in the dorsal and dorsolateral funiculi (Fig. 3.6B, C, D), whereas vOPCs (green) were distributed widely throughout the cross section of the cord (Fig. 3.6C). This confirms previous reports that dOPCs are less migratory than their vOPC counterparts. This could either be an intrinsic difference or reflect the fact that dOPCs appear late-after vOPCs have already colonized the cord-and are outcompeted by vOPCs for migration- or proliferation-inducing factors (e.g., platelet-derived growth factor, PDGF-AA). Consistent with the latter idea, dOPCs proliferate and migrate more than normal when vOLs are absent in *Nkx6.1/Nkx6.2* double-null mice (Cai et al., 2005; Vallstedt et al., 2005) and when the PDGF-AA supply is increased experimentally (Calver et al., 1998; van Heyningen et al., 2001).

Red (tdTom-expressing, dorsally derived) and green (GFP-expressing, ventrally derived) OL lineage cells in the dorsal and dorsolateral funiculi of the P6–P14 spinal cord were recorded from (median age P8). Patch-clamped cells were identified as OPCs and mature OLs from their morphology and membrane current properties, as described previously for recordings in brain slices. Spinal cord OPC-morphology cells, like those in brain, fell into two classes, either with or without Na^+ currents, and the mean capacitance of the cells without I_{Na} was larger (Fig. 3.7A). The membrane resistance of dOPCs and vOPCs with I_{Na} was not significantly different (Fig. 3.7B), and this was also true for dorsally and ventrally derived mature OLs. However, the resistance of vOPCs without I_{Na} was larger than that for dOPCs. This was the only electrophysiological difference I found between dOPCs and vOPCs, but it would

become insignificant if correction were made for multiple comparisons. The presence or absence of I_{Na} did not correlate with the developmental origin of the cells, because dOPCs and vOPCs were both found either with or without I_{Na} (10 of 16 dOPCs and 10 of 16 vOPCs expressed I_{Na}). In I_{Na}-expressing cells, the peak inward current (evoked by a step from −70 mV to +10 mV) was not significantly different between the two groups (Fig. 3.7C). Dorsally and ventrally derived mature OLs myelinated a similar range of number of internodes (between 2 and 6, the distribution of which did not differ significantly: $p = 0.21$ comparing dOLs and vOLs) (Fig. 3.7D). Consequently, the mean number of internodes did not differ significantly between dOLs and vOLs ($p = 0.23$) (Fig. 3.7E). There were no significant differences between dOPCs and vOPCs with I_{Na} in their responses to 100 µM GABA (at −40 mV) or to 100 µM kainate or 60 µM NMDA (at −70 mV) (Fig. 3.7F), nor between dOLs and vOLs in their responses to kainate and NMDA (Fig. 3.7G).

3.3.5 Tract preferences of dorsally and ventrally derived oligodendrocytes in the spinal cord

At P7, the most ventral part (base) of the dorsal columns, where the developing cortical spinal tracts (CSTs) run, was devoid of dOPCs/dOLs and contained few vOPCs/vOLs compared to other regions of developing white matter (Fig. 3.8B, E). This could be because most corticospinal projections have not yet reached the spinal cord; the first corticospinal axons reach lumbar (L5) spinal cord at P6–P9, and the CST does not achieve its full size until ~P14 (Bareyre et al., 2005; Gianino et al., 1999). It makes sense that OL lineage cells should be excluded from the paths of growing axons, since myelin components (several of which are expressed at a low level by OPCs) are known to be inhibitory for axon outgrowth. Since neither the CST nor the rubrospinal tracts (RSTs) could be specifically labelled at this early age, an anatomical atlas was referred to (Watson et al., 2008) to locate these tracts at P7 and P13. At P7, there were only a few ventrally derived OL lineage cells in the CST and even fewer dorsally derived cells (Fig. 3.8B, E). At cervical levels, for example, only ~8% of OL lineage cells in the CST were dorsally derived, the remaining ~92% being ventrally derived (Fig. 3.8H). By P13, there were many OL lineage cells in the CST, still mainly ventrally derived although the dorsal contribution had also increased (Fig. 3.8C, F). In the cervical CST, for example, the dorsal contribution had increased from ~8% to ~34% (Fig. 3.8H). In neighbouring dorsal tracts, such as the fasciculus gracilis and fasciculus cuneatus (which are ascending sensory tracts), the opposite was true - at cervical level, ~63% of labelled cells in these tracts were dorsally derived at P13 (data not shown). The RSTs in the

dorsolateral funiculi were equally populated by dorsally and ventrally derived OL lineage cells at P13 (50 ± 2% were dorsally derived, n = 3 mice). At this stage, only a minor proportion of labelled OL lineage cells in the ventral funiculus was dorsally derived (10 ± 3%, n = 3 mice).

These observations suggested that there were some tract preferences of dorsally and ventrally derived OLs. To see whether this persisted long-term, adult *Msx3-Cre:Sox10-GFP/tdTom* spinal cords were examined. Unexpectedly, it was found that the dorsal funiculus, especially the CST, was populated predominantly by dorsally derived OLs at P67 (Fig. 3.8D, G; I show that the cells are mainly OLs and not OPCs below in Fig. 3.9N-Q), the reverse of the situation at P7 and P13 (Fig. 3.8B, C, E, F). (The locations of tracts are shown in Fig. 3.8A.) This suggests that the dorsal OL lineage displaces the ventral lineage between P13 and P67 in this tract.

If the absolute number of vOLs in the dorsal funiculus did not change between P13 and P67, the number of vOLs per section would be expected to decrease ~1.5-fold because the length of the spinal cord increases ~1.5-fold during this time with a concomitant increase in volume (see section 2 of this chapter; since cells were counted in the whole area of the dorsal funiculus - i.e., a larger area at P67 than at P13 - growth in the radial plane is automatically taken into account). However, the number of vOLs per section across the whole area of the dorsal funiculus at cervical level decreased 3.8-fold between P13 and P67 (from 110 ± 9 to 29 ± 4, n = 3 mice) (Fig. 3.8I), which cannot be explained simply by the increased length of the cord-the absolute number of vOLs must have decreased ~2.5-fold (i.e., 3.8/1.5). The number of dOLs per section remained constant from P13 to P67 (156 ± 17 and 163 ± 26, respectively, n = 3 mice) (Fig. 3.8I). Because of the increased length of the cord, the absolute number of dOLs must therefore have increased ~1.5-fold during this period. Thus, the number of dOLs rises as the number of vOLs falls, suggesting that vOLs are replaced by dOLs. However, it is not simply a matter of one-to-one replacement because the total number of vOLs plus dOLs decreased modestly from P13 to P67 (from ~266 to ~192 per section).

To confirm the location of the CST, the anterograde tracer BDA was injected into the right primary motor cortex of P67 mice (performed by P.Anderson) and we examined the spinal cord 12 d later (see section 3.2). In 3 of 3 injected animals, the CST was labelled unilaterally on the left. Within the BDA-labelled area, the majority of OL lineage cells were dorsal in origin (red) at all rostrocaudal levels (Fig. 3.9A-C). For example, 88 ± 3% (n = 3 mice) of labelled OL lineage cells in the cervical CST were

dorsally derived (as shown previously in Fig. 3.8H). In addition, the RSTs were also labelled by unilateral BDA injection into the red nucleus in the midbrain. This was less reproducible - only 2 of 7 injected mice had any RST labelling. Using this BDA labelling as a guide, the cells in the region of the RST were counted and it was found that they were populated mostly by dorsally derived OLs (79 ± 5%, n = 3 mice; not shown). In contrast, ventral and ventrolateral tracts were occupied mainly by ventrally derived OPCs and OLs, as expected (Fig. 3.9D, E), although the proportion of dorsally derived cells increased with age, from 10 ± 3% (n = 3 mice) at P13 to 24 ± 4% (n = 3 mice) at P67.

At P67, the GFP and tdTom signal intensities in individual cells were reduced relative to P13 and the labelled cells were smaller, both effects being more pronounced in white matter compared to grey matter and more obvious for GFP than tdTom. The sum of GFP^+ and $tdTom^+$ cell counts in the dorsal funiculus at P67 amounted to 80 ± 5% (n = 3 mice) of all SOX10-immunoreactive cells in the dorsal funiculus, which is not significantly different (p = 0.22) from the number of $SOX10^+$ OL lineage cells that expressed GFP in *Sox10-GFP/tdTom* spinal cords at P13 (86 ± 4%, n = 4 mice) (Fig. 3.1H). Similarly, the sum of the GFP^+ and $tdTom^+$ cells in adult spinal cord white matter amounted to 89 ± 3% (n = 3 mice) of all $OLIG2^+$ cells (Fig. 3.9F-I), and 88 ± 4% (n = 3 mice) of all CC-1^+ cells (Fig. 3.9J-M), indicating that the majority of these cells are mature OLs. The sum of the GFP+ and tdTom+ cells in the spinal cord (at P13 and P67) did not reach 100%, suggesting that the *Sox10-GFP/tdTom* transgene does not recombine in all OLs in the spinal cord. However, despite this, since a consistent number of OLs (86 ± 4% and 80 ± 5%, at P13 and P67, respectively) are labelled with either GFP or tdTom at P13 and at P67, this suggests that the expression levels of either label do not fall below the levels of detection, and that the OL population can be reliably identified at both ages in the *Sox10-GFP/tdTom* reporter mouse. Also, almost all $SOX10^+$ cells in the adult were $OLIG2^+$, confirming them as OL lineage (98.4 ± 0.1% (n = 3 mice) of all SOX10+ cells were $OLIG2^+$ and 96.8 ± 0.4% (n = 3 mice) of all $OLIG2^+$ cells were $SOX10^+$ in double-immunolabel experiments (Fig. 3.9N-Q), further confirming OLs express both markers in the spinal cord in adulthood.

3.4 Discussion

Since the demonstration that there are both dorsally and ventrally derived populations of OL lineage cells in the spinal cord and brain (Spassky et al., 2001; Cai et al., 2005; Fogarty et al., 2005; Vallstedt et al., 2005; Kessaris et al., 2006), an outstanding question has been whether these are functionally identical or specialized in

some way (Miller, 2005). As the two populations of OLs are specified by different signalling pathways - the ventral cells depend on SHH, whereas the dorsal cells are SHH independent - it might be expected that the two populations differ. Additionally, different subtypes of OPCs and OLs have been described by a variety of criteria, including differences in the electrophysiological properties of OPCs (Chittajallu et al., 2004; Karadottir et al., 2008) in brain regions where these cells develop to produce a wide range of OL morphologies (del Rio-Hortega et al., 1921, 1928; Bjartmar et al., 1994; Weruaga-Prieto et al., 1996; Murtie et al., 2007; Bakiri et al., 2009; Vinet et al., 2010). In this chapter, I have shown, using a dual reporter mouse, that despite different sites of origin, dorsally- and ventrally-derived OL lineage cells are electrically and morphologically similar. However, despite being electrically identical, interesting differences in the settling positions of OL lineage cells that develop from dorsal and ventral regions of the spinal cord were discovered.

3.4.1 Dorsally and ventrally derived OL lineage cells are electrically similar

Using the dual-reporter mice, I was able to ask whether the ventrally and dorsally derived OL lineages correspond to different electrical subtypes. However, no significant electrophysiological differences could be detected between dOPCs and vOPCs. Both populations were an approximately 2:1 mixture of cells with or without significant voltage-gated Na^+ current, and their input resistances were similar. Because I defined OPCs solely by their morphology in these experiments, it is possible that, in addition to true NG2-expressing OPCs that lack voltage-gated Na^+ currents (Karadottir et al., 2008 and see chapter 4), some of the I_{Na}-negative cells I recorded from were already differentiating into OLs and had downregulated NG2 and Na^+ channel expression before changing their morphology (De Biase et al., 2010; Kukley et al., 2010). Both vOPCs and dOPCs had a similar membrane capacitance, arguing against a consistent morphological difference. vOLs and dOLs also appeared indistinguishable, having a similar membrane resistance and myelinating the same number of axons. vOPCs/vOLs and dOPCs/dOLs also reacted similarly to the neurotransmitter agonists kainate (to activate AMPA and kainate receptors), NMDA and GABA.

It is possible that other electrical differences between vOPCs and dOPCs could exist that were not examined by this study, for example they could differ in terms of the synapses they receive from neuronal axons. OPCs derived from different lineages may receive synaptic inputs from either excitatory or inhibitory neurons (or both), or the properties of these currents could be distinct (e.g. OPCs could receive synaptic inputs at different frequencies and/or amplitudes). The fact that both vOPCs and dOPCs

responded similarly to the application of excitatory and inhibitory neurotransmitters suggests that they express the appropriate receptors to respond to glutamate and/or GABA release from neuronal axons. Receiving different synaptic inputs from neuronal axons might provide an electrical mechanism by which OPC survival, differentiation and subsequent myelination could be controlled by specific tracts. Alternatively different molecular cues, which were not examined in this study, could account for the myelination of specific tracts as discussed in more detail below.

3.4.2 Tract preferences of dorsally and ventrally derived OLs

Interesting differences in the settling positions of OL lineage cells that develop from the dorsal versus the ventral VZ of the spinal cord were discovered. Since dorsal regions in the spinal cord are largely sensory, while ventral regions are largely motor, perhaps the modality of the axon is matched to the source of OLs (Miller, 2005). Consistent with previous studies, it was confirmed that vOPCs appear around E12.5 and migrate widely throughout the cross section of the cord, populating all developing white matter tracts, including those in the dorsal funiculus, before dOPCs appear around E15.5 (for review, see Richardson et al., 2006). dOPCs were less migratory and remained mainly (though not exclusively) in the dorsal half of the cord. Strikingly, they appeared gradually to displace ventrally derived cells from dorsal axon tracts. The dorsal and dorsolateral funiculi at cervical levels contained similar numbers of ventrally and dorsally derived OL lineage cells at ~P13 (e.g. ~50% were ventrally derived in the RSTs and ~66% in the CST) (Figs. 3.6B, 3.8H), but, after that, dorsally derived cells took over and by P67 comprised >80% of all OL lineage cells in the RST, CST, and the dorsal funiculus as a whole. The large majority of ventrally derived OL lineage cells in the dorsal funiculus were CC-1$^+$ differentiated OLs even at P13, so the fact that the absolute number of vOL lineage cells decreased after P13 while the dOL lineage did not change much (in the cervical cord at least, Fig. 3.8I) strongly suggests that dOLs have some selective advantage over vOLs in dorsal axon tracts.

The *Sox10-GFP/tdTom* dual reporter used in this study failed to detect ~14% of OL lineage cells in the P13 spinal cord using our *Sox10-GFP/tdTom* reporter - i.e., ~14% of SOX10$^+$ OPCs/OLs did not express GFP in the absence of Cre. In the brain, the equivalent figure was ~4%. There is no obvious explanation for why the *Sox10* transgene is apparently inactive in a proportion of OL lineage cells, or why this proportion should be higher in the spinal cord than the brain. In the calculations above, the assumption was made that the "missing" ~14% of cells does not include a disproportionate number of either ventrally or dorsally derived OL lineage cells. If all the

missing cells happened to be ventrally derived, or all happened to be dorsally derived (and if the assumption is made that the same percentage of such cells were missing at P67 as at P13), then the calculated decrease in the number of vOLs/section between P13 and P67 would still be 3.8-fold, but the final contribution of dOLs to the dorsal funiculus would be ~80% or ~88% of the total, respectively, rather than ~85%. Thus, although there is no reason to think that the missing cells should be mainly ventrally or dorsally derived, even if this were the case the conclusions in this study would not be greatly affected.

Competition for myelination between ventrally and dorsally derived OL lineage cells has been previously described in the corpus callosum and overlying cortex (Kessaris et al., 2006). In the brain, the fraction of OL lineage cells in the corpus callosum that was derived from the most ventral part of the forebrain VZ (*Nkx2.1*-expressing) started high but declined rapidly after birth, so that, by P10, <10% of OPCs/OLs in the corpus callosum (and even less in the cortex) were *Nkx2.1* derived, and by P30, there were essentially none, their place being taken by more dorsally derived OLs (Kessaris et al., 2006). Many factors could explain the apparent selective advantage that dOLs have over vOLs in dorsal axon tracts of the spinal cord observed in this study. dOLs might, for example, have a higher affinity than vOLs for dorsal axons or they might respond preferentially to survival factors released by dorsal axons. The homophilic cell adhesion molecule L1CAM appears to play an especially important role in the development and myelination of the CST compared to other spinal tracts (Joosten and Gribnau, 1989; Cohen et al., 1998; Dobson et al., 2001; Jakeman et al., 2006), so it is conceivable that the CST and other dorsal axons might have adhesive properties that favour dOLs over their ventral counterparts. Alternatively, inhibitory signals could be released from vOLs in the ventral spinal cord, preventing the migration and survival of dOLs outside of the dorsal spinal cord. Instead, there might be continual turnover of OLs in the dorsal funiculus and the dying OLs might be preferentially replaced by differentiating dOPCs.

At this point, the mechanism by which dOLs come to outnumber vOLs can only be speculated about. Whatever the mechanism, there is effectively a competition between the ventral and dorsal lineages. Gene expression profiling of vOL and dOL lineage cells from our dual reporter transgenic mouse, which was not within the scope of this study, may shed light on the mechanism by which dOLs outcompete vOLs. OLs may express different genes or higher levels of particular genes depending on their site of origin, for example dOLs may specifically express adhesion molecule genes or

survival genes, enabling them to reside within and myelinate dorsal tracts tracts more effectively.

3.4.3 Tract preferences of dorsally and ventrally derived OLs and consequences for remyelination

The finding that dOLs and vOLs compete to myelinate specific tracts within the spinal cord raises the question of whether this competition exists in the context of remyelination following a demyelinating disease or injury. In a recent study, Zhu et al., (2011b) investigated remyelination following focal demyelination of the spinal cord. In response to demyelination at a ventral region of the spinal cord, dOPCs migrated to, and proliferated in, the area of lesion, to provide a large number of newly differentiated oligodendrocytes (Zhu et al., 2011b). These data suggest that dOLs may provide an important source of OPCs for axon remyelination. It is plausible that vOLs predominantly myelinate neuronal axons during early development, whereas dOLs myelinate axons at later stages in life and play a more important role in myelin turnover and injury-induced remyelination. If a tendency exists for dOLs to dominate the remyelination process, this finding might influence our strategic approach to myelin regeneration in the future. For example in studies where OPCs are transplanted to promote remyelination (Windrem et al., 2008), it might be advantageous to transplant dOPCs rather than vOPCs or a mixture of the two.

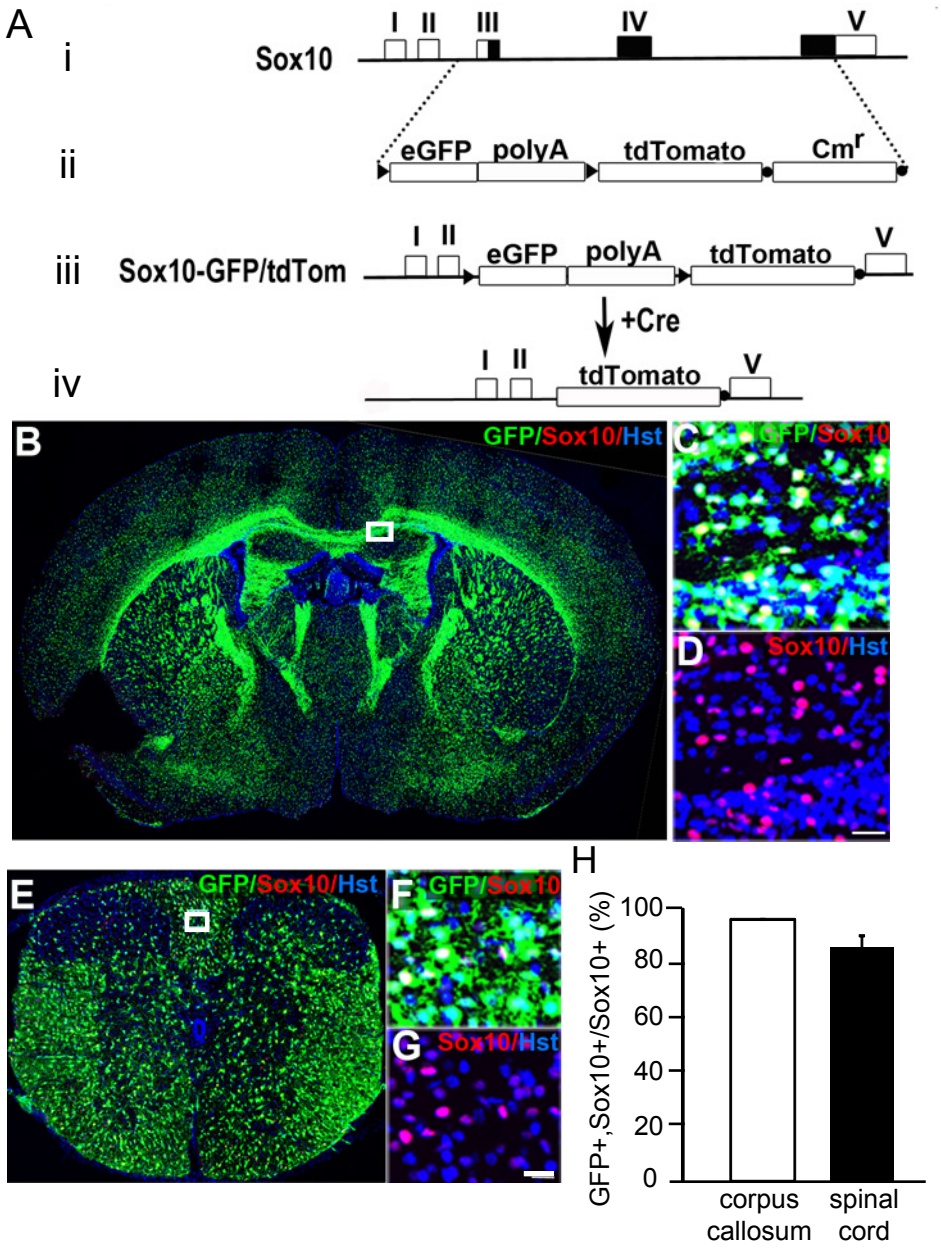

Figure 3.1. Generation and characterization of *Sox10-GFP/tdTom* dual reporter mice.

A. The DNA sequence displays the intron and exon structure of the Sox10 locus (**i**). The dashed section of DNA shows the Sox10 PAC (Phage Artificial Chromosome) sequence, loxP-eGFP-(polyA)4-loxP-tdTom-frt-CmR-frt (**ii**), that replaced the DNA between exons 3 and 5 (**i**). LoxP sites are represented by black arrows and Flippase recognition target (Frt) sites are represented as black circles (**ii**). The chloramphenicol resistance cassette (Cm^r), inserted to allow selection of correctly recombined clones in bacteria, was removed with flip-recombinase before microinjection into mouse embryos. In the absence of Cre recombinase, only eGFP is expressed since the polyA4 cassette directs the cleavage of the RNA transcript upstream of the tdTom (**iii**). When the Sox10-GFP/tdTom dual reporter mice are crossed with Cre mice, in $Sox10^+$ cells that express Cre, the eGFP-polyA cassette between the loxP sites is removed, activating the expression of tdTom instead (**iv**). As expected, in the absence of Cre, expression of GFP (green) was noted in a majority of $SOX10^+$ cells (red) in the forebrain (**B–D**) and spinal cord (**E–G**). Boxed areas in **B** and **E** are shown at higher magnification in **C**, **D**, and **F**, **G**, respectively. Cell counts at P10–P13 (**H**) revealed that ~96% (n = 3 mice) of SOX10+ cells in the corpus callosum and ~86% (n = 4 mice) of SOX10+ cells in the spinal cord white matter were GFP+ (data shown as mean ± SEM).Scale bars: D, G, 20 μm.

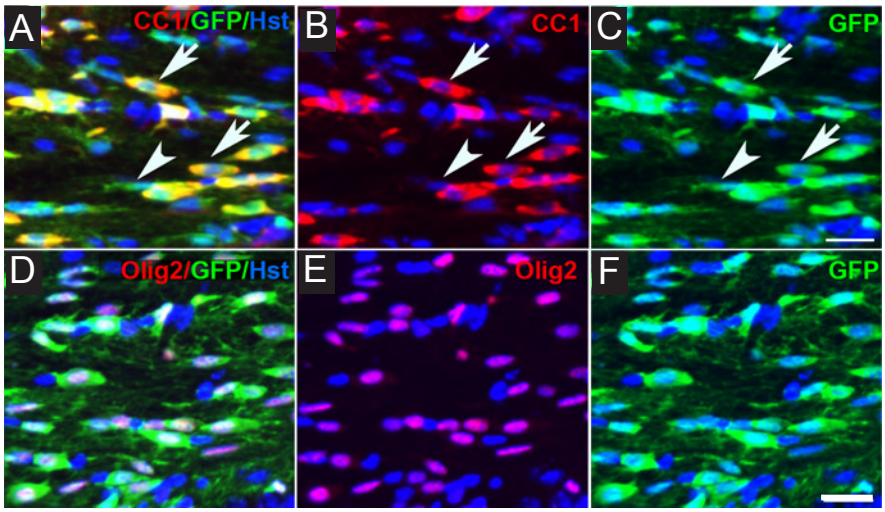

Figure 3.2. **The majority of oligodendrocyte lineage cells express GFP.**
GFP+ cells (green) were confirmed to be OL lineage by double immunolabeling spinal cord white matter for CC-1, which labels differentiated OLs (red, **A–C**), or anti-OLIG2, which labels all stages of the lineage (red, **D–E**). Arrows in **A–C** indicate GFP+ OLs that colabel with CC-1; arrowheads indicate GFP+, CC-1-negative OPCs. tdTom was not expressed in the absence of Cre (not shown). Cell nuclei were stained with Hoechst 33258 (Hst, blue). The images in **A–E** were taken in the corpus callosum at P12. Scale bars: **F**, 25 μm.

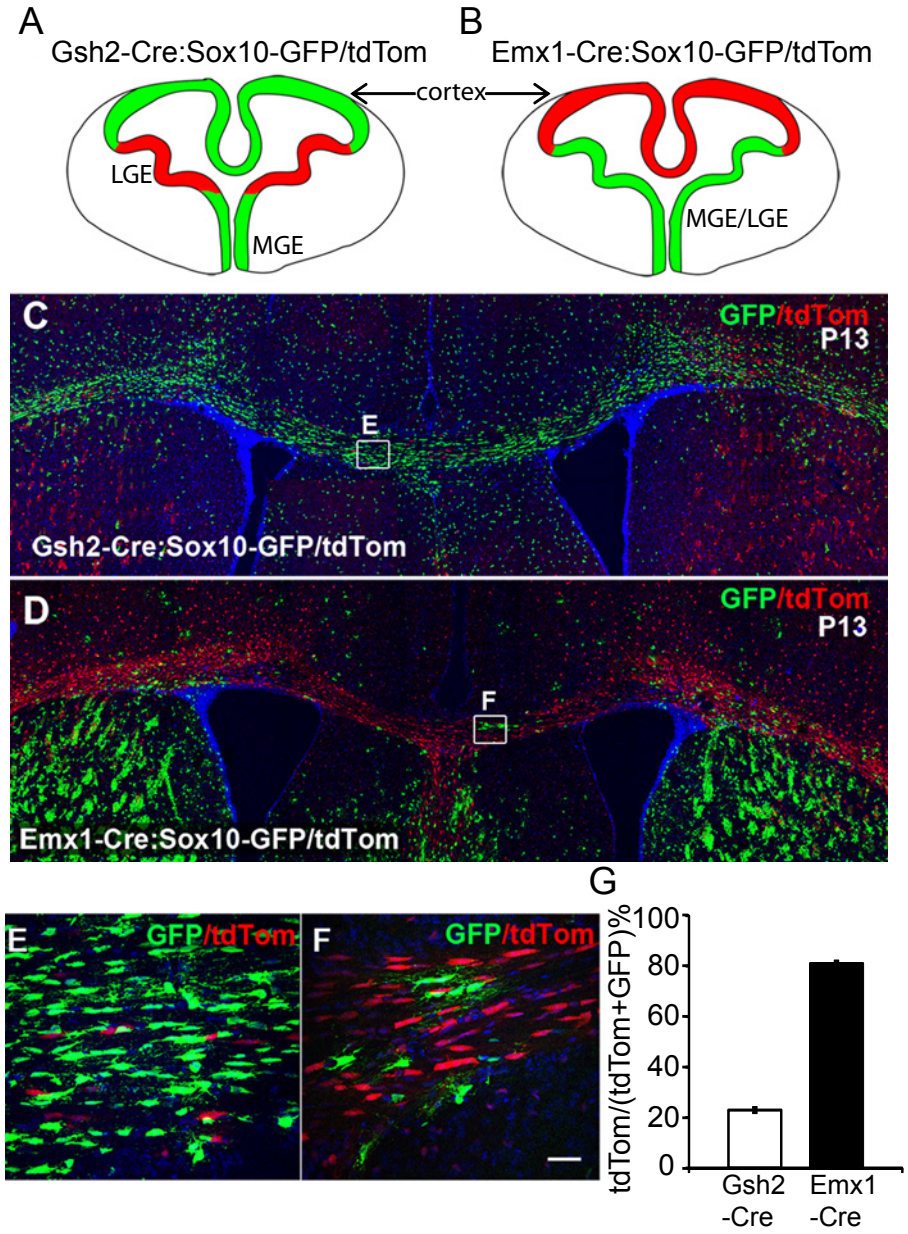

Figure 3.3. The corpus callosum is populated mainly by dorsally derived OLs. *Gsh2* is expressed only in the LGE and dorsal MGE (**A**, shown in red), whereas *Emx1* is expressed in the developing dorsal telencephalon (**B**, shown in red). In both A and B the colours green and red show the predicted fluoresence of OPCs derived from the regions shown, in the two mice. In *Gsh2-Cre: Sox10-GFP/tdTom* animals, the corpus callosum (CC) was populated mainly by unrecombined (green) OL lineage cells (**C**). Consistent with this, in *Emx1-Cre:Sox10-GFP/tdTom* animals, the CC was populated predominantly by recombined (red) OL lineage cells (**D**). Boxes in **C** and **D** are shown at higher magnification in **E** and **F**, respectively. Cell nuclei were poststained with Hoechst 33258 (Hst, blue). **G**, Cell counts in the CC at P12–P13 showed that ~20% (n = 6 mice) of the red labelled OL population in *Gsh2-Cre:Sox10-GFP/tdTom* were tdTom+, i.e., derived from MGE/LGE, whereas ~80% (n = 5 mice) of red labeled cells in the CC of *Emx1-Cre:Sox10-GFP/tdTom* were tdTom+, i.e., originating in the cortex. Data are presented as mean ± SEM. Scale bar: 20 μm.

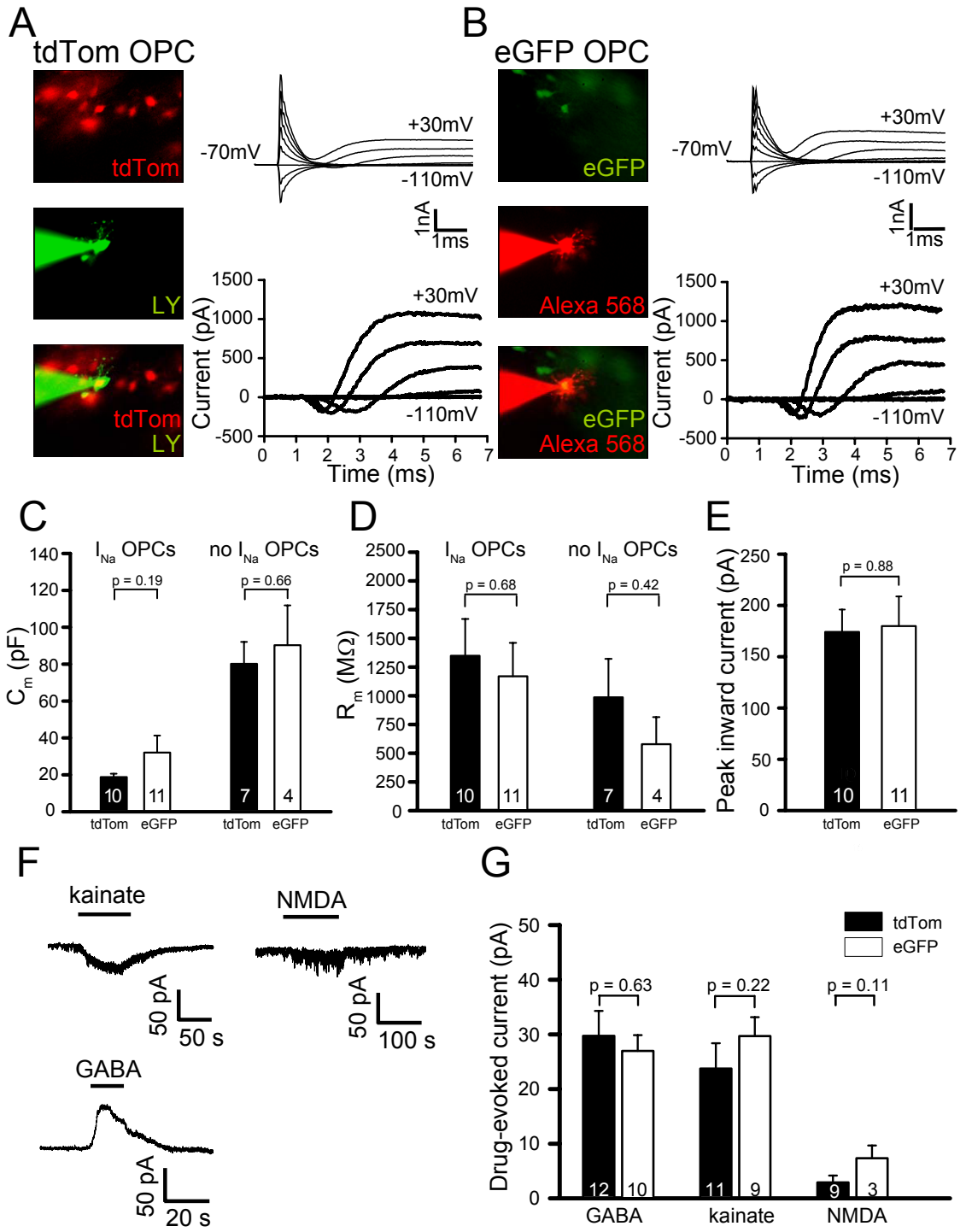

Figure 3.4. Electrophysiological properties of ventrally and dorsally derived OPCs in the corpus callosum.

A, A vOPC expressing tdTom under *Sox10* transcriptional control (in *Gsh2-Cre:Sox10-GFP/tdTom* mice; top) was whole-cell clamped with an internal solution containing Lucifer yellow (green: middle). Bottom panel shows overlay. Top current traces are in response to 20 mV steps from −70 mV. Bottom traces are after subtraction of the linearly scaled response to the step to −110 mV. **B**, As in **A** but for a dOPC expressing eGFP under *Sox10* control (in *Gsh2-Cre:Sox10-GFP/tdTom* mice). **C**, **D**, Comparison for vOPCs (tdTom) and dOPCs (eGFP), with and without Na^+ current, of membrane capacitance (**C**) and membrane resistance (**D**) at −70 mV. **E**, Comparison of peak net inward current evoked in I_{Na}-expressing OPCs by a step from −70 mV to +10 mV. **F**, Specimen responses of an OPC to kainate (100 μM) and NMDA (60 μM) at −70 mV and to GABA (100 μM) at −40 mV. **G**, Magnitude of drug-evoked currents (as in **E**) for vOPCs and dOPCs expressing I_{Na}.

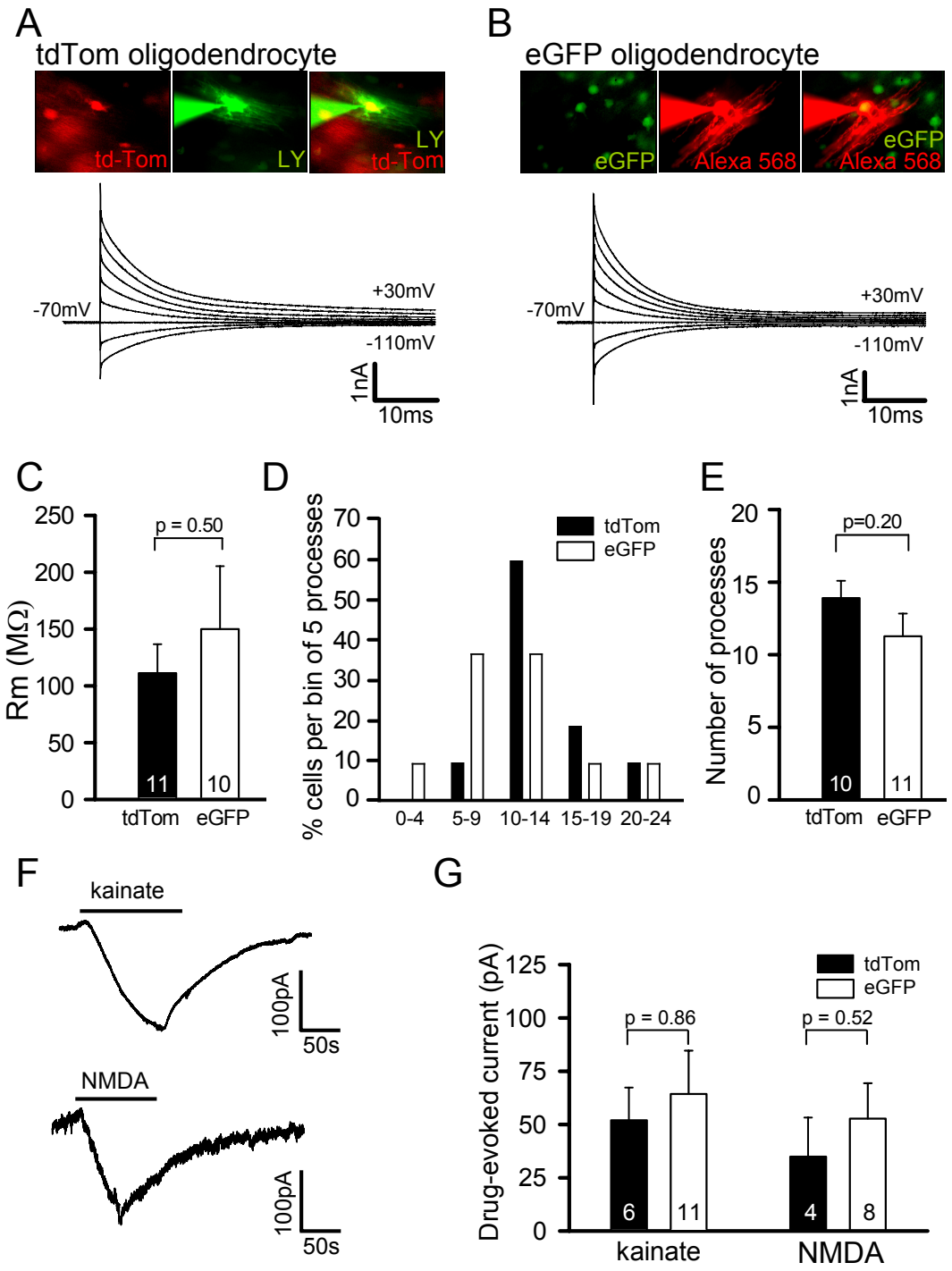

Figure 3.5. Comparison of the electrical properties of ventrally and dorsally derived mature oligodendrocytes (vOLs and dOLs) in the forebrain.
A, A vOL expressing tdTom in *Gsh2-Cre:Sox10-GFP/tdTom* mice (left) was whole-cell clamped with an internal solution containing Lucifer yellow (green: middle); thin green parallel processes are internodes. Right panel shows overlay. Current traces are in response to 20 mV steps from −70 mV. **B**, As in **A** but for a dOL expressing eGFP in *Gsh2-Cre:Sox10-GFP/tdTom* mice; thin red parallel processes are internodes. **C**, Comparison for vOLs (tdTom) and dOLs (eGFP) of membrane resistance at −70 mV. **D**, Percentage of vOLs (tdTom) and dOLs (eGFP) with different numbers of internodal processes (10 vOLs and 11 dOLs were studied). **E**, Mean number of internodal processes made by vOLs and dOLs. **F**, Specimen responses of an OL to kainate (100 μM) and NMDA (60 μM) at −70 mV. **G**, Magnitude of drug-evoked currents (as in **F**) for vOLs and dOLs. P values are from t tests.

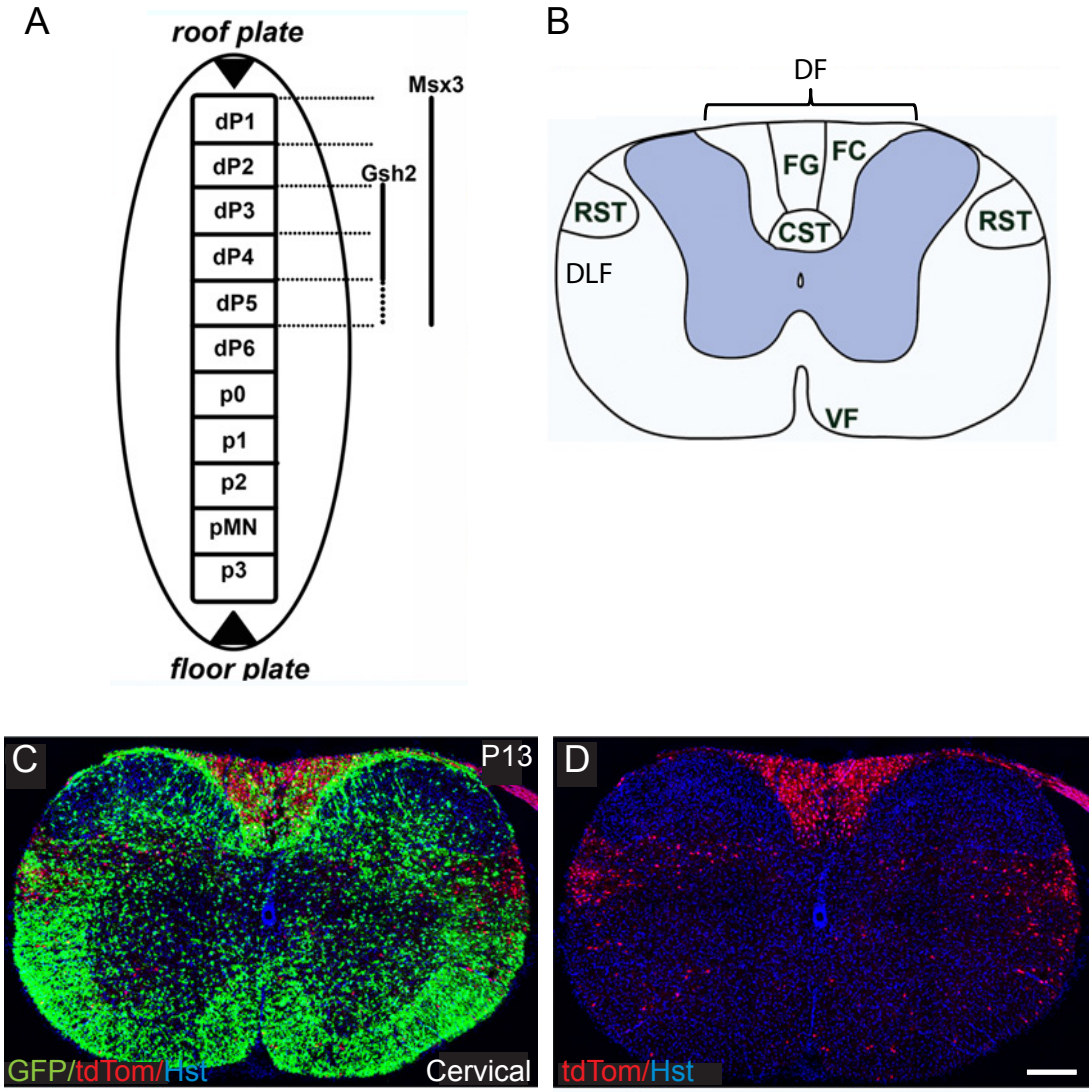

Figure 3.6. Origin and location of spinal dOPCs and vOPCs.
A, In the developing spinal cord *Msx3* is expressed in dorsal domains dP1–dP5, whereas *Gsh2* is expressed only in dP3–dP5. Hence, *Msx3-Cre:Sox10-GFP/tdTom* mice were used to examine dorsally derived OL lineage cells in the spinal cord. **B**, A schematic diagram of the adult spinal cord showing the tracts and regions examined. **C-D,** At P13, ventrally derived OPCs and OLs (green) are evenly spread throughout the spinal cord (**C**), whereas dorsally derived OL lineage cells (red) are mainly restricted to the dorsal and dorsolateral regions of the cord (**D**). Very few dorsally derived cells were observed in the ventral funiculus (VF). Note that the dorsal funiculus (DF) is dominated by dorsally derived (red) cells except for the ventralmost part (the contical spinal tracts (CSTs)), where ventrally derived (green) cells are more abundant. In the dorsolateral funiculus (DLF), where the rubrospinal tracts (RSTs) run, there appears to be an accumulation of dorsally derived cells. Cell nuclei were poststained with Hoechst 33258 (Hst, blue). Scale 250 µm.

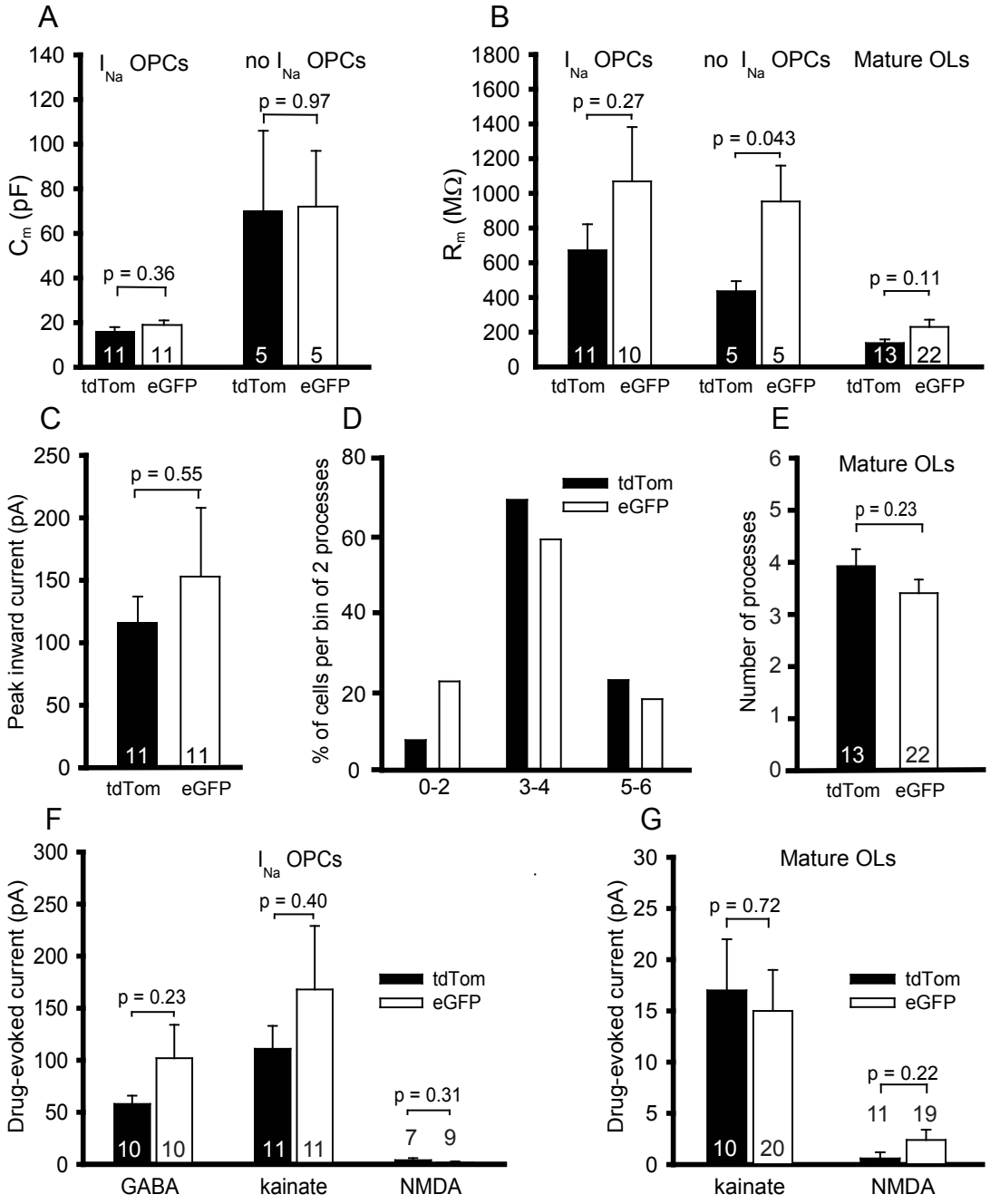

Figure 3.7. Dorsally and ventrally derived OL lineage cells in the spinal cord have similar electrical properties.

A–G, Electrical properties of spinal dorsally and ventrally derived OL lineage cells in *Msx3-Cre:Sox10-GFP/tdTom mice*. **A**, Membrane capacitance of dorsal (tdTom-expressing) and ventral (eGFP-expressing) OPC morphology cells. **B**, Membrane resistance at −70 mV of OPC morphology cells with and without I_{Na} and of mature OLs. **C**, Peak inward current evoked by depolarization from −70 mV to +10 mV in OPCs with I_{Na}. **D**, Percentage of dOLs and vOLs with different numbers of internodal processes (13 dOLs and 22 vOLs were studied). **E**, Mean number of internodal processes made by dOLs and vOLs. **F**, Drug-evoked currents in OPCs with I_{Na}. **G**, Drug-evoked currents in mature OLs. P values are from t tests.

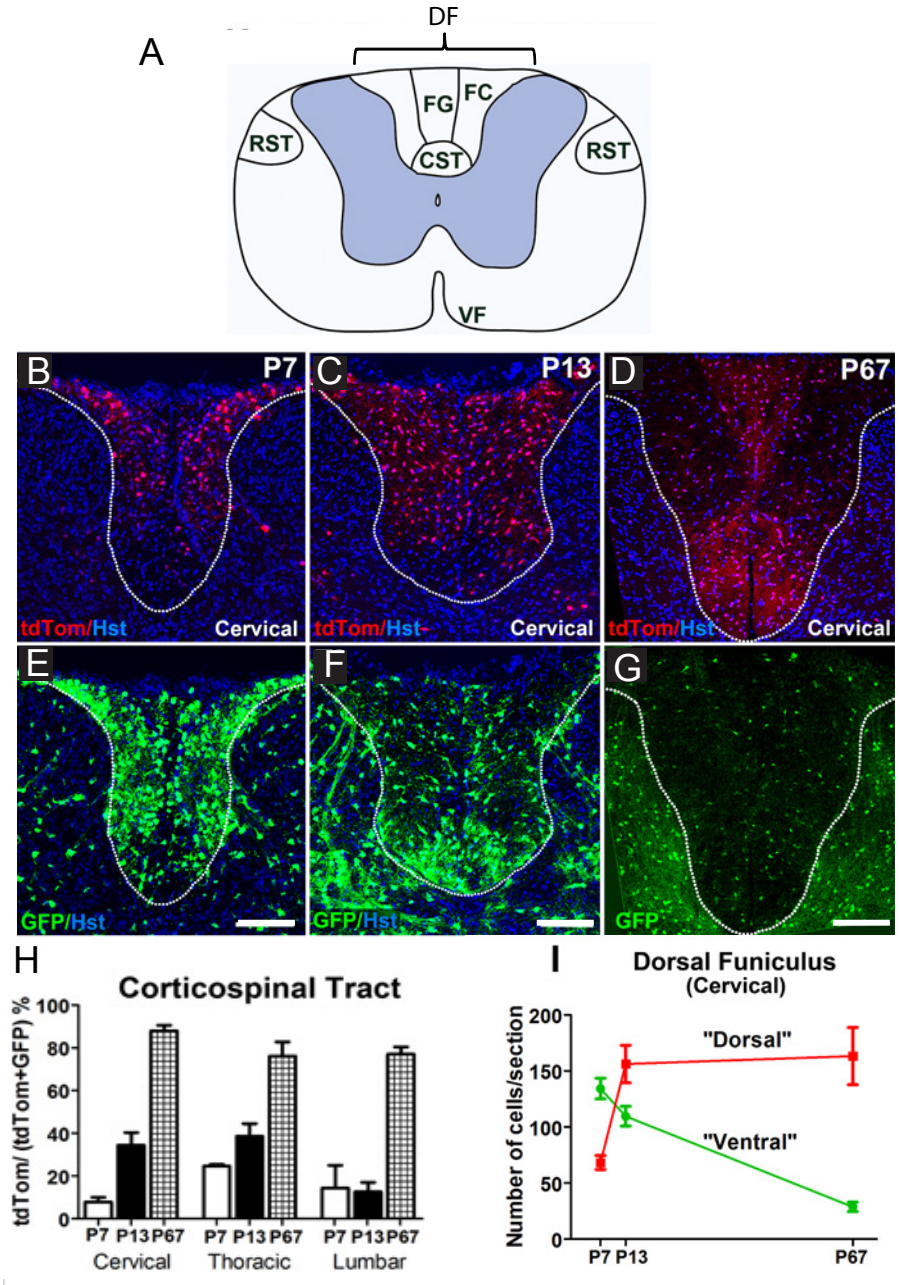

Figure 3.8. Corticospinal tracts are populated mainly by dorsally derived OL lineage cells in adulthood.

A, A schematic diagram of the adult spinal cord showing the tracts and regions examined. At P7, the majority of cells in the dorsal funiculus (DF) and especially the cortical spinal tract (CST) are ventrally derived (green) (**B** and **E**). By P13, the numbers of dorsally derived (red) cells increases in the DF (**C**), but the CST is still mainly populated by dorsally derived cells (green, **F**). This situation reverses by P67, when the entire DF, especially the CST (**D** and **G**), is populated mainly by dorsally derived OPCs and OLs as revealed by cell counts (**H**). Three sections per spinal level were counted for each animal: P7 (n = 2 mice) (**B, E**), P13 (n = 3) (**C, F**), and P67 (n = 3) (**D, G**). **I**, The absolute numbers of GFP+ (ventrally derived) cells/section in the dorsal funiculus (cervical level) decrease dramatically between P7 and P67, while tdTom+ (dorsally derived) cells increase in number during the same time frame. Scale bars,100 μm.

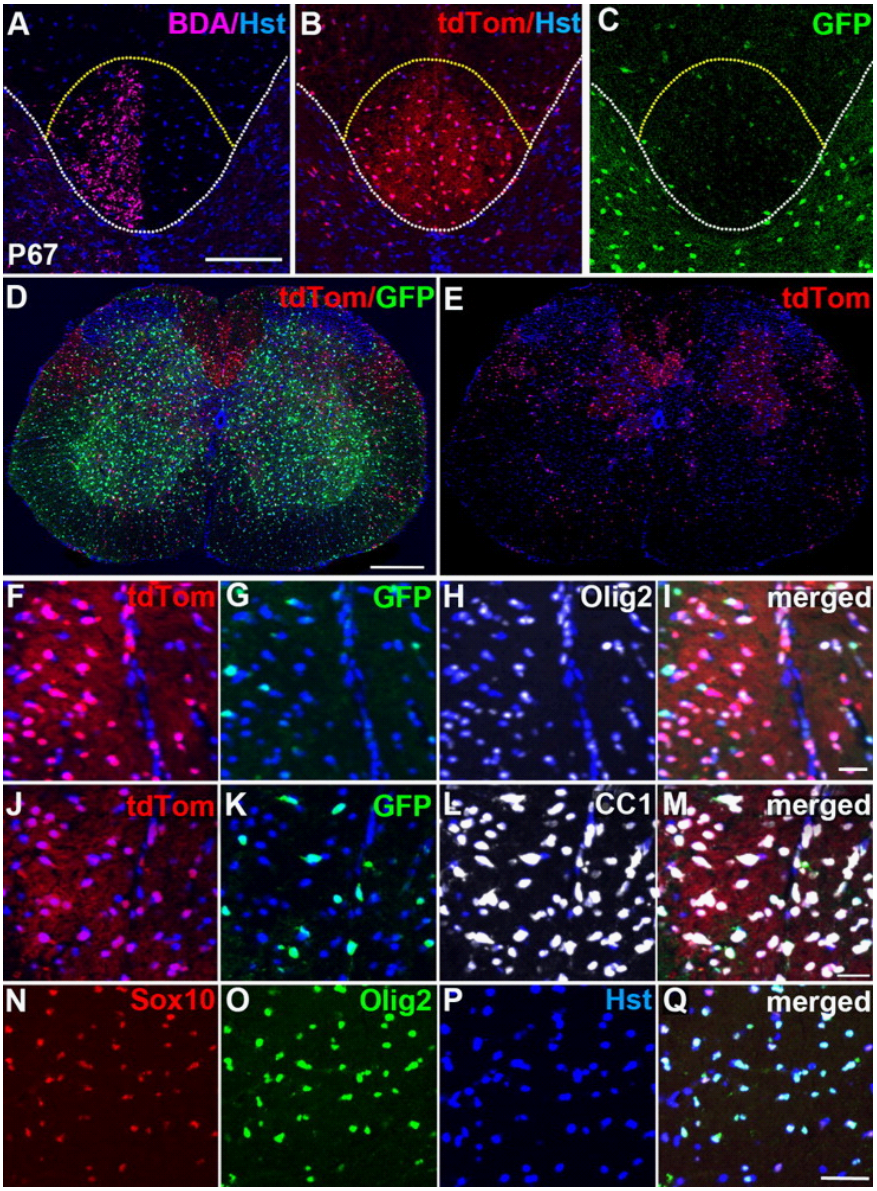

Figure 3.9. The *Sox10-GFP/tdTom* reporter faithfully identifies OL lineage cells in the adult.

A–C, BDA labeling confirmed that the majority of presumptive OL lineage cells in the adult CST are of dorsal origin (tdTom+). The white dotted line separates grey matter from white matter and the yellow dotted line outlines the CST. **D, E**, A cross-sectional image of an adult *Msx3-Cre:Sox10-GFP/tdTom* spinal cord shows that the dorsal funiculus (especially the CST) and dorsolateral funiculi (RST) contain mainly dorsally derived tdTom+ cells. tdTom+ (**F**, red) and GFP+ (**G**, green) cells together account for the great majority of OLIG2+ cells (**H–I**) in the adult spinal white matter. In addition, most CC-1+ differentiated OLs (**L–M**) colabeled for either tdTom (red, **J**) or GFP (green, **K**), confirming that the *Sox10-GFP/tdTom* reporter faithfully identifies OL lineage cells in the adult cord and also that a significant number of OL lineage cells were not “lost” in adulthood because of reduced GFP or tdTom expression. Almost all SOX10+ cells (red, N) also colabel for OLIG2 (green, O–Q) and vice versa in the adult spinal cord. Cell nuclei were poststained with Hoechst 33258 (Hst, blue). All images were taken from the cervical spinal cord. The images in F–Q were taken within the CST. Scale bars: A, 100 µm; D, 250 µm; I, M, 25 µm; Q, 35 µm.

Chapter 4: Properties and fate of oligodendrocyte precursor cells in the postnatal mouse brain

4.1 Introduction

As reviewed in chapter 1, whether all OPCs are the same is controversial. On the one hand it has been suggested that all OPCs express voltage-gated sodium (I_{Na}) and potassium channels, which are down-regulated when OPCs differentiate to form OLs (De Biase et al., 2010; Kukley et al., 2010). On the other hand, OPCs expressing NG2 in the rat cerebellar white matter fall into two classes: one that receives synaptic input, expresses I_{Na} and can generate action potentials, and another that lacks these attributes (Karadottir et al., 2008). Voltage-gated ion channel expression and spiking behaviour were also reported to differ between white and grey matter OPCs (Chittajallu et al., 2004). Furthermore, while it is undisputed that OPCs proliferate, there is great variation in the fraction of OPCs that are reported to be dividing. This has led to speculation about the existence of a permanently post-mitotic sub-population of OPCs that may have a distinct biological function in the brain. Finally, in addition to generating oligodendrocytes throughout the brain, OPCs have also been reported to be the source of new projection neurons in one region of the brain, the piriform cortex (Dayer et al., 2005; Tamura et al., 2007; Rivers et al., 2008; Guo et al., 2010). To resolve these issues over the diversity of OPCs, I patch-clamped OPCs in different brain regions to investigate their expression of voltage-gated ion channels, their proliferative capacity and their cell fate.

4.2 Methods

Transgenic mice

Sox10-GFP and *Pdgfrα-H2BGFP* knock-in mice (Hamilton et al., 2003; referred to as *Pdgfrα-GFP* mice) which fluorescently label oligodendrocyte lineage cells (see below) were used for the electrophysiology experiments described in this chapter. For the cell fate tracing experiments described in this chapter, *Pdgfrα-CreER*^{T2} BAC transgenic mice (Rivers et al., 2008) were crossed with Cre-sensitive reporter mice, either 1) homozygous *R26R-YFP* transgenic mice (Srinivas et al., 2001) to label OPCs and their all of their progeny with YFP or, 2) heterozygous *Tau-loxSTOP-lox-mGFP-IRES-NLS-LacZ-pA* (*Tau-mGFP*) mice (Hippenmeyer et al., 2005) to label any differentiating/differentiated oligodendrocytes and neurons generated by OPCs with

membrane targeted GFP (mGFP). These transgenic mice are described in detail chapter 2, section 13.

Tamoxifen administration

Tamoxifen was administered to activate Cre-mediated recombination and induce YFP or GFP labelling in oligodendrocyte lineage cells, as described in detail in chapter 2, section 13.5.

Brain slices

Coronal brain slices or parasagittal cerebellar slices (225 µm thick) were prepared from postnatal day 2, P7-P10 (referred to as P9), and P32-P34 (referred to as P33) *Sox10-GFP* or *Pdgfrα-GFP* mice (as described in chapter 2 section 1). Slices were superfused at ~33℃ with bicarbonate-buffered solution which contained the following (in mM): 126 NaCl, 24 $NaHCO_3$, 2.5 KCl, 1 NaH_2PO_4, 2.5 $CaCl_2$, 1 $MgCl_2$, 10 D-glucose, pH 7.4 (bubbled with 95% O_2/5% CO_2).

Patch-clamp recordings

Whole-cell recordings were made from OPCs that expressed GFP under transcriptional control of the *Sox10* or *Pdgfrα* promotor. Some mice were pre-labelled with EdU before recording to detect dividing cells, as described in chapter 2 section 13.7. OPCs were distinguished from differentiated OLs by morphology (OPCs are bipolar or stellate cells, OLs have long processes aligned with axons) and by the change in membrane current induced by changing the cell membrane potential from −110 to +30 mV in 20 mV steps. The steady-state I–V plots are approximately ohmic (linear) with mild outward rectification for mature OLs and more outwardly rectifying for OPCs (see Fig. 3.4 and 3.5). The peak net inward current (reflecting the difference between the inward I_{Na} and the subsequently activating voltage-dependent outward K^+ current) was quantified after subtracting the capacity current and an assumed ohmic leak current, which were scaled from the response to hyperpolarising pulses. Voltage responses to current injection were recorded from the cell's resting potential (applying 20 pA steps for 200 ms).

Electrodes were pulled from thick-walled borosilicate glass to a resistance of 6–9 MΩ and filled with a K-gluconate-based solution containing the following (in mM): 130 K-gluconate, 4 NaCl, 0.5 $CaCl_2$, 10 HEPES, 10 BAPTA, 4 MgATP, 0.5 Na_2GTP, and 2 K-Lucifer yellow (or 0.052 Alexa Fluor 568), pH 7.3 (adjusted with KOH). 1 µM TTX (Tocris) was added into the superfusion solution to block sodium currents.

After recording, the patch electrode was removed from the cell, leaving the soma intact. The slice was then immersion fixed in 4% (w/v) paraformaldehyde (PFA) in PBS at 21ºC for a minimum of 1 hour (maximum of 6 hours). These cells were also processed to detect GFP and NG2, with or without EdU, as described in chapter 2, section 14. Some slices were briefly fixed for 20 minutes at 21℃ to allow immunolabelling with anti-PDGFRα (this antibody is fixation sensitive).

EdU labelling and detection

In vivo EdU labelling to detect dividing cells was performed by my colleague Kaylene Young as described in chapter 2, section 14.

Tissue preparation and immunohistochemistry

Immunohistrochemistry was performed on cryosections or brain slices after patch-clamp recordings as described in detail in chapter 2, section 14.

Microscopy and cell counts

Images were collected on an Ultraview confocal microscope (Perkin Elmer) or LSM 510 (Zeiss) as Z stacks with 1 μm spacing. For quantification, 8 or more low magnification (20x objective) fields were collected within each anatomical region of interest, for each coronal brain section, including all layers of the medial motor cortex (Ctx), layer II of the anterior piriform cortices (aPC), and the corpus callosum (CC). Cells were counted manually, viewing each image in Adobe Photoshop or Image J. For post-electrophysiological confocal imaging of individual cells, the Alexa Fluor 568 dye-filled cell was located within the section and scored for EdU and NG2 expression, blind to the electrophysiology data for that cell. Fluorescence intensities and cell body diameters were measured in photomicrographs using Image J software.

Calculation of cell cycle time

For a homogeneous population of cycling cells, the fraction of cells that label with EdU (“labelling index”) is expected to increase linearly with the duration of BrdU/EdU exposure until all dividing cells are labelled (phase 1, Fig. 4.10B: Nowakowski et al., 1989). After this the labelling index cannot increase further and a plateau is reached (phase 2, Fig. 4.10B). The rate at which cells incorporate EdU is given by the slope (m) of phase 1 and was calculated by performing a linear regression analysis. The maximum labelling index (phase 2 plateau value) is known as the “growth fraction” (GF), which is expressed as a percentage of the total cell population. This was

calculated using only points at late times in the labelling curve, that were deemed not statistically significant from each other by ANOVA and were not already included in the linear regression analysis. The value of GF presented is the average from all mice that were analysed at the plateau. From these data, the length of the cell cycle Tc = GF/m was calculated (Nowakowski et al., 1989). Since Tc depends on the reciprocal of m, its standard error (s.e.Tc) is not symmetrical about the mean. However, for simplicity s.e. of Tc is shown as ± half of the full range, calculated as follows:

$$s.e._{Tc} = [\{(GF + s.e._{GF}) / (m - s.e._{m})\} - \{(GF - s.e._{GF}) / (m + s.e._{m})\}] / 2$$

Statistics

The statistical analysis is described in detail in chapter 2, section 15.

4.3 Results

4.3.1 Using transgenic mice to identify OL lineage cells in the postnatal brain

To investigate whether oligodendrogenic OPCs present throughout the postnatal mouse brain have electrical properties similar to the potentially neurogenic OPCs in the anterior piriform cortex (aPC), putative OPCs were identified by their intrinsic fluorescence in brain slices from *Pdgfrα-GFP* (Hamilton et al., 2003) or *Sox10-GFP* (Kessaris et al 2006) trangenic mice. *Sox10-GFP* transgenic mice have been previously shown to reliably label all oligodendrocyte lineage cells with GFP (Kessaris et al., 2006), but do not label OPCs specifically. As PDGFRα is expressed by OPCs but not by differentiated OLs (Nishyama et al., 2009), it might be expected that OPCs should be specifically labelled in the *Pdgfrα-GFP* mice. *Pdgfrα-GFP* transgenic mice have been previously used to identify embryonic OPCs (Hamilton et al., 2003) but the specificity of the GFP expression was not characterised postnatally. Therefore postnatal day 9 (P9) and P33 coronal brain sections from *Pdgfrα-GFP* mice were co-immunolabelled for GFP and the OL lineage marker OLIG2 (Fig. 4.1A-C). In the motor cortical area (henceforth called the motor cortex or Ctx), corpus callosum and anterior piriform cortex, more than 96% of all GFP^+ cells also expressed OLIG2 (Fig. 4.1G). As NG2-immunolabelling is intense in OPCs but is lost as they differentiate into OLs (Nishyama et al., 2009), additional sections were immunolabelled for GFP and NG2 (Fig. 4.1D-F) to determine what proportion of the GFP^+ cells are OPCs. At P9 ~93% of GFP antibody-labelled cells also labelled for NG2. However by P33 only ~70% of all GFP^+ cells in the motor cortex, ~30% of those in the corpus callousm, and ~60% in the anterior piriform cortex also expressed NG2 (Fig. 4.1G), suggesting that GFP persists

even after OPCs have turned into more mature oligodendroglial cells (which I represent as: $OLIG2^+$ $NG2^{neg}$). Therefore, in the postnatal brain of *Pdgfrα-GFP* transgenic mice, GFP labelling identifies cells of the OL lineage ($OLIG2^+$) but does not distinguish between OPCs and recently-differentiated OLs.

4.3.2 Expression of voltage-gated sodium channels defines two populations of OL lineage cell in the postnatal mouse brain

To investigate the electrophysiological properties of OL lineage cells, I whole-cell patch-clamped cells in white matter areas (corpus callosum (CC), and cerebellar white matter (CB WM)) and grey matter areas (motor cortex (Ctx), anterior piriform cortex (aPC), and cerebellar grey matter (CB GM)) of the postnatal brain. Identified by their GFP expression, OL lineage cells in the brain of postnatal *Pdgfrα-GFP* or *Sox10-GFP* mice could be divided into two broad classes of cell. One class (termed I_{Na}^+) produced a transient inward current after depolarisation beyond -30 mV (Fig. 4.2A-C), which was blocked by tetrodotoxin (TTX) (Fig. 4.3A), indicating that it was mediated by voltage-gated sodium channels (I_{Na}). This transient inward current was followed by activation of a more sustained outward, presumably K^+ current (I_K) (Fig. 4.2A-C) since in rat OPCs this has been shown to be abolished when internal K^+ is replaced with Cs^+ (Karadottir et al., 2008). In contrast, the other cell type (termed I_{Na}^{neg}) showed an essentially time-independent current-voltage (I-V) relationship at negative potentials, but often an outward (presumably K^+) voltage-gated current on depolarisation (Fig. 4.2D-F). When TTX was applied to this cell class, the I-V relationship remained unchanged (Fig. 4.3B), excluding the possibility that the K^+ conductance was masking a voltage-gated Na^+ current in these cells (n=3).

Owing to the rapid kinetics of I_{Na}, it partly overlaps with the transient capacity current, so the net inward current was quantified after subtracting the linearly scaled capacity transient and ohmic leak current that was evoked by a hyperpolarising pulse (Fig. 4.2, lower traces). The resulting peak inward current represents a combination of inward I_{Na} and outward I_K. To assess how the overlap of these currents alters the apparent magnitude of the voltage-gated Na^+ current, TTX was applied to some cells to isolate I_K (Fig. 4.3A). Subtraction of I_K in these cells from the total inward current resulted in a 2.5-fold increase in the amplitude of the net inward current (n=3) (Fig. 4.3A).

In the corpus callosum, the proportion of OPCs (defined by morphology) that expressed I_{Na} did not change significantly throughout development, being ~60-80% at

P2, P9 and P33 (Fig. 4.4A**;** 118 cells were studied in total). In contrast, the proportion of OPCs (defined by morphology) that expressed I_{Na}, in the motor cortex (Ctx) and cerebellar grey matter (CB GM), significantly decreased from ~80% early in development (P2, P9) to ~30% later in development (P33) (both $P<0.001$; Chi^2 test) (Fig. 4.4B; in total 141 cells in the Ctx, and 64 cells in the CB GM were studied). Interestingly, ~20% of OPCs (defined by morphology) lacked I_{Na} expression as early as P2, in both white and grey matter, suggesting that OPCs lacking I_{Na} are formed early in development, just after birth.

4.3.3 I_{Na} cells show regenerative action potential-like waves but do not express neuronal markers

It has been reported that some OPCs can fire action potentials in response to depolarisation (Chittajallu et al., 2004; Karadottir et al., 2008; Ge et al., 2009). In my study, depolarising current injection resulted in passive membrane responses in I_{Na}^{neg} GFP^+ cells (Fig. 4.5F), while I_{Na}^+ GFP^+ cells exhibited a range of action potential-like waves in response to depolarising current pulses (Fig. 4.5A-E). Early in development (P9) the majority of I_{Na}^+ GFP^+ cells (69/87) in both the grey and the white matter showed a single regenerative depolarisation (Fig. 4.5A-C). Single action potential-like events were also detected in 21 of 37 I_{Na}^+ GFP^+ cells in the white and the grey matter later in development (P33). A minority of I_{Na} expressing cells (3/124) exhibited repetitive action potential-like waves on depolarisation (Fig. 4.5D-E). Similar regenerative responses have been reported for OPCs in white (Chittajallu et al., 2004; De Biase et al., 2010) and grey matter regions (Chittajallu et al., 2004; Ge et al., 2009; De Biase et al., 2010) of the postnatal mouse brain.

Although I_{Na}^+ GFP^+ cells could generate action potential-like events, they were not like typical neuronal action potentials or those described for I_{Na}^+ OPCs in the rat cerebellar white matter (Karadottir et al., 2008). The action potential-like events had a higher threshold for activation (-21 ± 1.5 mV) than action potentials in neurons, their amplitudes increased somewhat with larger current injections (Fig. 4.5D-E), unlike neuronal action potentials, and the timescale of the spikes (4.3 ± 0.7 ms, measuring the duration at half of the amplitude) was longer than those for most neurons (for examples see Fig. 4.5D-E). This probably reflects the lower ratio of I_{Na} current magnitude to cell input resistance in mouse OPCs (mean peak inward current <300 pA, Fig. 4.9 below) than was previously found for rat OPCs (mean peak inward current ~ 1000 pA, Karadottir et al., 2008) and suggests that mouse I_{Na}^+ cells do not have a sufficient density of I_{Na} to fire *bone fide* action potentials.

As I_{Na}^+ GFP^+ cells were detected in all brain regions, including the white matter of the corpus callosum, it seemed unlikely that the excitability of the I_{Na}^+ GFP^+ cells analysed was a result of ectopic GFP expression by immature neurons or cortical interneurons. However, as some OPCs reportedly express immature neuronal markers such as TOAD-64 (turned on after division-64), doublecortin, Tuj1 and HuC/D (Belachew et al, 2003; Chittajallu et al, 2004; Tamura et al., 2007), suggesting that they might turn into neurons in various brain regions (reviewed by Richardson et al., 2011), I investigated this possibility by immunolabelling coronal brain sections from P9 and P33 *Pdgfrα-GFP* transgenic mice to detect GFP and a variety of neuronal markers (Fig. 4.6). At both ages, GFP-expressing cells in the motor cortex did not detectably express parvalbumin (Fig. 4.6A, M), somatostatin (Fig 4.6B, M), neuropeptide Y (Fig 4.6C, M), calbindin (Fig. 4.6D, M), reelin (Fig. 4.6E, M) and PSA-NCAM (Fig. 4.6L, M). While the vast majority of GFP-expressing cells also lacked calretinin labelling (Fig. 4.6F, M) and NeuN (Fig. 4.6I, M), a small number of cells that exhibited faint GFP expression were found to express calretinin (Fig. 4.6G, H, M) or NeuN (Fig. 4.6J, K, M) strongly, and so are presumed to be neurons. In the motor cortex, these presumptive neurons were located in the superficial cortex, concentrated near the brain mid-line. Even if the calretinin- and NeuN-expressing GFP^+ cells are separate populations, at P33 they would together still comprise only ~2% (and ~4% at P9) of all GFP^+ cells. Consistent with the findings in the motor cortex, GFP^+ cells in the anterior piriform cortex of P33 *Pdgfrα-GFP* transgenic mice rarely expressed neuronal markers – a small number co-labelled for PSA-NCAM (4/1820 GFP^+ cells examined; 4/606 PSA-$NCAM^+$ cells examined) and only 0.7% ± 0.2% of GFP^+ cells co-expressed NeuN.

The finding that GFP (driven by an OL-lineage cell promoter) is expressed by a small number of cells expressing neuronal markers is reminiscent of a study from Belachew et al. (2003), who suggested that the brightly-labelled GFP^+ $NG2^+$ OPCs that they observed in *CNPase-GFP* transgenic mice were able to generate faintly-labelled GFP^+ interneurons in the postnatal mouse hippocampus. These data might suggest either that some interneurons are generated from OPCs, and that the GFP fluorescence is residual and indicative of their origin, or that a small subset of cortical neurons have a very low level of *Pdgfrα* promoter activity and so become labelled with GFP.

By counting the number of neurons labelled for calretinin and NeuN, it was deduced that the GFP-labelled cells account for 11% ± 0.7% of calretinin-expressing and 0.14% ± 0.02% of NeuN-expressing neurons in the motor cortex at P9, and 14% ± 2% of calretinin-expressing and 0.2% ± 0.02% of NeuN-expressing neurons in the

motor cortex at P33. The GFP^+ neurons expressed low levels of GFP, which was ~8 times lower in intensity (averaged over the nucleus) than was detected in $NG2^+$ OPCs (GFP+ neurons 10.6 ± 1.0, OPCs 84.3 ± 0.1 arbitrary units) and ~3 times less than was detected in $NG2^{neg}$ OLs (35.0 ± 5.0 arbitrary units). The GFP^+ neurons were difficult to detect even by antibody labelling, so it is highly unlikely that they would have been selected for patch-clamping based on their intrinsic GFP fluorescence. Furthermore, patch-clamp recordings were performed in brain hemi-sections, therefore cells immediately bordering the cortical mid-line (where the GFP+ neurons tend to congregate) were not targeted, and the calretinin and NeuN expressing cells were too few in number (<5%) to account for the significant number of GFP^+ cells that I classify as excitable $I_{Na}{}^+$ GFP^+ cells (77% and 61% of the GFP^+ cells that were studied expressed I_{Na} in the motor cortex, at P9 and P33, respectively). I conclude that the great majority of the GFP^+ $I_{Na}{}^+$ cells that I recorded from were genuine OPCs and not neurons.

4.3.4 All GFP^+ cells that express NG2 strongly are proliferative and express I_{Na}

Based on GFP expression I was able to identify OL lineage cells, however I found that they were heterogeneous in terms of I_{Na} expression in all brain regions examined. The morphology of the Alexa Fluor 568-filled cells suggested that the expression of I_{Na} might be an OPC trait, while a lack of I_{Na} might be an OL trait. Morphology proved to be more useful for identifying putative OPCs in the white matter than in the grey matter. In white matter, GFP positive cells with OPC-like morphology (Fig. 4.7A) ($I_{Na}{}^+$ GFP^+ cell) could be easily distinguished from OLs with myelinating processes (Fig. 4.7B, $I_{Na}{}^{neg}$ GFP^+ cell). OPCs were defined as having bipolar or stellate morphology and OLs as having multiple long processes aligned with axons. This distinction was less obvious in grey matter (Fig. 4.7C, $I_{Na}{}^{neg}$ GFP^+ cell), because axons do not fasciculate in the grey matter as they do in white matter tracts, and myelin internodes are not all parallel with one another but oriented in various directions (Murtie et al., 2007; Vinet et al., 2010). Consequently, in the grey matter, on the basis of morphology alone some GFP^+ differentiated OLs might easily be mistaken for OPCs. In order to identify OPCs unambiguously in both grey and white matter it was necessary to perform post-recording immunohistochemistry for NG2. In the following section I correlated cell proliferation with expression of NG2 and I_{Na} in different brain regions.

Individual GFP^+ cells in the corpus callosum, motor cortex and anterior piriform cortex were whole-cell patch-clamped to determine whether or not they exhibited I_{Na}

and then dye-filled with Alexa Fluor-568. Dye filling not only revealed the cellular morphology but also permitted identification of the recorded cell after NG2 immunolabelling. Three categories of dye-filled cells were identified: (1) cells expressing NG2 strongly ($NG2^+$ cells) which I defined to be OPCs (Fig. 4.8A, C and E), (2) cells expressing low levels of NG2 limited to the soma or the base of some processes ($NG2^{low}$ cells) that were presumed to be early differentiating OLs (Fig. 4.8G), and (3) cells with no detectable NG2 ($NG2^{neg}$ cells) that were assumed to be OLs (Fig. 4.8I).

At both P9 and P33 and in all brain regions examined, I found that the $NG2^+$ GFP^+ cell population (Fig. 4.8A, C, E) was the same as the population of $I_{Na}{}^+$ GFP^+ excitable cells (Fig. 4.8.B, D, F). As expected, these $NG2^+$ $I_{Na}{}^+$ presumed OPCs were found to co-express PDGFRα (5 cells examined in the motor cortex, 7 cells in the anterior cortex) confirming them as OPCs. The magnitude of the net inward current generated by OPCs on depolarization from -70 mV to 10 mV was ~130-320 pA in all areas (Fig. 4.9A) and tended to decrease with age, falling by 21%, 61% or 31% from P9 to P33 in the CC, Ctx or aPC, respectively (Fig. 4.9A). Similarly, in all brain areas a reduction in membrane resistance (Fig. 4.9B) and peak outward current (Fig. 4.9C) was observed with age, whereas no consistent change in cell capacitance (a measure of cell size) could be detected with age (Fig. 4.9D). OPCs were consistently larger in grey matter than in white matter, irrespective of age (Fig. 4.9D). The resting membrane potential of OPCs ranged from between ~-85 and -94 mV (at P9, the resting membrane potential of OPCs was -94 ± 3.8 mV, -93 ± 2.6 mV, -92 ± 1.6 mV, in the corpus callosum (n=14), motor cortex (n=14) and anterior piriform cortex (n=10), respectively. At P33, the resting membrane potential of OPCs was -89 ± 1.9 mV, -86 ± 3.3 mV, -85 ± 2.3 mV, in the corpus callosum (n=22), motor cortex (n=18) and anterior piriform cortex (n=17), respectively) at each age and in each brain region. These data suggest that the intrinsic membrane properties of OPCs are subject to change during development but that I_{Na} expression is a universal property of OPCs in all brain areas throughout postnatal life.

The second category of GFP^+ cells, $NG2^{low}$ cells, had limited expression of NG2 (Fig. 4.8G). These cells had little to no I_{Na} (Fig. 4.8H; mean net inward current 24 ± 5pA in 9 cells) and are referred to as $NG2^{low}$ $I_{Na}{}^{low}$ cells. They were assumed to correspond to early differentiating OLs that are down-regulating their I_{Na} and NG2 expression, as previously described (De Biase et al., 2010; Kukley et al., 2010). The final category of GFP^+ cells ($NG2^{neg}$ OLs) lacked both NG2 labelling (Fig. 4.8I) and I_{Na}

expression (Fig. 4.8J) and therefore correspond to pre-myelinating or myelinating OLs (44 cells; $NG2^{neg}$ $I_{Na}{}^{neg}$ OLs), which I refer to collectively as OLs.

A number of studies have indicated the presence of a post-mitotic population of OPCs (defined by NG2 immunolabelling) within the postnatal mouse brain (reviewed by Richardson et al., 2011). In the piriform cortex, these post-mitotic OPCs have been suggested to comprise a substantial fraction (~50%) of the OPC population and to differentiate over time, providing a source of new projection neurons (Rivers et al., 2008; Guo et al., 2010). To assess the electrophysiological properties of dividing oligodendrogenic OPCs and the putative non-dividing neurogenic OPCs, the thymidine analogue EdU was administered to *Pdgfrα-GFP* mice for 5 days prior to making patch clamp recordings at P9, and for 12-13 days prior to making patch clamp recordings at P33. In addition to NG2-immunolabelling, slices were processed to detect EdU. These dosing regimens were selected to label all the proliferating OPCs in the white and grey matter of the brain, which were predicted from Psachoulia et al., (2009) to be approximately half of all OPCs. Unexpectedly, given this prediction, the vast majority of GFP^{+}, $NG2^{+}$, $I_{Na}{}^{+}$ OPCs that I analysed were EdU^{+}, and so were proliferating, irrespective of brain region or age. At P9, ~90% of $NG2^{+}$ $I_{Na}{}^{+}$ OPCs had divided in the previous five days (motor cortex, 8/9 OPCs; corpus callosum, 12/13 OPCs). At P33, 70-100% of all GFP^{+}, $NG2^{+}$, $I_{Na}{}^{+}$ OPCs were EdU-labelled in all regions (motor cortex, 17/24 OPCs; corpus callosum, 4/4 OPCs; aPC, 29/31 OPCs) (Fig. 4.8A-F). In contrast, none of the $NG2^{low}$ $I_{Na}{}^{low}$ cells analysed in the motor cortex of P33 mice (following ~13 days of EdU administration) had incorporated EdU (Fig. 4.8G, 9 cells analysed), consistent with *in vitro* data from Sugiarto et al. (2011), which suggested that, following an asymmetric OPC division, one cell begins to down regulate mitogenic proteins, commits to differentiating and will no longer incorporate BrdU, while the other cell maintains the expression of mitogenic proteins, remains an OPC and re-enters the cell cycle. This supports the idea that the $NG2^{low}$ $I_{Na}{}^{low}$ cells are early differentiating OLs, formed from a cell division that occurred more than 13 days earlier.

The large fraction of individual OPCs that were EdU^{+} following these patch-clamp recordings accurately reflected the total fraction of EdU^{+} OPCs quantified in each brain region when confocal analysis was performed of large numbers of OPCs immunolabelled for NG2. In motor cortex at P9, 90% ± 2% of $NG2^{+}$ OPCs were EdU^{+} and at P33, 83% ± 1% of $NG2^{+}$ OPCs were EdU^{+}, indicating that the high fraction of OPCs identified as proliferating was not the result of a cell selection bias when patch-

clamping, but instead indicated that a larger proportion of OPCs underwent cell division than was previously detected by Psachoulia et al. (2009) and Guo et al. (2010).

These data undermine previous reports, based on BrdU-cumulative labelling, that there is a post-mitotic population of OPCs in the brain (Rivers et al., 2008; Psachoulia et al., 2009, Guo et al., 2010; Simon et al., 2011). This in turn raises questions about the origins of new projection neurons in the anterior cortex, which were previously thought to derive from OPCs but which do not incorporate BrdU (Rivers et al. 2008; Guo et al., 2010) even after a long labelling period and thus are unlikely to be derived from dividing precursors such as OPCs. However, the EdU labelling experiments on motor cortex described above left open the possibility that there might be a local population of post-mitotic OPCs specifically in the anterior pirifrom cortex. To test this, EdU was administered to P21 and P60 mice via their drinking water for various time periods up to 35 days. Coronal brain sections were immunolabelled for PDGFRα and NG2 to detect OPCs, and were co-stained for EdU (Fig. 4.10A). When administering EdU from P21 the proportion of OPCs in the anterior piriform cortex that became EdU^+ was found to increase linearly with time ($r^2 > 0.96$) at a rate of 7.6% per day, until >98% of all OPCs were stably labelled after ~13 days (Fig. 4.10B). From P60 the fraction of EdU-labelled OPCs was found to increase linearly with time ($r^2 > 0.97$) at a rate of 3.15% per day until >98% of OPCs were labelled after ~30 days. From these data the cell cycle time for OPCs in the anterior piriform cortex was calculated as being approximately 12.9 ± 0.8 days at P21 and 31.3 ± 1.7 days at P60 (using the methods described section 2 of this chapter). These data show that all OPCs (defined by strong NG2 and PDGFRα expression) in the anterior piriform cortex are mitotically active, as in other regions of the forebrain.

4.3.5 OPCs generate exclusively OLs in the postnatal mouse brain

To determine what cell types are produced by OPCs in the corpus callosum, motor cortex and anterior piriform cortex, OPCs were labelled and traced using two cell tracing methods simultaneously: (1) extended EdU exposure to label all proliferating cells (including all OPCs and their differentiating progeny) and (2) Cre-lox fate mapping using *Pdgfrα-CreER^{T2}* mice. EdU was administered via the drinking water to *Pdgfrα-CreER^{T2} : R26R-YFP* mice continuously after P25 to pre-label all proliferating OPCs. Tamoxifen was then administered to these same mice on four consecutive days (P45-P48 inclusive) in order to activate Cre-mediated recombination and induce YFP expression in PDGFRα-positive OPCs (see experimental time line, Fig. 4.11A).

The identity of the starting population of YFP-labelled cells was confirmed by immunolabelling sections of *Pdgfrα-CreER^{T2} : R26R-YFP* mouse brains at P45+6, two days after the final dose of tamoxifen. Sections were immunolabelled for YFP and different combinations of OLIG2, NG2, PDGFRα, PSA-NCAM, NeuN or the microglial marker Iba1 (Fig. 4.11B, D). In the aPC, ~90% of all YFP$^+$ cells co-labelled for OLIG2 (>500 YFP$^+$ cells counted), most of which were OPCs, as 88% ± 4% of YFP$^+$ cells also co-labelled for NG2 (>600 YFP$^+$ cells counted) and 89% ± 1% co-labelled for PDGFRα (>400 YFP$^+$ cells counted) (Fig. 4.11D). At P45+6, <1% of YFP$^+$ cells in the anterior piriform cortex co-labelled for NeuN (>500 YFP$^+$ cells counted). These data confirmed that tamoxifen induced the YFP-labelling of OPCs but an insignificant number of NeuN$^+$ neurons. In addition to OPCs, a population of YFP$^+$ PSA-NCAM$^+$ cells were also detected in the aPC (Fig. 4.11B), which constituted 11% ± 6% of all YFP$^+$ cells (>400 YFP$^+$ cells counted). The YFP$^+$ PSA-NCAM$^+$ cells were smaller than OPCs, having cell bodies 5.2 ± 0.3 μm in diameter compared with 10.1 ± 0.5 μm for YFP$^+$ NG2$^+$ OPCs (20 cells measured in each case). These very small YFP$^+$ cells were also distinguished from OL lineage cells in the same region in that they did not express OLIG2 (Fig. 4.11C). Despite their small size, the YFP$^+$ PSA-NCAM$^+$ cells were not microglial cells as they did not express Iba1; indeed, no YFP$^+$ Iba1$^+$ cells were found in the anterior piriform cortex (>400 YFP$^+$ cells counted, Fig. 4.11D). Importantly, the YFP$^+$ PSA-NCAM$^+$ cells did not become EdU-labelled even when EdU was administered for 90 days (from P25 to P115; Fig. 4.12F). Therefore OPCs are the only EdU$^+$ YFP$^+$ double-labelled cells within the anterior piriform cortex, allowing their fate to be followed specifically *in vivo*.

Pdgfrα-CreER^{T2} : R26R-YFP mice were labelled with EdU from P25, tamoxifen was administered from P45-P48 (Fig. 4.11A) and the mice were analysed on P115 (P45+70). Coronal brain sections were double-immunolabelled for YFP and NG2 (OPCs), CC1 (OLs) or NeuN (neurons) (Fig. 4.12A-E). The sections were also processed to detect EdU. The vast majority of YFP$^+$ cells in the corpus callosum and motor cortex were OL-lineage cells that expressed NG2 or CC1. However, as previously reported (Rivers et al., 2008), YFP$^+$ neurons accumulated in the anterior piriform cortex where they were about as numerous as YFP$^+$, CC1$^+$ OLs (Fig. 4.11E). As expected, essentially all of the YFP$^+$ OPCs were EdU$^+$ in all brain regions examined (Fig. 4.12A, F) (<2% of YFP$^+$ OPCs escaped EdU-labelling). Therefore, all the differentiated progeny of YFP$^+$ EdU$^+$ OPCs would be expected to inherit both markers. This was true for YFP$^+$ CC1$^+$ OLs in the corpus callosum, motor cortex and anterior piriform cortex, which were clearly also EdU$^+$ (<4% of YFP$^+$ CC1$^+$ OLs escaped EdU-

labelling) (Fig. 4.12B-D, F), identifying them as cells that were generated from OPCs at some point between P45 and P115. However this was not true for the YFP^+ $NeuN^+$ neurons that accumulated in the anterior piriform cortex over the same time period. None of the YFP^+ $NeuN^+$ neurons had incorporated EdU (Fig. 4.12E, F) (>1000 YFP^+, $NeuN^+$ cells counted in 5 mice), indicating that they are not the progeny of YFP^+, EdU^+ OPCs in the postnatal mouse brain. This suggests that the YFP^+ anterior piriform cortex neurons were generated after P45 (when tamoxifen was given) by direct differentiation of precursor cells, as yet unidentified, that had were no longer proliferating and indeed must have undergone their final division before P25 (i.e. before EdU was administered).

4.3.6 YFP^+ $PSA\text{-}NCAM^+$ cells in the anterior piriform cortex are post-mitotic cells that are born before P25

The YFP^+ EdU^{neg} $PSA\text{-}NCAM^+$ cells that were identified in the anterior piriform cortex of P45+6 *Pdgfrα-CreER^{T2} : R26R-YFP* mice could be the source of the YFP^+ EdU^{neg} anterior piriform cortex neurons detected at P45+70. None of the rare YFP^+ $PSA\text{-}NCAM^+$ cells remaining in the anterior piriform cortex at P45+70 (Fig. 4.11B) were EdU^+ (Fig. 4.12F), indicating that, like the YFP^+ $NeuN^+$ cells, they were not the progeny of YFP^+ EdU^+ OPCs. In fact no $PSA\text{-}NCAM^+$ cells detected in the anterior piriform cortex at any age had incorporated EdU (>150 $PSA\text{-}NCAM^+$ cells examined in 3 mice), indicating that they were born before EdU exposure began on P25. Therefore these cells, which were previously suggested to be an intermediate between OPCs and projection neurons (Guo et al., 2010), are actually a post-mitotic population that is not generated after P25 from proliferating OPCs nor from proliferating neural stem cells. At P45+70, $PSA\text{-}NCAM^+$ cells represented only $0.5\% \pm 0.1\%$ of all YFP^+ cells within the aPC (>1200 YFP^+ cells examined in n=3 mice; Fig. 4.11E). This fraction is 20-fold less than at P45+6 (Fig. 4.11D), reflecting their dilution by the accumulating number of YFP^+ OLs and neurons. Rivers et al. (2008), determined that YFP^+ $NeuN^+$ cells are added to the aPC of *Pdgfrα-CreER^{T2} : R26R-YFP* transgenic mice at a rate of ~0.18 cells per 30 μm coronal brain section per day, from 30 days after tamoxifen administration. This equates to ~7 YFP^+ neurons per section by P45+70 ((70 days - 30 days) x 0.18 per day = 7.2). In this study, the total number of YFP^+ $PSA\text{-}NCAM^+$ cells per 30 μm coronal brain section fell from ~7 cells per section at P45+6 to an average of ~1 cell per section at P45+70 (average number in 12 sections across 3 mice from each timepoint), which suggests that YFP^+ $PSA\text{-}NCAM^+$ cells either die or differentiate over time. Interestingly

the fall of ~6 YFP^+ PSA-$NCAM^+$ cells/section, can be seen to almost match the number of YFP^+ $NeuN^+$ neurons added to the aPC in the same time frame.

4.4 Discussion

OPCs were originally assumed to be a homogeneous class of immature oligodendroglial cell, but have since been subdivided according to their electrical properties (Chittajallu et al., 2004; Karadottir et al., 2008), gene expression profiles (Gensert and Goldman, 2001; Mallon et al., 2002; Lin et al., 2009), proliferation rates (Psachoulia et al., 2009), response to injury (Keirstead et al., 1998; Lytle et al., 2009) and their abilities to differentiate into myelinating OLs (Mallon et al., 2002; Dimou et al., 2008) or other types of cells including neurons (Guo et al., 2010; Rivers et al., 2008; Zhu et al., 2008). There continues to be much debate over how many sub-types of OPC there might be, and the most appropriate way to classify them. To advance understanding of this issue, experiments were performed examining both the histological and electrophysiological properties of OPCs. In summary, these data determined that all postnatal OPCs defined by strong expression of the NG2 proteoglycan: (1) co-express the mitogenic receptor PDGFRα, (2) express I_{Na} and are electrically excitable, (3) are mitotically active and incorporate EdU, and (4) generate differentiated OLs but not neurons.

4.4.1 OPCs in the postnatal mouse brain are excitable but do not fire action potentials

Injecting current into OPCs led to regenerative action potential-like depolarization waves, consistent with previous studies in mice (Chittajallu et al., 2004; Ge et al., 2009; De Biase et al., 2010). These action potential-like waves differed from neuronal action potentials and the action potentials previously described for OPCs in the rat cerebellar white matter (Karadottir et al., 2008), as they required a larger depolarization for activation, their amplitudes increased with larger current injections and the timescale of the waves was longer. These regenerative events could be induced in OPCs in all brain areas, and at all developmental stages investigated, suggesting they are a universal property of OPCs.

The likelihood that a cell will generate an action potential is determined by the magnitude of the voltage-gated sodium current and the effective cell membrane resistance (which can be adversely reduced by the conductance of the seal between the patch electrode and the cell membrane (Bakiri et al., 2009)). Thus, the difference in spiking behaviour I observed in mouse OPCs compared to rat OPCs (Karadottir et al.,

2008) might reflect the fact that mouse OPCs have a 6-fold lower ratio of I_{Na} magnitude to membrane resistance than was previously found for rat I_{Na} OPCs (Karadottir et al., 2008). It is conceivable that, even in mouse OPCs, more robust spiking behaviour would be observed *in vivo* in the absence of shunting by the seal between the patch electrode and the cell.

I observed significant variation among OPCs in the amount of current required to initiate Na^+ spikes (for the most excitable cells the minimum current needed was 60 pA), in part reflecting differences in input resistances of the cells (Bakiri et al., 2009). White matter OPCs have been reported to receive ~140 synapses (Kukley et al., 2007), for each of which the miniature excitatory post-synaptic current (EPSC) at the resting potential is ~6 pA (Kukley et al., 2007; Kukley et al., 2010), implying that 10 simultaneous EPSCs would be needed to trigger this response *in vivo* (60 pA/ 6 pA). This is likely to happen more frequently in development when synchronized neuronal firing occurs in the cortex (Mao et al., 2001), hippocampus (Mohns and Blumberg, 2008), cerebellum (Watt et al., 2009) and retina (Demas et al., 2003; Meister et al., 1991). However, whether or not full action potentials are produced by mouse OPCs *in vivo*, activation of their voltage-gated sodium channels is likely to amplify excitatory synaptic inputs, raising intracellular calcium levels to regulate OPC development, so the expression of I_{Na} by OPCs might play a key role in regulating the developmental myelination of active circuits.

4.4.2 Is excitability a regulator of OPC proliferation?

All OPCs have I_{Na}, proliferate and generate OLs *in vivo* (Figs. 4.8-4.12). However the rate of OPC proliferation and OL production varies significantly between brain regions, with OPCs in the white matter dividing more rapidly than those in the grey matter (Power et al., 2002; Psachoulia et al., 2009; Rivers et al., 2008; Dimou et al., 2008; Simon et al., 2011). Many factors regulate OPC proliferation, such as PDGF-AA, basic fibroblast growth factor (FGF2), and sonic hedgehog (Collarini et al., 1992; Pringle et al., 1989; Zhu et al., 1999). Furthermore the expression of NG2 by OPCs has been reported to enhance ligand binding to PDGFRα and the fibroblast growth factor receptor (Goretzki et al., 1999). In the presence of growth factors, OPCs can proliferate in the absence of neurons (e.g. Collarini et al., 1992). However, there is evidence that neuronal activity also influences OPC proliferation *in vivo*. For example, injecting TTX into the eye, to block action potentials in retinal ganglion neurons, causes a large decrease in OPC proliferation in the optic nerve (Barres and Raff, 1993). This inhibitory effect of TTX could be alleviated by supplying exogenous PDGF-A to the optic nerve,

suggesting that electrical activity stimulates release of PDGF-A within the nerve, or enhances the responsiveness of OPCs to PDGF-A (Barres and Raff, 1993). There is also other evidence that links growth factor signalling and electrical activity. PDGFRα signalling maintains the expression of delayed outward-rectifying K^+ channels by OPCs (Chittajallu et al., 2005) and block of K^+ channels as a consequence of glutamatergic signalling to OPCs may inhibit their proliferation and lineage progression (Knutson et al., 1997).

I considered whether OPC proliferation rate might correlate with the density of voltage-gated potassium channels (Knutson et al., 1997). The cell cycle time for OPCs in the corpus callosum of the P21 mouse brain is ~3 days, which is significantly shorter than the cell cycle time for OPCs in the motor cortex (~18 days; Young, Psachoulia and Richardson, unpublished) or aPC (~ 13 days, see Fig. 4.10B). Perhaps coincidentally, in P33 mice the peak outward K^+ current was 2-fold larger in the corpus callosum compared to the other regions (Fig. 4.9D), consistent with a potential role for K^+ currents in promoting a higher proliferation rate in white matter compared to that in grey matter areas at late developmental times.

4.4.3 OPCs generate OLs but not neurons in the postnatal mouse forebrain.

It has been reported previously that OPCs generate new neurons in the postnatal mouse brain (Rivers et al., 2008; Guo et al., 2010). In this study very small numbers of YFP^+, $NeuN^+$ neurons were observed throughout the forebrain of *Pdgfrα-CreER^{T2} : R26R-YFP* mice at short times post-tamoxifen but, in most brain areas, these neurons did not accumulate with time post-tamoxifen, as one would predict if they were produced continually from YFP^+ precursors and survived long-term. Similar observations were made using an independently-generated *Pdgfrα-CreER^{T2}* line (Kang et al., 2010) and an *Ng2-CreER* line (Zhu et al., 2011a), prompting the suggestion that the rare labelled neurons were the result of sporadic activation of the *CreER* transgenes in a subset of neurons (Kang et al., 2010; Zhu et al., 2011a). However, in this study YFP^+-labelled neurons were also observed in the anterior piriform cortex (but not the posterior piriform cortex; KM Young and WD Richardson, unpublished) that survived and accumulated for months following tamoxifen treatment, confirming the earlier results of Rivers et al. (2008). A similar accumulation of $mGFP^+$ neurons was also observed with time in the aPC of *Pdgfrα-CreER^{T2} : Tau-mGFP* transgenic mice (Fig. 4.13), demonstrating that this is not an artefact of the particular reporter mouse used.

It is difficult to understand how this could come about unless these particular neurons are produced continuously in the postnatal aPC from a pool of precursors that become YFP-labelled at the time of tamoxifen treatment. In the earlier studies, the YFP-labelled neurons were consistently BrdU-negative, even after extended BrdU exposure, as were ~50% of OPCs, suggesting that a sub-population of mitotically quiescent OPCs might differentiate directly into new aPC neurons without an intervening cell division. Now, using an alternative thymidine analogue (EdU), all OPCs in the forebrain were found to be mitotically active (see Fig. 4.10) and therefore OPCs cannot be the source of new neurons in the anterior piriform cortex, which are consistently EdU-negative (Fig. 4.12F). Therefore, these data now agree with Kang et al. (2010) who found that all OPCs, but no neurons, incorporated BrdU after a long labelling period. Nevertheless, the fact that YFP^+ neurons accumulate in the anterior piriform cortex after tamoxifen treatment of the *Pdgfrα-CreER*^{T2} : *R26R-YFP* mice still requires explanation, as does the apparent discrepancy between our line of *Pdgfrα-CreER* mice and the line made and used by Kang et al. (2010), who did not see an accumulation of neurons in the piriform cortex. It is conceivable that our line, but not theirs, marks an unidentified population of *Pdgfrα*-expressing neurogenic precursor/stem cells that either resides in the CNS or arrives there via the blood. Further experiments, e.g. with *Pdgfrα-CreER* knock-in mice, will be required to resolve this.

In summary, these data show that OPCs throughout the postnatal brain are electrically excitable, proliferative and are the precursors of new oligodendrocytes, but not neurons, at least over the time period I have examined, i.e. after P25.

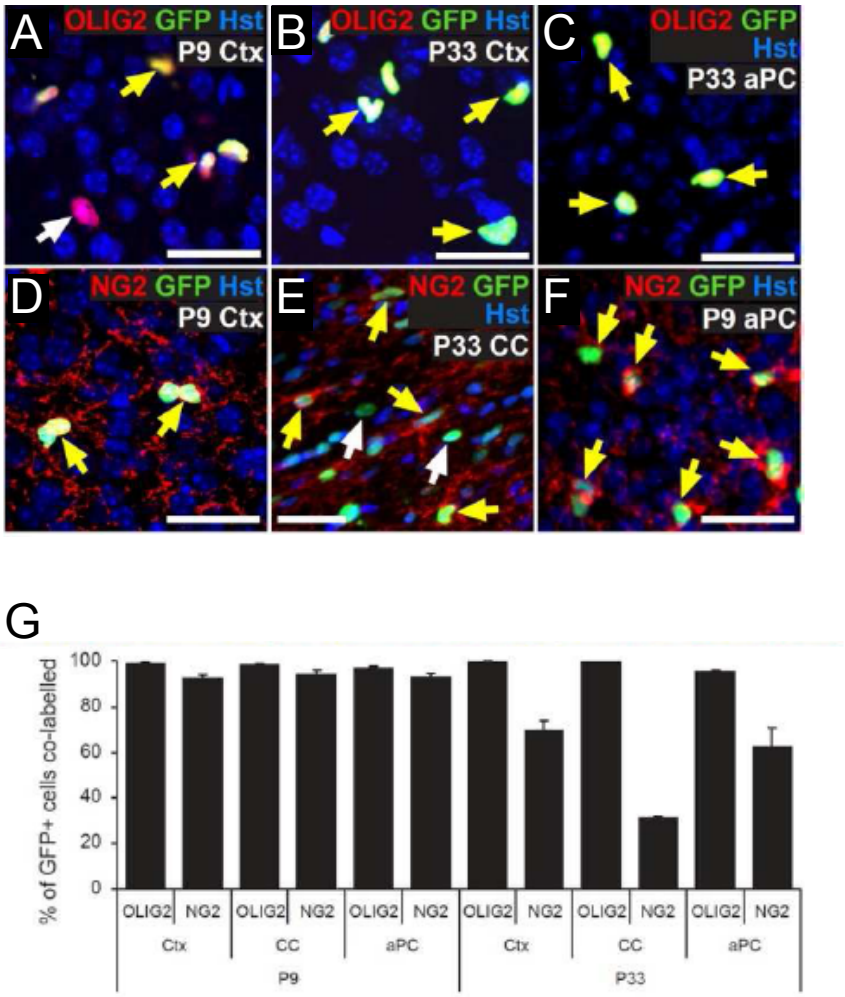

Figure 4.1. In *Pdgfra-GFP* mice GFP labels oligodendroglial cells in the postnatal brain.

A-F. Cryosections from P9 and P33 *Pdgfra-GFP* mice were immunolabelled to detect GFP (green) with either OLIG2 (red; **A-C**) or NG2 (red; **D-F**). Double-labelled cells are indicated by a yellow arrow, single labelled cells by a white arrow. Sections were also stained with Hoechst 33258 (Hst; blue) to detect cell nuclei. **G.** The proportions of GFP^+ cells that co-expressed each marker were quantified for the motor cortex (Ctx), corpus callosum (CC) and the anterior piriform cortex (aPC). The proportion of GFP+ cells that co-expressed NG2 fell significantly from P9 to P33 (ANOVA; $P< 0.01$). Scale bars: 20 µm.

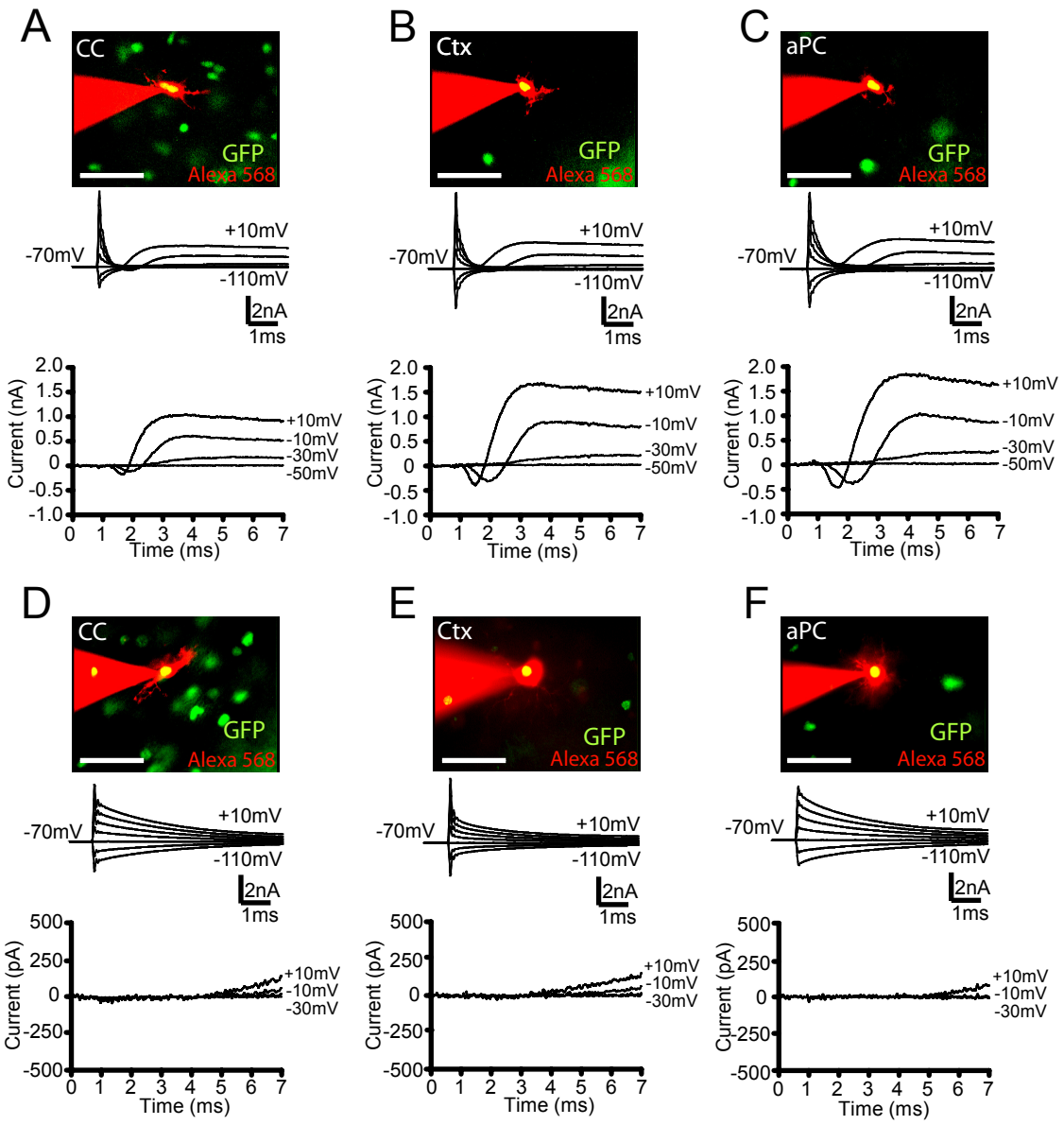

Figure 4.2. Two types of GFP⁺ OL lineage cell in the postnatal mouse brain.
A-F. Cells expressing GFP driven by the *Pdgfrα* promoter (green) were whole-cell patch-clamped and filled with Alexa Fluor-568 dye (red) (top image in columns **A-F**). Current responses (second panel of **A-F**) were recorded for GFP⁺ cells with and without I_{Na} (**A-C** and **D-F**, respectively), to 20 mV steps from -70 mV to -110 mV and to +10 mV. Voltage-gated currents were isolated by subtracting the capacity transient and ohmic leak current scaled linearly from that seen in response to evoked by a hyperpolarizing pulse (bottom sets of traces). Representative data, at either P9 (**A-D**) or P33 (**E, F**) from GFP⁺ cells in the corpus callosum (CC) (**A, D**), cortical grey matter (Ctx) (**B, E**) and anterior piriform cortex (aPC) (**C, F**) are shown. Scale bars: 50 μm

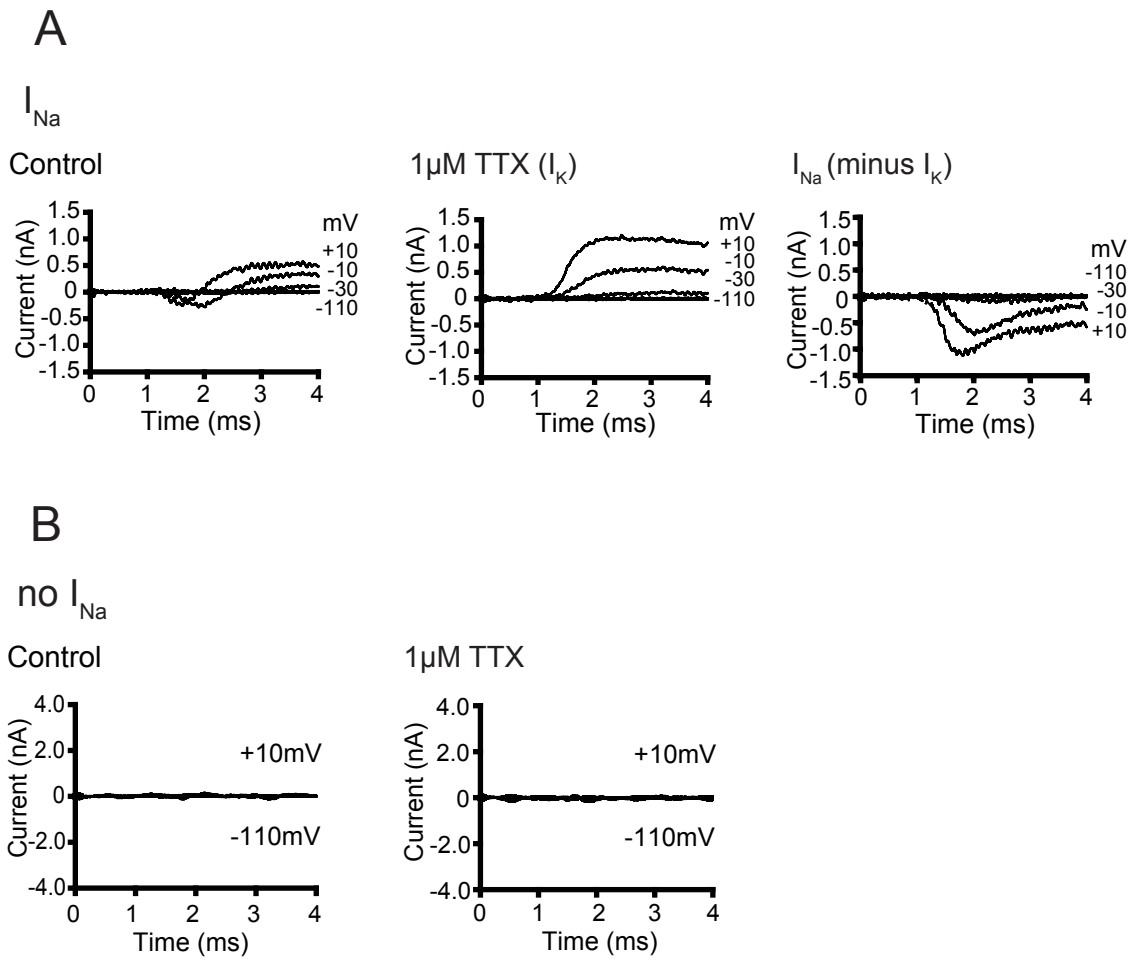

Figure 4.3. I_{Na} currents in GFP⁺ cells are blocked by TTX.
A, **Left**: Capacity transient and ohmic leak - subtracted responses of a GFP⁺ cell with I_{Na}, to 20 mV steps from -70 mV (to -110 mV and to +10 mV). **Middle**: 1 μM TTX blocked the inward Na^+ current. **Right**: Subtracting the voltage-gated K^+ current isolated in TTX from the total voltage-gated current gave the voltage-gated Na^+ current. **B**, **Left**: Capacity transient and ohmic leak - subtracted responses of a GFP⁺ cell without I_{Na}, to 20 mV steps from -70 mV (to -110 mV and to +10 mV). **Right**: TTX did not change the current response of the cell to voltage steps. Traces are representative of 3 GFP⁺ cells without I_{Na}.

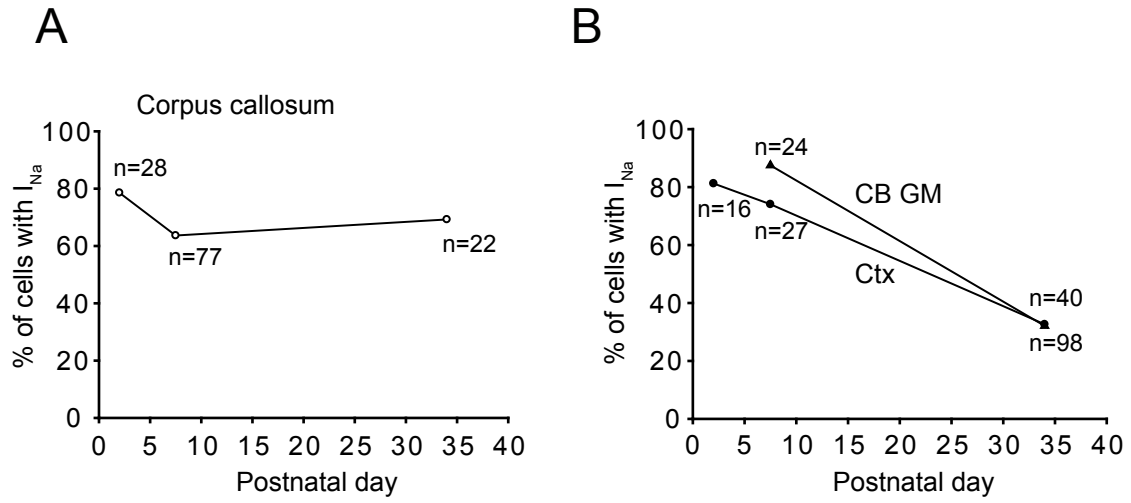

Figure 4.4. Two classes of OPC morphology cell can be detected early in development, and in all brain regions examined.
A,**B**,The percentage of OPCs that exhibit I_{Na} in white matter areas (**A**) (corpus callosum), and grey matter areas (**B**) cortex (Ctx); and cerebellar grey matter (CB GM) throughout development. Note that no significant difference could be detected in the proportion of cells expressing I_{Na} in the corpus callosum during development, however the proportion of cells expressing I_{Na} significantly decreased in the motor cortex ($P= 0.27 \times 10^{-3}$) and in the cerebellar grey matter ($P= 6.1 \times 10^{-5}$) between P9 and P30. These P values were obtained from a Chi^2 analysis with Yates small number correction.

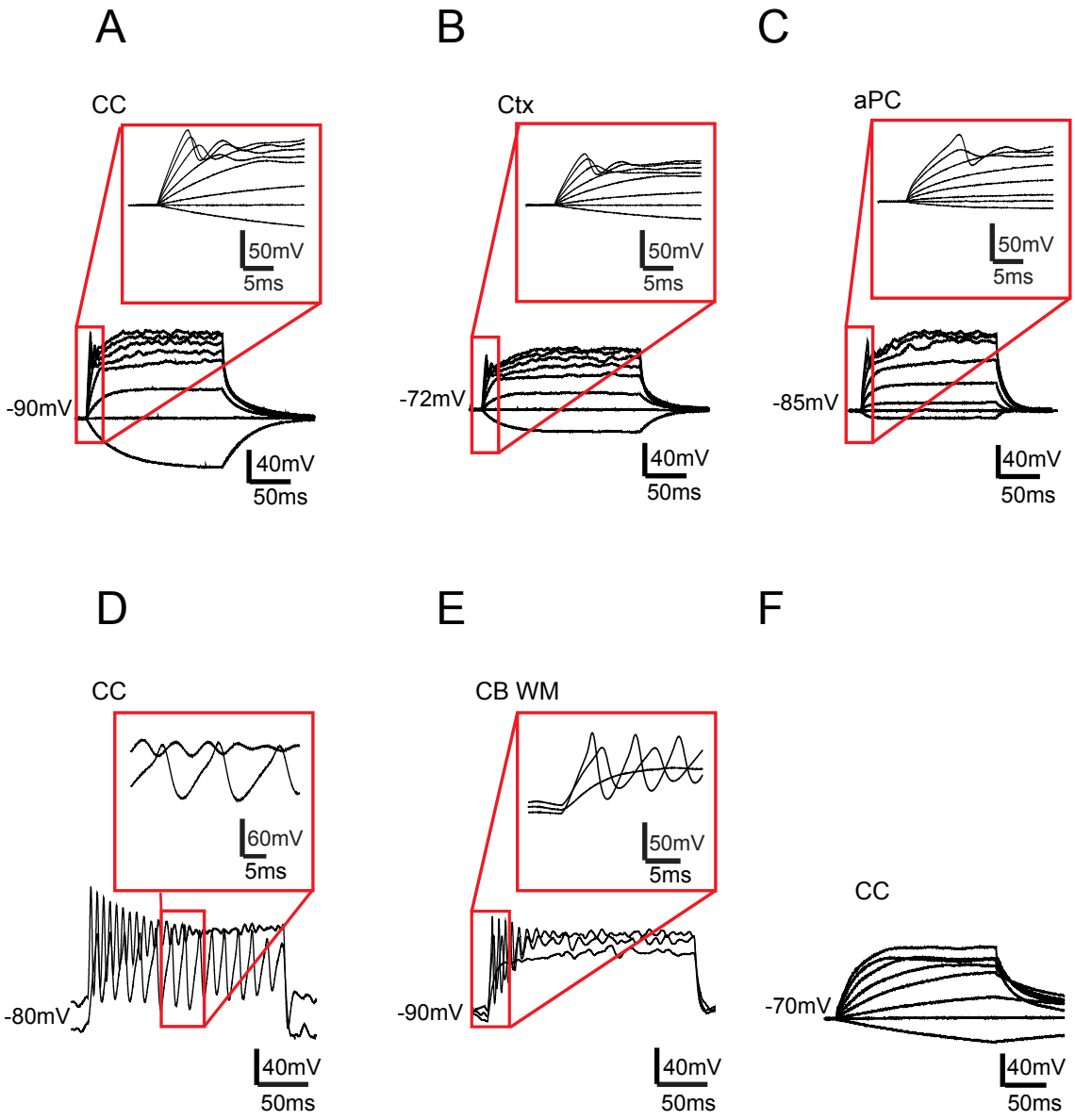

Figure 4.5. I_{Na}^+ GFP⁺ cells generate action potential-like events in response to current injection.

A-F, Responses of white and grey matter GFP+ cells to depolarizing current injection (-20, 0, 20, 60, 100, 160, 220 and 260 pA of current was injected). **A-C**, Current-clamp recordings for GFP+ cells with I_{Na}, at P9**,** in the corpus callosum (CC) **(A)**, cortical grey matter (Ctx) **(B)** and anterior piriform cortex (aPC) **(C). D-E**, Current-clamp recordings from GFP+ I_{Na} cells, which produce repetitive action potential-like waves in the corpus callosum at P33 (40, 140 pA was injected) (**D**), and cerebellar white matter (CB WM) at P9 (40, 80, 120 pA was injected) (**E**). Red boxes indicate the region of the trace that has been enlarged. **F**, Current-clamp recording of a GFP⁺ cell without I_{Na}, at P9 (-20, 0, 20, 60, 100, 160, 220 and 260 pA of current was injected), in the corpus callosum; similar responses were seen in cells lacking I_{Na} in all other brain areas examined.

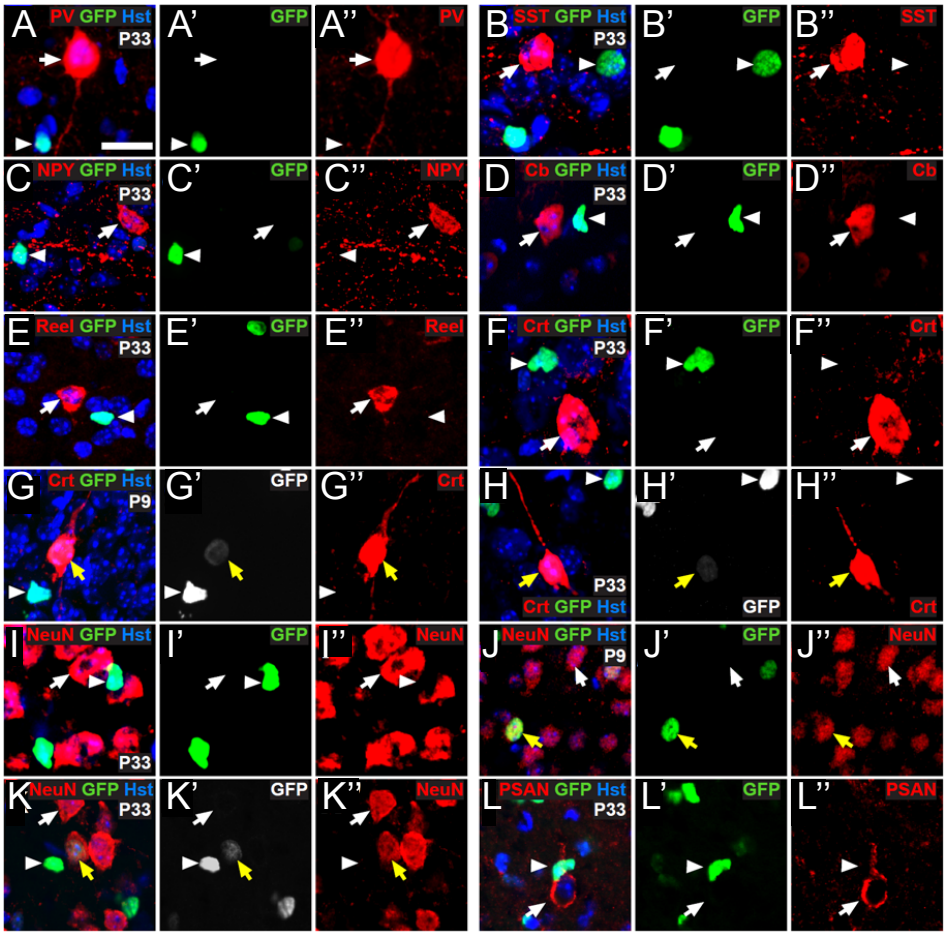

M

Neuronal marker	P9 GFP+ cells expressing marker (%)	No. P9 GFP+ cells examined	P33 GFP+ cells expressing marker (%)	No. P33 GFP+ cells examined
PV	0.00 ± 0.00	2114	0.09 ± 0.09	1612
SST	0.00 ± 0.00	2036	0.08 ± 0.08	2120
NPY	0.00 ± 0.00	2358	0.04 ± 0.04	2082
Cb	0.00 ± 0.00	2203	0.00 ± 0.00	2132
Reelin	0.09 ± 0.05	1967	0.20 ± 0.08	2605
Crt	3.59 ± 0.40	1671	1.48 ± 0.15	3365
NeuN	0.82 ± 0.07	1471	0.68 ± 0.12	2389
PSANCAM	-	-	0.00 ± 0.00	2633

Figure 4.6. A small proportion of calretinin⁺ interneurons express GFP in the medial motor cortex of *Pdgfrα-GFP* transgenic mice.
A-L, Cryosections from P9 and P33 *Pdgfrα-GFP* transgenic mice were co-stained to detect GFP (green) and a variety of neuronal markers (red): parvalbumin (PV; **A**), somatostatin (SST; **B**), neuropeptide Y (NPY; **C**), calbindin (cb; **D**), reelin (**E**), calretinin (crt; **F-H**), NeuN; (**I-K**) and PSA-NCAM (**L**). **M**, The number of single labelled GFP+ cells (white arrowheads in A-L), single labelled neuronal cells (white arrows) and co-labelled cells (yellow arrows) was counted. The table gives the proportion of GFP+ cells that co-expressed each neuronal marker. This was quantified in the motor cortex for 3 mice and is expressed as the average percentage ± s.e.m. The total number of GFP+ cells examined is also given. The only neuronal markers expressed by subsets of cortical GFP+ cells were calretinin and NeuN. Scale bars:15 μm (A, C-E, H, J-L) or 10 μm (B, F, G, I).

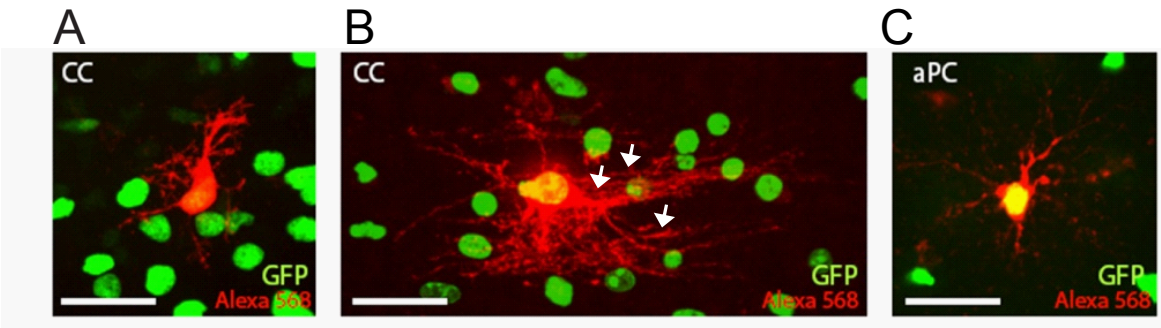

Figure 4.7. Morphology of *PDGFRα-GFP* expressing OPCs.
A-C GFP was mainly expressed by cells with typical OPC morphology in white and grey matter (e.g. dye-filled OPCs in the corpus callosum (CC) (**A**) and anterior piriform cortex (aPC) (**C**)), but GFP could also be occasionally detected in cells that were more advanced in their differentiation, with more oligodendrocyte-like morphology including myelinating internodes (e.g. dye-filled GFP expressing cell in the corpus callosum (CC) with some myelinating internodes labelled with white arrows, **B**). Scale bars: 30 μm.

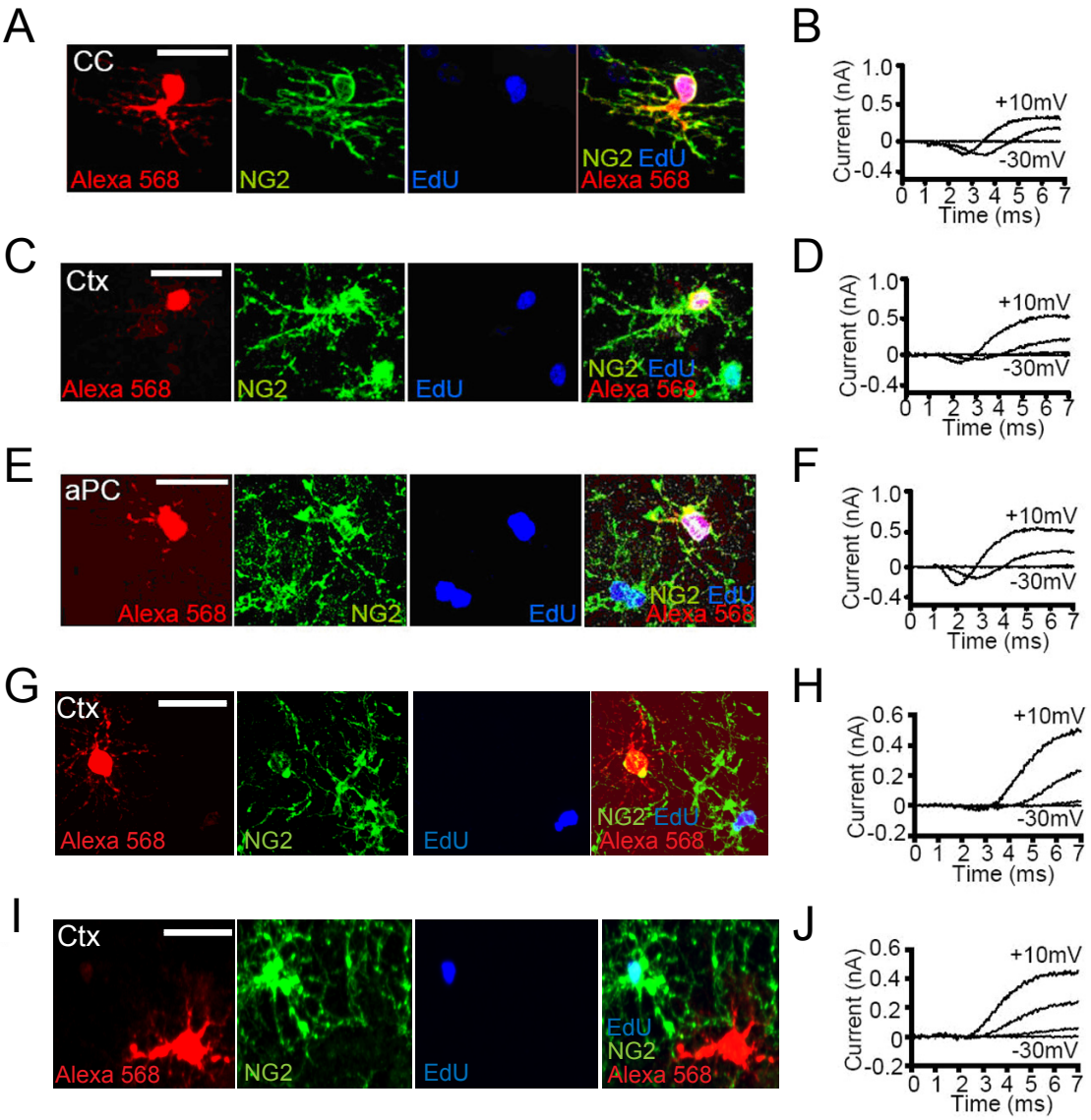

Figure 4.8. Characterisation of NG2$^+$ expression, I_{Na} expression and proliferation in GFP$^+$ OPCs.

A-J, Images of dye fills of whole-cell patch-clamped GFP$^+$ cells in corpus callosum (CC), cortical grey matter (Ctx) and anterior piriform cortex (aPC), and labelling for NG2 and EdU (left panel), together with current responses to depolarizing voltage steps in 20 mV increments from -70 mV (right panel). Cells fell into one of three groups: **A-F,** NG2$^+$ I_{Na}^+ mitotic (EdU$^+$) OPCs; **G-H,** NG2^{low} I_{Na}^{low} early differentiating OLs; and **I-J,** electrically passive OLs (NG2^{neg}, I_{Na}^{neg}). Scale bars: 20 μm.

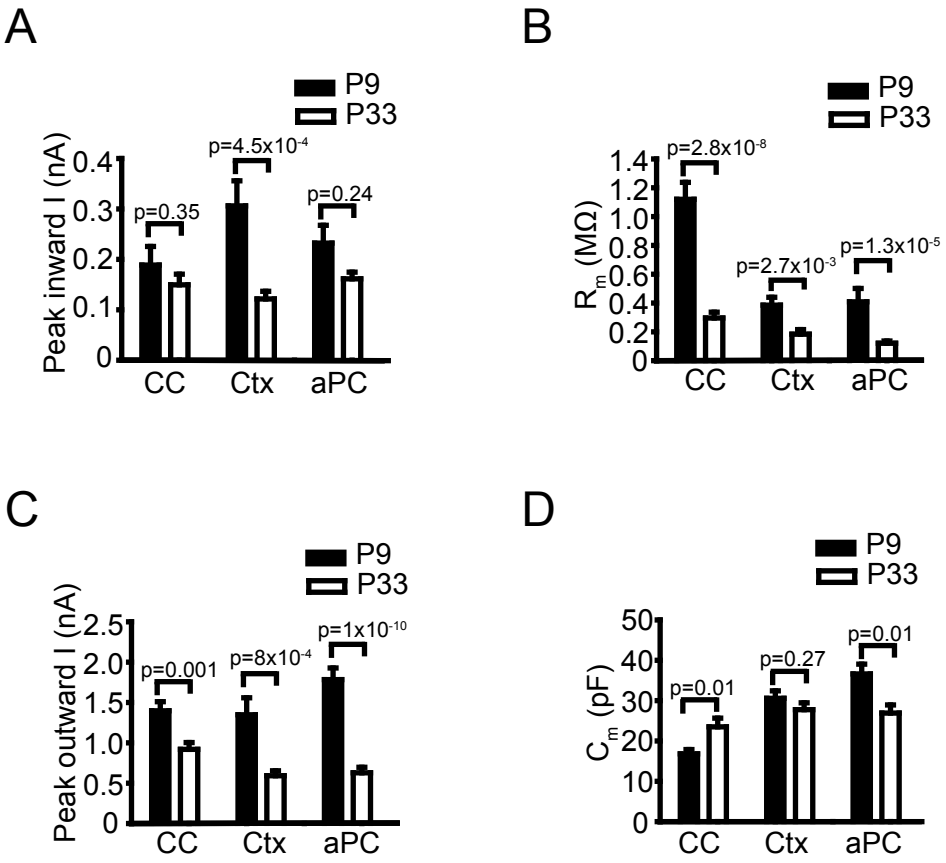

Figure 4.9. All NG2$^+$ OPCs express I_{Na}.
A-D, The average electrophysiological data for NG2$^+$ OPCs (mean ± s.e.m.) at P9 (corpus callosum (CC) n=20, motor cortex (Ctx) n=15, anterior piriform cortex (aPC) n=14 cells) and P33 (corpus callosum (CC) n=22, motor cortex (Ctx) n=17, anterior piriform (aPC) n=41 cells) are shown, including: **A**, peak inward current on depolarization from -70 mV to +10 mV, **B**, membrane resistance at -70 mV; **C**, peak outward current (on depolarization from -70 mV to +10 mV), and **D**, membrane capacitance at -70 mV.

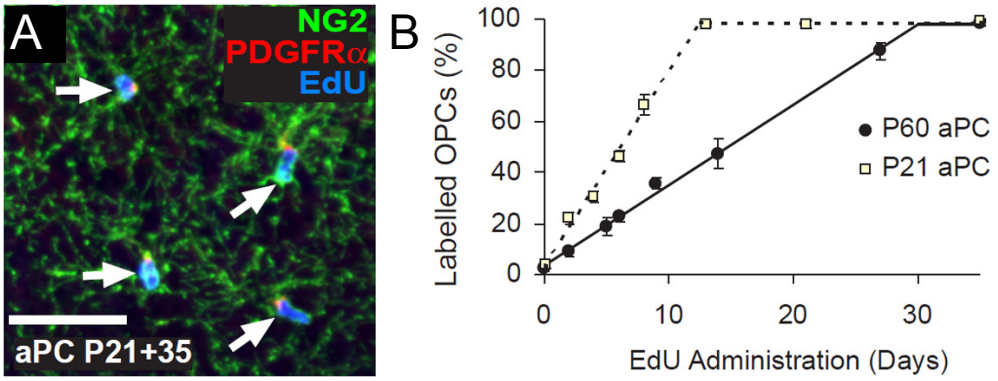

Figure 4.10. All NG2$^+$ OPCs in the anterior piriform cortex proliferate and incorporate EdU.
A, Coronal brain sections containing the anterior piriform cortex (aPC) immuno-labelled to detect PDGFRα (red) and NG2 (green) in order to identify OPCs, and then developed to visualize EdU incorporation (blue). **B,** The proportion of OPCs (PDGFRα$^+$ NG2$^+$) that had incorporated EdU as a function of EdU administration time (mean ± s.e.m., n=3 mice for each timepoint). Scale bar: 35 μm.

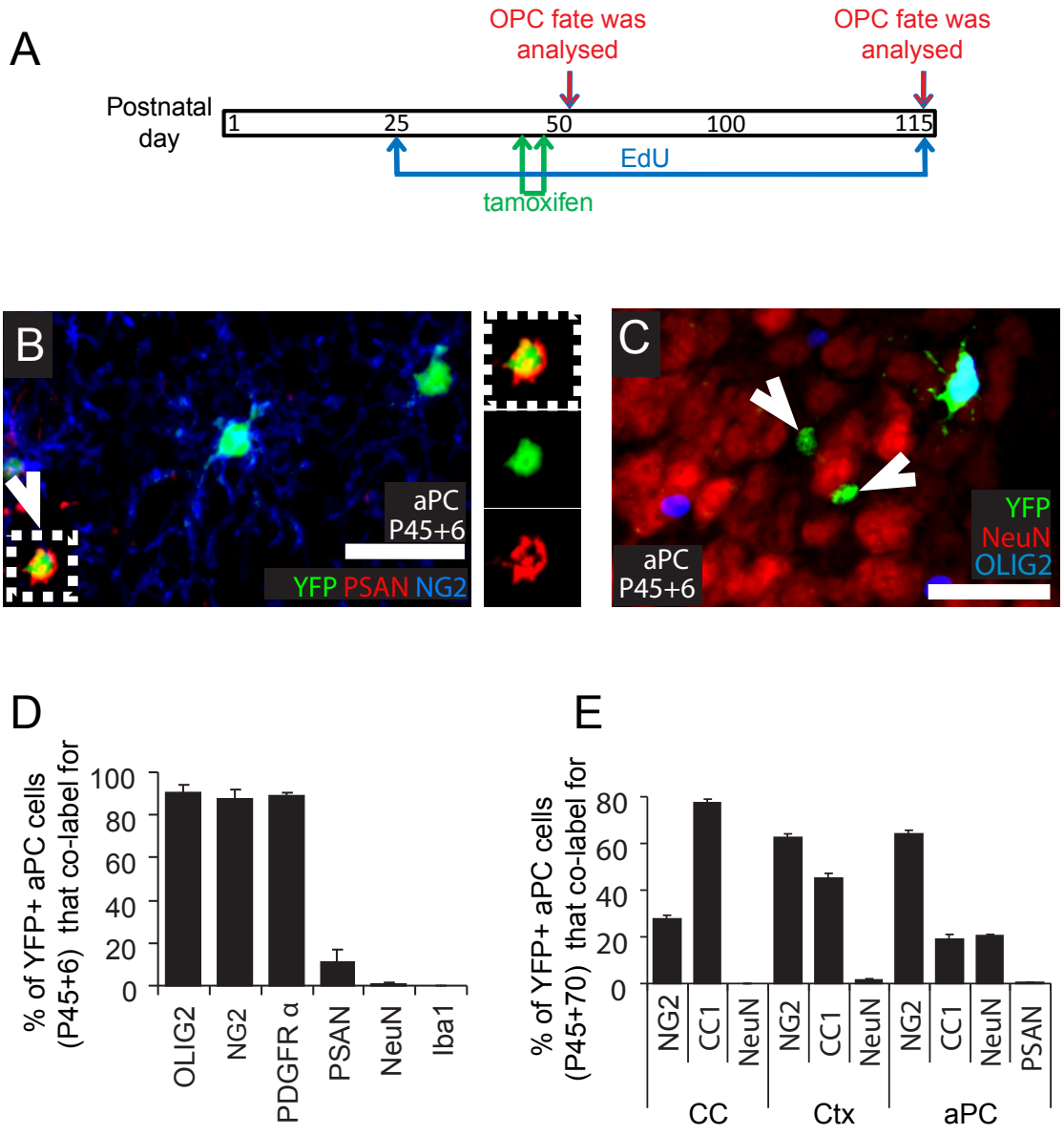

Figure 4.11. Characterisation of OPC cell fate in the postnatal mouse brain after activating Cre recombination to label OPCs with YFP.

A, *Pdgfrα-CreERT2 : R26R-YFP* transgenic mice received EdU from P25 to label dividing cells, as well as tamoxifen from P45-P48 to activate Cre recombination to label OPCs, and were perfusion fixed at P51 (P45+6) and P115 (P45+70). **B,** Immunolabelling of the anterior piriform cortex (aPC) of P45+6 *Pdgfrα-CreERT2 : R26R-YFP* transgenic mice for NG2 (blue), GFP (green) and PSANCAM (red) shows OPCs (centre and top right) as well as a small GFP$^+$ cell (arrow head) that also labels for PSANCAM. **C**, Immunolabelling of the anterior piriform cortex of P45+6 *Pdgfra -CreERT2 : R26R-YFP* transgenic mice for OLIG2 (blue), GFP (green) and NeuN (red). White arrowheads indicate unidentified YFP$^+$ cells in the anterior piriform cortex that lack OLIG2 expression. **D**, Proportions of YFP$^+$ cells in anterior piriform cortex (aPC) of P45+6 *Pdgfrα-CreERT2 : R26R-YFP* mouse brains that were either OPCs (NG2$^+$), OLs (CC1$^+$), neuroblasts (PSANCAM$^+$, PSAN), neurons (NeuN$^+$) or microglia (Iba1$^+$) (mean ± s.e.m, n=3 mice). **E**, Proportions of YFP$^+$ cells in the corpus callosum (CC), motor cortex (Ctx) and anterior piriform cortex (aPC) of P45+70 *Pdgfrα-CreERT2 : R26R-YFP* mice that were OPCs (NG2$^+$), OLs (CC1$^+$) or neurons (NeuN$^+$) (mean ± s.e.m, n=3 mice), and proportion in aPC that were PSANCAM$^+$. Scale bars: 30 μm.

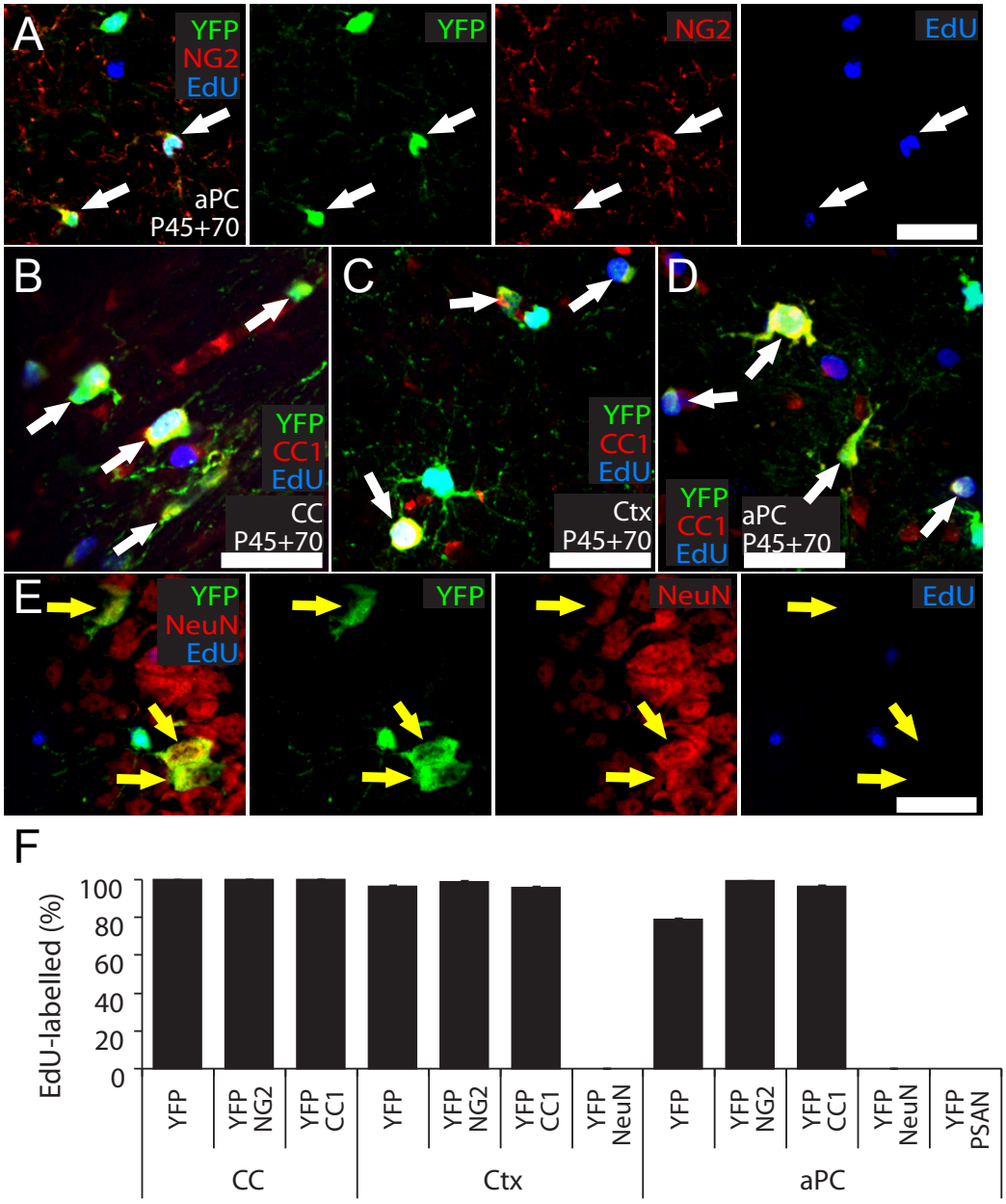

Figure 4.12. OPCs generate new OLs but not neurons in the postnatal mouse brain.

A-F, *Pdgfrα-CreERT2 : R26R-YFP* transgenic mice received EdU from P25 to label dividing cells, tamoxifen from P45 -P48 to activate Cre recombination to induce YFP expression in OPCs, and were perfusion fixed at P51 (P45+6) and P115 (P45+70). **A,** Immunolabelling of the anterior piriform cortex (aPC) for NG2 (red), GFP (green) and detection of EdU (blue). **B-D**, immunolabelling of the corpus callosum (CC) (**B**), cortex (Ctx) (**C**) and anterior piriform cortex (aPC) (**D**) for CC1 antigen (red) to define mature oligodendrocytes, GFP (green) and detection of EdU (blue). **E**, Immunolabelling of the aPC for NeuN (red), GFP (green) and detection of EdU (blue). **F**, Percentage of YFP^+ OPCs (YFP^+ $NG2^+$), YFP^+ OLs (YFP^+ $CC1^+$) and YFP^+ neurons (YFP^+ $NeuN^+$ or YFP^+ $PSAN^+$) that incorporated EdU (mean ± s.e.m, n=3 mice). All YFP^+ oligodendrocyte lineage cells incorporate EdU, but YFP^+ neurons never incorporate EdU. White arrows indicate triple-labelled cells. Yellow arrows indicate double-positive, but EdU-negative cells. Scale bars:30 μm.

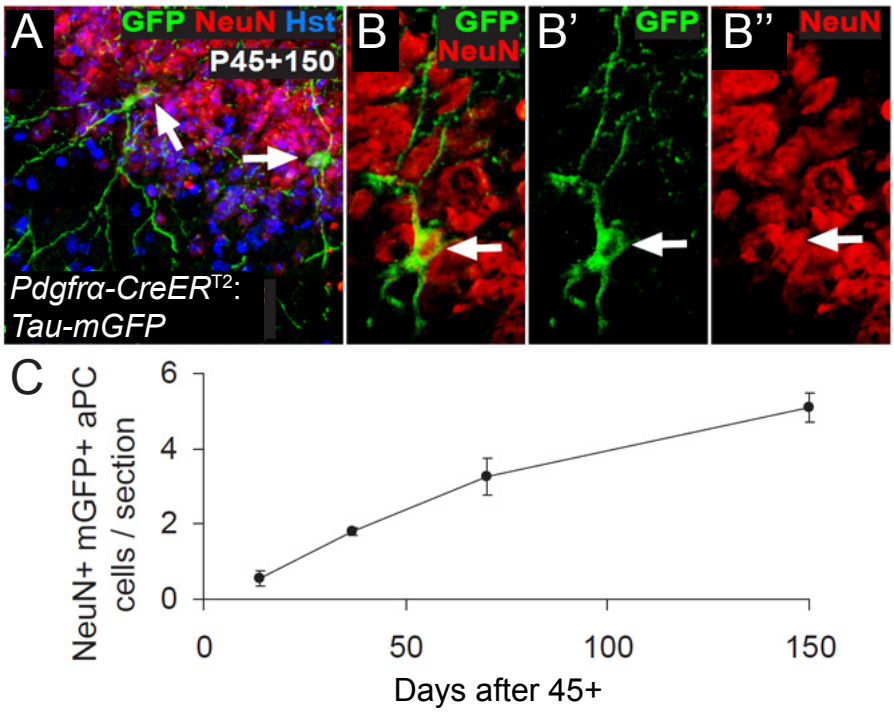

Figure 4.13. GFP$^+$ neurons accumulate in the aPC of postnatal *Pdgfrα-CreER^{T2} : Tau-mGFP* transgenic mice.

A-C, *Pdgfrα-CreER^{T2}* transgenic mice were crossed with a different reporter mouse that, following recombination, expresses a membrane targeted form of GFP (mGFP) under the control of the neuronal and oligodendroglial Tau promoter (*Tau-mGFP* reporter mice; Hippenmayer et al., 2005).The double heterozygous *Pdgfrα-CreER^{T2} : Tau-mGFP* transgenic mice received tamoxifen from P45-P48 to induce recombination in PDGFRα$^+$ cells, and were analysed at P45+ 14, 27, 70 and 150 days, by immunolabelling coronal brain sections to detect mGFP (green) and NeuN (red). Cell nuclei were stained with Hoechst 33258 (Hst; blue). **A**, A maximum intensity projection of a confocal image stack through a 30 µm brain section, demonstrating the location of mGFP$^+$ NeuN$^+$ neurons (white arrows) in layer II of the anterior piriform cortex (aPC). **B**, A single-scan (1 µm) confocal image through a mGFP$^+$ NeuN$^+$ neuron. **C**, Numbers of mGFP$^+$ NeuN$^+$ cells in the aPC of each 30 µm coronal brain section, showing a significant accumulation of mGFP$^+$ neurons with time. However this was smaller in magnitude than a previous report examining *Pdgfrα-CreER^{T2} : R26R-YFP* transgenic mice (Rivers et al, 2008), and likely reflects a difference in the recombination efficiencies of the two reporter lines.

Chapter 5: The effects of GABA on OPCs, mature oligodendrocytes and myelination

5.1. Introduction

During development or during plasticity and remyelination in the adult, the proliferation of oligodendrocyte precursor cells (OPCs) must generate the appropriate number of myelinating cells to ensheath the length of axon that needs to be myelinated. OPC proliferation and myelination are coordinated by communication between the axons to be myelinated and the developing oligodendrocyte lineage cells. As reviewed in chapter 1, this has long been known to involve growth factors such as PDGF-AA (Richardson et al., 1988; Barres & Raff, 1993) and neurotrophin-3 (Barres et al., 1994b). More recently, however, it has been discovered that OPCs receive excitatory and inhibitory synaptic input mediated by glutamate and GABA (Bergles et al., 2000; Lin & Bergles, 2004; Kukley et al., 2007, 2008; Ziskin et al., 2007; Káradóttir et al., 2008; Ge et al., 2009), raising the question of whether these neurotransmitters also regulate OPC development and myelination. In this chapter, I investigated the properties of GABA-evoked currents in oligodendrocyte lineage cells, and how GABAergic signalling regulates their proliferation, differentiation and myelination.

5.2. Methods

Transgenic mice and myelination assay

Sox10-GFP transgenic mice (described in detail in chapter 2, section 13.1-13.3) in which GFP is expressed in oligodendrocyte lineage cells (Kessaris et al., 2006), were used in an neocortical organotypic slice model of myelination (Rinholm et al., 2011) as described below.

Acute brain slices

Parasagittal cerebellar brain slices (225µm thick) were prepared from P7-P14 rats (as described in chapter 2, section 1). Slices were superfused at ~33℃ with bicarbonate buffered solution which contained the following (mM): 126 NaCl, 24 $NaHCO_3$, 1 NaH_2PO_4, 2.5 KCl, 1 $MgCl_2$, 2.5 (or 2 for EPSC experiments) $CaCl_2$, 10 D-glucose, pH 7.4 (bubbled with 95% O_2/5% CO_2).

Patch-clamp recordings

The electrophysiology of oligodendrocyte lineage cells was studied in acute parasagittal cerebellar slices, to mimic, as best as possible, the in vivo situation. Oligodendrocyte lineage cells were identified from their dye-fill morphology and I-V relations, and for some cells from post-recording antibody labelling, as described by Káradóttir et al. (2005, 2008). They were whole-cell clamped with pipettes with a series resistance of 8-20 MΩ. The electrophysiology of neurons was studied in the organotypic slice cultures used to study myelination. Neurons were identified from their dye-fill morphology and I-V relations, and were whole-cell clamped with pipettes of series resistance 5-15 MΩ. Electrode junction potentials were compensated. I-V relations were from responses to 200 msec voltage steps.

Electrodes were pulled from thick-walled borosilicate glass to a resistance of 6-9 MΩ for oligodendrocyte lineage cells and 2-5 MΩ for neurons. Electrodes were filled with Cs-gluconate (for oligodendrocytes) or K-gluconate (for OPCs and neurons) based solution containing (mM): 130 Cs- or K-gluconate, 4 NaCl, 0.5 $CaCl_2$, 10 HEPES, 10 BAPTA, 4 MgATP, 0.5 Na_2GTP, 2 K-Lucifer yellow (pH 7.3).

Synaptic currents were recorded in neurons at -40mV, analysed using Clampfit 10.1, and were defined to occur if their amplitude was >3 times the standard deviation of the current noise in a period without visible synaptic currents and their 10-90% decay time was longer than their rise time.

Organotypic cortical slice cultures and myelination assay

An assay for myelination was employed using brain slices in which transgenically labelled oligodendrocyte lineage cells fluoresce green, and neuronal axons and myelin are identified and quantified with immunofluorescence (Rinholm et al., 2011). This allowed assessment of whether changes in myelination reflected changes in the number of oligodendrocyte lineage cells, of axonal density or of the myelinating activity per oligodendrocyte lineage cell.

Coronal cortical slices from 8 day old transgenic mice were cut, and then cultured as described in chapter 2, section 2.3. After 2 weeks in culture the slices were fixed and immunolabelled with markers for myelin (MBP primary, and AlexaFluor 555 secondary antibodies) and axons (NF200 primary and Cy5.5 secondary antibodies: this emission is recoloured blue in the figures). Images (confocal Z stacks) were taken of myelination within the grey matter of the cortex, covering layers I-VI.

Myelination was quantified (using Metamorph or Image J) either by measuring (averaged over an 920 by 920 μm area) the peak intensity of MBP labelling divided by that of the axon labelling (NF200) in the confocal stack image with the largest intensity in each stack, to obtain a measure of myelination per axon (Rinholm et al., 2011), and then averaging over 2-6 stacks from each slice, or by counting the fraction of axons myelinated in four contiguous regions (Fig. 5.8, 30 μm by 25 μm). The amount of myelin per length of axon was measured by placing a 3 μm by 3 μm square over the first (from the top left corner) myelinated axon found crossing the top edge of each of the regions shown in Fig. 5.8 and integrating the MBP intensity over this 3 μm square area. Internode length (Fig. 5.10) was measured between two nodes of Ranvier, one at least of which was within a 92 μm by 160 μm region, and the internode was followed to its end even if that was outside the initial observation region. These internode lengths defined by MBP labelling are approximately 1 μm shorter than the length that would be measured from the centre of one node to the centre of the next. Measurements were also made of the number of nodes of Ranvier per field of view (Fig. 5.10), and the length of nodes of Ranvier (Fig. 5.10).

Immunohistochemistry and EdU labelling

Immunohistochemistry, in vitro EdU labelling and EdU detection were performed on organotypic slices as described in detail in chapter 2, section 14.

Statistics

The statistical analysis is described in detail in chapter 2, section 15.

5.3. Results

5.3.1 GABA-evoked currents in oligodendrocyte lineage cells

In acute brain slices, superfused GABA (100 μM) evoked a current in oligodendrocyte lineage cells in rat cerebellar white matter (Fig. 5.1 and 5.2) and mouse corpus callosum (chapter 3). In OPCs, this current was strongly inhibited by GABAzine (Fig. 5.1A, C). Applying GABAzine in the absence of superfused GABA had very little effect on the membrane current, suggesting there is little tonic GABA release onto these cells, at least in cerebellar slices (Fig. 5.1B). The magnitude of the GABA-evoked current did not differ significantly (Fig. 5.1D) between OPC-morphology cells that expressed or had down-regulated their voltage-gated Na^+ current (in contrast a decrease of glutamate-gated current is seen in cells lacking Na^+ currents: Káradóttir et al. (2008)). With the pipette $[Cl]_i$ chosen to set E_{Cl} to -87 mV, the GABA-evoked current

reversed at around -50 mV (Fig. 5.1D), which is more positive than the resting potential, so GABA would depolarize cells that were not voltage-clamped, as shown previously by Lin & Bergles, (2004). This positive value may largely reflect a contribution of HCO_3^- to the reversal potential (Kaila et al., 1989) which, for a permeability ratio of P_{HCO3}/P_{Cl} of 0.44 as is found in neurons (Fatima-Shad & Barry, 1993), will shift the reversal potential to -64 mV. Blocking accumulation of Cl^- inside the cell by NKCC1 transporters (Tyzio et al., 2011) using 100 μM bumetanide, moved the reversal potential negative by only 3.9±2.5 mV in 19 cells (10 with and 9 without voltage-gated Na^+ current, p= 0.14) (Fig. 5.1E), implying that operation of NKCC1 is not the main cause of the depolarised reversal potential.

GABA also evoked a current in cerebellar myelinating oligodendrocytes, which was strongly blocked by GABAzine (Fig. 5.2A). This current was unaffected by blocking $GABA_B$ receptors with CGP35348 (50 μM, Fig. 5.2B, I) or $GABA_C$ receptors with TPMPA (100 μM, Fig. 5.2C, I), and the $GABA_B$ agonist baclofen (40 μM) generated no current in 8 cells (data not shown). Inhibiting GAT-1 GABA transporters with 100 μM SKF-89976A (Fig. 5.2D, I), blocking ionotropic glutamate receptors with 25 μM NBQX and 50 μM AP5 (Fig. 5.2E, I), or blocking action potentials with 1 μM TTX (Fig. 5.2G, I), all had no effect on the GABA-evoked current (Fig. 5.2I). Thus, the current is not an uptake current, and is not a result of GABA depolarising neurons and triggering action potential evoked release of glutamate or some other agent. Furosemide, a $GABA_A$ receptor α_6 subunit blocker (Korpi et al., 1995), reduced the GABA-evoked current by 33±6% ($p=1.6X10^{-3}$) (Fig. 5.2F, I), suggesting that the $GABA_A$ receptors in oligodendrocytes may contain the α_6 subunit. However, this percentage block is far smaller than the almost 100% block found for tonic GABA receptor mediated currents in the nearby cerebellar granule cells (Rossi et al., 2003).

Unlike in OPCs, the GABA-evoked current in mature oligodendrocytes was inward at all potentials (Fig. 5.2H). This may suggest that the long cell processes are not well voltage-clamped by the pipette at the soma, so that at the ends of the processes the voltage remains below the reversal potential even when the soma is depolarised. Alternatively, GABA may generate an inward current in part by suppressing an outward K^+ current (Pastor et al., 1995), or part of the current may be generated by K^+ released when GABA depolarizes other cells in the slice (cf. Cheung et al., 2009). However, blocking K^+ channels (with 5mM 4-aminopyridine and 5 mM $BaCl_2$, or 5 mM 4-aminopyridine and 5 mM $BaCl_2$ together with 100 nM apamin and 20 mM TEA) had no effect on GABA-evoked currents in 12 mature oligodendrocytes (data

not shown). Despite uncertainty over the reason for the lack of reversal of the current at positive potentials, these data indicate that the GABA-evoked current is mediated by $GABA_A$ receptors (Berger et al., 1992; Pastor et al., 1995).

5.3.2 $GABA_A$ receptors are not activated on myelinating oligodendrocytes during ischaemia

The role of GABA in the response of oligodendrocyte lineage cells to pathological conditions like ischaemia was investigated, since GABA is known to be released in the white matter during ischaemia (Shimada et al., 1993). Application of a solution mimicking ischaemia (described in detail in chapter 2, section 2) evoked a slowly developing inward current (Fig. 5.3A). However, unlike application of glutamate receptor blockers which reduce ischaemia-evoked currents in oligodendrocytes and OPCs (Karadottir et al., 2005 and 2008), GABAzine did not reduce the ischaemia-evoked inward current (Fig. 5.3A, B). These data suggest that ischaemia-evoked GABA release does not greatly activate $GABA_A$ receptors on these cells, and does not significantly contribute to the ischaemic current.

5.3.3 Oligodendrocyte development in cultured cortical slices

To test the role of GABA in regulating oligodendrocyte development, organotypic brain slices were made from the frontal cortex of postnatal day 8 (P8) Sox10-GFP transgenic mice (Kessaris et al., 2006), in which oligodendrocyte lineage cells express GFP. Fixing slices after different durations in culture, and labelling with antibodies for neurofilament 200 (NF) and for myelin basic protein (MBP), allowed the imaging of neuronal processes as blue, oligodendrocyte lineage cells as green, and myelin as red (Fig. 5.4A).

Myelination develops over a period of about 2 weeks in these cultured slices (Fig. 5.4A, D). Initially many oligodendrocyte lineage cells are visible but, as neuronal processes develop, these become fewer in number as a result of cell death, and gradually myelin basic protein appears. Larger magnification pictures of the cultures (Fig. 5.4B, C) reveal that the great majority of the MBP is expressed in close apposition to neurofilament-labelled processes (only 11% of MBP labelled processes were not clearly wrapping neurofilament labelled axons, and these may be processes connecting internodes to the oligodendrocyte somata, or processes wrapping axons in which the neurofilament labelling was too weak to see). Thus, very few oligodendrocytes express MBP before they myelinate, and labelling is concentrated in

myelin around axons. Nodes of Ranvier are visible as gaps in the MBP labelling around axons (Fig. 5.4B and see below).

By counting the number of GFP expressing cells, and using the total fluorescence of NF antibody and MBP antibody as measures of the amount of neuronal processes and of myelin present (Rinholm et al., 2011), the progress of myelination in the cultures can be assessed as in Fig. 5.4D. During the first few days in culture the number of oligodendrocyte lineage cells increases as OPCs proliferate, which is followed by a decrease to below the initial number as cells die. After about a week in culture the number of neuronal processes reaches a plateau, while myelination continues to occur for at least another week. As a quantitative measure of the amount of myelin formed per neuronal process, the ratio of the MBP fluorescence to NF fluorescence was calculated (shown for different cortical layers in Fig. 5.4E). More detailed analyses of the percentage of axons myelinated and the myelin per individual axon are given below.

5.3.4 GABA, but not glutamate, regulates the number of oligodendrocyte lineage cells

To test the effect of endogenously released glutamate and GABA on the number of oligodendrocyte lineage cells generated, as a result of the balance between OPC proliferation and death, the NMDA receptor blocker MK-801 (50 μM), the AMPA/KA receptor blocker NBQX (25 μM), or the $GABA_A$ receptor blocker GABAzine (50 μM) were included in the culture medium from days 3 to 14 in vitro. Blocking NMDA receptors led to a 40±12% decrease (p=0.02) of the amount of neurofilament labelling in the cultures, probably because neurons need a basal level of NMDA receptor activation to survive (Hardingham & Bading, 2003), which precluded a meaningful analysis of whether NMDA receptors regulate myelination. However, deleterious effects on neurons were not observed when blocking AMPA/KA or $GABA_A$ receptors. When present from 3-14 days in vitro NBQX, which blocks excitatory synaptic transmission from axons to OPCs (Kukley et al., 2007; Ziskin et al., 2007), had no effect (Fig. 5.5A, B; p=0.99) on the number of oligodendrocyte lineage cells present at DIV14, nor on the amount of labelling for neurofilament or MBP (reduced by 3±11% (p=0.81) and increased by 4±6% (p=0.75) respectively, not shown). In contrast GABAzine, which blocks inhibitory synaptic transmission to OPCs (Lin & Bergles, 2004; Káradóttir et al., 2008), dramatically increased the number of oligodendrocyte lineage cells (Fig. 5.5A). Having NBQX present with the GABAzine (to reduce any neuronal excitability increase

produced by blocking $GABA_A$ receptors) did not significantly affect the increase produced by GABAzine (the increase was 0.5% larger, p=0.93, not shown).

Counting the number of GFP-labelled cells showed that GABAzine increased the number of oligodendrocyte lineage cells more than 2.6-fold in this particular experiment ($p=3x10^{-5}$, Fig. 5.5B; the mean increase over 7 independent sets of cultures was 1.76±0.08 fold ($p= 1.1x10^{-15}$, first 2 bars in Fig. 5.5G). Furthermore, this increase did not just lead to a larger population of OPCs that went on to die before or after differentiating into mature oligodendrocytes (as was seen previously by Calver et al. (1998) when increasing OPC proliferation with PDGF-A oversupplied from an integrated transgene). Using APC (adenomatous polyposis coli) antibody to define mature myelinating cells (Bhat et al., 1996) it was found that, by 2 weeks in culture, GABAzine had produced a large fractional increase in the number of mature (APC-expressing) oligodendrocytes (increased by 73%, Fig. 5.5C, D) as well as in the number of APC-negative NG2-expressing OPCs (increased by 48%, Fig. 5.5E, F). Since GABAzine increases the number of cells it follows that endogenous GABA, acting via $GABA_A$ receptors, normally acts to decrease the number of oligodendrocyte lineage cells, including mature oligodendrocytes.

Applying muscimol (10 μM), a $GABA_A$ receptor agonist, from days 3-14 in vitro had the opposite effect to GABAzine on the number of oligodendrocyte lineage cells present at DIV14 (Fig. 5.5G). Muscimol decreased the number of cells by 23±6% (p=0.0004, 32 slices). Thus, increases and decreases of $GABA_A$ receptor activation can bidirectionally alter oligodendrocyte lineage cell number.

The increase of the number of oligodendrocyte lineage cells produced by GABAzine did not depend on NKCC1 transporters accumulating Cl^- in the cell to shift positive the reversal potential for $GABA_A$ receptors (Lin & Bergles, 2004; Tyzio et al., 2011). NKCC1 was blocked with bumetanide (100 μM, present from 3-14 days in vitro), which on its own did not affect the number of oligodendrocyte lineage cells (p=0.2, 4^{th} bar in Fig. 5.5G). In the presence of bumetanide, adding GABAzine or muscimol produced a 1.71±0.12 fold increase ($p=2x10^{-7}$) or a 28±5% decrease (p=0.02), respectively, in the number of oligodendrocyte lineage cells present, i.e. changes that were not significantly different to those seen in the absence of bumetanide (Fig. 5.5G).

In contrast to the effects of blocking or activating $GABA_A$ receptors, blocking $GABA_B$ receptors with 50 μM CGP35348 or activating them with 10 μM baclofen had no effect on the number of oligodendrocyte lineage cells present (decreased by

12±8%, p=0.15, and increased by 2±8%, p=0.81, respectively, Fig 5.5G), unlike a previous report for pure OPC cultures (Luyt et al., 2007) in which activation of $GABA_B$ receptors increased OPC proliferation.

5.3.5 GABA regulates the proliferation and death of oligodendrocyte lineage cells

GABAzine could increase the number of oligodendrocyte lineage cells either by blocking a GABA-mediated suppression of OPC proliferation (as was previously suggested for neural precursor cells: LoTurco et al., 1995), or by blocking GABA-evoked cell death (Fig. 5.4D shows less GFP-labelled cells at 10-14 days in vitro than at 3-7 days in vitro, so some death of oligodendrocyte lineage cells is occurring). To investigate this GABAzine was applied from 3-6 days in vitro, i.e. the period in Fig. 5.4D when OPC proliferation dominates). At day 6, NG2-expressing OPCs accounted for the majority of the oligodendrocyte lineage cells (68.5±2.8% in control slices and 74.6±2.4% in GABAzine treated slices, not significantly different, p= 0.11). By DIV6, GABAzine had evoked a similar percentage increase in the number of oligodendrocyte lineage cells (1.72±0.04 fold, $p=8x10^{-7}$, Fig. 5.5H) as when it was applied from 3-14 days in vitro (1.76±0.08 fold, Fig. 5.5G).

Using the thymidine analogue EdU to define dividing cells (Chehrehasa et al., 2009), I found that GABAzine significantly increased the fraction of OPCs (NG2-expressing cells) that were dividing (from 70.6±2.8% in control slices to 93.4±0.7% in GABAzine treated slices, $p=4.0x10^{-9}$) between days 4 and 6 *in vitro* (Fig. 5.6A, B, C). In addition, I assessed the number of oligodendrocyte lineage cells undergoing apoptotic cell death at day 6 *in vitro* by labelling slices for cleaved caspase-3 (Sánchez-Gómez et al., 2003; Fig. 5.6D, E). GABAzine significantly reduced the proportion of Sox10-GFP cells undergoing apoptosis (from 1.9 ±0.2% in control slices to 1.2±0.1% in GABAzine treated slices, p=0.003, Fig. 5.6F). Thus, GABAzine regulates the number of oligodendrocyte lineage cells by increasing their proliferation and by decreasing their death, implying that endogenous GABA release normally suppresses proliferation and increases cell death. It is unclear whether these are two separate actions of $GABA_A$ receptors or whether GABA alters a single developmental pathway to switch the cell from a proliferative state to a state where more of them die.

5.3.6 Endogenous GABA release decreases myelination

The increased number of APC-expressing cells in Fig. 5.5C-D indicates the possibility that GABA could control, not only the number of OPCs produced, but also the amount of myelination carried out. Figure 5.7 analyses the effect on myelination in

cortical slices of blocking the effects of endogenous GABA on $GABA_A$ receptors with GABAzine, or of activating $GABA_A$ receptors with muscimol (10 μM, present from days 3-14 in vitro). As in Fig. 5.5B, GABAzine greatly increased the number of GFP-expressing oligodendrocyte lineage cells present (by 1.83±0.09 fold, $p=2x10^{-14}$, Fig. 5.7A, B) while muscimol decreased the number present by 25±7% ($p=3x10^{-4}$). In contrast to this effect on oligodendrocyte lineage cells, neurofilament labelling was unaffected by either GABAzine or muscimol (Fig. 5.7C, D), showing that $GABA_A$ receptor activation has little effect on the growth of neuronal processes.

The changes in the number of oligodendrocyte lineage cells induced by exposure to GABAzine or muscimol produced significant alterations in myelination. Total MBP fluorescence was increased by 42±19% by GABAzine (p=0.01, Fig. 5.7E, F) and decreased by 33±7% by muscimol ($p=1x10^{-4}$). As a simple index of myelination per neuronal process, the summed fluorescence of the MBP present was normalised by the summed fluorescence of the neurofilament present. GABAzine increased this index by 26±10% (p=0.03, Fig. 5.7G, H) while muscimol decreased it by 37±6% ($p=9x10^{-4}$).

To determine whether the increase of myelination was due to a larger fraction of axons becoming myelinated, or to more myelin wrapping each axon, the fraction of neurofilament-labelled axons that were wrapped with MBP in four contiguous 30 μm x 25 μm rectangular areas per image were counted (Fig. 5.8A). This revealed that GABAzine increased by 25±6% (p=0.003) the fraction of axons myelinated, without producing a significant change in the number of axons present (Fig. 5.8B, C). In addition, by selecting only axons that were myelinated, and measuring the MBP fluorescence associated with a standard length of such axons (Fig. 5.8D), it was found that GABAzine also increased the amount of myelin labelling per length of myelinated axon by 28±11% (p=0.03, Fig. 5.8E). This might reflect an increase in the average thickness of the myelin around each axon, or an increase in the diameter of the axon (accurate measurement of which is beyond the resolution of the images) without an increase in myelin thickness, or both. Any of these scenarios would increase the conduction velocity of the underlying axon. Thus, GABAzine increases both the fraction of axons myelinated and the amount of myelin per axon, implying that endogenous GABA release normally has the opposite effects.

5.3.7 The effects of GABA are not via altered neuronal activity

The effects of endogenous GABA release on the number of oligodendrocyte lineage cells and on myelination could be mediated directly by the $GABA_A$ receptors I have demonstrated in Fig. 5.1 and 5.2 to be present on oligodendrocyte lineage cells.

Alternatively, blocking neuronal $GABA_A$ receptors might change neuronal activity, which could alter myelination by changing the release of growth factors (see Introduction) or of glutamate (Wake et al., 2011). I therefore assessed action potential activity in the cultured slices (after 8 days in vitro) by whole-cell patch-clamping neurons in the grey matter of the cortex and quantifying the frequency of TTX-suppressible synaptic currents they received at -40 mV. Prolonged application of GABAzine did not significantly change the action potential evoked EPSC rate (0.97±0.79 Hz in 12 cells in control slices, 1.13±0.64 Hz in 10 cells in GABAzine treated slices, p=0.88; Fig. 5.9). This lack of a large long-term effect of GABAzine could reflect homeostatic alteration of cell properties to regulate firing rate but, surprisingly, even at the onset of GABAzine application there was no significant change of EPSC rate (decreased from 1.46±0.84 to 0.98±0.44 Hz in 12 cells, including both spontaneous and action potential evoked EPSCs, p=0.57), possibly because GABA has both excitatory and inhibitory actions at this stage of development (Mohajerani & Cherubini, 2005) perhaps in different cell types (Sauer et al., 2012).

5.3.8 Endogenous GABA increases internode length

The large decrease in the number of oligodendrocyte lineage cells produced by endogenous GABA release (i.e. the opposite of the GABAzine effect in Fig. 5.5B) implies that there will be fewer OPCs competing to myelinate the same number of axons which, in addition to resulting in less axons becoming myelinated as described above, may result in each oligodendrocyte having to make longer internodes to myelinate the same length of axon. To analyse this, nodes of Ranvier were identified using antibody to ankyrin G, or as gaps in the MBP-labelling of the GFP-filled myelinating processes of oligodendrocytes (Fig. 5.10A).

GABAzine increased (p=0.02), while muscimol decreased (p=0.02), the mean number of nodes in each 146 μm square field of view (Fig. 5.10B). The 47% increase in node density produced by GABAzine is nearly 2-fold larger than the 25% increase in the number of axons myelinated (Fig. 5.8B), implying that GABAzine decreases the separation of nodes along axons, i.e. decreases the internode length. GABAzine and muscimol did not alter the lengths of the nodes themselves, whether quantified as the length of the gap between MBP-labelled processes (Fig. 5.10C), as the length between the ends of GFP-filled processes (Fig. 5.10D, which is shorter than the gap between the MBP labelling, because MBP is not expressed in the last 0.5 μm of the myelinating processes), or as the length of the ankyrin labelling of the axon (Fig. 5.10E).

The lengths of internodes were measured by tracing them from one node of Ranvier to the next. All internodal segments were measured that had one end in 92 μm by 160 μm regions (Fig. 5.10F), and the internodes were then followed to their ends even if they were outside the initial region. The resulting distribution of internode lengths differed significantly between control slices and GABAzine-exposed slices (Fig. 5.10G, $p=3x10^{-7}$ by Kolmogorov-Smirnov test), corresponding to a 13% decrease of mean internode length (from 52.7±1.2 to 46.6±1.7 μm, p=0.003) in GABAzine treated slices (Fig. 5.10H). In fact there is more shift of the distribution of internode lengths at shorter lengths, and the Gaussian fits to the distributions in Fig. 5.10G predict a 21% decrease of mean length in GABAzine. Thus, endogenous GABA release normally increases internode length.

5.4 Discussion

5.4.1 GABA evokes a current in all oligodendrocyte lineage cells

Application of GABA evoked currents in cells at all stages of the oligodendrocyte lineage, which were mediated by activation of $GABA_A$ receptors (Fig. 5.1 and Fig. 5.2). These data contradict previous work reported by Kirchhoff and Kettenmann (1992) suggesting that GABA responses disappear as OPCs differentiate into mature oligodendrocytes. OPCs are more spatially compact than mature cells, facilitating the control of the cell's voltage and intracellular Cl^-, and they displayed a reversing GABA-evoked I-V relationship. However, the reversal potential of the GABA-evoked current was more positive than the value of E_{Cl} (-87 mV) and slightly more positive than the reversal potential of -64 mV predicted assuming a significant HCO_3^- permeability of the channel (Fatima-Shad and Berry, 1993) from the Cl^- and HCO_3^- concentrations present in the solutions inside and outside the cell. Immature neurons are known to maintain a high $[Cl^-]_i$ because of the expression of the Cl^- accumulating transporter NKCC1, and a low level of the Cl^- extruding transporter KCC2, and therefore GABA exerts a depolarising rather than a hyperpolarising response in the immature brain ((Ben-Ari, 2002) but see Rheims et al. (2009) and Tyzio et al. (2011) for further discussion). Similarly, activation of $GABA_A$ receptors in OPCs has been reported to induce membrane depolarisation since the intracellular concentration of Cl^- is also high (Lin and Bergles, 2004). However, in OPCs, blocking NKCC1 with bumetanide did not significantly change the reversal potential of GABA-evoked currents (Fig. 5.1E).

The depolarisation evoked by $GABA_A$ receptors generates a $[Ca^{2+}]_i$ elevation by activating voltage gated Na^+ channels, raising $[Na^+]_i$ and thus reversing Na^+/Ca^{2+} exchangers (Tong et al., 2009). Interestingly, this unique Ca^{2+} signalling pathway has been shown to be involved in OPC migration (Tong et al., 2009). The data in this chapter suggest a further functional role of GABA in regulating OPC cell number and myelination, which will be discussed in more detail below.

In contrast to the OPCs, mature oligodendrocytes showed an inward current in response to GABA application at all potentials (Fig. 5.2). Previously, this has been attributed to GABA both activating a Cl^- influx through $GABA_A$ receptors and suppressing an inward rectifier K^+ conductance (Pastor et al., 1995). However, blocking K^+ channels with agents such as $BaCl_2$ which blocks inward rectifiers, indicated that the latter effect was not occurring in these experiments. In addition, application of glutamate receptor blockers and TTX had no effect on the GABA-evoked current in mature cells, further suggesting that GABA is not acting via an indirect pathway, activating neurons which release glutamate or K^+ onto oligodendrocytes. Finally, no evidence was found for the presence of $GABA_B$ or $GABA_C$ receptors in mature cells, which could contribute to the GABA-evoked current. In summary, these data indicate that the GABA-evoked response is mediated by $GABA_A$ receptors located on the oligodendrocytes, and the unusual I-V relationship may be a direct consequence of the complex morphology of these cells resulting in poor voltage-control of voltage and perhaps $[Cl^-]_i$ in the long processes.

GABAergic signalling to oligodendrocyte lineage cells could also play a role in pathological conditions. GABA is released in the white matter during ischaemia (Shimada et al., 1993) which may activate the $GABA_A$ receptors present on oligodendrocytes and their precursors. It is currently unclear whether GABA release exerts a beneficial effect by limiting depolarisation produced by glutamate release (Lutz, 1992) or a harmful effect since Cl^- influx facilitates water influx leading to cell swelling (Allen and Attwell, 2004). However, my data demonstrate that $GABA_A$ receptors are not significantly activated on myelinating oligodendrocytes during ischaemia, as application of GABAzine did not block or reduce ischaemia-evoked currents (Fig. 5.3). Interestingly, a suppression of $GABA_A$ responses during ischaemia has been reported for neurons (Allen et al., 2004).

5.4.2 Regulation of oligodendrocyte lineage cell number by GABA

Proliferation of oligodendrocyte precursor cells has been suggested to occur for a period that is regulated by an intrinsic clock (Raff et al., 1988) or to be controlled by

the availability of growth factors (Calver et al., 1998; van Heyningen et al., 2001), while differentiation of OPCs has been suggested to require a critical density of OPCs (Rosenberg et al., 2008). The data presented in this chapter reveal a previously unknown factor exercising a major influence on the number and density of oligodendrocyte lineage cells *in situ* in cerebral cortical slices, i.e. release of the neurotransmitter GABA.

Blocking the effects of endogenous GABA on $GABA_A$ receptors, using GABAzine, nearly doubled the number of oligodendrocyte lineage cells that are produced and survive, while increasing activation of $GABA_A$ receptors with exogenous muscimol reduced the number (Fig. 5.5G). In contrast, blocking glutamatergic excitation with NBQX had no effect on the number of oligodendrocyte lineage cells, and GABAzine produced the same increase in oligodendrocyte lineage cell number in the presence of NBQX (Fig. 5.5A-B, and associated text). This result, and the fact that GABAzine did not have a significant effect on neuronal activity, suggest that the actions of GABA are not mediated by an alteration of neuronal firing or a subsequent change of glutamate release acting on AMPA/KA receptors in OPCs, but reflect a direct action of GABA on oligodendrocyte lineage cells.

Endogenously released GABA reduces the number of oligodendrocyte lineage cells by two possibly linked mechanisms. First, it suppresses OPC proliferation (since GABAzine increases proliferation: Fig. 5.6A-C), as was previously suggested to occur for neural precursor cells (LoTurco et al., 1995). Second, it increases the death of oligodendrocyte lineage cells (since GABAzine decreases that death: Fig. 5.6D-F), cell death is known to occur both at the OPC stage and after differentiation into pre-myelinating oligodendrocytes (Barres et al., 1992; Trapp et al., 1997). As a result, the number of oligodendrocyte lineage cells which are produced and survive is determined not only by an endogenous clock and/or the availability of growth factors (Raff et al., 1988; Calver et al., 1998; van Heyningen et al., 2001), but also by locally released GABA.

The suppressive effect of GABA on the proliferation of neural precursor cells was suggested to be produced by membrane depolarization (LoTurco et al., 1995). However, although $GABA_A$ receptors are excitatory during early development (Lin & Bergles, 2004; Tyzio et al., 2011), the effects of GABA on oligodendrocyte development did not depend on NKCC1 transporters creating a high $[Cl^-]_i$ to make the reversal potential of GABA evoked currents more positive (Fig. 5.1E), since blocking NKCC1 with bumetanide did not alter the effect of GABAzine (Fig. 5.5G).

5.4.3 Regulation of myelination by GABA

Activation of $GABA_A$ receptors by endogenous GABA does not just decrease the number of OPCs produced, but also decreases the number of mature myelinating cells (Fig. 5.5C-D). As a result of this, blocking GABA's action with GABAzine led to an increase in myelination per axon (Fig. 5.7H), both because more axons become myelinated and because each myelinated axon has more myelin (Fig. 5.8C-E). GABAzine also decreased the mean internode length (Fig. 5.10). Although the mechanisms determining internode length are not understood at all, a simple explanation for why GABAzine decreases the internode length is that, when the number of OPCs is increased (Fig. 5.5E, F), there are more cells competing to myelinate the fixed number of axons present (Figs. 5.7C, D; 5.8B), so each ends up myelinating a shorter axon segment.

The GABA that regulates OPC development in these experiments is presumably released by interneurons in the grey matter (Lin & Bergles, 2004; Vélez-Fort et al., 2010). GABA released from inhibitory projection axons at synapses onto OPCs in some white matter tracts (e.g. from cerebellar Purkinje cell axons: Káradóttir et al., 2008) could have a similar influence in the white matter. OPCs themselves may modify the GABA concentration that they experience, because they express plasma membrane GABA transporters (Cahoy et al., 2008) and have even been suggested to release GABA by reversal of these transporters (Gallo et al., 1991). In addition the structure of interneuron–OPC synapses changes during development, so that at later times the peak GABA concentration experienced by the OPCs is reduced (Vélez-Fort et al., 2010), perhaps reducing the influence of GABA on OPC proliferation.

For grey matter OPCs, the timing of excitatory synaptic input is similar to that in nearby neurons (Mangin et al., 2008) suggesting that, if the same is true for inhibitory synaptic currents, then OPC development will be locally regulated by nearby interneurons. Consequently, the activity of interneurons could tune the conduction speed of nearby axons, and a differential density or activity of interneurons along the path of a set of axons might lead to a spatial variation of the fraction of axons that become myelinated, or a spatial variation of the internode length in the axons that do become myelinated. A spatial variation of internode length has been reported for axons in the auditory system (Seidl et al., 2010).

5.4.4 GABA actions on oligodendrocyte lineage cells and consequences for physiology and pathology in the brain

The effects of GABAzine show that release of endogenous GABA decreases myelination and increases internode length. This offers two separate ways in which GABA can tune the arrival time of action potentials. If, as a result of GABA release during development, some axons are prevented from becoming myelinated, then that will delay the arrival of action potentials at the ends of those axons. However, for axons that do become myelinated the longer internode length will, at least for the relatively short internodes characterised in Fig. 5.10, increase the conduction speed, because the internode length will be below the optimal length needed to maximise conduction speed (Brill et al., 1977). Further work is necessary to establish whether either of these mechanisms serves to tune the conduction speed of myelinated axons in order to beneficially influence information processing.

These data also have potential clinical implications, for brain cancer and for promoting remyelination. The reduction of oligodendrocyte precursor proliferation by GABA could explain an experimentally observed inverse correlation between the density of $GABA_A$ receptors and the malignancy of glioma cells (Jussofie et al., 1994; Labrakakis et al., 1998) some of which may develop from OPCs (Patt et al., 1996). This would suggest that pharmacologically increasing GABAergic signalling in gliomas may reduce cell proliferation and increase cell death, and hence reduce their malignancy. Furthermore, the fact that GABA modulates myelination during normal development raises the possibility that it may do the same during remyelination by adult OPCs in pathologies like multiple sclerosis and spinal cord injury. Excitatory axons make synapses onto adult OPCs during remyelination (Etxeberria et al., 2010), raising the possibility that the same might occur for inhibitory axons in the grey matter or in white matter tracts containing inhibitory axons. If this does occur, local block of $GABA_A$ signalling might serve to increase the number of OPCs available to carry out remyelination.

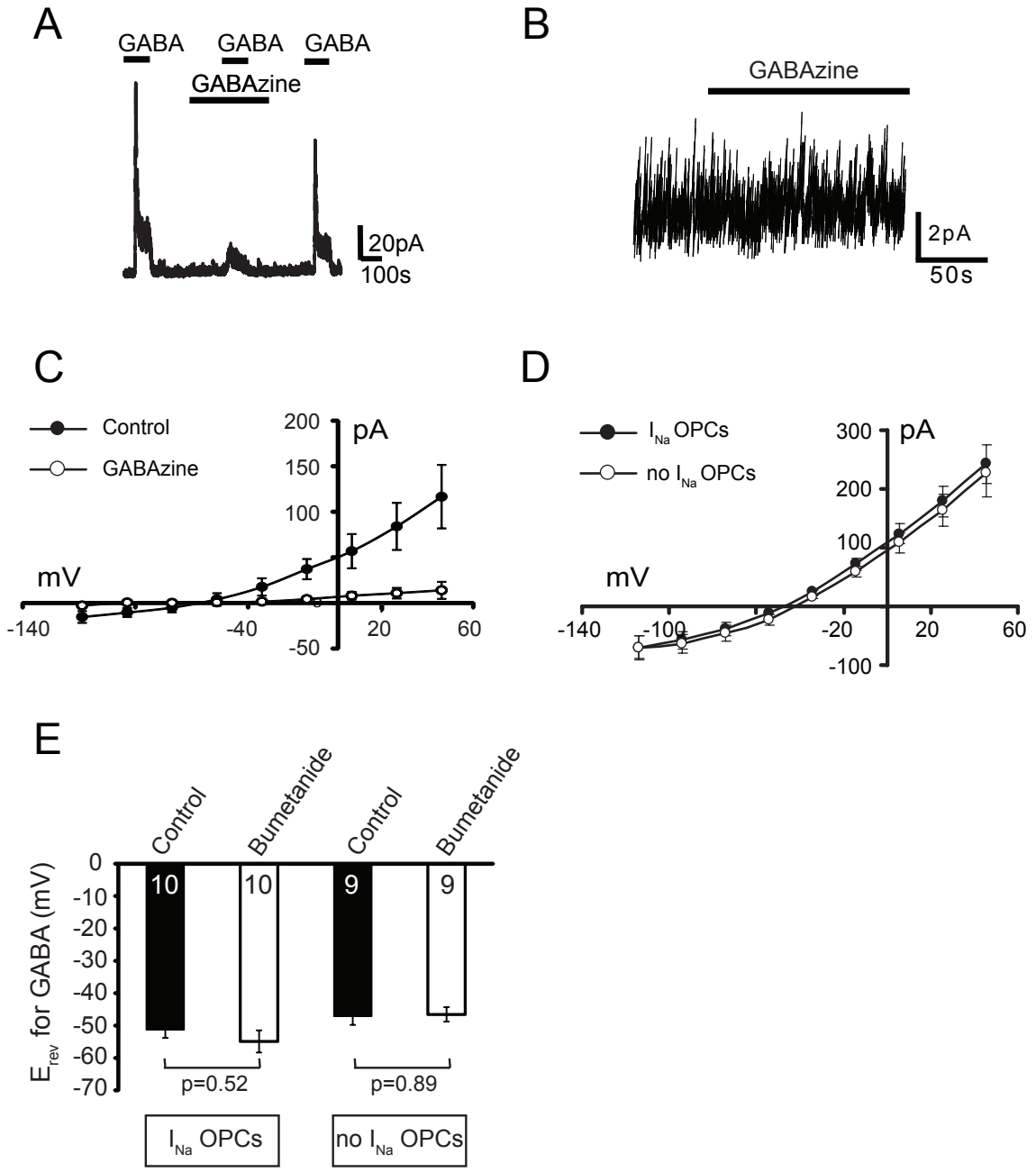

Figure 5.1. GABA evokes a current via $GABA_A$ receptors in OPCs.
A, GABA (100 μM) evoked an outward current at depolarised potentials which was effectively blocked by the $GABA_A$ receptor blocker GABAzine (10 μM). **B**, GABAzine did not affect the baseline current in OPCs. **C,** Mean GABA-evoked IV relationship for OPCs with and without GABAzine (10μM). **D,** Mean GABA-evoked IV relationship for OPCs with I_{Na} (closed circles) and without I_{Na} (no I_{Na}) (open circles), which reverse at a more positive potential than the predicted E_{Cl} (-87 mV), possibly because of a contribution of HCO_3^- to the current. **E**, Blocking accumulation of Cl- inside the cell by NKCC1 transporters with 100 μM bumetanide did not significantly change the reversal potential in OPCs with or without I_{Na}. Numbers of cells are shown on the bars.

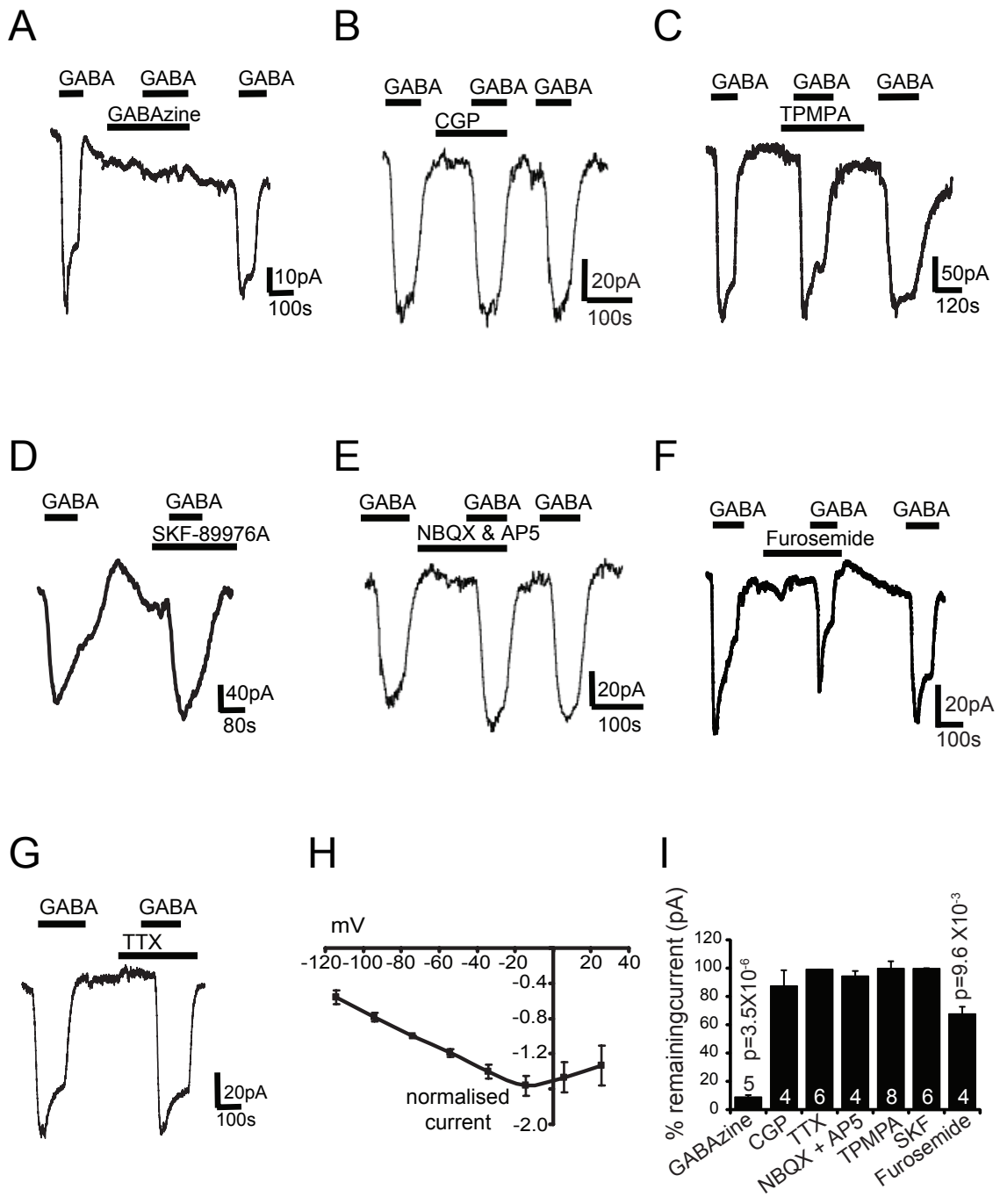

Figure 5.2. GABA evokes a current mediated via $GABA_A$ receptors in mature oligodendrocytes.

A-G, Current response at -74 mV of cerebellar oligodendrocytes to 100 μM GABA, and the effect on the current of a $GABA_A$ receptor blocker (**A**: 10 μM GABAzine), a $GABA_B$ receptor blocker (**B**: 50 μM CGP35348), a $GABA_C$ blocker (**C**: 100 μM TPMPA), a GAT-1 transporter blocker (**D**: 100 μM SKF-89976A), blockers of AMPA/KA and NMDA receptors (**E**: 25 μM NBQX and 50 μM D-AP5) , a $GABA_A$ receptor α_6 subunit blocker (D: 100μM furosemide), and an action potential blocker (**G**: 1 μM TTX). **H**, I-V relation for GABA-evoked current in 14 oligodendrocytes (normalised to the value at -70 mV). **I**, Percentage of current remaining unblocked in the blockers shown, number of cells are shown on the bars and p values (Holm-Bonferroni corrected for multiple comparisons) are shown where the changes were significant.

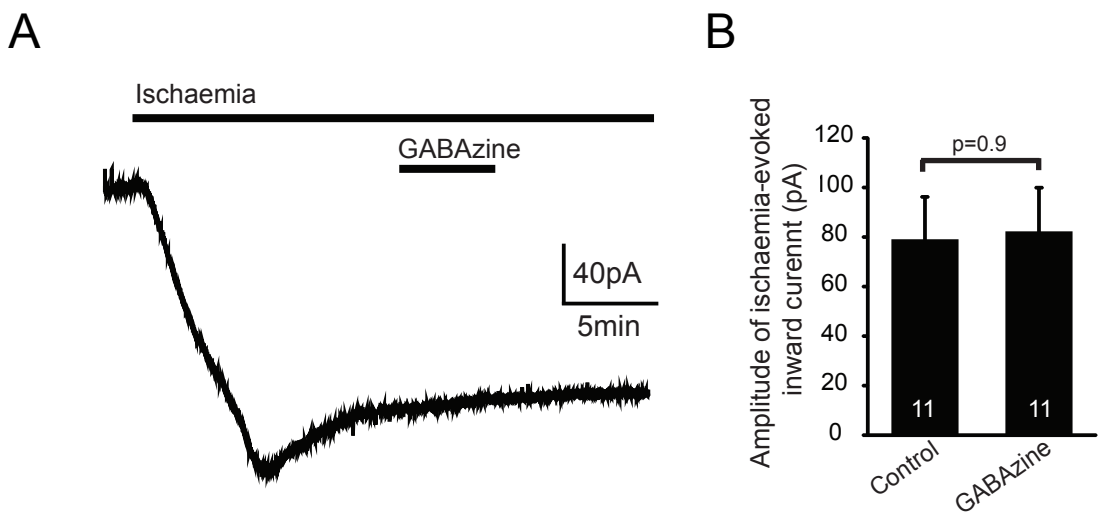

Figure 5.3. The ischaemia-evoked inward current in mature oligodendrocytes is not affected by blocking $GABA_A$ receptors.
A, Membrane current at -74 mV in a mature oligodenddrocyte during simulated ischaemia (glucose and O_2 were replaced with sucrose and N_2, and antimycin and iodoacetate were added to the recording solution to block ATP production by glycolysis and oxidative phosphorylation). $GABA_A$ receptors were blocked (with 10 μM GABAzine) during the period when the ischaemia-evoked current sags back somewhat from its initial peak. **B**, Blocking $GABA_A$ receptors with 10 μM GABAzine did not significantly reduce the ischaemic-evoked inward current in mature oligodendrocytes. Numbers of cells are shown on the bars.

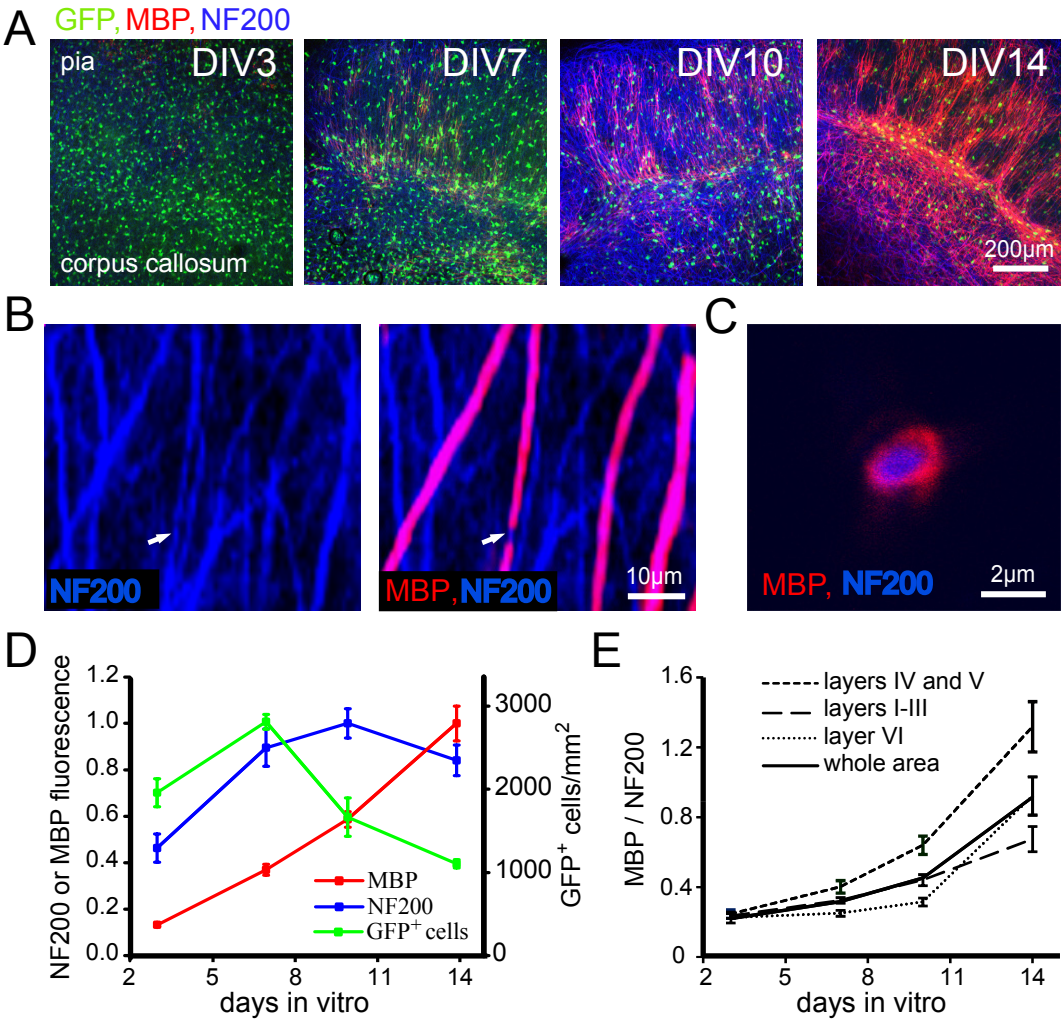

Figure 5.4. Development of myelination in cultured cortical slices.
A, Cortical slices from mice with oligodendrocyte lineage cells expressing GFP (under control of the Sox10 promoter, green) after different numbers of days in vitro (DIV). Blue is antibody to neurofilament 200 (NF200) and shows axons; red is antibody to myelin basic protein (MBP). Slice orientation is approximately with the pial surface at the top and the corpus callosal surface at the bottom. Band of heavy myelination at DIV14 is in layers IV-V (the Baillarger lines corresponding to the stria of Gennari in the striate cortex). **B**, Higher magnification view of cultures showing neurofilament in axons, some of which are wrapped with MBP containing myelin (green GFP channel not shown). Gap in the MBP covering one axon is a node of Ranvier (indicated by the white arrow). **C**, A myelinated axon imaged in cross section, showing MBP closely opposed to the neurofilament labelled axon. **D**, Mean values of numbers of GFP expressing cells/mm^2 (green, right axis) and mean fluorescence (left axis) of NF200 (blue) and MBP (red) averaged over 920 µm by 920 µm images (8-15 images at different ages). **E**, Development with time of the amount of myelin per axon, quantified as ratio of MBP to NF200 fluorescence averaged over the different cortical layers indicated.

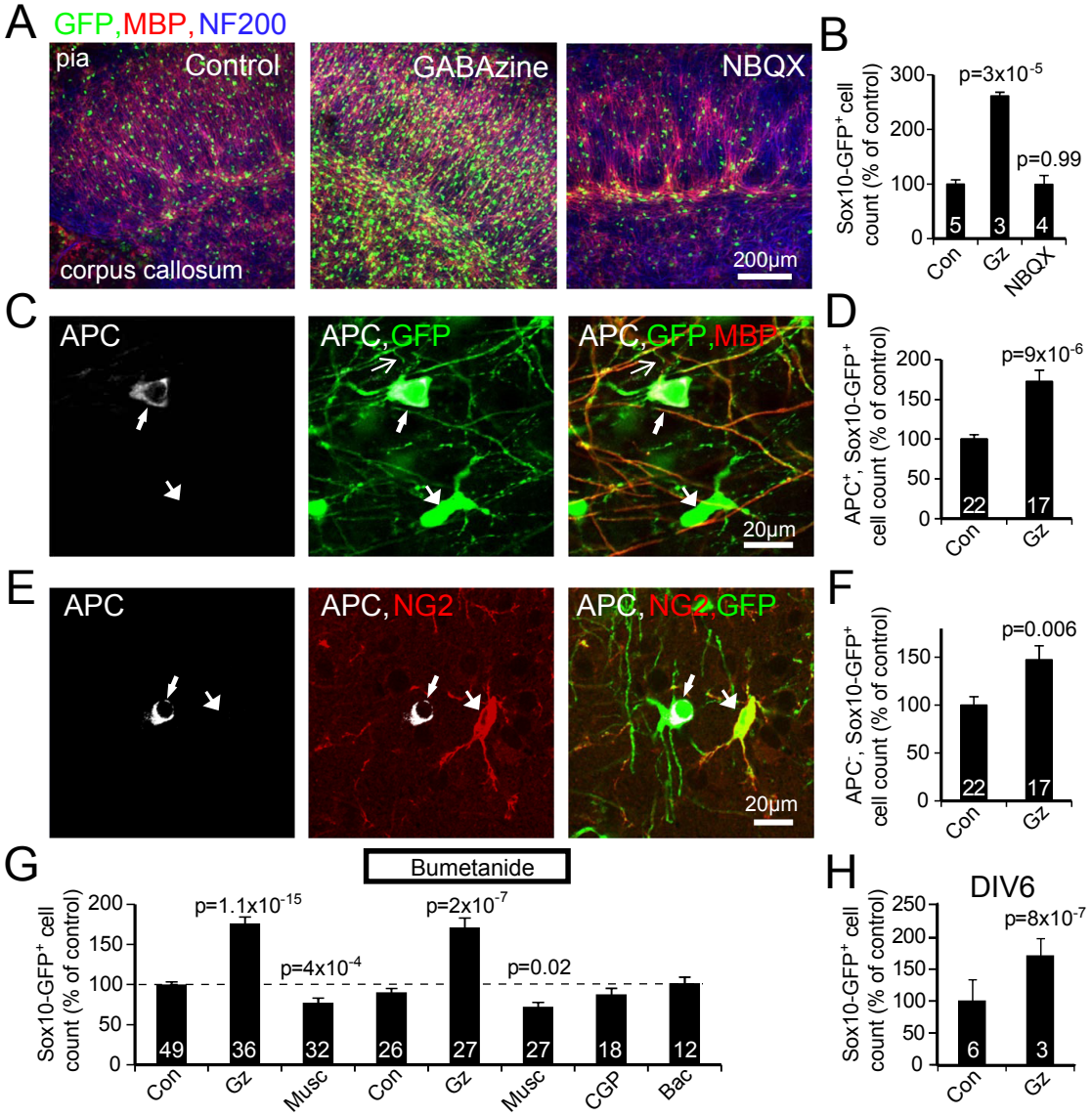

Figure 5.5. Blocking $GABA_A$Rs increases the number of oligodendrocyte lineage cells.

A, Cortical slices at DIV14 after culture in control conditions, or with $GABA_A$ or AMPA/KA receptors blocked with GABAzine or NBQX respectively. **B**, Number of GFP expressing oligodendrocyte lineage cells in each condition, normalised to the number in control conditions (numbers on bars are numbers of slices). **C**, Labelling of oligodendrocyte lineage cells (expressing GFP, green) for the mature oligodendrocyte marker APC (white) and for MBP (red). Top arrowed cell expresses APC, as well as MBP in its myelinating processes (top thin arrow indicates a primary process linking the arrowed soma to a MBP expressing process), unlike the bottom cell. **D**, Number of cells expressing GFP and APC in the presence of GABAzine, normalised to the number in control conditions. **E**, Labelling of oligodendrocyte lineage cells (expressing GFP, green) for APC (white) and for the OPC marker NG2 (red). Unlike the left cell which expresses APC, the right arrowed cell lacks APC and expresses NG2. **F**, Number of cells expressing GFP but not APC in the presence of GABAzine, normalised to the number in control conditions. **G**, Number of Sox10-GFP-expressing cells in all experiments performed, in control conditions and with the indicated drugs present from DIV3-14 (Gz=GABAzine, Musc=muscimol, CGP=CGP35348, Bac=baclofen). P values are Holm-Bonferroni corrected for 5 comparisons for Gz, Musc, Bumetanide, CGP, Bac, and for 2 comparisons when comparing GABAzine or muscimol with control or comparing Bumetanide+Gz or Bumetanide+Musc with Bumetanide. **H**, Effect of GABAzine from DIV3-6 on the number of GFP expressing cells at DIV6.

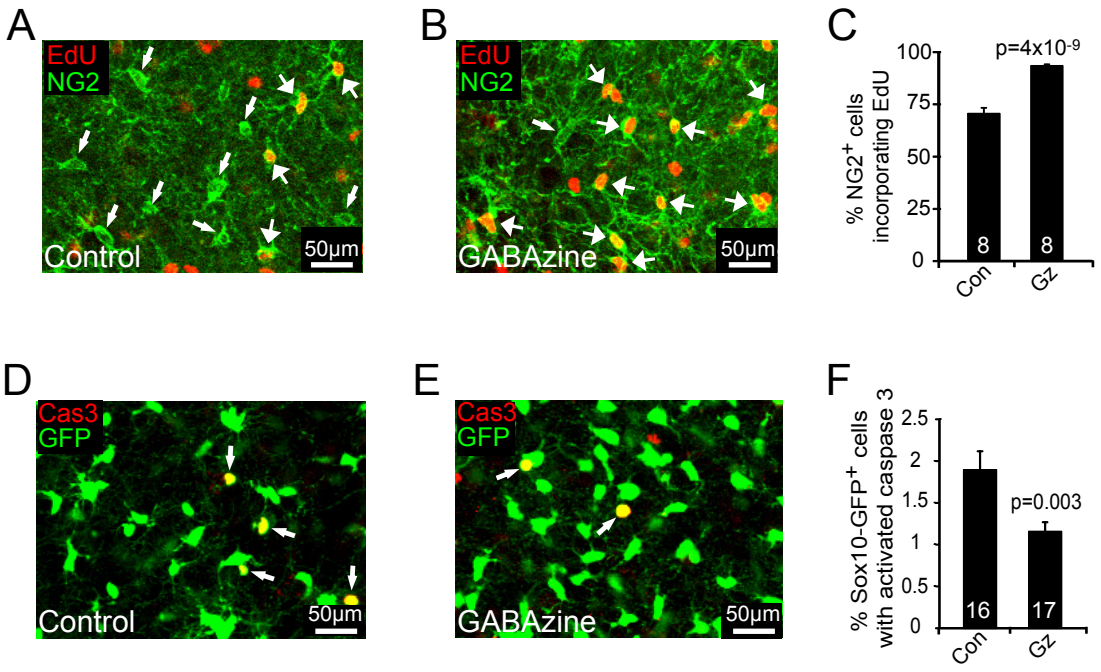

Figure 5.6. GABA regulates the proliferation and death of oligodendrocyte lineage cells

A-B, Example of EdU labelling (red) in NG2 expressing cells (green) with and without GABAzine. **C**, Quantification of fraction of OPCs dividing between DIV4-6. **D-E**, Example of cleaved caspase 3 labelling (red) in SOX10-GFP expressing cells (green) with and without GABAzine. **F**, Quantification of fraction of oligodendrocyte lineage cells labelling for cleaved caspase 3 at DIV6. Number of slices analysed are shown on the bars.

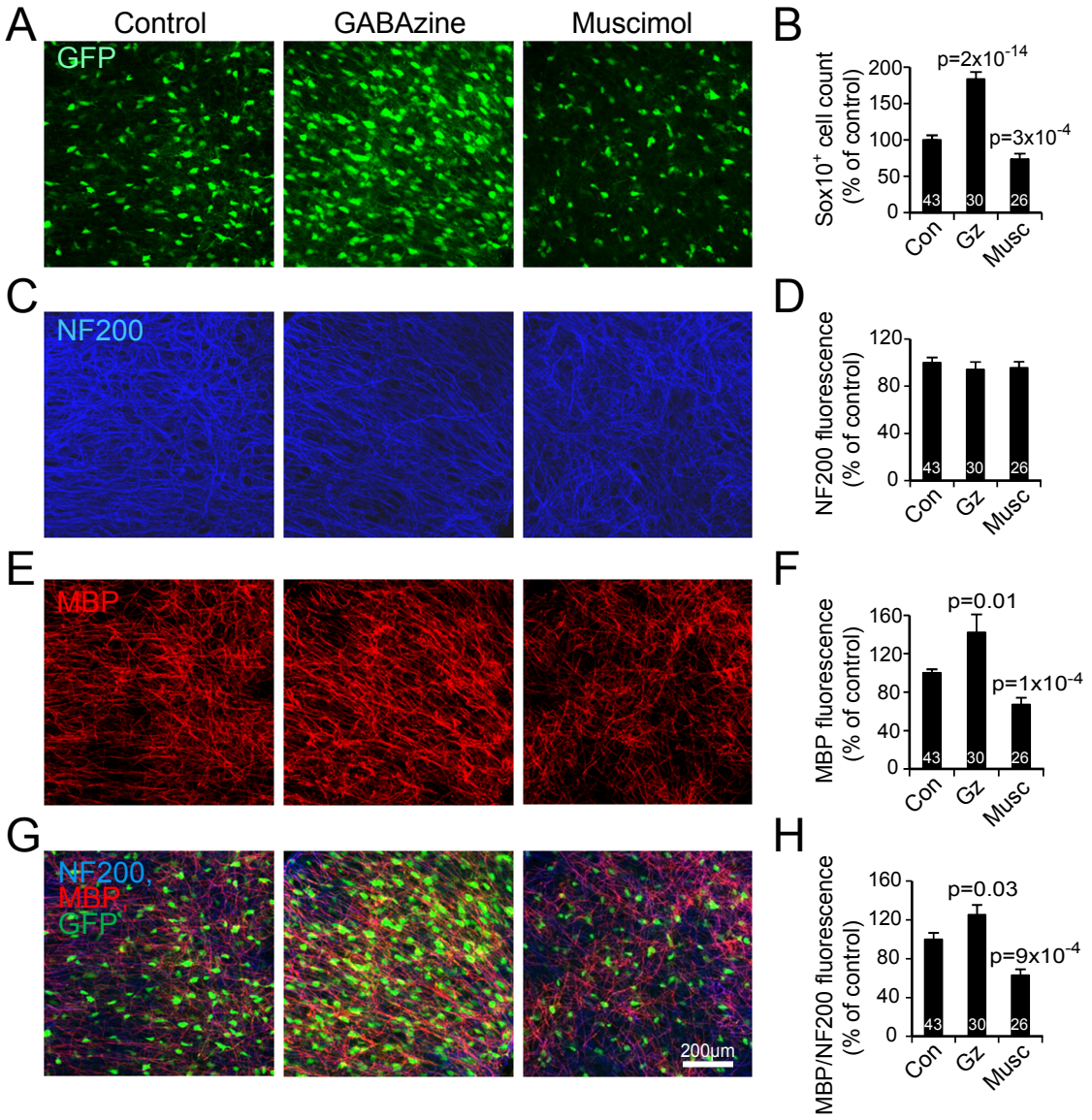

Figure 5.7. Endogenous GABA release decreases myelination.
A, C, E, G, Cortical slices at DIV14 after culture in control conditions, or with GABAzine or muscimol present from DIV3-14, showing labelling for (**A**) Sox10-GFP, (**C**) neurofilament (NF200), (**E**) MBP and (**G**) all the labels. **B, D, F**, Quantification (averaged over the whole image) of the labelling in the panels to the left (panel B is similar to the first 3 bars in Fig. 5.5G but using data only for the slices from which panels D, F and H were obtained). **H**, Ratio of labelling for MBP to that for NF200.

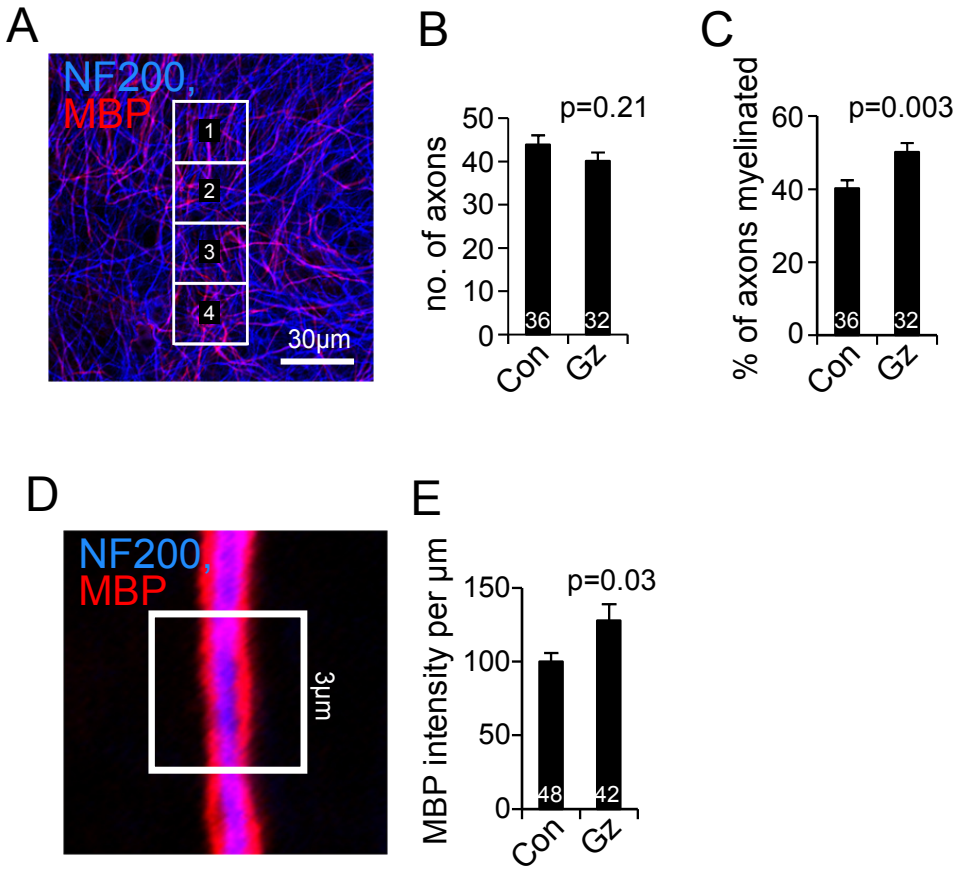

Figure 5.8. GABAzine increases both the fraction of axons myelinated and the amount of myelin per axon.
A, Specimen labelling with superimposed squares for quantification of the fraction of NF200-expressing axons (blue) that are myelinated (i.e. wrapped with MBP, red). **B, C**, GABAzine from DIV3-14 has no significant effect on the number of axons present per rectangle (**B**) but increases the percentage of axons myelinated (**C**). **D**, Specimen image of myelinated axon, with 3 µm long region of interest used to quantify the amount of MBP per micron of axon. **E**, Effect of GABAzine on MBP fluorescence intensity per micron of axon. Numbers on bars are images analysed.

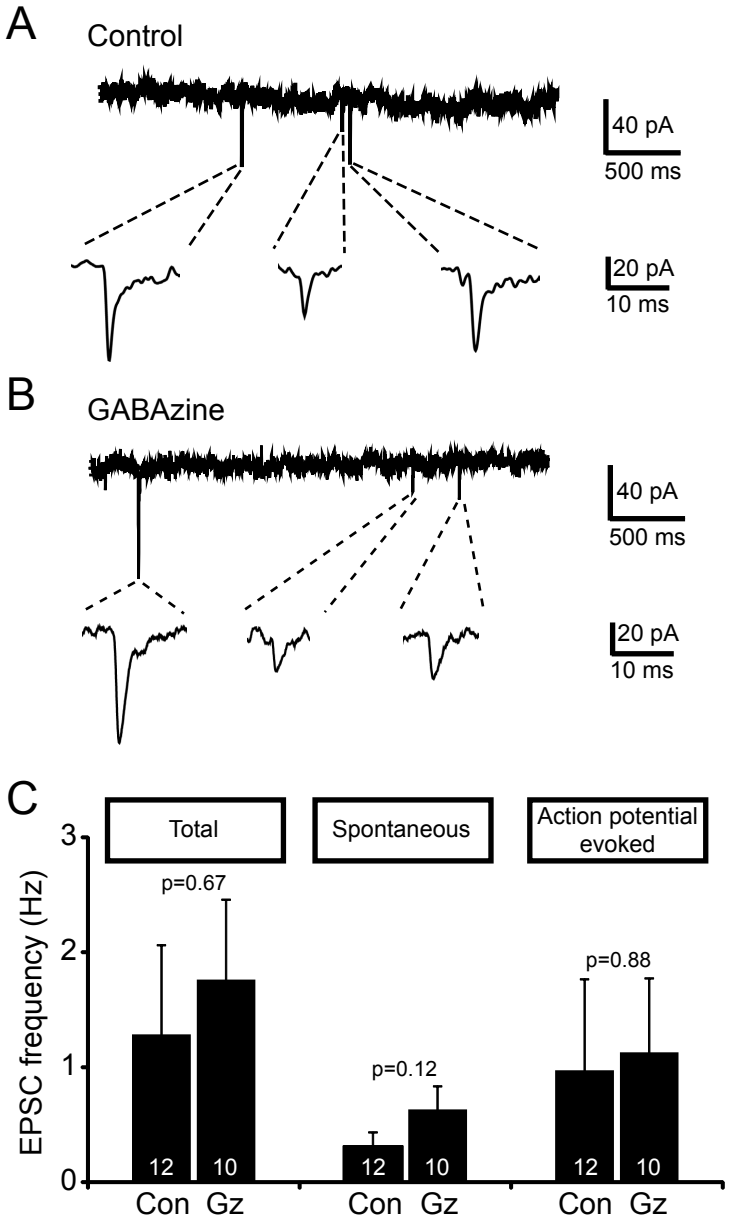

Figure 5.9. Effect of GABAzine on the activity of neurons.
A, Specimen trace showing EPSCs in a pyramidal neuron clamped to -40mV. **B**, EPSCs in a neuron after 8 days in GABAzine. **C**, Mean frequency, in control or GABAzine-treated slices, of all EPSCs, of spontaneous EPSCs recorded in 1 μM TTX, and of action potential evoked EPSCs blocked by TTX. Number of cells shown on bars.

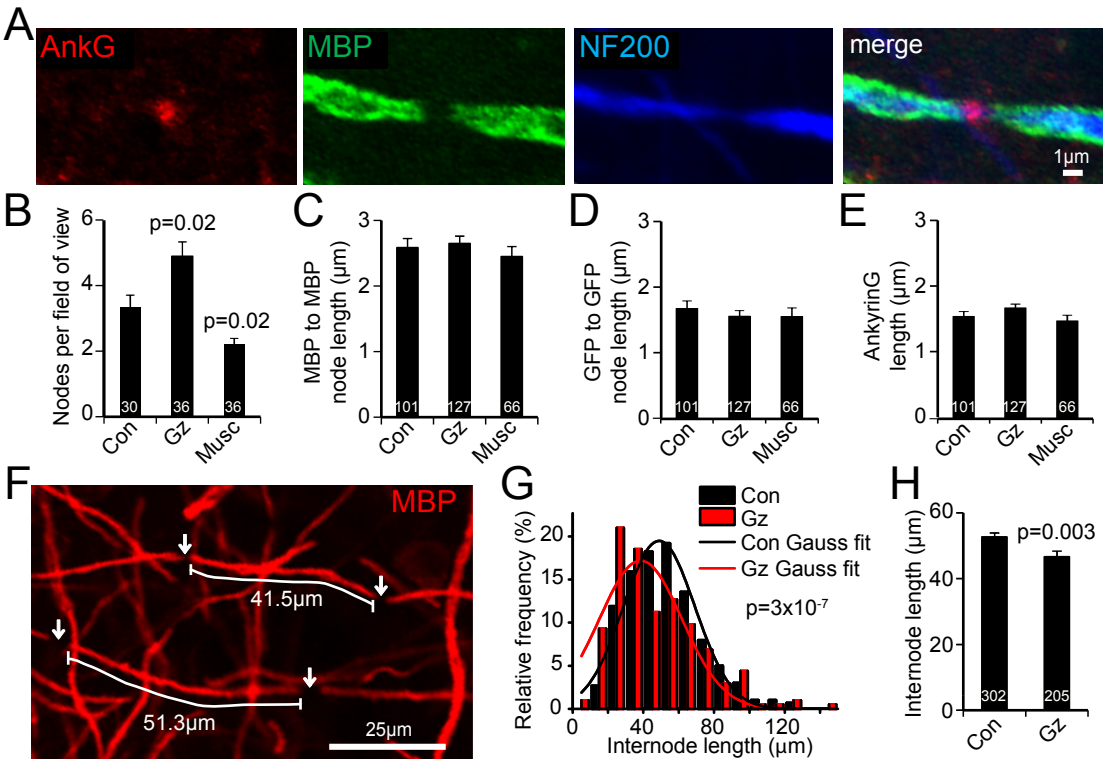

Figure 5.10. Endogenous GABA release increases internode length.
A, Myelinated axon node of Ranvier labelled for ankyrin G (Ank G), myelin basic protein (MBP) and neurofilament (NF200); right panel shows merged image. **B**, Number of nodes per 146 μm square field of view at DIV14, in control conditions, or with GABAzine or muscimol present from DIV3-14. Numbers on bars are fields of view; 6-10 fields were taken per slice. **C-E**, Node lengths (measured from all the nodes imaged for panel B) in different conditions assessed as: (**C**) gap between end of internodal MBP labelling, (**D**) gap between internodal GFP, and (**E**) length of ankyrin G labelling. Numbers on bars are nodes. (**F**) Example of internode length measurement. Nodes are identified as gaps in GFP and MBP labelling. (**G**) Distribution of internode lengths, L in 10 μm bins), at DIV14, in control conditions (in eight 92 μm x 160 μm images from 4 slices), or with GABAzine present from DIV3-14 (7 images from 4 slices). Fits are Gaussian curves, $\{A/[\sigma\sqrt{(2\pi)}]\}\exp\{-(L-M)2/2\sigma2)\}$, with parameters A=991, mean length M=48.9 μm, σ=20.3 μm in control and A=1004, M=38.5 μm, σ=23.3 μm in GABAzine. P value showing significantly different distributions is from Kolmogorov-Smirnov test. **H**, Mean internode length from (**G**); numbers on bars are internodes.

Chapter 6: Other pilot PhD projects

The experiments described in this chapter detail two less developed research projects I performed during my PhD. In this chapter I investigate nitric oxide signalling to oligodendrocyte lineage cells (section 6.1) and activity-dependent nodal plasticity (section 6.2), and each project will be described in turn.

6.1 Nitric oxide regulation of the membrane properties of oligodendrocyte lineage cells and myelination

6.1.1 Introduction

Nitric oxide (NO) signalling regulates many processes in the central nervous system, including cell proliferation, neuronal development, and learning and memory (Contestabile and Ciani, 2004; Bicker, 2005; Garthwaite, 2008). In the absence of pathology, NO is synthesised by nitric oxide synthase (NOS), an enzyme found in neurons (nNOS) and endothelial cells (eNOS) (Seidel et al., 1997). The canonical pathway for NO signal transduction is via activation of guanylyl cyclase (GC) to produce cGMP, which in turn regulates the function of protein kinases, phosphodiesterases, and ion channels (reviewed by Garthwaite, 2008). NO can thereby affect neuronal function by modulating neuronal excitability and firing rate (Ahern et al., 2002; Frick and Johnston, 2005; Steinert et al., 2008; Artinian et al., 2010).

In addition to modulating neuronal activity, NO has been reported to influence the properties of oligodendrocytes. In particular, a recent study suggested that inhaled NO (a controversial therapy used to treat hypoxic respiratory failure in neonates) increased myelination in neonatal mice, by increasing OPC proliferation and differentiation (Olivier et al., 2010). A subpopulation of oligodendrocyte lineage cells are reported to express GC for cGMP synthesis (Tanaka et al., 1997), and some OPCs exhibit a small hyperpolarisation-activated inward current (I_h) produced by hyperpolarisation activated cyclic nucleotide-modulated cation channels (HCN), which can be modulated by the cGMP level (Lin and Bergles, 2002). In a study by Garthwaite et al. (2006), NO derived from vascular endothelial cells was reported to activate GC in axons, raising the cGMP level, and causing membrane depolarisation by activating HCN channels. Conceivably the depolarisation of axons observed could reflect a primary action of NO on oligodendrocytes.

NO is reported to play a role in the pathology of many diseases involving oligodendrocytes, including multiple sclerosis (Smith and Lassmann., 2002; Li et al., 2011) and periventricular leukomalacia (Baud et al., 2004). There is abundant evidence that NO production is significantly raised in multiple sclerosis lesions (Smith and Lassmann, 2002). This increase in NO is due to an upregulation of inducible NOS by reactive microglia/macrophages. The increased levels of NO can react with superoxide to form peroxynitrite, which is a highly toxic reactive nitrogen species, and leads to the death of oligodendrocytes (Zhang et al., 2006a). These reactive nitrogen species have been recognised to play a crucial role in the formation of white matter lesions in disease models of multiple sclerosis (Hooper et al., 1997; Volpe et al., 2003).

In contrast, NO is reported to be protective against cell injury because NO is a weak oxidant and reacts more readily as an antioxidant by neutralizing other free radicals (Rosenberg et al., 1999). NO has also been suggested to prevent oligodendrocyte death by increasing cGMP production and activating cGMP-dependent signalling pathways which, in turn, can inhibit mitochondrial pore transition and apoptosis in response to certain types of excitotoxic injury (Benjamins and Nedelkoska, 2007). Collectively, these studies suggest that NO may play either a harmful or protective role in oligodendrocyte injury and further work will be required to improve our understanding of this issue.

In this chapter I report work investigating the membrane effects of NO signalling in both OPCs and oligodendrocytes, by applying an NO donor, or decreasing endogenous NO production, and recording any resulting changes in membrane currents. In addition, I investigated the effects of NO on myelination using the organotypic cortical slice model of myelination described in chapter 5.

6.2.2 Methods

Transgenic mice

Sox10-GFP transgenic mice (described in detail in chapter 2, section 13.1-13.3) in which GFP is expressed in oligodendrocyte lineage cells (Kessaris et al., 2006), were used for patch-clamp recording and in an organotypic slice model of myelination (Rinholm et al., 2011, and chapter 5).

Brain slices

Coronal forebrain or parasagittal brain slices (225 µm thick) were prepared from P6-9 *Sox10-GFP* transgenic mice (as described in chapter 2 section 1). Slices were

superfused at ~37℃ with bicarbonate buffered solut ion which contained the following (mM); 126 NaCl, 24 $NaHCO_3$, 1 NaH_2PO_4, 2.5 KCl, 1 $MgCl_2$, 2.5, $CaCl_2$, 10 D-glucose, pH 7.4 (bubbled with 95% O_2/5% CO_2).

Nitric oxide donors

Diazeniumdiolate NO donors were used with varying NO release half-lives. For patch-clamp recordings the NO donor PAPA-NONOate was used, as it has a short NO release half-life of 15 min (37℃), at pH 7.4. PAPA -NONOate was chosen for patch-clamp recordings to look at fast time scale responses to NO. For organotypic slice culture experiments the NO donor DETA-NONOate was used, as it has a longer NO release half-life of 20 hours (37℃), at pH 7.4. DE TA-NONOate was chosen for culture experiments because it produces NO for long time periods, enabling assessment of the effect of prolonged increases in NO levels.

Patch-clamp recordings

The electrophysiology of oligodendrocyte lineage cells was studied in acute coronal forebrain and parasagittal cerebellar slices. Oligodendrocyte lineage cells were identified from their GFP-fluorescence, dye-fill morphology and I-V relations. They were whole-cell clamped with pipettes with a series resistance of 8-20 MΩ.

Electrodes were pulled from thick-walled borosilicate glass to a resistance of 6-9 MΩ for oligodendrocyte lineage cells. Electrodes were filled with K-gluconate based solution containing (mM): 130 K-gluconate, 4 NaCl, 0.5 $CaCl_2$, 10 HEPES, 10 BAPTA, 4 MgATP, 0.5 Na_2GTP, 2 K-Lucifer yellow (pH 7.3).

Organotypic cortical slice cultures and myelination assay

An assay for myelination in brain slices was used in which oligodendrocyte lineage cells fluoresce green, and neuronal axons and myelin are identified and quantified with immunofluorescence (Rinholm et al., 2011). This allowed assessment of whether changes in myelination reflected changes in the number of oligodendrocyte lineage cells, axonal density or the myelinating activity per oligodendrocyte lineage cell. The myelination assay is described in detail in chapter 5.

Immunohistochemistry

Immunohistochemistry was performed on organotypic slices as described in chapter 2, section 14 and chapter 5.

Statistics

The statistical analysis is described in detail in chapter 2, section 15.

6.2.3 Results

In cortical and cerebellar brain slices of *Sox10-GFP* transgenic mice, application of an NO donor (1 and 10 µM PAPA-NONOate) did not evoke a current in OPCs (Fig. 6.1A, n=10 cells) or in myelinating oligodendrocytes (Fig. 6.1B, n=3 cells). Data in Fig. 6.1A, B are shown at -40 mV, but no current change was seen at any voltage. Additionally, blocking endogenous nitric oxide production by inhibiting nitric oxide synthase (NOS) (with 100 µM N(G)-methyl-L-arginine (L-NMMA)) did not evoke a current in OPCs (Fig. 6.1A, n=10 cells) or in myelinating oligodendrocytes (Fig. 6.1B, n=3 cells). These data suggest that NO signalling does not evoke detectable membrane currents in oligodendrocyte lineage cells.

NO exerts its biological effects by activating GC and increasing cGMP levels, which can modulate HCN ion channels (Ingram and Williams, 1996). HCN channels respond to hyperpolarisation by activating with a time constant of ~100 ms, producing a slowly activating I_h current (Wilson and Garthwaite, 2010). I investigated HCN channel expression in OPCs by applying a series of long hyperpolarising voltage steps to try to activate I_h currents. However, no significant current with the time course of I_h could be detected in OPCs in the corpus callosum (n=4 cells) or motor cortex (n=4 cells) (Fig. 6.1C).

To test the possible role of NO in regulating oligodendrocyte development and myelination, organotypic slices were made from the frontal cortex of postnatal day 8 *Sox10-GFP* transgenic mice (Kessaris et al., 2006), as described in detail in chapter 5. Slices were fixed after 14 days in culture, and labelling with antibodies to neurofilament 200 (NF) and myelin basic protein (MBP), allowed for the imaging of neuronal processes as blue, oligodendrocyte lineage cells as green, and myelin as red (Fig. 6.2A).

Myelination developed over a period of 2 weeks, as seen in chapter 5. By measuring the total fluorescence of GFP expressing cells, the number of oligodendrocyte lineage cells was assessed (Rinholm et al., 2011), and by using the total fluorescence of NF antibody and MBP antibody as measures of the amount of neuronal processes and of myelin present, the progress of myelination was assessed. To test the effect of endogenously released NO on the number of oligodendrocyte lineage cells generated, NOS blockers (100 µM L-nitroarginine (L-NNA), or 50 µM

N(G)-methyl-L-arginine (L-NMMA)) were included in the culture medium from days 3 to 14 *in vitro*. Blocking NOS had no significant effect on the number of oligodendrocyte lineage cells (Fig. 6.2A, B; p=0.4 and p=0.06 for L-NNA and L-NMMA, respectively), nor on the amount of myelination, measured as the ratio of total MBP to total NF fluorescence (Fig. 6.2A, C; p=0.6 and p=0.7 for L-NNA and L-NMMA, respectively). In addition, a NO donor (100 µM or 200 µM DETA-NONOate) was included in the culture medium from days 3 to 14 in vitro, to increase the concentration of NO exogenously. Increasing NO levels had no significant effect on the number of oligodendrocyte lineage cells (Fig. 6.2A, B; p=0.3 and p=0.07 for 100 µM and 200 µM DETA-NONOate, respectively), nor on the amount of myelination, measured as the ratio of MBP to NF (Fig. 6.2A, C; p=0.9 and p=0.6 for 100 µM and 200 µM DETA-NONOate, respectively). Although the effects of L-NMMA and DETA-NONOate come close to statistical significance, L-NMMA decreases the NO level while DETA-NONOate increases it, yet both drugs decreased the number of oligodendrocyte lineage cells present, ruling out an effect of NO. These data contradict a previous report by Olivier et al. (2010; see section 6.1.1), and suggest that NO signalling does not significantly affect the number oligodendrocyte lineage cell generated or myelination.

6.2.4 Discussion

It is well established that the transmitter NO can modulate the activity of neurons within the CNS, however the role of NO in brain development is poorly understood. In particular, very little is known about NO signalling to oligodendrocyte lineage cells and how this signalling affects oligodendrocyte lineage development and myelination. Therefore, I investigated NO-evoked membrane currents in oligodendrocyte lineage cells and the effects of NO on myelination.

My data suggest that neither endogenous nor exogenous NO evoke detectable currents in oligodendrocyte lineage cells. Additionally, OPCs in the corpus callosum or motor cortex were not found to express I_h currents mediated by HCN channels (an ion channel which can be modulated by cGMP), unlike OPCs in the hippocampus which are reported to express small I_h currents (Lin and Bergles, 2002). Furthermore, unlike the neurotransmitter GABA which decreases oligodendrocyte lineage cell number and myelination (see Chapter 5), increasing or decreasing NO levels did not significantly change the number of oligodendrocyte lineage cells generated, nor myelination. This finding contradicts a previous report by Oliver et al. (2010), in which rodent pups were exposed to inhaled NO, which increased OPC proliferation and myelination. However, NO also plays an important role in the regulation of blood flow (reviewed by Toda and

Okamura 2003), and it is therefore possible that exposure to inhaled NO increases blood flow to white matter tracts which results in an increase in myelination. Finally, NO signalling may play an important role in oligodendrocyte injury, which was not investigated in this chapter.

6.2 Activity dependent myelination and nodal plasticity

6.2.1 Introduction

Information transmission in the brain is generally considered to be modulated primarily in the grey matter, where dendrites integrate inputs from many presynaptic neurons, and the postsynaptic cell bodies 'decide' how or whether to convert this chemical information into an electrical signal. In the white matter, this electrical signal – already at the all-or-none stage – is simply propagated, with no scope for changes in information content until the next synaptic junction. However, this view is becoming outdated with increasing evidence that the timing of the action potential arrival at synapses is critical to information processing in the brain. Importantly, this timing can be regulated by myelin in the white matter, which determines action potential conduction speed. During development, for example, myelination is adjusted to ensure that cortical inputs from different thalamic nuclei arrive at the same time (Salami et al., 2003). During experience-dependent auditory maturation, the internode length is increased in longer brainstem pathways to ensure coincident input arrival with information arriving on shorter brainstem pathways, in order to allow sound localisation (Seidl et al., 2010). Finally, during learning in humans, there is evidence for increased myelination with increased piano practice (Bengtsson et al., 2005) and juggling (Scholz et al., 2009).

These are long-term changes, but it also seems possible that a mechanism could exist for altering conduction speed in the short-term, given the importance of input arrival time for several fast information integrating processes in the grey matter, for example, spike-timing dependent plasticity (STDP) (Markram et al., 1997; Bi and Poo, 1998) and dendritic sequence discrimination (Branco et al., 2010). My colleague, Lee Cossell has shown theoretically that an effective and energetically efficient way of quickly fine-tuning conduction speed would be to exo- or endocytose membrane at the nodes of Ranvier, thus decreasing or increasing conduction speed, respectively, by altering the nodal capacitance. Similarly, it was recently shown that the axon initial segment (AIS) – which has similar structural and functional features to the node of Ranvier – can change in size and position in an activity- and calcium-dependent

manner (Grubb and Burrone, 2010; Kuba et al., 2010). Myelinated axons experience activity-evoked calcium increases, possibly through influx at the node (Zhang et al., 2006b), which might promote the insertion or removal of membrane and Na^+ channels at the node, I therefore investigated whether, in response to activity, nodes might undergo adjustments, which affect the conduction speed of action potential propagation.

6.2.2 Methods

Optic nerve preparation

Optic nerves were removed from P21 rats (when myelination should be around 70% complete, Foster et al., 1982), as described in detail in chapter 2, section 2.1.4. Optic nerves were superfused at ~33℃ with bicarbonate-buffered solution which contained the following (in mM); 126 NaCl, 24 $NaHCO_3$, 1 NaH_2PO_4, 2.5 KCl, 1 $MgCl_2$, 2.5, $CaCl_2$, 10 D-glucose, pH 7.4 (bubbled with 95% O_2/5% CO_2).

Compound action potential recordings

To record the optic nerve compound action potential (CAP), the optic nerve was stimulated using a suction electrode filled with bicarbonate-buffered solution as described above. The optic nerve was stimulated using a using 0.2 ms, 2–8 V pulses, at 0.033 Hz (a low stimulus strength was used to avoid activation of the small number (Tennekoon et al., 1977) of unmyelinated axons present at this age). The CAP was recorded as a current using an Axon Axopatch 200B patch clamp with a second suction electrode at least 2 mm from the stimulating electrode. The suction electrode technique is described in detail in chapter 2, section 12.

CAPs were recorded for 20 minutes in bicarbonate-buffered solution to establish a stable baseline recording before application of high [K^+] (15mM KCl) to depolarise the optic nerve for 10 minutes. This procedure mimics, but more briefly, the depolarisation protocol of Grubb and Burrone (2010) which altered the AIS structure. Following depolarisation, CAPs were recorded for a further 20 minutes in bicarbonate-buffered solution to assess recovery and any lasting changes in conduction velocity. Optic nerves were included in the analysis if the amplitude of the CAP recovered to within 10% of the control amplitude (n=6 nerves).

Statistics

The statistical analysis is described in detail in chapter 2, section 15.

6.2.3 Results

CAPs were recorded from the optic nerves of P21 rats (when myelination should be around 70% complete; Foster et al., 1982). The time from the stimulus artefact to the peak of the CAP was measured, and a change in this latency was interpreted as a change in conduction velocity. To depolarise the axons I superfused optic nerves with high [K^+] (15 mM KCl; Grubb and Burrone, 2010) for 10 minutes (Fig. 6.3A). This significantly decreased the CAP amplitude ($p=0.0031$, in 6 control and 6 high [$K^{+]}$ treated nerves) and increased the CAP latency ($p= 7.0 \times 10^{-6}$, in 6 control and 6 high [K^+] treated nerves) i.e. decreased the conduction velocity (Fig. 6.3A-C), which was probably due to depolarisation producing sodium channel inactivation. To assess any long lasting changes in conduction velocity, I selected only those nerves that recovered to within 10% of their original amplitude (n=6 for control, and high [K^+] conditions) (Fig. 6.3C). In optic nerves treated with high [K^+], the latency of the mean CAP recovered by ~95% (Fig. 6.3B). However, the latency of the mean CAP the control optic nerves also decreased to ~95% of their original latency (Fig. 6.3B) after recording for 30 minutes. Indeed, no significant difference could be detected in the conduction velocity of CAPs between control and nerves treated with high [K^+] ($p= 0.67$), suggesting that nodal plasticity is not occurring in this preparation.

In addition to depolarising optic nerves with high [K^+], more physiological electrical stimulation trains were also applied to optic nerves to look for nodal plasticity. Several stimulation trains, including a train similar to that shown to shift the AIS (Grubb and Burrone, 2010) (20 Hz bursts of 5 pulses every 5 s), a train used to induce STDP (Markram et al., 1997) (20 Hz bursts of 5 spikes for 1 min) and more vigorous tetanic stimulation classically used to induce LTP (100 Hz for 10 sec) were applied to optic nerves (data not shown). These types of electrical stimulation evoked a pattern of changes to the CAP similar to that seen with depolarisation with high [K^+]: a decrease in amplitude and increase in latency during stimulation, followed by recovery to original values, with no observable lasting change in conduction velocity.

6.2.4 Discussion

Depolarisation of the myelinated optic nerve (with either high [K^+], or physiological stimulation found to induce various types of neuronal plasticity), did not change action potential conduction velocity, which suggests that nodal plasticity is not occurring in this preparation. However, this does not rule out the idea that the action potential conduction velocity might be regulated on a fast timescale at the node of Ranvier. It is possible that this novel form of plasticity may occur but was below the

threshold for detection in the optic nerve preparation, where there are different cell classes present with different conduction speeds, making accurate measurement of individual axons speeds impossible. Alternatively, nodal plasticity may require a feedback signal from the postsynaptic cell, which was not present in the optic nerve preparation. Such a feedback mechanism is attractive, given that it is within the postsynaptic cell that the action potential timing is critical. Further work in acute brain slices, looking at the input arrival times to a single postsynaptic cell whilst stimulating presynaptic inputs from a myelinated nerve, at different times relative to applying a postsynaptic depolarisation, may allow determination of whether this kind of nodal plasticity exists.

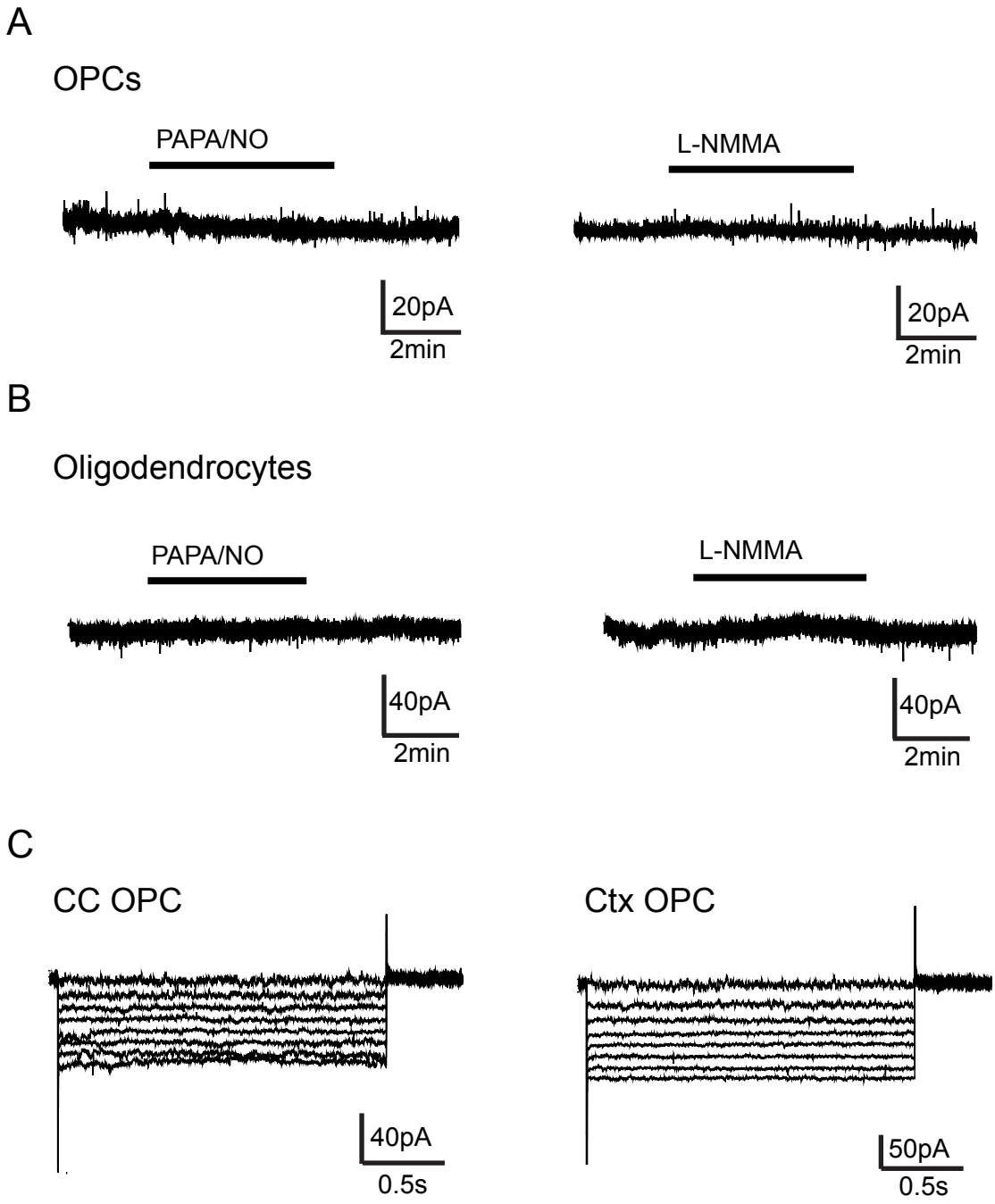

Figure 6.1. Nitric oxide-evoked currents can not be detected in oligodendrocyte lineage cells.

A,B, Application of a nitric oxide donor (10 μM PAPA-NONOate) or inhibiting endogenous nitric oxide production by blocking nitric oxide synthase (100 μM N(G)-methyl-L-arginine (L-NMMA)) did not evoke a detectable current in OPCs (**A**, n=10 cells) or in mature oligodendrocytes (**B**, n=3 cells) clamped to -30 mV. **C,D**, Expression of hyperpolarisation-activated cyclic nucleotide-modulated cation (HCN) channels, which can be modulated by nitric oxide, was investigated in OPCs. A series of hyperpolarising voltage steps (from a holding potential of -45 mV, hyperpolarising voltage steps in 10 mV increments from -55 mV to -115 mV) were applied to activate HCN channels, however no detectable HCN channel conductance was observed in OPCs in the corpus callosum (CC) (**C**, n=4 cells) or motor cortex (Ctx) (**D**, n=4 cells).

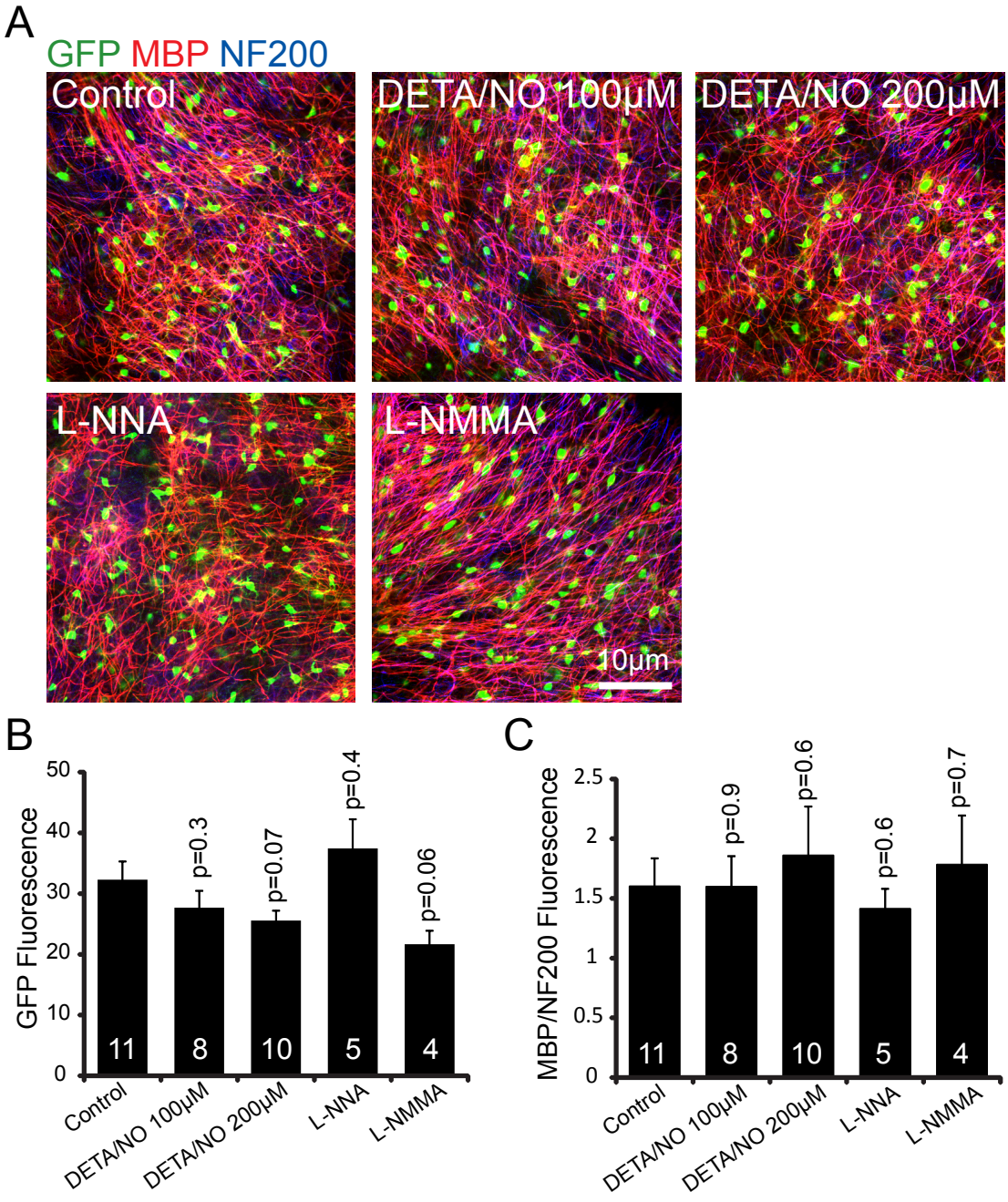

Figure 6.2. Nitric oxide does not affect oligodendrocyte cell number or myelination.
A, Cortical slices at DIV14 after culture in control conditions, or with a nitric oxide donor (100 µM or 200 µM DETA-NONOate), or with a nitric oxide synthase inhibitor (100 µM L-nitroarginine (L-NNA), or 50 µM N(G)-methyl-L-arginine (L-NMMA)) present from DIV3-14, showing labelling for Sox10-GFP (green), neurofilament (blue) and MBP (red). **B,** Quantification (averaged over the whole image) of the GFP fluorescence. **C**, Quantification of the ratio of labelling for MBP to that for NF200. Numbers on the bars represent the number of slices analysed.

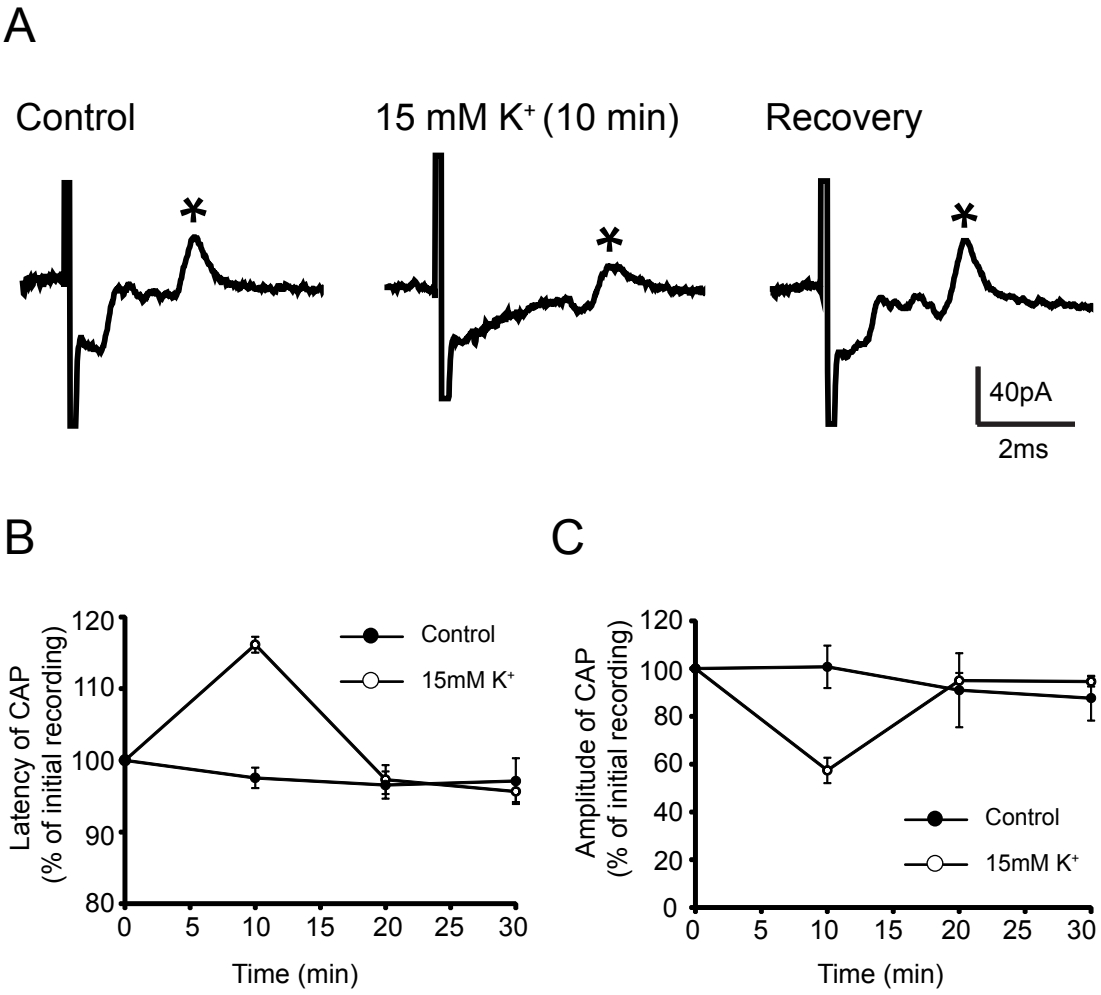

Figure 6.3. Investigating node of Ranvier plasticity in the optic nerve.
A, Compound action potentials (CAP) were recorded from P21 (when ~70% of myelination has occurred) optic nerves using suction electrodes (the experimental set-up is described in detail in chapter 2, section 12). CAPs were recorded every 3 seconds, and their peak latency and peak amplitude were measured across conditions (at points marked by asterisk in **A**, in relation to the baseline value immediately preceding the artefact). **Left**: A representative trace of a CAP recorded during control conditions (in bicarbonate-buffered solution). **Middle**: a representative trace of a CAP recorded after application of 15 mM K^+ for 10 minutes to depolarise the nerve. During depolarisation the CAP amplitude decreased and the latency of the peak increased. **Right:** a representative trace of a CAP recorded 20min after removal of 15 mM K^+ (in bicarbonate-buffered solution). The amplitude and latency of the CAP peak recovered and was not disimilar to the CAP recorded before depolarisation. **B, C**, Mean latency (**B**) and amplitude (**C**) as a percentage of the inital CAP recording (n=6 optic nerves in control and 15 mM K^+ conditions).

Chapter 7: Final discussion

In this section, I will review the main results I have obtained throughout my PhD and suggest future experiments which could further the research I have carried out.

7.1 Dorsally- and ventrally-derived oligodendrocytes have similar electrical properties but myelinate preferred tracts

7.1.1 Discussion

Oligodendrocytes are generated from both dorsal and ventral germinal regions in the embryonic forebrain and spinal cord, under the influence of different inductive signals. Since the discovery of dorsally- and ventrally-derived populations of oligodendrocytes, an important question has been whether they are functionally identical or differ functionally in some way. Using a dual-reporter mouse, I have shown that, despite different sites of origin, dorsally- and ventrally-derived oligodendrocyte lineage cells are electrically and morphologically similar.

However, despite being electrically identical, interesting differences in the settling positions of oligodendrocyte lineage cells that develop from dorsal and ventral regions of the spinal cord were discovered. These data suggest that competition exists between dorsally- and ventrally-derived oligodendrocytes for the myelination of specific tracts. In a recent study, Zhu et al. (2011b) demonstrated that dorsally-derived OPCs were able to migrate to, and produce new oligodendrocytes in, a focal lesion in the ventral spinal cord. These data suggest that dorsally-derived OPCs could provide an important source of new oligodendrocytes for axon remyelination after injury. At this point, the mechanism by which dorsal oligodendrocytes outnumber ventral oligodendrocytes in either myelination or remyelination can only be speculated about, and further experiments detailed below may shed light on this mechanism.

7.1.2 Suggestions for further work

Despite examining many of the electrical properties and morphological properties of dorsally- and ventrally-derived oligodendrocyte lineage cells, they appeared to be electrically and morphologically identical. It is possible that other electrical differences between dorsally- and ventrally-derived oligodendrocyte lineage cells could exist that were not examined by this study. For example, dorsal OPCs and ventral OPCs could differ in terms of the synapses they receive from neuronal axons. Conceivably OPCs derived from different lineages may receive synaptic inputs from

either excitatory or inhibitory neurons (or both), or the properties of these currents could be distinct (e.g. OPCs could receive synaptic inputs at different frequencies or with different amplitudes). The fact that both dorsal and ventral OPCs responded similarly to the application of excitatory and inhibitory neurotransmitters suggests that they express the appropriate receptors to respond to glutamate and/or GABA release from neuronal axons. Receiving synaptic inputs with different properties from neuronal axons could provide an electrical mechanism by which OPC survival, differentiation and subsequent myelination could be controlled by specific tracts. Therefore, it would be interesting to examine and compare the properties of the synaptic input to dorsal and ventral OPCs.

Alternatively, different molecular cues which were not examined in this study could account for the myelination of specific tracts. For example, dorsally- and ventrally-derived oligodendrocyte lineage cells may express different genes or higher levels of particular genes depending on their site of origin. In the context of this study, dorsally-derived oligodendrocyte lineage cells may specifically express adhesion molecules or survival genes, which enable them to reside within and myelinate the dorsal tracts in the spinal cord more effectively. In order to assess such differences, gene expression profiling of dorsally- and ventrally-derived oligodendrocyte lineage cells from the dual reporter mouse could be carried out.

At present, it is well established that newly born mature oligodendrocytes are generated from OPCs throughout life (Rivers et al., 2008; Psachoulia et al., 2009). Activity dependent changes in myelination have also been suggested to occur in the human brain in adulthood. For example, when people learn motor tasks such as piano playing (Bengtsson et al., 2005), changes in myelination have been observed. However, although I have shown that all OPCs proliferate, it is not known whether dorsally- and ventrally-derived OPCs can both contribute towards the production of these newly born oligodendrocytes in adulthood. It would be of interest to assess whether dorsally- or ventrally-derived OPCs, or a mixture of both, generate these new oligodendrocytes, which could contribute to myelin turnover and activity-dependent changes in myelination in the adult brain.

Furthermore, the finding that dorsally-derived oligodendrocyte lineage cells compete to myelinate specific tracts within the spinal cord raises the question of how such a competition operates in the context of remyelination. During remyelination, OPCs must proliferate and differentiate in order to generate new oligodendrocytes to repair demyelinated axons. It has been suggested that dorsally-derived OPCs can

migrate to, and produce new oligodendendrocytes in a focal lesion in the spinal cord (Zhu et al., 2011b). It would be interesting to investigate the signalling mechanisms which induce dorsally-derived OPCs proliferate, and differentiate more effectively into myelinating oligodendrocytes after injury, when compared to their ventrally-derived counterparts. In addition, transplantation of OPCs has been shown to promote remyelination (Windrem et al., 2008), therefore it would be of interest to see whether transplanted dorsally-derived or ventrally-derived OPCs dominate during the remyelination process.

7.2 Properties and fate of oligodendrocyte precursor cells in the postnatal mouse brain

7.2.1 Discussion

OPCs were originally assumed to be a homogeneous class of immature oligodendroglial cell, but have since been subdivided according to their electrical properties (Chittajallu et al., 2004; Karadottir et al., 2008), gene expression profiles (Gensert and Goldman, 2001; Mallon et al., 2002; Lin et al., 2009), proliferation rates (Psachoulia et al., 2009), response to injury (Keirstead et al., 1998; Lytle et al., 2009) and their abilities to differentiate into myelinating OLs (Mallon et al., 2002; Dimou et al., 2008) or other types of cells including neurons (Guo et al., 2010; Rivers et al., 2008; Zhu et al., 2008). There continues to be much debate over how many sub-types of OPC there might be, and the most appropriate way to classify them. To advance understanding of this issue, I performed experiments examining both the histological and electrophysiological properties of OPCs. In summary, these data determined that all postnatal OPCs defined by strong expression of the NG2 proteoglycan: (1) co-express the mitogenic receptor PDGFRα, (2) express I_{Na} and are electrically excitable, but do not fire *bona fide* action potentials, (3) are mitotically active and incorporate EdU, and (4) generate differentiated OLs but not neurons.

In addition, two further classes of oligodendrocyte lineage cell were observed. One group of cells expressed low levels of NG2 and little to no I_{Na}, which were assumed to correspond to early differentiating OPCs, that are down-regulating their I_{Na} and NG2 expression, as previously described (De Biase et al., 2010; Kukley et al., 2010). This group likely corresponds to the no I_{Na} OPCs reported by Karadottir et al. (2008). The other group of cells lacked both NG2 labelling and I_{Na} expression, and therefore correspond to pre-myelinating or myelinating oligodendrocytes. Taken

together, these data suggest that OPCs are in fact a homogenous population of cells, which downregulate their expression of NG2 and PDGFRα, and voltage-gated channels as they differentiate into myelinating oligodendrocytes. At this point, these data point to a link between Na^+ and/or K^+ channel expression and OPC proliferation and differentiation, but further work, as suggested below, is required to fully understand the these voltage-gated channels in OPCs.

7.2.2 Suggestions for further work

I have demonstrated that injecting current into OPCs led to regenerative action potential-like depolarisations in all brain areas and developmental stages examined, consistent with previous studies in mice (Chittajallu et al., 2004; Ge et al., 2009; De Biase et al., 2010). It is likely that activation of voltage-gated Na^+ channels in OPCs acts to amplify excitatory synaptic inputs to OPCs, raising intracellular Ca^{2+} levels to regulate OPC development. Expression of I_{Na} in OPCs might also play a key role in regulating the developmental myelination of active circuits and activity-dependent myelination in the adult brain. It would be interesting to conditionally knock-out voltage-gated Na^+ channels in OPCs during developmental myelination and in adulthood. Following the deletion of Na^+ channels, any changes in the properties of OPCs could be assessed, such as their ability to proliferate and differentiate, along with the amount of myelin that they make.

Voltage-gated K^+ channel expression by OPCs has been suggested to regulate growth-factor mediated proliferation (Knutson et al., 1997; Chittajallu et al., 2005). Therefore, I considered whether OPC proliferation rate might correlate with the density of voltage-gated K^+ channels expressed by OPCs. The cell cycle time for OPCs in the corpus callosum is reported to be significantly shorter than the cell cycle time for OPCs in the motor cortex (Psachoulia et al., 2009). Coincidentally, the peak outward K^+ current was 2-fold larger in the corpus callosum compared to the motor cortex, consistent with a potential role for K^+ currents in promoting proliferation. The function role of K^+ channel expression in OPCs could be assessed *in vivo*, by conditionally knocking out these channels during development and in adulthood. After the deletion of these channels the development and differentiation of OPCs could be compared with that in OPCs expressing K^+ channels, along with any changes in the myelination that the cells produce.

In addition to the differentiation of OPCs into oligodendrocytes which myelinate neuronal axons, several groups have previously reported that OPCs generate new neurons in the postnatal mouse brain (Rivers et al., 2008; Guo et al., 2010). In this

study, lineage tracing experiments using *Pdgfrα-CreER^{T2}:R26-YFP* transgenic mice, demonstrated the labelling of newly formed YFP^{+} oligodendrocytes and neurons. The neurons accumulated in the anterior piriform cortex of the brain, consistent with previous studies (Rivers et al., 2008; Guo et al., 2010). It was assumed that these neurons are produced continuously from a pool of precursors in the piriform cortex that become YFP-labelled after tamoxifen treatment. In the earlier studies, the YFP-labelled neurons were consistently BrdU-negative, even after extended BrdU exposure, leading the authors to speculate that a subpopulation of mitotically quiescent OPCs might be differentiating into the new neurons in the piriform cortex (Rivers et al., 2008; Guo et al., 2010). In this study, using an alternative thymidine analogue (EdU), all OPCs were found to be mitotically active, and so cannot be the source of the new neurons in the piriform cortex, which were again found to be consistently mitotically inactive. These data now agree with a study by Kang et al. (2010) who, using an independently generated line of *Pdgfrα-CreER^{T2}* mice, failed to detect any newly generated long-term surviving neurons, derived from OPCs, in the piriform cortex or elsewhere in the forebrain. The fact that YFP expressing neurons (which are not generated by OPCs) accumulate in the *Pdgfrα-CreER^{T2}:R26-YFP* in this study, but not in the Kang et al. (2010) study, still requires explanation. It is possible that the transgenic mouse line used in this study, but not theirs, marks an unidentified population of *Pdgfrα*-expressing neurogenic precursor/stem cells that either resides in the CNS or arrives via the blood. Experiments identifying this population of *Pdgfrα*-expressing neurogenic precursor/stem cells and following their fate, would confirm whether or not new neurons are being produced in the adult piriform cortex (that are not generated by OPCs), a brain area in the olfactory bulb circuitry, which is known to be highly plastic with new neurons being added to the olfactory neuroepithelium of the nose and to the olfactory bulb, in adulthood (Young et al., 2007). Further experiments, for example using a *Pdgfrα-CreER* knock-in transgenic mouse line, would be required to resolve this.

7.3 The effects of GABA on OPCs, mature oligodendrocytes, and myelination

7.3.1 Discussion

Myelination is controlled by interactions between developing axons and OPCs, which are in part mediated by growth factors. However, OPCs also receive excitatory and inhibitory input from neuronal axons, raising the question of whether neurotransmitters also regulate OPC development and myelination. In this thesis, I

confirm earlier reports that GABA evokes a current, which is mediated by $GABA_A$ receptors, in all oligodendrocyte lineage cells. Using a cerebral cortical slice model of myelination, I investigated whether GABAergic signalling can regulate the OPC proliferation, differentiation, and myelination. Interestingly, GABA acting on $GABA_A$ receptors halves the number of OPCs, thereby controlling the number of myelinating cells available to ensheath axons. GABA reduces the number of OPCs by two separate mechanisms, firstly, it suppresses OPC proliferation, and secondly, it increases the death of oligodendrocyte lineage cells. As a result of the reduced number of OPCs, GABA reduces the fraction of axons myelinated, reduces the amount of myelin on axons that do become myelinated, and increases the length of the myelin internodes wrapped around the axons.

At present, the function of GABAergic input to OPCs is not well understood, but these data indicate that GABA plays a role in OPC development and myelination. However, these data contradict previous studies reporting that GABA had no effect on OPC development (Gallo et al., 1996; Yuan et al., 1998). Instead, the GABA-mediated suppression of OPC proliferation observed here is more similar to that previously reported for neural precursor cells (LoTurco et al., 1995).

In this study, the effects of endogenous GABA release on the number of the oligodendrocyte lineage cells and on myelination could be mediated directly by $GABA_A$ receptors present on oligodendrocyte lineage cells, or alternatively blocking neuronal $GABA_A$ receptors might change neuronal activity, which could alter myelination indirectly by changing the release of growth factors or glutamate (Wake et al., 2011). In support of the idea that GABA acts directly on OPCs, in this study GABAzine (which blocks $GABA_A$ receptors) did not have a significant effect on neuronal activity, suggesting that the actions of GABA on oligodendrocyte lineage cells are not mediated by an alteration of neuronal firing and a subsequent release of growth factors and/or glutamate. Further experiments, which are detailed below, could be carried out to determine whether GABA is acting directly on OPCs.

7.3.2 Suggestions for further work

Firstly, in order to demonstrate that the GABA-mediated effect on OPCs is dependent on the synaptic release of GABA, the myelinating slice cultures could be treated with botulinum toxin, which cleaves the synaptic release protein SNAP-25 to inhibit vesicle fusion and neurotransmitter release (Wake et al., 2011; Welch et al., 2000). Secondly, the synaptic currents in OPCs could be assessed, to demonstrate that following treatment with GABAzine, the GABAergic synaptic input to OPCs is

reduced. Furthermore, GABA receptors could be specifically knocked-out of OPCs using a conditional $GABA_A$ receptor knock-out mouse, or alternatively siRNAs could be cell specifically introduced via viral infection to knock-out $GABA_A$ receptors in OPCs in the myelinating cultures. Following the deletion of $GABA_A$ receptors from OPCs, changes in OPC proliferation, differentiation and myelination could be assessed. Collectively, data from these experiments would further test the idea that GABA release from neurons is acting directly on the $GABA_A$ receptors on OPCs to regulate their proliferation, differentiation and myelination.

Another question that remains unanswered is: how does GABA regulate the proliferation of OPCs in order to control the number of OPCs available to myelinate axons? Studies investigating the $GABA_A$ receptor regulation of neural stem cell proliferation provide a hint of the mechanism by which GABA may regulate OPC proliferation. Like neural stem cells (LoTurco et al., 1995), GABA appears to reduce the proliferation of OPCs. In neural stem cells, GABA, acting on $GABA_A$ receptors, signals through S-phase checkpoint kinases of the phosphatidylinositol-3-OH kinase-related kinase (PIKKs) family, to regulate the cell cycle and proliferation (Andang et al., 2008; Fernando et al., 2011). In particular, GABA acts through the PIKK protein, ATR, which activates another PIKK protein, ATM, by phosphorylation. Then, ATM phosphorylates histones (in particular the H2AX-variant) in the cell nucleus, resulting in decreased DNA synthesis, a slower progression through S-phase of the cell cycle, and a slower rate of cell proliferation (Andang et al., 2008; Fernando et al., 2011). It would be of interest to investigate whether GABA regulates OPC proliferation by a similar mechanism. In order to assess this, the organotypic slice cultures could be immuno-labelled with an antibody to the phosphorylated form of H2AX (γ-H2AX), and the proportion of OPCs expressing γ-H2AX in control slices could be compared with proportion of γ-H2AX expressing OPCs in slices treated with either GABAzine or muscimol. In addition, ATR phosphorylation of ATM could be blocked using a specific ATR kinase inhibitor (Andang et al., 2008), to assess whether the $GABA_A$ receptor dependent reduction in the number of proliferating OPCs is regulated by a similar mechanism to that in neural stem cells.

At present, it is not clear whether blocking $GABA_A$ receptors increases the overall number of axons myelinated, or just accelerates myelination. It would be of interest to assess whether eventually, after a longer time period in culture, the control slices would reach a similar level of myelination. Furthermore, the speed of developmental myelination could be assessed in mice in which $GABA_A$ receptors have been specifically knocked-out of OPCs.

GABA not only reduces the fraction of axons myelinated, but also appears to reduce the amount of myelin on the axons that do become myelinated. This GABA-mediated change in myelin thickness could be assessed further by performing electron microscopy on the organotypic slice cultures and measuring the g-ratio of the myelinated axons. In addition to increasing the fraction of myelinated axons, and the amount of myelin, GABA also increased the length of the internodes. Presumably, the increase in internode length was due to the large decrease of the overall number of oligodendrocyte lineage cells produced, implying that there will be fewer OPCs competing to myelinate the same number of axons, which results in each oligodendrocyte having to make longer internodes to myelinate the same length of axon. This increase in internode length could increase the action potential conduction velocity. However, there is an optimal internode length that maximises conduction speed (Brill et al., 1977). Indeed, if axons become myelinated with internodes that are much longer than the optimal length, the conduction velocity can actually decrease, due to less voltage transmission from one node to the next, so that the Na^+ conductance at the next node takes longer to activate (Brill et al., 1977). It would be of interest to assess the extent to which the GABA-mediated change in internode length affects the conduction velocity of myelinated axons, and whether this change tunes the conduction speed in order to beneficially influence information processing. The conduction velocity could be measured experimentally by looking at the input arrival times at a single post-synaptic cell whilst stimulating the presynaptic inputs from a defined position on a myelinated axon. Alternatively, the action potential conduction velocity could be assessed in myelinated axons with the use of voltage-sensitive dyes. Using either technique, the conduction velocity could be compared in neurons in control slices with neurons in slices treated with GABAzine.

Finally, the fact that GABA can modulate developmental myelination raises the possibility that it may do so during remyelination. In support of this, excitatory axons have been reported to make synapses onto OPCs during remyelination (Etxeberria et al., 2010). Therefore, it is possible that inhibitory axons in the grey matter or in white matter tracts may make synapses with OPCs during remyelination. It would be interesting to look at GABAergic signalling to OPCs following a lesion, to assess whether blocking GABAergic signalling can increase the number of OPCs available to myelinate neuronal axons after injury.

7.4 Conclusion

The experiments performed in this thesis investigated the electrical properties of OPCs, and how signalling to these cells regulates their proliferation, differentiation and myelination. Firstly, I have demonstrated that oligodendrocyte lineage cells derived from different embryonic sites are electrically similar, however, despite having indistinguishable electrical properties, dorsally-derived oligodendrocytes myelinated specific tracts in the spinal cord. Secondly, I have shown that OPCs in different brain regions have similar properties in terms of their expression of voltage-gated ion channels, precursor proteins and proliferative capacity. Finally, having determined that all OPCs apparently have similar membrane properties, I investigated whether the inhibitory neurotransmitter GABA can regulate OPC proliferation, differentiation and myelination. Endogenously released GABA was found to reduce the number of oligodendrocyte lineage cells formed, reduce the amount of myelin per axon and increase internode length. These results demonstrate that GABA, presumably released from inhibitory interneurons, can regulate OPC development and myelination. However, further work is required to shed light on the functional role of voltage-gated ion channels in OPCs and how expression of these channels modulates OPC proliferation, differentiation and myelination.

Bibliography

Abremski K, Hoess R (1984) Bacteriophage P1 site-specific recombination. Purification and properties of the Cre recombinase protein. J Biol Chem 259:1509-1514.

Aguirre A, Gallo V (2004) Postnatal neurogenesis and gliogenesis in the olfactory bulb from NG2-expressing progenitors of the subventricular zone. J Neurosci 24:10530-10541.

Ahern GP, Klyachko VA, Jackson MB (2002) cGMP and S-nitrosylation: two routes for modulation of neuronal excitability by NO. Trends Neurosci. 25:510-7

Akopian G, Kressin K, Derouiche A, Steinhauser C (1996) Identified glial cells in the early postnatal mouse hippocampus display different types of Ca2+ currents. Glia 17:181-194.

Allen NJ, Attwell D (2004) The effect of simulated ischaemia on spontaneous GABA release in area CA1 of the juvenile rat hippocampus. J Physiol 561:485-498.

Allen NJ, Rossi DJ, Attwell D (2004) Sequential release of GABA by exocytosis and reversed uptake leads to neuronal swelling in simulated ischemia of hippocampal slices. J Neurosci. 24:3837-49.

Allen NJ, Karadottir R, Attwell D (2005) A preferential role for glycolysis in preventing the anoxic depolarization of rat hippocampal area CA1 pyramidal cells. J Neurosci 25:848-859.

Altman J, Bayer SA (1984) The development of the rat spinal cord. Adv Anat Embryol Cell Biol 85:1-164.

Andang M, Hjerling-Leffler J, Moliner A, Lundgren TK, Castelo-Branco G, Nanou E, Pozas E, Bryja V, Halliez S, Nishimaru H, Wilbertz J, Arenas E, Koltzenburg M, Charnay P, El MA, Ibanez CF, Ernfors P (2008) Histone H2AX-dependent GABA(A) receptor regulation of stem cell proliferation. Nature 451:460-464.

Apps R, Garwicz M (2005) Anatomical and physiological foundations of cerebellar information processing. Nat Rev Neurosci 6:297-311.

Armendariz BG, Bribian A, Perez-Martinez E, Martinez A, de CF, Soriano E, Burgaya F (2012) Expression of Semaphorin 4F in neurons and brain oligodendrocytes and the regulation of oligodendrocyte precursor migration in the optic nerve. Mol Cell Neurosci 49:54-67.

Artinian L, Tornieri K, Zhong L, Baro D, Rehder V (2010) Nitric oxide acts as a volume transmitter to modulate electrical properties of spontaneously firing neurons via apamin-sensitive potassium channels. J Neurosci. 30:1699-711.

Arroyo EJ, Sirkowski EE, Chitale R, Scherer SS (2004) Acute demyelination disrupts the molecular organization of peripheral nervous system nodes. J. Comp. Neurol 479:424–434

Attali B, Wang N, Kolot A, Sobko A, Cherepanov V, Soliven B (1997) Characterization of delayed rectifier Kv channels in oligodendrocytes and progenitor cells. J Neurosci 17:8234-8245.

Attwell D, Laughlin SB (2001) An energy budget for signaling in the grey matter of the brain. J Cereb Blood Flow Metab 21:1133-1145.

Baas D, Legrand C, Samarut J, Flamant F (2002) Persistence of oligodendrocyte precursor cells and altered myelination in optic nerve associated to retina degeneration in mice devoid of all thyroid hormone receptors. Proc Natl Acad Sci U S A 99:2907-2911.

Back SA, Luo NL, Borenstein NS, Levine JM, Volpe JJ, Kinney HC (2001) Late oligodendrocyte progenitors coincide with the developmental window of vulnerability for human perinatal white matter injury. J Neurosci 21:1302-1312.

Bakiri Y, Attwell D, Karadottir R (2009) Electrical signalling properties of oligodendrocyte precursor cells. Neuron Glia Biol1-9.

Bakiri Y, Karadottir R, Cossell L, Attwell D (2011) Morphological and electrical properties of oligodendrocytes in the white matter of the corpus callosum and cerebellum. J Physiol 589:559-573.

Bansal R, Kumar M, Murray K, Morrison RS, Pfeiffer SE (1996) Regulation of FGF receptors in the oligodendrocyte lineage. Mol Cell Neurosci 7:263-275.

Bareyre FM, Kerschensteiner M, Misgeld T, Sanes JR (2005) Transgenic labeling of the corticospinal tract for monitoring axonal responses to spinal cord injury. Nat Med 11:1355-1360.

Barres BA, Hart IK, Coles HS, Burne JF, Voyvodic JT, Richardson WD, Raff MC (1992) Cell death and control of cell survival in the oligodendrocyte lineage. Cell 70:31-46.

Barres BA, Koroshetz WJ, Swartz KJ, Chun LL, Corey DP (1990) Ion channel expression by white matter glia: the O-2A glial progenitor cell. Neuron 4:507-524.

Barres BA, Lazar MA, Raff MC (1994a) A novel role for thyroid hormone, glucocorticoids and retinoic acid in timing oligodendrocyte development. Development 120:1097-1108.

Barres BA, Raff MC (1993) Proliferation of oligodendrocyte precursor cells depends on electrical activity in axons. Nature 361:258-260.

Barres BA, Raff MC (1994) Control of oligodendrocyte number in the developing rat optic nerve. Neuron 12:935-942.

Barres BA, Raff MC, Gaese F, Bartke I, Dechant G, Barde YA (1994b) A crucial role for neurotrophin-3 in oligodendrocyte development. Nature 367:371-375.

Bartel DP (2004) MicroRNAs: genomics, biogenesis, mechanism, and function. Cell 116:281-297.

Baud O, Li J, Zhang Y, Neve RL, Volpe JJ, Rosenberg PA (2004) Nitric oxide-induced cell death in developing oligodendrocytes is associated with mitochondrial dysfunction and apoptosis-inducing factor translocation. Eur J Neurosci. 20:1713-26.

Belachew S, Chittajallu R, Aguirre AA, Yuan X, Kirby M, Anderson S, Gallo V (2003) Postnatal NG2 proteoglycan-expressing progenitor cells are intrinsically multipotent and generate functional neurons. J Cell Biol 161:169-186.

Ben-Ari Y (2002) Excitatory actions of gaba during development: the nature of the nurture. Nat Rev Neurosci 3:728-739.

Bengtsson SL, Nagy Z, Skare S, Forsman L, Forssberg H, Ullen F (2005) Extensive piano practicing has regionally specific effects on white matter development. Nat Neurosci 8:1148-1150.

Benjamins JA and Nedelkoska L (2007) Cyclic GMP-dependent pathways protect differentiated oligodendrocytes from multiple types of injury. Neurochem Res. 32:321-9.

Berger T, Walz W, Schnitzer J, Kettenmann H (1992) J Neurosci Res 31:21-27.

Bergles DE, Roberts JD, Somogyi P, Jahr CE (2000) Glutamatergic synapses on oligodendrocyte precursor cells in the hippocampus. Nature 405:187-191.

Bhat, R.V., Axt, K.J., Fosnaugh, J.S., Smith, K.J., Johnson, K.A., Hill, D.E., Kinzler,K.W., and Baraban, J.M. (1996) Expression of the APC tumor suppressor protein in oligodendroglia. Glia 17, 169-174.

Bi GQ, Poo MM (1998) Synaptic modifications in cultured hippocampal neurons: dependence on spike timing, synaptic strength, and postsynaptic cell type. J Neurosci 18:10464-10472.

Bicker G (2005) STOP and GO with NO: nitric oxide as a regulator of cell motility in simple brains. Bioessays 27:495-505.

Bjarnason GA, Jordan RC, Sothern RB (1999) Circadian variation in the expression of cell-cycle proteins in human oral epithelium. Am J Pathol 154:613-622.

Bjartmar C, Hildebrand C, Loinder K (1994) Morphological heterogeneity of rat oligodendrocytes: electron microscopic studies on serial sections. Glia 11:235-244.

Bjelke B, Seiger A (1989) Morphological distribution of MBP-like immunoreactivity in the brain during development. Int J Dev Neurosci 7:145-164.

Borges K, Kettenmann H (1995) Blockade of K+ channels induced by AMPA/kainate receptor activation in mouse oligodendrocyte precursor cells is mediated by Na+ entry. J Neurosci Res 42:579-593.

Borges K, Ohlemeyer C, Trotter J, Kettenmann H (1994) AMPA/kainate receptor activation in murine oligodendrocyte precursor cells leads to activation of a cation conductance, calcium influx and blockade of delayed rectifying K+ channels. Neuroscience 63:135-149.

Bormann J, Kettenmann H (1988) Patch-clamp study of gamma-aminobutyric acid receptor Cl- channels in cultured astrocytes. Proc Natl Acad Sci U S A 85:9336-9340.

Branco T, Clark BA, Hausser M (2010) Dendritic discrimination of temporal input sequences in cortical neurons. Science 329:1671-1675.

Brill MH, Waxman SG, Moore JW, Joyner RW (1977) Conduction velocity and spike configuration in myelinated fibres: computed dependence on internode distance. J Neurol Neurosurg Psychiatry 40:769-774.

Brinkmann BG, Agarwal A, Sereda MW, Garratt AN, Muller T, Wende H, Stassart RM, Nawaz S, Humml C, Velanac V, Radyushkin K, Goebbels S, Fischer TM, Franklin RJ, Lai C, Ehrenreich H, Birchmeier C, Schwab MH, Nave KA (2008) Neuregulin-1/ErbB signaling serves distinct functions in myelination of the peripheral and central nervous system. Neuron 59:581-595.

Bryant MR, Marta CB, Kim FS, Bansal,R (2009) Phosphorylation and lipid raft association of fibroblast growth factor receptor-2 in oligodendrocytes. Glia 57:935-46.

Bullmann T, Hartig W, Holzer M, Arendt T (2010) Expression of the embryonal isoform (0N/3R) of the microtubule-associated protein tau in the adult rat central nervous system. J Comp Neurol 518:2538-2553.

Bunge RP, Bunge MB, Bates M (1989) Movements of the Schwann cell nucleus implicate progression of the inner (axon-related) Schwann cell process during myelination. J Cell Biol 109:273-284.

Burne JF, Staple JK, Raff MC (1996) Glial cells are increased proportionally in transgenic optic nerves with increased numbers of axons. J Neurosci 16:2064-2073.

Butt AM, Duncan A, Hornby MF, Kirvell SL, Hunter A, Levine JM, Berry M (1999) Cells expressing the NG2 antigen contact nodes of Ranvier in adult CNS white matter. Glia 26:84-91.

Butt AM, Ibrahim M, Berry M (1997) The relationship between developing oligodendrocyte units and maturing axons during myelinogenesis in the anterior medullary velum of neonatal rats. J Neurocytol 26:327-338.

Burzomato V, Frugier G, Pérez-Otaño I, Kittler JT, Attwell D (2010) The receptor subunits generating NMDA receptor mediated currents in oligodendrocytes. J Physiol. 588:3403-14.

Cahoy JD, Emery B, Kaushal A, Foo LC, Zamanian JL, Christopherson KS, Xing Y, Lubischer JL, Krieg PA, Krupenko SA, Thompson WJ, Barres BA (2008a) A transcriptome database for astrocytes, neurons, and oligodendrocytes: a new resource for understanding brain development and function. J Neurosci 28:264-278.

Cahoy JD, Emery B, Kaushal A, Foo LC, Zamanian JL, Christopherson KS, Xing Y, Lubischer JL, Krieg PA, Krupenko SA, Thompson WJ, Barres BA (2008b) A transcriptome database for astrocytes, neurons, and oligodendrocytes: a new resource for understanding brain development and function. J Neurosci 28:264-278.

Cai J, Qi Y, Hu X, Tan M, Liu Z, Zhang J, Li Q, Sander M, Qiu M (2005) Generation of oligodendrocyte precursor cells from mouse dorsal spinal cord independent of Nkx6 regulation and Shh signaling. Neuron 45:41-53.

Calver AR, Hall AC, Yu WP, Walsh FS, Heath JK, Betsholtz C, Richardson WD (1998) Oligodendrocyte population dynamics and the role of PDGF in vivo. Neuron 20:869-882.

Chang A, Nishiyama A, Peterson J, Prineas J, Trapp BD (2000) NG2-positive oligodendrocyte progenitor cells in adult human brain and multiple sclerosis lesions. J Neurosci 20:6404-6412.

Chatterjee N, Stegmuller J, Schatzle P, Karram K, Koroll M, Werner HB, Nave KA, Trotter J (2008) Interaction of syntenin-1 and the NG2 proteoglycan in migratory oligodendrocyte precursor cells. J Biol Chem 283:8310-8317.

Chatterton JE, Awobuluyi M, Premkumar LS, Takahashi H, Talantova M, Shin Y, Cui J, Tu S, Sevarino KA, Nakanishi N, Tong G, Lipton SA, Zhang D (2002) Excitatory glycine receptors containing the NR3 family of NMDA receptor subunits. Nature 415:793-798.

Chehrehasa, F., Meedeniya, A.C., Dwyer, P., Abrahamsen, G., and Mackay-Sim, A. (2009) EdU, a new thymidine analogue for labelling proliferating cells in the nervous system. J. Neurosci. Meth. 177, 122-130.

Chen-Goodspeed M, Lee CC (2007) Tumor suppression and circadian function. J Biol Rhythms 22:291-298.

Cheung G, Kann O, Kohsaka S, Fäerber K, Kettenmann H (2009) GABAergic activities enhance macrophage inflammatory protein-1alpha release from microglia (brain macrophages) in postnatal mouse brain. J Physiol 587:753-68

Chittajallu R, Aguirre A, Gallo V (2004) NG2-positive cells in the mouse white and grey matter display distinct physiological properties. J Physiol 561:109-122.

Chittajallu R, Aguirre AA, Gallo V (2005) Downregulation of platelet-derived growth factor-alpha receptor-mediated tyrosine kinase activity as a cellular mechanism for K+-channel regulation during oligodendrocyte development in situ. J Neurosci 25:8601-8610.

Chittajallu R, Chen Y, Wang H, Yuan X, Ghiani CA, Heckman T, McBain CJ, Gallo V (2002) Regulation of Kv1 subunit expression in oligodendrocyte progenitor cells and their role in G1/S phase progression of the cell cycle. Proc Natl Acad Sci U S A 99:2350-2355.

Collarini EJ, Kuhn R, Marshall CJ, Monuki ES, Lemke G, Richardson WD (1992) Down-regulation of the POU transcription factor SCIP is an early event in oligodendrocyte differentiation in vitro. Development 116:193-200.

Chong SY, Rosenberg SS, Fancy SP, Zhao C, Shen YA, Hahn AT, McGee AW, Xu X, Zheng B, Zhang LI, Rowitch DH, Franklin RJ, Lu QR, Chan JR (2012) Neurite outgrowth inhibitor Nogo-A establishes spatial segregation and extent of oligodendrocyte myelination. Proc Natl Acad Sci U S A 109:1299-1304.

Chung K, Coggeshall RE (1983) Numbers of Axons in Lateral and Ventral Funiculi of Rat Sacral Spinal Cord. The Journal of Comparative Neurology 214:72-78

Chung K, Sharma J, Coggeshall RE (1985) Numbers of Myelinated and Unmyelinated Axons in the Dorsal, Lateral, and Ventral Funiculi of the White Matter of the S2 Segment of Cat Spinal Cord. The Journal of Comparative Neurology 234:117-121

Cohen NR, Taylor JS, Scott LB, Guillery RW, Soriano P, Furley AJ (1998) Errors in corticospinal axon guidance in mice lacking the neural cell adhesion molecule L1. Curr Biol 8:26-33.

Coman I, Barbin G, Charles P, Zalc B, Lubetzki C (2005) Axonal signals in central nervous system myelination, demyelination and remyelination. J Neurol Sci 233:67-71.

Contestabile A and Ciani E (2004) Role of nitric oxide in the regulation of neuronal proliferation, survival and differentiation. Neurochem Int. 45:903-14

Dayer AG, Cleaver KM, Abouantoun T, Cameron HA (2005) New GABAergic interneurons in the adult neocortex and striatum are generated from different precursors. J Cell Biol. 168:415-27.

Davies JE, Miller RH (2001) Local sonic hedgehog signaling regulates oligodendrocyte precursor appearance in multiple ventricular zone domains in the chick metencephalon. Dev Biol 233:513-525.

Davis AA, Temple S (1994) A self-renewing multipotential stem cell in embryonic rat cerebral cortex. Nature 372:263-266.

Dawson MR, Polito A, Levine JM, Reynolds R (2003) NG2-expressing glial progenitor cells: an abundant and widespread population of cycling cells in the adult rat CNS. Mol Cell Neurosci 24:476-488.

De Biase LM, Kang SH, Baxi EG, Fukaya M, Pucak ML, Mishina M, Calabresi PA, Bergles DE (2011) NMDA receptor signaling in oligodendrocyte progenitors is not required for oligodendrogenesis and myelination. J Neurosci 31:12650-12662.

De Biase LM, Nishiyama A, Bergles DE (2010) Excitability and synaptic communication within the oligodendrocyte lineage. J Neurosci 30:3600-3611.

del Rio-Hortega P (1921) Estudios sobre la neuroglia. La glia de escasas radiaciones oligodendroglia. Bol Real Soc Espan Hist Nat 21:63–92.

del Rio-Hortega P (1928) Tercera aportación al conocimiento morfológico e interpretación funcional de la oligodendroglia. Mem Real Soc Espan Hist Nat14:40–122.

Demas J, Eglen SJ, Wong RO (2003) Developmental loss of synchronous spontaneous activity in the mouse retina is independent of visual experience. J Neurosci 23:2851-2860.

Demerens C, Stankoff B, Logak M, Anglade P, Allinquant B, Couraud F, Zalc B, Lubetzki C (1996) Induction of myelination in the central nervous system by electrical activity. Proc Natl Acad Sci U S A 93:9887-9892.

Deng W, Rosenberg PA, Volpe JJ, Jensen FE (2003) Calcium-permeable AMPA/kainate receptors mediate toxicity and preconditioning by oxygen-glucose deprivation in oligodendrocyte precursors. Proc Natl Acad Sci U S A 100:6801-6806.

Dimou L, Simon C, Kirchhoff F, Takebayashi H, Gotz M (2008) Progeny of Olig2-expressing progenitors in the gray and white matter of the adult mouse cerebral cortex. J Neurosci 28:10434-10442.

Dingledine R, Borges K, Bowie D, Traynelis SF (1999) The glutamate receptor ion channels. Pharmacol Rev 51:7-61.

Dobson CB, Villagra F, Clowry GJ, Smith M, Kenwrick S, Donnai D, Miller S, Eyre JA (2001) Abnormal corticospinal function but normal axonal guidance in human L1CAM mutations. Brain 124:2393-2406.

Dubois-Dalcq M, Behar T, Hudson L, Lazzarini RA (1986) Emergence of three myelin proteins in oligodendrocytes cultured without neurons. J Cell Biol 102:384-392.

Dugas JC, Cuellar TL, Scholze A, Ason B, Ibrahim A, Emery B, Zamanian JL, Foo LC, McManus MT, Barres BA (2010) Dicer1 and miR-219 Are required for normal oligodendrocyte differentiation and myelination. Neuron 65:597-611.

Edwards FA, Konnerth A, Sakmann B, Takahashi T (1989) A thin slice preparation for patch clamp recordings from neurones of the mammalian central nervous system. Pflugers Arch 414:600-612.

Engel U, Wolswijk G (1996) Oligodendrocyte-type-2 astrocyte (O-2A) progenitor cells derived from adult rat spinal cord: in vitro characteristics and response to PDGF, bFGF and NT-3. Glia 16:16-26.

Etxeberria A, Mangin JM, Aguirre A, Gallo V (2010) Adult-born SVZ progenitors receive transient synapses during remyelination in corpus callosum. Nat Neurosci 13:287-289.

Fatima-Shad K, Barry PH (1993) Anion permeation in GABA- and glycine-gated channels of mammalian cultured hippocampal neurons. Proc Biol Sci. 253:69-75

Feinberg K, Eshed-Eisenbach Y, Frechter S, Amor V, Salomon D, Sabanay H, Dupree JL, Grumet M, Brophy PJ, Shrager P, Peles E (2010) A glial signal consisting of gliomedin and NrCAM clusters axonal Na+ channels during the formation of nodes of Ranvier. Neuron 65:490-502.

Fern R, Moller T (2000) Rapid ischemic cell death in immature oligodendrocytes: a fatal glutamate release feedback loop. J Neurosci 20:34-42.

Fernando RN, Eleuteri B, Abdelhady S, Nussenzweig A, Andang M, Ernfors P (2011) Cell cycle restriction by histone H2AX limits proliferation of adult neural stem cells. Proc Natl Acad Sci U S A 108:5837-5842.

Ffrench-Constant C, Raff MC (1986) Proliferating bipotential glial progenitor cells in adult rat optic nerve. Nature 319:499-502.

Fields RD (2008) White matter in learning, cognition and psychiatric disorders. Trends Neurosci 31:361-370.

Fogarty M, Richardson WD, Kessaris N (2005) A subset of oligodendrocytes generated from radial glia in the dorsal spinal cord. Development 132:1951-1959.

Foster RE, Connors BW, Waxman SG (1982) Rat optic nerve: electrophysiological, pharmacological and anatomical studies during development. Brain Res 255:371-386.

Frick A, Johnston D (2005) Plasticity of dendritic excitability. J Neurobiol 64:100-15.

Friede RL (1972) Control of myelin formation by axon caliber (with a model of the control mechanism). J Comp Neurol 144:233-252.

Fruttiger M, Karlsson L, Hall AC, Abramsson A, Calver AR, Bostrom H, Willetts K, Bertold CH, Heath JK, Betsholtz C, Richardson WD (1999) Defective oligodendrocyte development and severe hypomyelination in PDGF-A knockout mice. Development 126:457-467.

Fulton BP, Burne JF, Raff MC (1992) Visualization of O-2A progenitor cells in developing and adult rat optic nerve by quisqualate-stimulated cobalt uptake. J Neurosci 12:4816-4833.

Fulton D, Paez PM, Fisher R, Handley V, Colwell CS, Campagnoni AT (2010) Regulation of L-type Ca++ currents and process morphology in white matter oligodendrocyte precursor cells by golli-myelin proteins. Glia 58:1292-1303.

Furusho M, Dupree JL, Nave KA, Bansal R (2012) Fibroblast growth factor receptor signaling in oligodendrocytes regulates myelin sheath thickness. J Neurosci 32:6631-6641.

Gallo, V., Patrizio, M., and Levi, G. (1991) GABA release triggered by the activation of neuron-like non-NMDA receptors in cultured type 2 astrocytes is carrier-mediated. Glia 4:245-255.

Gallo V, Zhou JM, McBain CJ, Wright P, Knutson PL, Armstrong RC (1996) Oligodendrocyte progenitor cell proliferation and lineage progression are regulated by glutamate receptor-mediated K+ channel block. J Neurosci 16:2659-2670.

Gard AL, Pfeiffer SE (1993) Glial cell mitogens bFGF and PDGF differentially regulate development of O4+GalC- oligodendrocyte progenitors. Dev Biol 159:618-630.

Garthwaite G, Bartus K, Malcolm D, Goodwin D, Kollb-Sielecka M, Dooldeniya C, Garthwaite J. (2006) Signaling from blood vessels to CNS axons through nitric oxide. J Neurosci. 26:7730-40.

Garthwaite J (2008) Concepts of neural nitric oxide-mediated transmission. Eur J Neurosci. 27:2783-802

Ge WP, Yang XJ, Zhang Z, Wang HK, Shen W, Deng QD, Duan S (2006) Long-term potentiation of neuron-glia synapses mediated by Ca2+-permeable AMPA receptors. Science 312:1533-1537.

Ge WP, Zhou W, Luo Q, Jan LY, Jan YN (2009) Dividing glial cells maintain differentiated properties including complex morphology and functional synapses. Proc Natl Acad Sci U S A 106:328-333.

Geiger JR, Melcher T, Koh DS, Sakmann B, Seeburg PH, Jonas P, Monyer H (1995) Relative abundance of subunit mRNAs determines gating and Ca2+ permeability of AMPA receptors in principal neurons and interneurons in rat CNS. Neuron 15:193-204.

Gensert JM, Goldman JE (1997) Endogenous progenitors remyelinate demyelinated axons in the adult CNS. Neuron 19:197-203.

Gery S, Komatsu N, Baldjyan L, Yu A, Koo D, Koeffler HP (2006) The circadian gene per1 plays an important role in cell growth and DNA damage control in human cancer cells. Mol Cell 22:375-382.

Gianino S, Stein SA, Li H, Lu X, Biesiada E, Ulas J, Xu XM (1999) Postnatal growth of corticospinal axons in the spinal cord of developing mice. Brain Res Dev Brain Res 112:189-204.

Gilbert P, Kettenmann H, Schachner M (1984) gamma-Aminobutyric acid directly depolarizes cultured oligodendrocytes. J Neurosci 4:561-569.

Goretzki L, Burg MA, Grako KA, Stallcup WB (1999) High-affinity binding of basic fibroblast growth factor and platelet-derived growth factor-AA to the core protein of the NG2 proteoglycan. J Biol Chem 274:16831-16837.

Grubb MS, Burrone J (2010) Activity-dependent relocation of the axon initial segment fine-tunes neuronal excitability. Nature 465:1070-1074.

Gudz TI, Komuro H, Macklin WB (2006) Glutamate stimulates oligodendrocyte progenitor migration mediated via an alphav integrin/myelin proteolipid protein complex. J Neurosci 26:2458-2466.

Guo F, Maeda Y, Ma J, Xu J, Horiuchi M, Miers L, Vaccarino F, Pleasure D (2010) Pyramidal neurons are generated from oligodendroglial progenitor cells in adult piriform cortex. J Neurosci 30:12036-12049.

Guo F, Maeda Y, Ko EM, Delgado M, Horiuchi M, Soulika A, Miers L, Burns T, Itoh T, Shen H, Lee E, Sohn J, Pleasure D (2012) Disruption of NMDA receptors in oligodendroglial lineage cells does not alter their susceptibility to experimental autoimmune encephalomyelitis or their normal development. J Neurosci 32:639-45

Guzman-Marin R, Suntsova N, Bashir T, Szymusiak R, McGinty D (2007) Cell proliferation in the dentate gyrus of the adult rat fluctuates with the light-dark cycle. Neurosci Lett 422:198-201.

Hardingham GE, Bading H (2003) The Yin and Yang of NMDA receptor signalling. Trends Neurosci. 26:81-9

Hamann M, Rossi DJ, Mohr C, Andrade AL, Attwell D (2005) The electrical response of cerebellar Purkinje neurons to simulated ischaemia. Brain 128:2408-2420.

Hamano K, Iwasaki N, Takeya T, Takita H (1996) A quantitative analysis of rat central nervous system myelination using the immunohistochemical method for MBP. Brain Res Dev Brain Res 93:18-22.

Hamano K, Takeya T, Iwasaki N, Nakayama J, Ohto T, Okada Y (1998) A quantitative study of the progress of myelination in the rat central nervous system, using the immunohistochemical method for proteolipid protein. Brain Res Dev Brain Res 108:287-293.

Hamill OP, Marty A, Neher E, Sakmann B, Sigworth FJ (1981) Improved patch-clamp techniques for high-resolution current recording from cells and cell-free membrane patches. Pflugers Arch 391:85-100.

Hamilton TG, Klinghoffer RA, Corrin PD, Soriano P (2003) Evolutionary divergence of platelet-derived growth factor alpha receptor signaling mechanisms. Mol Cell Biol 23:4013-4025.

Hansen AJ (1985) Effect of anoxia on ion distribution in the brain. Physiol Rev 65:101-148.

Hayakawa K, Pham LD, Som AT, Lee BJ, Guo S, Lo EH, Arai K (2011) Vascular endothelial growth factor regulates the migration of oligodendrocyte precursor cells. J Neurosci 31:10666-10670.

Hayashi T, Seki T, Sato K, Iwai M, Zhang WR, Manabe Y, Abe K (2001) Expression of polysialylated neural cell adhesion molecule in rat brain after transient middle cerebral artery occlusion. Brain Res 907:130-133.

Heng JI, Moonen G, Nguyen L (2007) Neurotransmitters regulate cell migration in the telencephalon. Eur J Neurosci 26:537-546.

Hippenmeyer S, Vrieseling E, Sigrist M, Portmann T, Laengle C, Ladle DR, Arber,S (2006) A developmental switch in the response of DRG neurons to ETS transcription factor signaling. PLoS Biol 3: 878-890

Honke K, Hirahara Y, Dupree J, Suzuki K, Popko B, Fukushima K, Fukushima J, Nagasawa T, Yoshida N, Wada Y, Taniguchi N (2002) Paranodal junction formation and spermatogenesis require sulfoglycolipids. Proc Natl Acad Sci U S A 99:4227-4232.

Hooper DC, Bagasra O, Marini JC, Zborek A, Ohnishi ST, Kean R, Champion JM, Sarker AB, Bobroski L, Farber JL, Akaike T, Maeda H, Koprowski H (1997) Prevention of experimental allergic encephalomyelitis by targeting nitric oxide and peroxynitrite: implications for the treatment of multiple sclerosis. Proc Natl Acad Sci U S A. 94:2528-33.

Horner PJ, Power AE, Kempermann G, Kuhn HG, Palmer TD, Winkler J, Thal LJ, Gage FH (2000) Proliferation and differentiation of progenitor cells throughout the intact adult rat spinal cord. J Neurosci 20:2218-2228.

Hossain-Ibrahim MK, Rezajooi K, Stallcup WB, Lieberman AR, Anderson PN (2007) Analysis of axonal regeneration in the central and peripheral nervous systems of the NG2-deficient mouse. BMC Neurosci 8:80.

Huxley AF, Stampfli R (1949) Evidence for saltatory conduction in peripheral myelinated nerve fibres. J Physiol 108:315-339.

Ingram SL, Williams JT (1996) Modulation of the hyperpolarization-activated current (Ih) by cyclic nucleotides in guinea-pig primary afferent neurons. J Physiol. 492:97-106.

Ioannidou K, Anderson KI, Strachan D, Edgar JM, Barnett SC (2012) Time-lapse imaging of the dynamics of CNS glial-axonal interactions in vitro and ex vivo. PLoS One 7:e30775.

Ishibashi T, Dakin KA, Stevens B, Lee PR, Kozlov SV, Stewart CL, Fields RD (2006) Astrocytes promote myelination in response to electrical impulses. Neuron 49:823-32.

Jackson EL, Garcia-Verdugo JM, Gil-Perotin S, Roy M, Quinones-Hinojosa A, Vandenberg S, Alvarez-Buylla A (2006) PDGFR alpha-positive B cells are neural stem cells in the adult SVZ that form glioma-like growths in response to increased PDGF signaling. Neuron 51:187-199.

Jakeman LB, Chen Y, Lucin KM, McTigue DM (2006) Mice lacking L1 cell adhesion molecule have deficits in locomotion and exhibit enhanced corticospinal tract sprouting following mild contusion injury to the spinal cord. Eur J Neurosci 23:1997-2011.

Jeffress LA (1948) A place theory of sound localization. J Comp Physiol Psychol 41:35-39.

Jenkins SM, Bennett V (2002) Developing nodes of Ranvier are defined by ankyrin-G clustering and are independent of paranodal axoglial adhesion. Proc Natl Acad Sci U S A 99:2303-2308.

Jensen AM, Chiu SY (1993) Expression of glutamate receptor genes in white matter: developing and adult rat optic nerve. J Neurosci 13:1664-1675.

Joosten EA, Gribnau AA (1989) Immunocytochemical localization of cell adhesion molecule L1 in developing rat pyramidal tract. Neurosci Lett 100:94-98.

Jussofie, A., Reinhardt, V., and Kalff, R. (1994) GABA binding sites: their density, their affinity to muscimol and their behaviour against neuroactive steroids in human gliomas of different degrees of malignancy. J. Neural Transm Gen. Sect. 96, 233-241.

Kaila K, Pasternack M, Saarikoski J, Voipio J (1989) Influence of GABA-gated bicarbonate conductance on potential, current and intracellular chloride in crayfish muscle fibres. J Physiol 416:161-81

Kang SH, Fukaya M, Yang JK, Rothstein JD, Bergles DE (2010) NG2+ CNS glial progenitors remain committed to the oligodendrocyte lineage in postnatal life and following neurodegeneration. Neuron 68:668-681.

Karadottir R, Cavelier P, Bergersen LH, Attwell D (2005) NMDA receptors are expressed in oligodendrocytes and activated in ischaemia. Nature 438:1162-1166.

Karadottir R, Hamilton NB, Bakiri Y, Attwell D (2008) Spiking and nonspiking classes of oligodendrocyte precursor glia in CNS white matter. Nat Neurosci 11:450-456.

Kaplan MR, Meyer-Franke A, Lambert S, Bennett V, Duncan ID, Levinson SR, Barres BA (1997) Induction of sodium channel clustering by oligodendrocytes. Nature 386:724-8

Keirstead HS, Levine JM, Blakemore WF (1998) Response of the oligodendrocyte progenitor cell population (defined by NG2 labelling) to demyelination of the adult spinal cord. Glia 22:161-170.

Kessaris N, Fogarty M, Iannarelli P, Grist M, Wegner M, Richardson WD (2006) Competing waves of oligodendrocytes in the forebrain and postnatal elimination of an embryonic lineage. Nat Neurosci 9:173-179.

Kettenmann H, Gilbert P, Schachner M (1984) Depolarization of cultured oligodendrocytes by glutamate and GABA. Neurosci Lett 47:271-276.

Kimura F, Baughman RW (1997) GABAergic transcallosal neurons in developing rat neocortex. Eur J Neurosci 9:1137-1143.

Kirchhoff F, Kettenmann H (1992) GABA Triggers a [Ca2+]i Increase in Murine Precursor Cells of the Oligodendrocyte Lineage. Eur J Neurosci 4:1049-1058.

Knutson P, Ghiani CA, Zhou JM, Gallo V, McBain CJ (1997) K+ channel expression and cell proliferation are regulated by intracellular sodium and membrane depolarization in oligodendrocyte progenitor cells. J Neurosci 17:2669-2682.

Kondo T, Raff M (2000) Oligodendrocyte precursor cells reprogrammed to become multipotential CNS stem cells. Science 289:1754-1757.

Korpi ER, Kuner T, Seeburg PH, Lüddens H (1995) Selective antagonist for the cerebellar granule cell-specific gamma-aminobutyric acid type A receptor. Mol Pharmacol. 47:283-9

Kuba H, Oichi Y, Ohmori H (2010) Presynaptic activity regulates Na(+) channel distribution at the axon initial segment. Nature 465:1075-1078.

Kucharova K, Stallcup WB (2010) The NG2 proteoglycan promotes oligodendrocyte progenitor proliferation and developmental myelination. Neuroscience 166:185-194.

Kukley M, Capetillo-Zarate E, Dietrich D (2007) Vesicular glutamate release from axons in white matter. Nat Neurosci 10:311-320.

Kukley M, Nishiyama A, Dietrich D (2010) The fate of synaptic input to NG2 glial cells: neurons specifically downregulate transmitter release onto differentiating oligodendroglial cells. J Neurosci 30:8320-8331.

Kumada T, Komuro H (2004) Completion of neuronal migration regulated by loss of Ca(2+) transients. Proc Natl Acad Sci U S A 101:8479-8484.

Kumar SS, Huguenard JR (2001) Properties of excitatory synaptic connections mediated by the corpus callosum in the developing rat neocortex. J Neurophysiol 86:2973-2985.

Labrakakis, C., Patt, S., Hartmann, H., and Kettenmann, H. (1998) Functional $GABA_A$ receptors on human glioma cells. Eur. J. Neurosci. 10, 231-238.

Lang EJ, Rosenbluth J (2003) Role of myelination in the development of a uniform olivocerebellar conduction time. J Neurophysiol 89:2259-2270.

Lappe-Siefke C, Goebbels S, Gravel M, Nicksch E, Lee J, Braun PE, Griffiths IR, Nave KA (2003) Disruption of Cnp1 uncouples oligodendroglial functions in axonal support and myelination. Nat Genet 33:366-374.

Lee EC, Yu D, Martinez de Velasco J, Tessarollo L, Swing DA, Court DL, Jenkins NA, Copeland NG (2001) A highly efficient *Escherichia coli*-based chromosome engineering system adapted for recombinogenic targeting and subcloning of BAC DNA. Genomics 73:56–65

Levine JM (1994) Increased expression of the NG2 chondroitin-sulfate proteoglycan after brain injury. J Neurosci 14:4716-4730.

Levine JM, Reynolds R, Fawcett JW (2001) The oligodendrocyte precursor cell in health and disease. Trends Neurosci 24:39-47.

Levine JM, Stincone F, Lee YS (1993) Development and differentiation of glial precursor cells in the rat cerebellum. Glia 7:307-321.

Li S, Mealing GA, Morley P, Stys PK (1999) Novel injury mechanism in anoxia and trauma of spinal cord white matter: glutamate release via reverse Na+-dependent glutamate transport. J Neurosci 19:RC16.

Li S, Vana AC, Ribeiro R, Zhang Y (2011) Distinct role of nitric oxide and peroxynitrite in mediating oligodendrocyte toxicity in culture and in experimental autoimmune encephalomyelitis. Neuroscience 184:107-19

Lin SC, Bergles DE (2002) Physiological characteristics of NG2-expressing glial cells. Journal of Neurocytology 31:537-549.

Lin SC, Bergles DE (2004) Synaptic signaling between GABAergic interneurons and oligodendrocyte precursor cells in the hippocampus. Nat Neurosci 7:24-32.

Lin SC, Huck JH, Roberts JD, Macklin WB, Somogyi P, Bergles DE (2005) Climbing fiber innervation of NG2-expressing glia in the mammalian cerebellum. Neuron 46:773-785.

Lin G, Mela A, Guilfoyle EM, Goldman JE (2009) Neonatal and adult O4(+) oligodendrocyte lineage cells display different growth factor responses and different gene expression patterns. J Neurosci Res. 87:3390-402.

Liu X, Lu Y, Zhang Y, Li Y, Zhou J, Yuan Y, Gao X, Su Z, He C (2012) Slit2 Regulates the Dispersal of Oligodendrocyte Precursor Cells via Fyn/RhoA Signaling. J Biol Chem.

LoTurco JJ, Owens DF, Heath MJ, Davis MB, Kriegstein AR (1995) GABA and glutamate depolarize cortical progenitor cells and inhibit DNA synthesis. Neuron 15:1287-1298.

Lu QR, Yuk D, Alberta JA, Zhu Z, Pawlitzky I, Chan J, McMahon AP, Stiles CD, Rowitch DH (2000) Sonic hedgehog--regulated oligodendrocyte lineage genes encoding bHLH proteins in the mammalian central nervous system. Neuron 25:317-29.

Lutz PL (1992) Mechanisms for anoxic survival in the vertebrate brain. Annu Rev Physiol 54:601-618.

Luyt, K., Slade, T.P., Dorward, J.J., Durant, C.F., Wu, Y., Shigemoto, R., Mundell, S.J., Váradi, A., and Molnár, E. (2007) Developing oligodendrocytes express functional $GABA_B$ receptors that stimulate cell proliferation and migration. J. Neurochem. 100, 822-840.

Lytle JM, Chittajallu R, Wrathall JR, Gallo V (2009) NG2 cell response in the CNP-EGFP mouse after contusive spinal cord injury. Glia. 57:270-85.

Major G (1993) Solutions for transients in arbitrarily branching cables: III. Voltage clamp problems. Biophysical Journal 65:469–49

Mallon BS, Shick HE, Kidd GJ, Macklin WB (2002) Proteolipid promoter activity distinguishes two populations of NG2-positive cells throughout neonatal cortical development. J Neurosci. 22:876-85.

Mangin JM, Kunze A, Chittajallu R, Gallo V (2008) Satellite NG2 progenitor cells share common glutamatergic inputs with associated interneurons in the mouse dentate gyrus. J Neurosci 28:7610-7623.

Mao BQ, Hamzei-Sichani F, Aronov D, Froemke RC, Yuste R (2001) Dynamics of spontaneous activity in neocortical slices. Neuron 32:883-898.

Markram H, Lubke J, Frotscher M, Sakmann B (1997) Regulation of synaptic efficacy by coincidence of postsynaptic APs and EPSPs. Science 275:213-215.

Mathis C, Denisenko-Nehrbass N, Girault JA, Borrelli E (2001) Essential role of oligodendrocytes in the formation and maintenance of central nervous system nodal regions. Development 128:4881-4890.

Matsumoto Y, Tsunekawa Y, Nomura T, Suto F, Matsumata M, Tsuchiya S, Osumi N (2011) Differential proliferation rhythm of neural progenitor and oligodendrocyte precursor cells in the young adult hippocampus. PLoS One 6:e27628.

Matute C, Sanchez-Gomez MV, Martinez-Millan L, Miledi R (1997) Glutamate receptor-mediated toxicity in optic nerve oligodendrocytes. Proc Natl Acad Sci U S A 94:8830-8835.

Mayer M, Bogler O, Noble M (1993) The inhibition of oligodendrocytic differentiation of O-2A progenitors caused by basic fibroblast growth factor is overridden by astrocytes. Glia 8:12-19.

McAlpine D, Grothe B (2003) Sound localization and delay lines--do mammals fit the model? Trends Neurosci 26:347-350.

Meintanis S, Thomaidou D, Jessen KR, Mirsky R, Matsas R (2001) The neuron-glia signal beta-neuregulin promotes Schwann cell motility via the MAPK pathway. Glia 34:39-51.

Melendez-Vasquez CV, Rios JC, Zanazzi G, Lambert S, Bretscher A, Salzer JL (2001) Nodes of Ranvier form in association with ezrin-radixin-moesin (ERM)-positive Schwann cell processes. Proc. Natl. Acad. Sci. USA, 98:1235–1240

Meister M, Wong RO, Baylor DA, Shatz CJ (1991) Synchronous bursts of action potentials in ganglion cells of the developing mammalian retina. Science 252:939-943.

Metzger D, Clifford J, Chiba H, Chambon P (1995) Conditional site-specific recombination in mammalian cells using a ligand-dependent chimeric Cre recombinase. Proc Natl Acad Sci U S A 92:6991-6995.

Michailov GV, Sereda MW, Brinkmann BG, Fischer TM, Haug B, Birchmeier C, Role L, Lai C, Schwab MH, Nave KA (2004) Axonal neuregulin-1 regulates myelin sheath thickness. Science 304:700-3

Micu I, Jiang Q, Coderre E, Ridsdale A, Zhang L, Woulfe J, Yin X, Trapp BD, McRory JE, Rehak R, Zamponi GW, Wang W, Stys PK (2006) NMDA receptors mediate calcium accumulation in myelin during chemical ischaemia. Nature 439:988-992.

Miller RH (2002) Regulation of oligodendrocyte development in the vertebrate CNS. Prog Neurobiol 67:451-467.

Miller RH (2005) Dorsally derived oligodendrocytes come of age. Neuron 45:1-3.

Milner R, Ffrench-Constant C (1994) A developmental analysis of oligodendroglial integrins in primary cells: changes in alpha v-associated beta subunits during differentiation. Development 120:3497-3506.

Mohajerani, M.H., Cherubini, E. (2005) Spontaneous recurrent network activity in organotypic rat hippocampal slices. Eur. J. Neurosci. 22, 107-118.

Mohns EJ, Blumberg MS (2008) Synchronous bursts of neuronal activity in the developing hippocampus: modulation by active sleep and association with emerging gamma and theta rhythms. J Neurosci 28:10134-10144.

Murtie JC, Macklin WB, Corfas G (2007) Morphometric analysis of oligodendrocytes in the adult mouse frontal cortex. J Neurosci Res 85:2080-2086.

Nacher J, Alonso-Llosa G, Rosell D, McEwen B (2002) PSA-NCAM expression in the piriform cortex of the adult rat. Modulation by NMDA receptor antagonist administration. Brain Res 927:111-121.

Nash B, Thomson CE, Linington C, Arthur AT, McClure JD, McBride MW, Barnett SC (2011) Functional duality of astrocytes in myelination. J Neurosci. 31:13028-38.

Nery S, Wichterle H, Fishell G (2001) Sonic hedgehog contributes to oligodendrocyte specification in the mammalian forebrain. Development 128:527-540.

Neusch C, Rozengurt N, Jacobs RE, Lester HA, Kofuji P (2001) Kir4.1 potassium channel subunit is crucial for oligodendrocyte development and in vivo myelination. J Neurosci 21:5429-5438.

Nishiyama A, Komitova M, Suzuki R, Zhu X (2009) Polydendrocytes (NG2 cells): multifunctional cells with lineage plasticity. Nat Rev Neurosci 10:9-22.

Nishiyama A, Lin XH, Giese N, Heldin CH, Stallcup WB (1996) Co-localization of NG2 proteoglycan and PDGF alpha-receptor on O2A progenitor cells in the developing rat brain. J Neurosci Res 43:299-314.

Nowakowski RS, Lewin SB, Miller MW (1989) Bromodeoxyuridine immunohistochemical determination of the lengths of the cell cycle and the DNA-synthetic phase for an anatomically defined population. J Neurocytol 18:311-8.

Olivier P, Loron G, Fontaine RH, Pansiot J, Dalous J, Thi HP, Charriaut-Marlangue C, Thomas JL, Mercier JC, Gressens P, Baud O (2010) Nitric oxide plays a key role in myelination in the developing brain. J Neuropathol Exp Neurol. 69:828-37.

Ono K, Yasui Y, Rutishauser U, Miller RH (1997) Focal ventricular origin and migration of oligodendrocyte precursors into the chick optic nerve. Neuron 19:283-292.

Orban PC, Chui D, Marth JD (1992) Tissue- and site-specific DNA recombination in transgenic mice. Proc Natl Acad Sci U S A 89:6861-6865.

Paez PM, Fulton DJ, Spreur V, Handley V, Campagnoni AT (2010) Multiple kinase pathways regulate voltage-dependent Ca2+ influx and migration in oligodendrocyte precursor cells. J Neurosci 30:6422-6433.

Park E, Velumian AA, Fehlings MG (2004) The role of excitotoxicity in secondary mechanisms of spinal cord injury: a review with an emphasis on the implications for white matter degeneration. J Neurotrauma 21:754-774.

Pastor A, Chvatal A, Sykova E, Kettenmann H (1995) Glycine- and GABA-activated currents in identified glial cells of the developing rat spinal cord slice. Eur J Neurosci 7:1188-1198.

Patneau DK, Wright PW, Winters C, Mayer ML, Gallo V (1994) Glial cells of the oligodendrocyte lineage express both kainate- and AMPA-preferring subtypes of glutamate receptor. Neuron 12:357-371.

Patt S, Labrakakis C, Bernstein M, Weydt P, Cervós-Navarro J, Nisch G, Kettenmann H (1996) Neuron-like physiological properties of cells from human oligodendroglial tumors. Neuroscience. 71:601-11.

Pekcec A, Loscher W, Potschka H (2006) Neurogenesis in the adult rat piriform cortex. Neuroreport 17:571-574.

Pende M, Holtzclaw LA, Curtis JL, Russell JT, Gallo V (1994) Glutamate regulates intracellular calcium and gene expression in oligodendrocyte progenitors through the activation of DL-alpha-amino-3-hydroxy-5-methyl-4-isoxazolepropionic acid receptors. Proc Natl Acad Sci U S A 91:3215-3219.

Pirker S, Schwarzer C, Wieselthaler A, Sieghart W, Sperk G (2000) GABA(A) receptors: immunocytochemical distribution of 13 subunits in the adult rat brain. Neuroscience 101:815-850.

Poliak S, Salomon D, Elhanany H, Sabanay H, Kiernan B, Pevny L, Stewart CL, Xu X, Chiu SY, Shrager P, Furley AJ, Peles E (2003) Juxtaparanodal clustering of Shaker-like K+ channels in myelinated axons depends on Caspr2 and TAG-1. J Cell Biol 162:1149-1160.

Power J, Mayer-Proschel M, Smith J, Noble M (2002) Oligodendrocyte precursor cells from different brain regions express divergent properties consistent with the differing time courses of myelination in these regions. Dev Biol 245:362-375.

Pringle N, Collarini EJ, Mosley MJ, Heldin CH, Westermark B, Richardson WD (1989) PDGF A chain homodimers drive proliferation of bipotential (O-2A) glial progenitor cells in the developing rat optic nerve. EMBO J 8:1049-1056.

Psachoulia K, Jamen F, Young KM, Richardson WD (2009) Cell cycle dynamics of NG2 cells in the postnatal and ageing brain. Neuron Glia Biol 5:57-67.

Qian X, Davis AA, Goderie SK, Temple S (1997) FGF2 concentration regulates the generation of neurons and glia from multipotent cortical stem cells. Neuron 18:81-93.

Raff MC, Miller RH, Noble M (1983) A glial progenitor cell that develops in vitro into an astrocyte or an oligodendrocyte depending on culture medium. Nature 303:390-396.

Raff MC, Lillien LE, Richardson WD, Burne JF, Noble MD. (1988) Platelet-derived growth factor from astrocytes drives the clock that times oligodendrocyte development in culture. Nature 333, 562-565.

Ransom BR, Walz W, Davis PK, Carlini WG (1992) Anoxia-induced changes in extracellular K+ and pH in mammalian central white matter. J Cereb Blood Flow Metab 12:593-602.

Reimann F, Ashcroft FM (1999) Inwardly rectifying potassium channels. Curr Opin Cell Biol 11:503-508.

Remahl S, Hildebrand C (1990) Relations between axons and oligodendroglial cells during initial myelination. II. The individual axon. J Neurocytol 19:883-898.

Reynolds R, Hardy R (1997) Oligodendroglial progenitors labeled with the O4 antibody persist in the adult rat cerebral cortex in vivo. J Neurosci Res 47:455-470.

Reynolds R, Wilkin GP (1988) Development of macroglial cells in rat cerebellum. II. An in situ immunohistochemical study of oligodendroglial lineage from precursor to mature myelinating cell. Development 102:409-425.

Rheims S, Holmgren CD, Chazal G, Mulder J, Harkany T, Zilberter T, Zilberter Y (2009) GABA action in immature neocortical neurons directly depends on the availability of ketone bodies. J Neurochem 110:1330-8

Richardson WD, Kessaris N, Pringle N (2006) Oligodendrocyte wars. Nat Rev Neurosci 7:11-18.

Richardson WD, Pringle N, Mosley MJ, Westermark B, Dubois-Dalcq M (1988) A role for platelet-derived growth factor in normal gliogenesis in the central nervous system. Cell 53:309-319.

Rinholm JE, Hamilton NB, Kessaris N, Richardson WD, Bergersen LH, Attwell D (2011) Regulation of oligodendrocyte development and myelination by glucose and lactate. J Neurosci 31:538-48.

Rivers LE, Young KM, Rizzi M, Jamen F, Psachoulia K, Wade A, Kessaris N, Richardson WD (2008) PDGFRA/NG2 glia generate myelinating oligodendrocytes and piriform projection neurons in adult mice. Nat Neurosci 11:1392-1401.

Robinson RA and Stokes RH (1965) Electrolyte Solutions (2nd). Butterworth, London.

Rosenberg PA, Li Y, Ali S, Altiok N, Back SA, Volpe JJ (1999) Intracellular redox state determines whether nitric oxide is toxic or protective to rat oligodendrocytes in culture. J Neurochem. 73:476-84.

Rosenberg SS, Kelland EE, Tokar E, De la Torre AR, Chan JR (2008) The geometric and spatial constraints of the microenvironment induce oligodendrocyte differentiation. Proc Natl Acad Sci U S A 105:14662-14667.

Rossi DJ, Oshima T, Attwell D (2000) Glutamate release in severe brain ischaemia is mainly by reversed uptake. Nature 403:316-21.

Rossi DJ, Hamann M, Attwell D (2003) Multiple modes of GABAergic inhibition of rat cerebellar granule cells. J Physiol. 548:97-110

Rouach N, Byrd K, Petralia RS, Elias GM, Adesnik H, Tomita S, Karimzadegan S, Kealey C, Bredt DS, Nicoll RA (2005) TARP gamma-8 controls hippocampal AMPA receptor number, distribution and synaptic plasticity. Nat Neurosci 8:1525-1533.

Roy K, Murtie JC, El-Khodor BF, Edgar N, Sardi SP, Hooks BM, Benoit-Marand M, Chen C, Moore H, O'Donnell P, Brunner D, Corfas G (2007) Loss of erbB signaling in oligodendrocytes alters myelin and dopaminergic function, a potential mechanism for neuropsychiatric disorders. Proc Natl Acad Sci U S A 104:8131-8136.

Salami M, Itami C, Tsumoto T, Kimura F (2003) Change of conduction velocity by regional myelination yields constant latency irrespective of distance between thalamus and cortex. Proc Natl Acad Sci U S A 100:6174-6179.

Salter MG, Fern R (2005) NMDA receptors are expressed in developing oligodendrocyte processes and mediate injury. Nature 438:1167-1171.

Salzer JL (2003) Polarized domains of myelinated axons. Neuron 40:297-318.

Sánchez-Gómez, M.V., Alberdi, E., Ibarretxe, G., Torre, I., and Matute, C. (2003) caspase-dependent and caspase-independent oligodendrocyte death mediated by AMPA and kainate receptors. J. Neurosci. 23, 9519-9528.

Sauer, J-F., Strüber, M, and Bartos, M. (2012) Interneurons provide circuit-specific depolarization and hyperpolarization. J. Neurosci. 32, 4224-4229.

Scholz J, Klein MC, Behrens TE, Johansen-Berg H (2009) Training induces changes in white-matter architecture. Nat Neurosci 12:1370-1371.

Seidl AH, Rubel EW, Harris DM (2010) Mechanisms for adjusting interaural time differences to achieve binaural coincidence detection. J Neurosci 30:70-80.

Seidel B, Stanarius A, Wolf G (1997) Differential expression of neuronal and endothelial nitric oxide synthase in blood vessels of the rat brain. Neurosci Lett. 1997 239:109-12.

Seki T, Arai Y (1993) Distribution and possible roles of the highly polysialylated neural cell adhesion molecule (NCAM-H) in the developing and adult central nervous system. Neurosci Res 17:265-290.

Shaner NC, Campbell RE, Steinbach PA, Giepmans BN, Palmer AE, Tsien RY (2004) Improved monomeric red, orange and yellow fluorescent proteins derived from Discosoma sp. red fluorescent protein. Nat Biotechnol 22:1567-1572.

Shapiro LA, Ng KL, Kinyamu R, Whitaker-Azmitia P, Geisert EE, Blurton-Jones M, Zhou QY, Ribak CE (2007) Origin, migration and fate of newly generated neurons in the adult rodent piriform cortex. Brain Struct Funct 212:133-148.

Sherman DL, Brophy PJ (2005) Mechanisms of axon ensheathment and myelin growth. Nat Rev Neurosci 6:683-690.

Shi J, Marinovich A, Barres BA (1998) Purification and characterization of adult oligodendrocyte precursor cells from the rat optic nerve. J Neurosci 18:4627-4636.

Shimada N, Graf R, Rosner G, Heiss WD (1993) Ischemia-induced accumulation of extracellular amino acids in cerebral cortex, white matter, and cerebrospinal fluid. J Neurochem 60:66-71.

Sim FJ, Zhao C, Penderis J, Franklin RJ (2002) The age-related decrease in CNS remyelination efficiency is attributable to an impairment of both oligodendrocyte progenitor recruitment and differentiation. J Neurosci 22:2451-2459.

Simon C, Gotz M, Dimou L (2011) Progenitors in the adult cerebral cortex: cell cycle properties and regulation by physiological stimuli and injury. Glia 59:869-881.

Smith KJ, Lassmann H. (2002) The role of nitric oxide in multiple sclerosis. Lancet Neurol. 1:232-41.

Sobottka B, Ziegler U, Kaech A, Becher B, Goebels N (2011) CNS live imaging reveals a new mechanism of myelination: the liquid croissant model. Glia 59:1841-1849.

Soliven B, Szuchet S, Arnason BG, Nelson DJ (1988) Voltage-gated potassium currents in cultured ovine oligodendrocytes. J Neurosci 8:2131-2141.

Soliven B, Szuchet S, Arnason BG, Nelson DJ (1989) Expression and modulation of K+ currents in oligodendrocytes: possible role in myelinogenesis. Dev Neurosci 11:118-131.

Sontheimer H, Trotter J, Schachner M, Kettenmann H (1989) Channel expression correlates with differentiation stage during the development of oligodendrocytes from their precursor cells in culture. Neuron 2:1135-1145.

Spassky N, Heydon K, Mangatal A, Jankovski A, Olivier C, Queraud-LeSaux F, Goujet-Zalc C, Thomas JL, Zalc B (2001) Sonic hedgehog-dependent emergence of oligodendrocytes in the telencephalon: evidence for a source of oligodendrocytes in the olfactory bulb that is independent of PDGFRalpha signaling. Development 128:4993-5004.

Srinivas S, Watanabe T, Lin CS, William CM, Tanabe Y, Jessell TM, Costantini F (2001) Cre reporter strains produced by targeted insertion of EYFP and ECFP into the ROSA26 locus. BMC Dev Biol 1:4

Steinert JR, Kopp-Scheinpflug C, Baker C, Challiss RA, Mistry R, Haustein MD, Griffin SJ, Tong H, Graham BP, Forsythe ID (2008) Nitric oxide is a volume transmitter regulating postsynaptic excitability at a glutamatergic synapse. Neuron 60:642-56.

Stensaas LJ, Stensaas SS (1968) Astrocytic neuroglial cells, oligodendrocytes and microgliacytes in the spinal cord of the toad. II. Electron microscopy. Z Zellforsch Mikrosk Anat 86:184-213.

Sternberg N, Hamilton D (1981) Bacteriophage P1 site-specific recombination. I. Recombination between loxP sites. J Mol Biol 150:467-486.

Stevens B, Porta S, Haak LL, Gallo V, Fields RD (2002) Adenosine: a neuron-glial transmitter promoting myelination in the CNS in response to action potentials. Neuron 36:855-868.

Sturrock RR (1980) Myelination of the mouse corpus callosum. Neuropathol Appl Neurobiol 6:415-420.

Sugiarto S, Persson AI, Munoz EG, Waldhuber M, Lamagna C, Andor N, Hanecker P, Ayers-Ringler J, Phillips J, Siu J, Lim DA, Vandenberg S, Stallcup W, Berger MS,

Bergers G, Weiss WA, Petritsch C (2011) Asymmetry-defective oligodendrocyte progenitors are glioma precursors. Cancer Cell 20:328-340.

Sugihara I, Lang EJ, Llinas R (1993) Uniform olivocerebellar conduction time underlies Purkinje cell complex spike synchronicity in the rat cerebellum. J Physiol 470:243-271.

Sugimoto Y, Taniguchi M, Yagi T, Akagi Y, Nojyo Y, Tamamaki N (2001) Guidance of glial precursor cell migration by secreted cues in the developing optic nerve. Development 128:3321-3330.

Sussman CR, Vartanian T, Miller RH (2005) The ErbB4 neuregulin receptor mediates suppression of oligodendrocyte maturation. J Neurosci 25:5757-62.

Suzuki N, Bekkers JM (2006) Neural coding by two classes of principal cells in the mouse piriform cortex. J Neurosci 26:11938-11947.

Suzuki N, Bekkers JM (2007) Inhibitory interneurons in the piriform cortex. Clin Exp Pharmacol Physiol 34:1064-1069.

Tamura Y, Kataoka Y, Cui Y, Takamori Y, Watanabe Y, Yamada H (2007) Multi-directional differentiation of doublecortin- and NG2-immunopositive progenitor cells in the adult rat neocortex in vivo. Eur J Neurosci 25:3489-3498.

Tanaka J, Markerink-van Ittersum M, Steinbusch HW, De Vente J (1997) Nitric oxide-mediated cGMP synthesis in oligodendrocytes in the developing rat brain. Glia. 19:286-97.

Taveggia C, Thaker P, Petrylak A, Caporaso GL, Toews A, Falls DL, Einheber S, Salzer JL (2008) Type III neuregulin-1 promotes oligodendrocyte myelination. Glia 56:284-293.

Tekki-Kessaris N, Woodruff R, Hall AC, Gaffield W, Kimura S, Stiles CD, Rowitch DH, Richardson WD (2001) Hedgehog-dependent oligodendrocyte lineage specification in the telencephalon. Development 128:2545-2554.

Tekkok SB, Goldberg MP (2001) Ampa/kainate receptor activation mediates hypoxic oligodendrocyte death and axonal injury in cerebral white matter. J Neurosci 21:4237-4248.

Temple S, Raff MC (1986) Clonal analysis of oligodendrocyte development in culture: evidence for a developmental clock that counts cell divisions. Cell 44:773-779.

Tennekoon GI, Cohen SR, Price DL, McKhann GM. (1977) Myelinogenesis in optic nerve. A morphological, autoradiographic, and biochemical analysis. J Cell Biol. 72:604-16.

Tessier-Lavigne M, Attwell D, Mobbs P, Wilson M (1988) Membrane currents in retinal bipolar cells of the axolotl. J Gen Physiol 91:49-72.

Toda N, Okamura T (2003) The pharmacology of nitric oxide in the peripheral nervous system of blood vessels. Pharmacol Rev 55:271-324.

Tomimoto H, Ihara M, Wakita H, Ohtani R, Lin JX, Akiguchi I, Kinoshita M, Shibasaki H (2003) Chronic cerebral hypoperfusion induces white matter lesions and loss of oligodendroglia with DNA fragmentation in the rat. Acta Neuropathol 106:527-534.

Tong XP, Li XY, Zhou B, Shen W, Zhang ZJ, Xu TL, Duan S (2009) Ca(2+) signaling evoked by activation of Na(+) channels and Na(+)/Ca(2+) exchangers is required for GABA-induced NG2 cell migration. J Cell Biol 186:113-128.

Trapp BD, Nishiyama A, Cheng D, Macklin W (1997) Differentiation and death of premyelinating oligodendrocytes in developing rodent brain. J Cell Biol 137:459-468.

Tripathi RB, Clarke LE, Burzomato V, Kessaris N, Anderson PN, Attwell D, Richardson WD (2011) Dorsally and ventrally derived oligodendrocytes have similar electrical properties but myelinate preferred tracts. J Neurosci 31:6809-6819.

Trotter J (2005) NG2-positive cells in CNS function and the pathological role of antibodies against NG2 in demyelinating diseases. J Neurol Sci 233:37-42.

Tyzio R, Allene C, Nardou R, Picardo MA, Yamamoto S, Sivakumaran S, Caiati MD, Rheims S, Minlebaev M, Milh M, Ferré P, Khazipov R, Romette JL, Lorquin J, Cossart R, Khalilov I, Nehlig A, Cherubini E, Ben-Ari Y (2011) Depolarizing actions of GABA in immature neurons depend neither on ketone bodies nor on pyruvate. J Neurosci. 31:34-45.

Ullen F (2009) Is activity regulation of late myelination a plastic mechanism in the human nervous system? Neuron Glia Biol 5:29-34.

Vallstedt A, Klos JM, Ericson J (2005) Multiple dorsoventral origins of oligodendrocyte generation in the spinal cord and hindbrain. Neuron 45:55-67.

Van Straaten HW, Hekking JW, Wiertz-Hoessels EJ, Thors F, Drukker J (1988) Effect of the notochord on the differentiation of a floor plate area in the neural tube of the chick embryo. Anat Embryol (Berl) 177:317-324.

Van't Veer A, Du Y, Fischer TZ, Boetig DR, Wood MR, Dreyfus CF (2009) Brain-derived neurotrophic factor effects on oligodendrocyte progenitors of the basal forebrain are mediated through trkB and the MAP kinase pathway. J Neurosci Res 87:69-78.

Van Heyningen P, Calver AR, Richardson WD (2001) Control of progenitor cell number by mitogen supply and demand. Curr. Biol. 11:232-241

Vautier F, Belachew S, Chittajallu R, Gallo V (2004) Shaker-type potassium channel subunits differentially control oligodendrocyte progenitor proliferation. Glia 48:337-345.

Velez-Fort M, Maldonado PP, Butt AM, Audinat E, Angulo MC (2010) Postnatal switch from synaptic to extrasynaptic transmission between interneurons and NG2 cells. J Neurosci 30:6921-6929.

Vinet J, Lemieux P, Tamburri A, Tiesinga P, Scafidi J, Gallo V, Sik A (2010) Subclasses of oligodendrocytes populate the mouse hippocampus. Eur J Neurosci 31:425-438.

Volpe JJ. Cerebral white matter injury of the premature infant-more common than you think. Pediatrics 112:176-80.

Von BG, Trotter J, Kettenmann H (1991) Expression and Developmental Regulation of a GABAA Receptor in Cultured Murine Cells of the Oligodendrocyte Lineage. Eur J Neurosci 3:310-316.

Vora P, Pillai PP, Zhu W, Mustapha J, Namaka MP, Frost EE (2011) Differential effects of growth factors on oligodendrocyte progenitor migration. Eur J Cell Biol 90:649-656.

Voyvodic JT (1989) Target size regulates calibre and myelination of sympathetic axons. Nature 342:430-433.

Wake H, Lee PR, Fields RD (2011) Control of local protein synthesis and initial events in myelination by action potentials. Science 333:1647-1651.

Watson C, Paxinos G, Kayoliaglu G (2008) The spinal cord: a Christopher and Dana Reeve Foundation text and atlas (Academic, New York).

Watt AJ, Cuntz H, Mori M, Nusser Z, Sjostrom PJ, Hausser M (2009) Traveling waves in developing cerebellar cortex mediated by asymmetrical Purkinje cell connectivity. Nat Neurosci 12:463-473.

Waxman SG, Bennett MV (1972) Relative conduction velocities of small myelinated and non-myelinated fibres in the central nervous system. Nat New Biol 238:217-219.

Weiler N, Wood L, Yu J, Solla SA, Shepherd GM (2008) Top-down laminar organization of the excitatory network in motor cortex. Nat Neurosci 11:360-366.

Welch MJ, Purkiss JR, Foster KA (2000) Sensitivity of embryonic rat dorsal root ganglia neurons to Clostridium botulinum neurotoxins. Toxicon 38:245-258.

Werner P, Pitt D, Raine CS (2001) Multiple sclerosis: altered glutamate homeostasis in lesions correlates with oligodendrocyte and axonal damage. Ann Neurol 50:169-180.

Weruaga-Prieto E, Eggli P, Celio MR (1996) Topographic variations in rat brain oligodendrocyte morphology elucidated by injection of Lucifer Yellow in fixed tissue slices. J Neurocytol 25:19-31.

Wigley R, Butt AM (2009) Integration of NG2-glia (synantocytes) into the neuroglial network. Neuron Glia Biol 5:21-28.

Wilson GW, Garthwaite J (2010) Hyperpolarization-activated ion channels as targets for nitric oxide signalling in deep cerebellar nuclei. Eur J Neurosci. 31:1935-45

Windrem MS, Schanz SJ, Guo M, Tian GF, Washco V, Stanwood N, Rasband M, Roy NS, Nedergaard M, Havton LA, Wang S, Goldman SA (2008) Neonatal chimerization with human glial progenitor cells can both remyelinate and rescue the otherwise lethally hypomyelinated shiverer mouse. Cell Stem Cell 2:553-565.

Wolswijk G, Noble M (1989) Identification of an adult-specific glial progenitor cell. Development 105:387-400.

Yoshioka A, Hardy M, Younkin DP, Grinspan JB, Stern JL, Pleasure D (1995) Alpha-amino-3-hydroxy-5-methyl-4-isoxazolepropionate (AMPA) receptors mediate excitotoxicity in the oligodendroglial lineage. J Neurochem 64:2442-2448.

Young KM, Fogarty M, Kessaris N, Richardson WD (2007) Subventricular zone stem cells are heterogeneous with respect to their embryonic origins and neurogenic fates in the adult olfactory bulb. J Neurosci 27:8286-8296.

Yuan X, Eisen AM, McBain CJ, Gallo V (1998) A role for glutamate and its receptors in the regulation of oligodendrocyte development in cerebellar tissue slices. Development 125:2901-2914.

Zhang G, Gurtu V, Kain SR (1996) An enhanced green fluorescent protein allows sensitive detection of gene transfer in mammalian cells. Biochem Biophys Res Commun 227:707-711.

Zhang Y, Wang H, Li J, Dong L, Xu P, Chen W, Neve RL, Volpe JJ, Rosenberg PA (2006a) Intracellular zinc release and ERK phosphorylation are required upstream of 12-lipoxygenase activation in peroxynitrite toxicity to mature rat oligodendrocytes. J Biol Chem. 281:9460-70.

Zhang CL, Wilson JA, Williams J, Chiu SY (2006b) Action potentials induce uniform calcium influx in mammalian myelinated optic nerves. J Neurophysiol 96:695-709.

Zhang Y, Bekku Y, Dzhashiashvili Y, Armenti S, Meng X, Sasaki Y, Milbrandt J, Salzer JL (2012) Assembly and maintenance of nodes of ranvier rely on distinct sources of proteins and targeting mechanisms. Neuron 73:92-107.

Zhao X, He X, Han X, Yu Y, Ye F, Chen Y, Hoang T, Xu X, Mi QS, Xin M, Wang F, Appel B, Lu QR (2010) MicroRNA-mediated control of oligodendrocyte differentiation. Neuron 65:612-626.

Zhou Q, Choi G, Anderson DJ (2001) The bHLH transcription factor Olig2 promotes oligodendrocyte differentiation in collaboration with Nkx2.2. Neuron 3:791-807

Zhu G, Mehler MF, Zhao J, Yu YS, Kessler JA (1999) Sonic hedgehog and BMP2 exert opposing actions on proliferation and differentiation of embryonic neural progenitor cells. Dev Biol 215:118-129.

Zhu X, Hill RA, Dietrich D, Komitova M, Suzuki R, Nishiyama A (2011a) Age-dependent fate and lineage restriction of single NG2 cells. Development 138:745-753.

Zhu Q, Whittemore SR, Devries WH, Zhao X, Kuypers NJ, Qiu M (2011b) Dorsally-derived oligodendrocytes in the spinal cord contribute to axonal myelination during development and remyelination following focal demyelination. Glia 59:1612-1621.

Zhu X, Bergles DE, Nishiyama A (2008) NG2 cells generate both oligodendrocytes and gray matter astrocytes. Development 135:145-157.

Ziskin JL, Nishiyama A, Rubio M, Fukaya M, Bergles DE (2007) Vesicular release of glutamate from unmyelinated axons in white matter. Nat Neurosci 10:321-330.

Zonouzi M, Renzi M, Farrant M, Cull-Candy SG (2011) Bidirectional plasticity of calcium-permeable AMPA receptors in oligodendrocyte lineage cells. Nat Neurosci 14:1430-1438.